University College London
Great Ormond Street Institute of Child Health

Varicella zoster virus vasculopathy

Dr Elena Moraitis, MBBS

Submitted for the degree of Doctor of Philosophy
Infection, Inflammation and Rheumatology Section
University College London
Great Ormond Street Institute of Child Health

I, Elena Moraitis, confirm that the work presented in this thesis is my own. Where information has been derived from other sources, I confirm that this has been indicated in this thesis.

Acknowledgements

The seeds of this journey were sown many years ago in my childhood home, where my parents instilled in me a strong passion for exploring and learning. That this passion has made it to these printed pages is due to the strong support of so many people, but none more so than Despina Eleftheriou and Paul Brogan. Despina and Paul, I have been truly fortunate to have you as my PhD supervisors. Heartfelt thanks for your unfailing belief in me, for the support and encouragement throughout the journey, for challenging me and making me grow. Your scientific and clinical knowledge will never cease to amaze me. I am also hugely grateful to Judith Breuer, Vijeya Ganesan and Nigel Klein, secondary supervisors, for support and direction. I will forever be in debt to Ying Hong, one of the nicest people imaginable, for the help, constant reassurance, invaluable advice and guidance. Thanks to Ebun for her help and patience when untangling the knots of RNAseq and not only. Thank you to Ariane, Sira, Claire, Annette and Sonia for being an amazing and helpful team. Special thanks to Charris and Athina for being such a supportive and fun friends and colleagues, and for cheering me up no end along the bumpy way. Thank you and appreciation to Muthana and the colleagues at GOSH, a constant source of encouragement. Lastly, but never least, thanks to my parents for the support and the amazing chances they've given me over the years and to my husband for putting up with me along the journey. Most importantly, thank you to Antonios, my son, for being a ray of sunshine.

Elena Moraitis, January 2018

Thesis abstract

Varicella zoster virus (VZV) associated vasculopathy has long been identified as a major risk factor for arterial ischaemic stroke (AIS) in both adults and children. The exact mechanisms of VZV-induced pathological vascular remodelling leading to AIS have however not been fully elucidated, thus hampering current therapeutic approaches for AIS prevention. Previous immunohistochemical analysis of the morphology and composition of the arterial wall, and the location of viral antigen in the adventitia of patients with early VZV cerebral vasculopathy suggested that human brain vascular adventitial fibroblasts (HBVAF) may be the point of VZV entry into the cerebral arterial wall.

In this thesis, I explored the hypothesis that VZV exerts direct pathogenic effects affecting different cells of the vasculature that could result in occlusive cerebral vasculopathy. I showed that following infection *in vitro*, VZV promotes HBVAF transdifferentiation to myofibroblasts, with subsequent proliferation and migration as identified by induction of α-SMA and EdU expression, and scratch assay repair. RNAseq profile analysis of VZV-infected HBVAF revealed significant upregulation of a number of genes in the infected cells, highlighting pathways possibly underlying the morphological changes described. I also examined the interaction of VZV-infected HBVAF with endothelial cells, and showed activation and dysfunction in cultured endothelial cells induced by conditioned media from VZV-infected HBVAF. Further experiments revealed that VZV-infected HBVAF release proinflammatory cytokines and chemokines that could contribute to the pathogenesis of cerebral arteriopathy. Lastly, I explored whether some of these

effects on endothelial cells could be mediated by microparticle (MP) release. MP are membrane vesicles that are released from cells upon activation or during apoptosis, and are key inflammatory and endothelial dysfunction mediators in several vascular diseases. I showed that MP derived from VZV infected HBVAF contain VZV particles as detected by flow cytometry, electron microscopy and mass spectrometry. These MP-VZV complexes could infect healthy HBVAF, and might suggest a completely novel mechanism of VZV infectivity with potential relevance to viral induced changes locally in the cerebral vasculature.

In conclusion, these novel findings suggest that in the context of VZV related cerebral arteriopathy, HBVAF are important players for initiation and propagation of vascular inflammation and remodelling, and that MP act as key facilitators of cross talk an viral propagation between endothelial cells and neighbouring HBVAFs. These observations suggest an entirely novel mechanism of VZV vasculopathy that furthers our understanding of the pathogenesis of AIS.

Impact statement

One in five patients with AIS and cerebral arteriopathy will have a stroke recurrence. To date epidemiological studies linked VZV with AIS but the exact mechanism is unknown, limiting the therapeutic approaches to stop progression and secondary stroke prevention. The diagnosis of VZV vasculopathy is based on the clinical features and history of chickenpox; cerebrospinal fluid analysis for VZV IgG was advocated but it is still not part of the routine clinical practice. Treatment with aciclovir and steroids has been suggested in adults, but the addition of steroids to the treatment of childhood VZV related AIS is not routine due to the lack of delineation if inflammation plays a role in this condition.

The findings of this study suggest that VZV related AIS is the effect of progressive vascular remodeling as a result of productive viral infection of arteries initiated from the adventitial fibroblast. Changes in these cells in response to infection trigger a change in the local microenvironment with the development of a proinflammatory profile of these cells. This in turn leads to an aberrant cross talk between these cells and endothelial cells to trigger a proinflammatory and procoagulant endothelial phenotype, with decreased capacity of repair, potentially further contributing to the arterial changes leading to the development of AIS. Although limited by the fact that this is an *in vitro* not *in vivo* model, these discoveries contribute to the understanding of the role of

antiviral treatments and use of steroids for the treatment of patients with VZV arteriopathy. My model could also impact on the development of further studies to investigate the potential of reversing these pathological changes perhaps also with the use of other novel agents. The transcriptomic data will also assist in the identification of pathways of relevance to vascular remodeling in this condition. This can contribute to identification of novel therapeutic approaches to target the vascular remodeling and inflammatory changes in VZV-related cerebral arteriopathy, to be further confirmed in other models.

The development of a diagnostic or prognostic biomarker would be a useful tool for the clinicians looking after these patients. A pilot analysis suggests that plasma microparticles from patients with VZV vasculopathy carry VZV proteins, triggering a large prospective study to confirm if this could be a diagnostic biomarker.

AIS occurs at up to 12 months post VZV infection. It is useful in a prospective study to stratify the patients according to the proximity of the AIS to the VZV and also with regards to recurrence and investigate if any differences in the MP profiles (numbers, origin, viral signature, functional role in transmitting infection, proinflammatory phenotype). This could assist with identification of patients at risk of progression and enable the development of treatment according to the MP profile displayed.

This study identified the association of VZV with microparticles and this discovery is of potential relevance for other VZV related conditions. Rich data was generated for further research in VZV vasculopathy with a particular focus in deepening the understanding of clinical and therapeutic implications.

Abbreviations

Abbreviation	Definition
AIS	Arterial ischaemic stroke
AnV	Annexin V
BSA	Bovine serum albumin
CA	Catheter angiography
CASCADE	Childhood AIS Standardized Classification and Diagnostic Evaluation
cDNA	Complementary DNA
CMV	Cytomegalovirus
cPACNS	Chilhood primary angiitis of central nervous system
CPE	Cytopathic effect
CSF	Cerebrospinal fluid
CNS	Central nervous system
CT	Computed Tomography
DNA	Deoxyribonucleic acid
DWI	Diffusion-weighted imaging
ECM	Extracellular matrix
EV	Extracellular vesicles
FBS	Fetal bovine serum
FCA	Focal cerebral arteriopathy
FDR	False discovery rate
FFPE	formalin-fixed paraffin-embedded
FLAIR	Fluid-attenuated inversion recovery
GCA	Giant cell arteritis
GFP	Green fluorescent protein

HAV	Hepatitis A virus
HBVAF	Human brain vascular adventitial fibroblasts
HCV	Hepatitis C virus
HELF	Human embryonic lung fibroblasts
HIV	Human immunodeficiency virus
HSV	Herpex simplex virus
HUVEC	Human umbilical vein endothelial cells
ICA	Internal carotid artery
ICAM-1	Intercellular adhesion molecule-1
IE62	Immediate early protein 62
IHC	Immunohistochemistry
IPSS	International Pediatric Stroke Study
LC-MS/MS	Liquid chromatography-tandem mass spectrometry
MCA	Middle cerebral artery
MCP-1	Monocyte chemoattractant protein-1
MFI	Median fluorescence intensity
MOI	Multiplicity of infection
MP	Microparticles
MRI	Magnetic resonance imaging
NO	Nitric oxide
ORF	Open reading frame
PCR	Polymerase chain reaction
PD-L1	Programmed death-ligand 1
PFA	Paraformadehyde
PH	Pulmonary hypertension
PPP	Platelet poor plasma
PVA	Post varicella arteriopathy

ROS	Reactive oxygen species
RNAseq	RNA sequencing
SEM	Scanning electron microscopy
SM-MHC	Smooth muscle myosin, heavy chain
TCA	Transient cerebral arteriopathy
TEM	Transmission electron microscop
TIA	Transient ischaemic attack
TNF- α	Tumor necrosis factor – α
TOAST	Trial of Org 10172 in Acute Stroke Treatment
TOF-MRA	Time of flight magnetic resonance angiogram
VCAM-1	Vascular cell adhesion molecule-1
VIPS	Vascular effects of Infection in Pediatric Stroke
VZV	Varicella zoster virus
vwMRI	Vessel wall magnetic resonance imaging
α-SMA	Alpha-smooth muscle actin

Table of contents

Acknowledgements **3**

Thesis abstract **4**

Abbreviations **6**

Table of contents **13**

List of tables **21**

List of figures **22**

1 Introduction **27**

1.1. Varicella zoster virus (VZV) **27**

1.2. Varicella zoster virus-related vasculopathy **30**

1.2.1. Varicella zoster virus-related arterial ischemic stroke 30

1.2.1.1. Arterial ischemic stroke definition 30

1.2.1.2. Arterial ischaemic stroke epidemiology 32

1.2.1.3. Clinical presentation of AIS 34

1.2.1.4. Arterial ischaemic stroke imaging 36

1.2.1.5. Risk Factors for arterial ischemic stroke 39

1.2.1.6. Cerebral arteriopathies in arterial ischemic stroke 44

1.2.1.7. Epidemiological studies linking Varicella zoster virus with arterial ischemic stroke 47
1.2.1.8. Clinical features and investigation of Varicella zoster virus-related arteriopathy 49
1.2.1.9. The mechanism of Varicella zoster virus-related arteriopathy 56
1.2.1.10. The structure of arteries: characteristics of systemic and cerebral arteries 60
1.2.2. Varicella zoster virus and extracranial vasculopathy 63
1.3. Hypothesis and Aims 67
2 General methods and materials 68
2.1. Varicella zoster virus (VZV) 68
2.1.1. Virus strains 68
2.1.2. Viral proteins 69
2.2. Cells 70
2.3. Tissue culture media 71
2.4. Antibodies 72
2.5. Protein(s) used for flow cytometry and immunohistochemistry 75
2.6. Cell preparation 75
2.6.1. HBVAF 75
2.6.2. HUVEC 76
2.6.3 MEWO cells 76
2.7. Cell subculture 76
2.8. Cell counting 77

2.9. Freezing cells....78

2.10. Recovery of frozen cells....78

2.11. Cytokines....78

2.12. Varicella zoster virus stock production....79

2.12.1. Varicella zoster virus stock titration....81

2.12.2. Assessment of cellular changes in response to VZV infection using microscopy....83

2.13. Varicella zoster virus infection of HBVAF....84

2.13.1. HBVAF direct infection with mitotically inactivated MeWo cells associated VZV....85

2.13.2. HBVAF cell to cell infection....87

2.14. Statistical analysis....90

3. Human brain vascular adventitial fibroblast differentiation, proliferation and migration in response to VZV infection....91

3.1. Summary....91

3.2. Introduction....92

3.2.1 Adventitial vascular fibroblast as regulators of vascular wall structure and function....92

3.3. Aims....95

3.4. Methods....96

3.4.1. Fluorescent activated cell sorting for HBVAF differentiation and proliferation....96

3.4.1.1. Surface and intracellular marker identification....96

3.4.1.2. Proliferation assay 97
3.4.1.3. Flow cytometry data analysis 100
3.4.2. Scratch assay 102
3.5. Results 105
3.5.1. HBVAF are permissive to Varicella zoster virus infection *in vitro* 105
3.5.2. HBVAF activation and differentiation in response to VZV infection 111
3.5.3. HBVAF proliferation in response to VZV infection 114
3.5.4. Migratory capacity of human brain adventitial fibroblasts in response to Varicella zoster virus infection 116
3.6. Discussion 119
4. Microparticles and their role in Varicella zoster virus vasculopathy 123
4.1. Summary 123
4.2. Introduction 125
4.2.1. The interplay between endothelial activation and endothelial dysfunction in vascular disease 125
4.2.2. Cellular microparticles 130
4.3. Hypothesis 135
4.4. Methods 135
4.4.1. Fluorescence activated cell sorting of HBVAF-derived microparticles 135
4.4.1.1. Isolation of MP from HBVAF 135
4.4.1.2. Preparation of monoclonal antibodies and labelling of MP with Annexin V 136

4.4.1.3. Flow cytometric analysis of MP 137
4.4.2. Quantification of soluble cytokines and chemokines in HBVAF culture supernatants 141
4.4.3. Fluorescence activated cell sorting for human umbilical vein endothelial cell activation and dysfunction in response to Varicella zoster virus infection 142
4.4.3.1. Production of HBVAF culture conditioned media 142
4.4.3.2. HBVAF conditioned media fractionation 142
4.4.3.3. HUVEC incubation with conditioned media/MP /MP-free fractions harvested from VZV -infected HBVAF culture 143
4.4.3.4. Fluorescent activated cell sorting for human umbilical vein endothelial cell CD54 expression 143
4.4.3.5. Reactive oxygen species detection by Flow Cytometry 144
4.4.4. Qualitative mass spectrometric analysis of the proteomic profile of MP released by HBVAF in response to VZV infection 145
4.4.4.1. Sample preparation 145
4.4.4.2. Liquid chromatography tandem-mass spectrometry 147
4.4.5. Transmission electron microscopy (TEM) of MP and MP-free pellets 150
4.4.6. HBVAF incubation with MP harvested from infected cultures 152
4.4.7. Circulating MP in children with VZV-related AIS 154
4.4.7.1. Patients 154
4.4.7.2. Healthy controls and disease controls 154

4.4.7.3. Isolation of MP from platelet poor plasma 154
4.5. Results 155
4.5.1. Assessment of endothelial cell activation in response to stimulation with conditioned media derived from VZV-infected HBVAF 155
4.5.2. Assessment of endothelial cellular oxidative stress in response to stimulation with conditioned media derived from VZV-infected HBVAF 158
4.5.3. Assessment of the soluble factors in conditioned media harvested from VZV-infected HBVAF 160
4.5.3.1. Quantification of proinflammatory cytokine and chemokine secretion released by VZV-infected HBVAF.....160
4.5.4. Flow cytometry study of MP derived from HBVAF 166
4.5.4.1. HBVAF release MP in response to VZV infection 167
4.5.4.2. Study of endothelial activation and cellular oxidative stress in response to stimulation with MP derived from VZV-infected HBVAF 169
4.5.4.3. Flow cytometry analysis of MP derived from VZV-infected HBVAF 174
4.5.5. Mass spectrometric analysis of MP derived from VZV-infected HBVAF 178
4.5.6. Transmission electron microscopy study of MP shed by VZV-infected HBVAF.....190
4.5.7. Productive infection of HBVAF by MP from VZV-infected cells.....196
4.5.8. Circulating MP in plasma from children with VZV-related AIS 202
4.6. Discussion 205

5. Analysis of the gene expression profile in human brain vascular adventitial fibroblasts in response to Varicella zoster virus infection 218

5.1. Summary 218

5.2. Introduction 219

5.3. Aims 221

5.4. Methods 222

5.4.1. Cell preparation for RNA extraction 222

5.4.2. RNA extraction 222

5.4.3. cDNA library preparation, quality control and RNA sequencing 223

5.4.4. Read alignment, count conversion and gene set enrichment analysis 224

5.4.5. Statistical analysis 224

5.5. Results 225

5.5.1. Description of raw data 225

5.5.2. Principal component analysis 226

5.5.3. Data normalization 228

5.5.4. Visualisation of RNAseq results 229

5.5.5. Overview of transcriptomic data analysis 231

5.6. Discussion 248

6. Analysis of gene expression profile changes in HUVEC in response to activation by MP derived from VZV-infected HBVAF 253

6.1. Summary 253

6.2. Introduction 254

6.3. Aims 255

6.4. Methods 255

6.5. Results 257

6.5.1. Description of raw data 257

6.5.2. Principal component analysis 258

6.5.3. Data normalization 259

6.5.4. Visualisation of the RNAseq results 260

6.5.5. Overview of the transcriptomic analysis 262

6.6. Discussion 269

7 General discussion and future directions 272

8 Publications from this thesis 281

9 References 281

List of tables

Table 2-1. Varicella zoster viral proteins.....69

Table 2-2. Primary antibodies for flow cytometry and immunohistochemistry.....73

Table 4-1. Comparison of mean cytokine levels secreted by VZV-infected HBVAF and mock-infected HBVAF.....164

Table 4-2. Viral proteins identified in microparticle pellets derived from Varicella zoster virus-infected human brain vascular adventitial fibroblasts by mass spectrometry 181

Table 5-1. List of top 20 altered genes identified with altered expression in VZV-infected HBVAF by RNAseq.....232

Table 5-2. Top differentially expressed genes with read counts in VZV-infected HBVAF by RNAseq.....240

Table 5-3. Top pathways that were found to be significantly altered in VZV-infected HBVAF.....244

Table 6-1. Number of genes differentially expressed in response to incubation of HUVEC with MP or culture media from VZV-infected HBVAF.....263

List of figures

Figure 1.1. Radiological phenotype of post-varicella arteriopathy in childhood.....53

Figure 1.2. Radiological phenotype of varicella vasculitis in children.....54

Figure 1.3. Histological aspects of the arterial wall.....62

Figure 2.1. Flow cytometric analysis of VZV protein expression in virus-infected HBVAF shown at different serial dilutions of the virus.....86

Figure 2.2. Schematic representation of experiments inducing VZV HBVAF cell to cell infection.....88

Figure 2.3. Time course of VZV protein expression in VZV infected HBVAF following cell to cell infection.....89

Figure 3.1. Flow cytometric plots for detection of proliferating HBVAF using Click-iT Plus EdU flow cytometry assay.....99

Figure 3.2. Flow cytometry for EdU and VZV IE 62 detection in HBVAF.....100

Figure 3.3. HBVAF are susceptible to infection by VZV in vitro.....107

Figure 3.4. Flow cytometric analysis of GFP VZV ORF23, VZV gH and VZV IE62 protein expression on VZV-infected HBVAF.....110

Figure 3.5. VZV induces HBVAF differentiation to myofibroblasts.....113

Figure 3.6. Co-staining of HBVAF for detection of α-SMA and VZV gE proteins.....114

Figure 3.7. VZV infection enhances HBVAF proliferation.....115
Figure 3.8. Migratory potential of HBVAF in response to VZV infection.....118
Figure 4.1. The role of endothelial activation and endothelial dysfunction in vascular disease. (Adapted from Liao KJ, 2013).....128
Figure 4.2. Flow cytometric detection of MP released from HBVAF.....139
Figure 4.3. Conversion equation for calculation of MP number per mL of media from flow cytometer counts.....140
Figure 4.4. Basic schematic representation of a typical experimental workflow for protein identification and characterisation using liquid chromatography tandem-mass spectrometry (LC-MS/MS) (From J Cottrell, 2010).....147
Figure 4.5. Effect of conditioned media from VZV-infected HBVAF on HUVEC CD54 expression. 157
Figure 4.6. Conditioned media harvested from VZV-infected HBVAF induces ROS production in endothelial cells.....159
Figure 4.7. Analysis of cytokine and chemokine levels released by VZV-infected and mock-infected HBVAF, 48 hours post infection.....163
Figure 4.8. Time course of cytokine secretion in VZV-infected HBVAF.....165
Figure 4.9. Enumeration of MP in culture supernatants of infected fibroblasts.....169
Figure 4.10. MP from VZV-infected HBVAF induce CD54 upregulation in HUVEC.....171
Figure 4.11. MP harvested from VZV-infected HBVAF stimulate ROS production in endothelial cells.....172

Figure 4.12. Study to assess for potential cytokine contamination of MP pellets isolated from culture supernatants of VZV-infected HBVAF.....,,173
Figure 4.13. MP released from VZV-infected HBVAF harbour viral proteins.....177
Figure 4.14. Venn diagram of number of proteins identified in MP from control mock-infected HBVAF and MP from VZV-infected HBVAF.....179
Figure 4.15. Representative transmission electron micrographs of MP in mock or VZV-infection experiments.....194
Figure 4.16. MP derived from VZV-infected HBVAF can facilitate infection of healthy cells.....196
Figure 4.17. Circulating MP in children with VZV-related AIS.....204
Figure 5.1. Total number of mapped and counted reads for each sample for gene expression profiles of HBVAF: VZV- or mock-infected.....226
Figure 5.2. Principal Component Analysis, with percentages of variance associated with each axis for gene expression profiles of HBVAF: VZV- or mock-infected.....227
Figure 5.3. Boxplots of raw and normalized read counts for gene expression profiles in HBVAF VZV- or mock-infected.....229
Figure 5.4. Volcano plot of the comparison between gene expression profiles of HBVAF: VZV- or mock-infected.....230
Figure 5.5. Heatmap illustrating hierarchical clustering analysis of the top 20 significantly altered genes in VZV-infected and mock-infected HBVAF.....231

Figure 5.6. Top pathways that were found to be significantly upregulated in VZV-infected HBVAF.....242
Figure 5.7. Top pathways that were found to be significantly down-regulated in VZV-infected HBVAF.....243
Figure 6.1. Schematic summary of RNAseq experiments examining gene expression profile changes in HUVEC incubated with MP or conditioned media derived from VZV-infected HBVAF.....256
Figure 6.2. Total number of mapped and counted reads for each HUVEC sample processed following incubation with MP or conditioned media.....257
Figure 6.3: Principal Component Analysis, with percentages of variance associated with each axis for HUVEC gene expression profiles examined under different conditions.....259
Figure 6.4. Boxplots of raw and normalized read counts for HUVEC gene expression profiles examined under different conditions.....260
Figure 6.5. Volcano plot of the comparison between gene expression profiles of HUVEC incubated with conditioned media or MP derived from VZV-infected HBVAF.....261
Figure 6.6. Number of significant differentially expressed genes across 4 comparisons.....264
Figure 6.7. Heatmap illustrating hierarchical clustering analysis of the significantly altered gene expression in endothelial cells incubated with MP or media from VZV - and mock-infected HBVAF.....266

Figure 6.8. Pathways that were found to be significantly altered in HUVEC incubated with MP from infected HBVAF- cluster 2.....268
Figure 6.9. Pathways that were found to be significantly altered in HUVEC incubated with MP from infected HBVAF - cluster 5.....269
Figure 7.1. VZV-induced changes in HBVAF: an in vitro model of cerebral arteriopathy.....276

1 Introduction

1.1. Varicella zoster virus (VZV)

VZV belongs to the *Herpesviridae* family, *Alphaherpesviridae* subfamily (along with Herpes simplex viruses 1 and 2), and is an exclusively human DNA neurotropic virus (Abendroth et al. 2010). The virus can cause two distinct diseases: varicella (chickenpox) and herpes zoster (shingles). The primary infection (varicella) presents with a vesicular rash which varies from a few vesicles to a widespread confluent rash, with or without fever and malaise. The virus is spread via respiratory droplets or contact with fluid, and the incubation period is 10-21 days (Gershon et al, 2015). This pattern and length of incubation period likely reflect the time required for the virus to spread after infecting the epithelial cells of the respiratory mucosa to the tonsils and other lymphoid tissue. Subsequently, infected T-cells carry the virus via the blood stream to the skin sites of replication and possibly other organs (Gershon et al, 2015). However, lack of an animal model has limited the understanding of the exact mechanisms of VZV infection and virus propagation (Breuer and Whitley, 2007). During primary infection VZV establishes lifelong latency in neurons of cranial nerve ganglia, dorsal root ganglia, and autonomic ganglia along the entire neuraxis by gaining access to the neuronal bodies either by retrograde transport from skin or via T-cell viraemia. The virus can reactivate from latency and travel by anterograde transaxonal transport from the neuronal bodies to the skin, and cause herpes zoster, characterized by a vesicular dermatomal rash and pain

(Gershon et al, 2015).

When intact, VZV viral particles have a diameter of 80–120 nm (sometimes up to 200 nm) and a spherical or pleomorphic morphology (Zerboni et al. 2014, Harson et al, 1995). The herpesviruses share a common virion morphology, and a group of approximately 40 conserved genes that play key roles during viral replication (Owen et al, 2015). Similar to all herpesviruses, the VZV virion has four distinct components: envelope, tegument, and capsid core with the genome (Zerboni et al. 2014). The linear 125000 bp double-stranded DNA genome encodes at least 71 open reading frames (ORF), with an electron-dense core packaged into an icosahedral nucleocapsid that is made up of proteins (Cohen et al., 2010). It is believed that all the VZV genes are expressed during lytic replication of the virus which results in productive infection, whilst a number of studies have reported that only a restricted number of VZV genes are expressed during latency (Abendroth et al. 2010, Steiner et al, 2007, Ambadala et al, 2007). Sixty four of the 71 VZV ORF have homologs in human simplex virus (HSV). Capsids are surrounded by a tegument layer comprised of proteins including the IE62, IE63, IE4, ORF9, ORF10, ORF47 and ORF66 proteins, several of which function in regulating viral gene expression (Arvin and Gilden, 2013). The outer component of the virus is a lipid-rich envelope derived from cellular membranes with incorporated viral glycoproteins, including major ones such as: gE, the most abundant VZV glycoprotein which facilitates the virus entry to the cell; and gH, the major fusogen again with a role in virus entry to the cell (Zerboni et al. 2014). In addition, VZV requires gE for viral replication in contrast to other

alphaherpesviruses which replicate in the absence of gE (Montalvo et al, 1985, Cohen et al, 2007).

Cryo-electron tomography showed the herpes simplex virus-1 capsid to be asymmetrically placed inside the viral envelope, with the tegument layer ranging in thickness from approximately 5 nm at the “proximal” pole to around 35 nm at the “distal” pole (Grünewald et al, 2003). As HSV-1 and VZV have a very similar ultrastructure, this is likely the case for VZV also.

According to the most widely-accepted model, the lytic phase of VZV infection commences with virus particle entry to the cells, a process poorly understood, presumed either by fusion of the virion envelope with the plasma membrane or by endocytosis. The tethering of the virions to the cells likely occurs after reversible interaction of viral glycoproteins with heparan sulphate proteoglycans, abundantly expressed on the cell surface of almost all cells (Owen et al, 2015). After cell entry, the virions uncoat, and then the inner tegument proteins, such as the immediate-early protein 62 (IE62) major viral protein that functions as a transcription factor, are released and transported to the nucleus along with the nucleocapsid before *de novo* protein synthesis occurs. As has been demonstrated in cells infected by HSV, VZV gene transcription is believed to occur in an order that results in the synthesis of viral proteins categorised as immediate-early (transcription regulators), early (replication factors), and late (structural proteins), based on the kinetics of their expression after virus entry to the cell (Reichelt et al. 2009). Viral gene transcription, translation and new viral DNA synthesis is followed by assembly of new virions, enveloping and egress

(Zerboni et al. 2014). IE62, the major viral transactivator has been shown to be localized to the nucleus early in infection (Reichelt et al., 2009) and initiates immediate early gene expression (Arvin and Gilden, 2013), to be later moved to the cytoplasm for incorporation into the tegument of newly produced virions (Lynch et al., 2002). Reichelt and colleagues have studied the VZV replication cycle and kinetics of virion assembly in human embryonic lung fibroblast (HELF), demonstrating that one complete single cell replication cycle ending with the generation of infectious VZV particles takes between 9 and 12 hours (Reichelt et al. 2009).

1.2. Varicella zoster virus-related vasculopathy

1.2.1. Varicella zoster virus-related arterial ischemic stroke

1.2.1.1. Arterial ischemic stroke definition

In 1970 the World Health Organization introduced a definition of stroke as: “rapidly developing clinical signs of focal (or global) disturbance of cerebral function, lasting more than 24 hours or leading to death, with no apparent cause other than that of vascular origin” (Aho et al. 1980). In view of recent advances in modern brain imaging which showed that permanent injury can occur sooner than the 24 hour inclusion criterion, this definition is now considered suboptimal. In recognition of this, the American Heart Association and American Stroke Association have jointly provided an expert consensus “updated definition of

stroke for 21st century" as follows: "central nervous system infarction in brain, spinal cord, or retinal cell death attributable to ischaemia, based on pathological, imaging, or other objective evidence of cerebral, spinal cord, or retinal focal ischaemic injury in a defined vascular distribution; or clinical evidence of cerebral, spinal cord, or retinal focal ischaemic injury based on symptoms persisting ≥24 hours or until death, and other aetiologies excluded" (Sacco et al. 2013).

Stroke can occur in all age groups, and despite advances in diagnosis and treatment, is still associated with significant morbidity and mortality (Ganesan et al. 2000, Ferro et al, 2010).

The subtypes of stroke are ischaemic stroke (including arterial ischaemic stroke and cerebral sinovenous thrombosis), and haemorrhagic stroke (which includes intra-cerebral and subarachnoid haemorrhage) (Amlie-Lefond et al. 2008, Ferro et al, 2010). Paediatric stroke can also be subdivided according to age of onset into ischaemic perinatal stroke (with presentation up to the 28th postnatal day); and later childhood stroke (>28 days of age) (Amlie-Lefond et al. 2008).

Arterial ischaemic stroke (AIS) is defined as a focal neurological deficit with acute- onset, attributable to cerebral infarction in an arterial distribution (Mackay et al. 2011). The focus of this study will be AIS as defined above, in the context of Varicella zoster virus associated vasculopathy.

1.2.1.2. Arterial ischaemic stroke epidemiology

AIS is the second leading cause of death behind ischemic heart disease; is the leading case of disability in adults; and is one of the top ten causes of death in children (Benjamin et al, 2017). Two-thirds of children who survive a stroke will experience significant lifelong impairment (Mallick and O'Callaghan. 2010). Stroke at all ages thus represents a catastrophic event from the patient's perspective.

The incidence of stroke in the general adult population is 88 - 149 per 100,000 adults per year (Lee et al, 2011; Rothwell et al, 2004; Hippisley-Cox et al, 2004; Poisson et al, 2014). Data have consistently suggested a decline in stroke incidence and mortality over the recent decades, in association with increased use of preventive treatments, improving understanding of the risk factors and improvement in cardiovascular risk factor modification (Benjamin et al, 2017; Rothwell et al, 2004). Most adult AIS epidemiological studies focus on patients older than 50 years of age, with the majority having mean ages in the 60s (Poisson et al, 2014; Rothwell et al, 2004; Hippisley-Cox et al, 2004). A minority of studies have suggested an incidence of AIS in young adults (ages between 15- 20 through 40-50 years) between 3 and 11 per 100,000 (Naess et al, 2002; Putaala et al, 2009). Interestingly, even if overall there has been a significant decline in stroke incidence and mortality rates, age-adjusted stroke death rates have remained higher in black populations than in white populations; and the former also have higher stroke incidence (Howard VJ, 2013). The higher prevalence of risk factors in black populations, particularly hypertension and

diabetes mellitus, have been recognized as potential contributing factors.

A number of studies have investigated the incidence of stroke in children. The overall incidence of childhood stroke (ischaemic and haemorrhagic), ranges from 1.3 to 13 per 100,000 children per year, with rates for ischaemic stroke ranging from 0.2 to 7.9 per 100,000 children per year (Mallick and Ganesan. 2014; Mallick and O'Callaghan. 2010; Fullerton et al, 2003; DeVeber 2000; Earley et al. 1998; Giroud et al. 1995; Satoh et al, 1991). The large differences in the reported study incidence rates likely reflect differences in the design of the studies, inclusion criteria, methodology, size of the study, as well as geographical regions or ethnicity of the study population.

An analysis of data from the Canadian Pediatric Ischemic Stroke Registry reported on an estimated incidence of 3.3 per 100,000 children per year for childhood ischaemic stroke (DeVeber et al. 2000), whilst a later retrospective study of a Californian-wide paediatric population estimated an overall incidence of stroke of 2.3 per 100,000 children per year, and a rate of ischaemic stroke of 1.2 per 100,000 children per year (Fullerton et al. 2003).

Recently a UK study, the largest prospective population-based study of childhood AIS until now, reported an incidence of AIS of 1.6 per 100,000 children per year (Mallick, Ganesan et al. 2014). A Californian study and a later International Paediatric Stoke Study both found a small but statistically significant AIS higher incidence in boys (Fullerton et al. 2003; Golomb et al. 2009). In contrast with the above studies, a recent UK prospective study did not detect a difference in the

risk of AIS between sexes, although this latter study was relatively small and possibly underpowered to detect a significant difference between the sexes (96 children with AIS).

In terms of ethnicity, both the Californian and UK studies mentioned above identified that black children were at higher risk of AIS than were white children, a finding largely reflecting the increased prevalence of sickle-cell disease in the black population (Mallick et al. 2014; Fullerton et al. 2003). A UK-based study also found that Asian children are at increased risk of stroke, in contrast with the study from Fullerton *et al (Mallick et al, 2014).* This may be explained by the ancestral differences of the Asian populations in England and California (Mallick et al. 2014; Fullerton et al. 2003).

Of note, in both adult and paediatric populations, approximately 20% of patients with AIS will have stroke recurrence (Benjamin et al, 2017; Fullerton et al, 2016; Ganesan et al. 2006; Fullerton et al. 2003).

1.2.1.3. Clinical presentation of AIS

Sudden onset of hemiparesis, aphasia, ataxia, hemianopia and/or the loss of consciousness are common and well recognised symptoms of arterial ischemic stroke in adults (Rivkin et al, 2016).

Both adults and children experience strokes that affect very similar vascular territories in the brain. However, children may present differently depending on

their age, making the diagnosis of paediatric stroke more challenging than in adults, particularly for younger children, who may present with atypical signs.

Focal features, in particular hemiparesis, are the most common presenting feature of AIS in children, but diffuse features (such as seizures or reduced conscious level) also may occur, albeit more rarely (Fox et al. 2012). A number of patients have transient ischaemic attacks (TIA), with signs resolving within 24 hours. However they may still have cerebral infarction on imaging (Ganesan V. 2010; Ganesan et al. 2003). Seizures can also be a presenting features of stroke in children, along with diffuse features like a decreased level of consciousness (Abend et al, 2011; Zimmer et al. 2007).

Other clinical features at presentation include visual disturbance; facial weakness; speech disturbance; headache or vomiting (Mallick, Ganesan et al. 2014; Ganesan 2010; Ganesan et al. 2003). Signs of raised intracranial pressure or coma in children with large infarcts have also been described at presentation of AIS, and these patients may require hospitalization in paediatric intensive care units (Fox et al. 2012). Posterior circulation stroke in childhood can present with ataxia, vertigo, or vomiting (Ganesan et al. 2002).

The clinician facing a child with acute focal neurological deficit is often challenged to rule out other conditions which can present in a similar way with ischaemic stroke: infectious causes of encephalitis, brain tumors, hemiplegic migraine, haematoma, posterior reversible encephalopathy syndrome, venous sinus thrombosis, demyelinating disorders; or mitochondrial encephalopathy with

stroke-like episodes (Kirkham, 1999; Shellhaas et al. 2006), amongst other metabolic causes.

1.2.1.4. Arterial ischaemic stroke imaging

In terms of localization, the majority of events in AIS occur within the anterior cerebral circulation, commonly involving the middle cerebral artery territories (Jones et al. 2010). The posterior circulation is involved more frequently in cranio-cervical arterial dissection (Ganesan et al. 2002; Mackay et al. 2010).

Imaging is the cornerstone for the diagnosis of ischaemic stroke, and can delineate acute, subacute and chronic ischaemic brain lesions. In AIS, it is also crucial for considering treatment strategies for AIS in the young. In recent years, a major focus of research in this field has focussed on improving accuracy and speed of diagnosis using imaging techniques, in order to facilitate optimal and timely patient management. For example, imaging may identify which patients will be benefit more from revascularization therapies, thus permitting personalised therapeutic decisions and improving individual patient outcoms. Computed tomography (CT) / CT angiography or magnetic resonance (MR) / MR angiography imaging are used to identify arterial occlusion, to exclude haemorrhage and stroke mimics, and to define the extent of brain infarct (Vilela and Rowley, 2017).

In the acute ischemic stroke assessment by MRI and CT imaging, essential

evaluations include that of the brain parenchyma (to detect the AIS and exclude haemorrhage and stroke mimics); and of the vascular tree to detect the presence, nature, site, and extent of arterial occlusion. Additional evaluation is directed towards assessment of the collateral circulation status, clot type/extension and potential viable brain tissue assessment (Vilela and Rowley, 2017). In adults, posterior circulation strokes and patients with good arterial collateral circulation may have a longer time window for treatment.

MRI, due to a greater sensitivity and specificity for the diagnosis of stroke or conditions mimicking stroke, is now the gold standard for the investigation of AIS. However, there are often limitations in the clinical practice with regard to access to MRI. Computed tomography (CT) scanning is still performed in some adult and paediatric centres, as it is generally more widely available as the initial investigation modality, and in addition has a role in excluding conditions such as intracerebral haemorhage (Vilela and Rowley, 2017; Jones et al. 2010). There is no doubt about the superiority of MRI over CT as an investigation modality of AIS, however. In a study in which the appearance of acute cerebral infarction was evaluated on MR images and CT scans obtained in 31 patients within 24 hours of the event, Bryan *et al.* demonstrated that acute infarcts are easier to detect on MRI than CT, with 82% of MRI positive within the first 24 hours compared with only 58% visible on CT (Bryan et al. 1991). In addition, in comparison to CT, MRI is particularly superior for the detection of infarcts within the posterior circulation where CT is limited by beam hardening artifact from the skull base (Jones et al. 2010; Bryan et al. 1991). Also, lacunar infarcts are better

visualized on MRI (Wardlaw et al. 2001).

MR imaging usually includes standard T2-weighted axial images that show tissue contrast well and sagittal and coronal T1 weighted images that maximize contrast between the cerebral tissue and cerebrospinal fluid (CSF) and provide morphological information (Jones et al. 2010; Baird et al. 1998). In addition fluid-attenuated inversion recovery (FLAIR) suppression of the signal from the CSF increases the visibility of periventricular lesions (Jones et al. 2010; Schaefer et al. 2002). Of note, diffusion weighted imaging (DWI) is able to detect ischaemic regions of the brain before any changes are detectable on conventional MRI (Jones et al. 2010; Gadian et al. 2000).

Catheter angiography (CA) is the gold standard when evaluating for a medium- and small-vessel vasculopathy, but is associated with risk of stroke itself, and requires specialist facilities and trained operators (Jones et al. 2010); it remains the investigation of choice for detection of equivocal cases of arteriopathy (Aviv e t al. 2007). In addition, time of flight magnetic resonance angiography (TOF-MRA) has been shown to be as sensitive as conventional angiography in many cases for the detection of vasculopathy of the internal carotid artery (ICA) and the proximal segments of the middle and anterior cerebral arteries (Jones et al. 2010). Of note, TOF-MRA can overestimate the severity and length of a stenosis (Jones et al. 2010). Contrast-enhanced MRA also has a role, although the spatial resolution of MRA makes accurate interrogation of medium and small-calibre intracranial arteries difficult (Ishimaru et al. 2007; Yang et al. 2002).

High-resolution intracranial vessel wall MR imaging (vwMRI) is an adjunct to conventional angiographic imaging with CTA, MRA, or digital substraction angiography and is already used on a clinical basis in many centers worldwide. Vessel wall MR imaging could have multiple potential academic and clinical uses for the assessment of ischemic stroke and intracranial hemorrhage (Mandell et al, 2017). vwMRI has emerged in recent years with the goal of evaluating vascular pathology of the intracranial arteries (de Havenon et al, 2016), and vwMRI sequences have high spatial resolution and directly image the vessel wall by suppressing blood signal. With vwMRI, it is also possible to identify distinct morphologic and enhancement patterns of atherosclerosis that can provide important information about stroke aetiology and recurrence risk in adults (de Havenon et al, 2017).

1.2.1.5. Risk Factors for arterial ischemic stroke

In adults, the TOAST (trial of ORG 10172 in acute stroke treatment) aetiological classification of stroke is the most widely used system for establishing the cause of ischemic stroke (Adams et al, 2012). It categorizes stroke etiology into one of five subtypes: large-artery atherothromboembolic, cardioembolic, small-vessel thrombotic, other etiology, or undetermined etiology (Madden et al, 1995).

In the TOAST system, the stroke could be attributed to large artery

atherosclerosis if the patient had clinical findings consistent with an infarction affecting the cerebral cortex or both deep and cortical structures, the brain stem, or cerebellum. There should be an evidence for risk factors for accelerated atherosclerosis or symptomatic atherosclerotic disease (coronary artery disease, aortic disease, and peripheral arterial disease) in other anatomic locations (Adams and Biller 2015). Supportive imaging findings would be detection of a branch or large hemispheric, brain stem, or cerebellar infarction. Vascular imaging would demonstrate either intracranial or extracranial stenosis or occlusion at the usual sites for atherosclerosis such as the origin of the internal carotid artery. Subsequently, evidence of atherosclerotic disease as seen on magnetic resonance arteriography or computed tomographic angiography also was added. Patients with one of the traditional lacunar syndromes, such as pure motor hemiparesis, would be considered as having the subtype of stroke secondary to small artery occlusion. These patients should have evidence of arterial hypertension or diabetes mellitus, which are recognized risk factors for this arterial cause of stroke in adults (Adams and Biller 2015).

The neurological findings among patients with stroke attributed to cardioembolism would be similar to those with strokes secondary to large artery atherosclerosis. In addition, the patient would have evidence of heart disease. The brain imaging findings also would be similar to those found among patients with thromboembolism secondary to large artery atherosclerosis but in addition, brain imaging findings consistent with acute ischemic lesions in multiple vascular territories would be supportive of the diagnosis of cardioembolic stroke (Adams

and Biller 2015). The category of stroke of other determined cause is a small group in most studies of stroke in adults with a higher rate in young adults and includes nonatherosclerotic vasculopathies, including cervical artery dissection and hypercoagulable states (Madden et al, 1995). The last category includes patients with undetermined cause of stroke, reflecting the difficulty in making a aetiological diagnosis in a small number of cases.

A number of criticisms have been raised regarding the reliability and validity of the TOAST causative classification of stroke (Landau and Nassief, 2005; Amarenco et al, 2009). The overall inter-rater agreement for the TOAST system is now regarded as moderate, and reliability is reported as high for atherosclerosis and cardioembolism ($\kappa = 0.80$) but low for small vessel disease ($\kappa = 0.53$) and strokes of undetermined cause ($\kappa = 0.40$) (Meschia et al, 2006).

In young adults (aged between 18 and 49 years), risk factors such as and smoking, hypertension, diabetes, hyperlipidemia are highly prevalent, with substance abuse, carotid/vertebral artery dissections, arteriopathies, use of contraceptive drugs, migraine, pregnancy, and rare genetic conditions among others also included (Stark and Cole, 2017). Historically, the aetiological features for AIS in young adults have been regarded as different from the 'traditional' risk factors in older adults, but a recent increase in stroke incidence in young adults has been found to be associated with an increase in the prevalence of important risk factors including hypertension, hypercholesterolaemia, diabetes mellitus and obesity (Maaijwee et al, 2014).

In contrast, the risk factors for AIS in children are markedly different from those in adults (Ganesan et al. 2003; DeVeber 2003; Lo et al. 2009). A large proportion of children with AIS have another medical diagnosis that predisposes them to stroke, for example sickle cell disease, congenital heart disease, acute systemic diseases or genetic disorders (Mallick et al. 2014; Ganesan et al. 2003; Mackay et al. 2011). Several studies have proposed a large number of factors that are associated with childhood AIS. The term 'risk factor' has been widely used in the literature to describe these factors; however, there is not enough evidence to prove direct causality in many instances, and it has been suggested that these risk factors are 'presumptive' rather than 'definite' (Mallick et al. 2014).

Additional data on risk factors for childhood AIS have emerged from large cohort studies. A study which included more than 200 children conducted at Great Ormond Street Hospital identified arteriopathies in more than 80% of cases, and emphasized possible roles for chickenpox, and trauma in the development of AIS in previously healthy children (Ganesan et al. 2003). In contrast, Sträter *et al.* found a lower rate of arteriopathy (18 %) and a markedly higher rate of thrombophilia in a German study. This was suggested to be explained by the genetic traits of that population and the extent of investigation of the cases included in the study. Infection was identified in around 10% of cases (Sträter et al. 2002). A recent epidemiological study of paediatric stroke conducted in an area which gathers around 50% of the UK paediatric population identified arteriopathies as the major risk factor for AIS (Mallick et al. 2014). In this study,

an infectious trigger was reported in 28% cases of AIS. These findings are in keeping with the results of a large study which extracted data from the International Paediatric Stroke Study (IPSS) registry (Mackay et al. 2011) discussed in more detail below.

The IPSS was initiated in 2002 by a group of Paediatric neurologists from Canada, the US, and UK with further participation from over 30 countries, "enabling standardized data collection on the diagnosis, investigation, treatment and outcome assessment of children with stroke" to permit international multicenter stroke studies based on large cohorts of children. A limitation of the IPSS is, as with many other international data collection studies, the variability in the clinical approach and investigation in individual collaborating centers. In the IPSS study mentioned above, which included 676 children from 30 centers in 10 countries to analyse the AIS risk factors, the main categories identified were arteriopathies (in more than 50%), infection (in around 25%), acute head and neck disorders, cardiac disorders, acute systemic conditions, and chronic systemic conditions (sickle cell disease and connective tissue disorders) (Mackay et al. 2011). Of note, in less than 10% of cases no risk factors were found. In summary, these studies have all identified cerebral arteriopathy and infection as major risk factors of paediatric AIS.

Of note, cerebral arteriopathy was significantly associated with AIS recurrence in a number of studies. VIPS (Vascular effects of Infection in Pediatric Stroke) was an international prospective case control study which enrolled 357 children with AIS and 355 children with no stroke from 37 countries on 5 continents, with AIS

within 3 weeks of enrolment and ages above 28 days (Fullerton et al. 2016). The study was completed in 2014. In this study, infection in the week prior to AIS conferred a 6.3 fold increase in risk for AIS (Fullerton et al. 2015). In the VIPS study, the cumulative stroke recurrence rate was 6.8% at one month and 12% at one year, despite treatment of cases at tertiary centers with paediatric stroke expertise, and initial use of antithrombotic medications for secondary stroke prevention (Fullerton et al. 2016). The only predictor of recurrence was the presence of an arteriopathy, with one in five children with a definite arteriopathy presenting with recurrence by 1 year, and 75% of recurrences occurring within the first 12 weeks after the index stroke. Two other studies have investigated the recurrence of paediatric AIS. In a Northern Californian population-based study the cumulative recurrence rate was 15% at one year, whilst in a mixed prospective and retrospective study conducted at Great Ormond Street Hospital which included 212 children with AIS, the 5-year cumulative recurrence rate was 18% (Ganesan et al. 2006; Fullerton et al. 2007).

Viral infections have also emerged as risk factors for stroke. VZV, human immunodeficiency virus (HIV) and cytomegalovirus (CMV), amongst others, have all been linked with stroke in adults and in children (Nagel et al, 2010).

1.2.1.6. Cerebral arteriopathies in arterial ischemic stroke

As shown in the above section, the current evidence suggests that cerebral

arteriopathies are a leading risk factor of childhood AIS and are associated with a high rate of stroke recurrence. They are less studied in adults, where the 'traditional' risk factors for stroke are prevalent.

Cerebral arteriopathies are currently defined and categorized on the basis of MRA findings. The majority of radiological findings are intracranial, although in up to 25% of cases extracranial cervical disease is identified (Ganesan et al. 2011). IPSS developed the Childhood AIS Standardized Classification and Diagnostic Evaluation (CASCADE) classification system which is based on the anatomic location of the abnormality, in an attempt to improve consistency in terminology and enable comparisons between prospective studies and clinical trials (Bernard et al. 2012). Sebire *et al.* proposed a classification system of cerebral arteriopathies including moyamoya (occlusive disease of the terminal internal carotid arteries with basal collaterals), vasculitis, arterial dissection, transient cerebral arteriopathy (TCA) and post-varicella angiopathy (PVA) (Sebire et al. 2004).

TCA, the most common arteriopathy described in the context of pediatric AIS, is a focal occlusive disease of the terminal internal carotid or proximal middle/anterior cerebral artery, which has been initially characterized as having a course showing stabilization or resolution on vascular imaging within an arbitrary defined interval of 6 months of the index AIS case (Sebire et al. 2004; Chabrier et al. 1998). However, cases have been described which show improvement after periods longer than 6 months (Danchaivijitr et al. 2006; Braun et al. 2009). Since the above definition of TCA is based on radiological documentation of the lesion

evolution, and many children with AIS are not re-imaged, in 2009 the IPSS coined the term focal cerebral arteriopathy of childhood (FCA) (Amlie-Lefond et al 2009). FCA is defined as TCA, but without the requirement to show evolution with re-imaging. When FCA is preceded by VZV infection in the 12 months prior to AIS, these children are considered to have post-varicella arteriopathy (PVA) (Sebire et al. 1998; Sebire et al. 1999; Askalan et al. 2001; Lanthier et al. 2005). There is confusion in the literature between FCA and PVA, which are both considered monophasic inflammatory arteriopathies and in fact radiologically indistinguishable.

One more aspect of controversy in the literature is the possible overlap between FCA and childhood primary angiitis of the central nervous system (cPACNS) (Elbers et al. 2008; Eleftheriou et al. 2009). The clinical presentation and radiological features are often similar, and further confusion arises from the fact that patients with FCA fulfil the Calabrese et al. criteria for cPACNS (Calabrese et al. 1988), and also from the lack of sensitivity of the investigations available for cPACNS and the difficulty of obtaining tissue for histologic diagnosis.

A recent prospective international study has shown that the presence of an arteriopathy increased the risk of recurrence 5-fold when compared with an idiopathic AIS (Fullerton et al, 2016). The 1-year recurrence rate in this study was around 25% for transient cerebral arteriopathy (Fullerton et al, 2016).

1.2.1.7. Epidemiological studies linking Varicella zoster virus with arterial ischemic stroke

Chickenpox was the first infection linked in the literature with AIS, and in the recent years other viral infections have emerged as risk factors for stroke. The first description of VZV vasculopathy seems to come from Cravioto and Feigin more than 50 years ago (Cravioto and Geigin, 1959).

The incidence and prevalence of VZV-related AIS is unknown. Estimates extrapolated from previous studies in children revealed that 7 to 31% of AIS is related to VZV (Askalan et al, 2001; Amlie-Lefond et al, 2009). Studies also showed that 1 in 15,000 cases of Varicella is associated with stroke (Askalan et al, 2001), and that in FCA stroke is preceded by varicella in 44% of cases (Braun et al, 2009). In adults, VZV vasculopathy is more common in immunocompromised than in immunocompetent individuals (Nagel et al, 2010), with VZV infection of the CNS detected in 1.5 to 4.4% of autopsy cases of immunocompromised patients (Petito et al, 1986; Grey et al, 1994).

In a case- control study, in 1999, Sebire and colleagues compared 11 children with AIS to 44 healthy controls, and showed that 64% versus 9% of children in the AIS and control group, respectively, had varicella at a median of 6 weeks prior to the stroke (Sebire et al. 1999). Two years later, a prospective cohort study which recruited 70 consecutive children presenting with AIS at two Canadian institutions reported that 1 in 3 cases of AIS followed varicella (Askalan

et al. 2001).

In 2014, 2 large studies confirmed the link between VZV and AIS (Thomas et al. 2014; Breuer et al. 2014). Thomas and colleagues found a 4- fold increased risk of stroke in children within 6 months of chickenpox in a self-controlled case series analysis of data from 4 general practice databases in the UK (Thomas et al. 2014). Breuer and colleagues conducted a retrospective cohort study of a large number of herpes zoster cases and matched controls which showed that herpes zoster is an independent risk factor for vascular disease under 40 years of age in the UK population (Breuer et al. 2014). In this study, the risk of stroke and transient ischemic attacks was 1.74 and 2.42-fold increased, respectively, in patients under 40 years of age with zoster (Breuer et al. 2014). In the same year, a UK based self-controlled case series study showed demonstrated a 1.23-fold increased risk of stroke over time at 1–26 weeks after zoster, and no increase at later times (Langan et al., 2014). In the same study, a stronger effect was observed for patients with ophthalmic zoster, rising to a >3-fold increase in the risk of stroke at 5-12 weeks after zoster (Langan et al., 2014).

Two studies, conducted in Taiwan and Denmark, observed a 17-30% increase in the risk of stroke in adults within 1 year following zoster (Kang et al., 2009; Sreenivasan et al., 2013). In a US-based community cohort study of older patients, the risk of stroke within 3 months of zoster was found to be 1.53-fold increased (Yawn et al, 2016).

The results of the VIPS study with regards to the role of herpesviruses

specifically in the development of childhood AIS were recently published (Elkind et al, 2016). These results confirm the findings of previous studies in a large international prospective study, showing that herpesviruses could act as a trigger for paediatric AIS, even if the symptomatology of infection was subclinical (Elkind et al. 2016). Elkind and colleagues included in this study 326 cases of AIS and 115 trauma controls with no stroke, with acute blood samples, of which 187 AIS cases had serological testing on paired convalescent samples. There was no difference between cases and controls in terms of serological evidence of past herpesvirus infection (IgG positive and IgM negative). However, serologic evidence of acute herpesvirus infection doubled the odds of childhood AIS, even after adjusting for confounding factors. Of the cases with acute herpesvirus infection, 32% had Herpes simplex virus (HSV) infection, and 18% had VZV infection (Elkind et al. 2016).

Taken together, these studies provide significant epidemiological evidence to demonstrate that VZV (and other herpesviruses) infection increases risk of AIS in children and adults.

1.2.1.8. Clinical features and investigation of Varicella zoster virus-related arteriopathy

VZV-related AIS typically presents with acute contralateral hemiplegia weeks to months following (usually) ophthalmic distribution zoster in adults or chickenpox

in children (Reshef et al, 1985; Nagel et al, 2010).

The literature, mainly concerning adult patients, describes patients with VZV-related vasculitis. VZV cerebral vasculitis and VZV-related arteriopathy are regarded as two distinct populations, based on clinical presentation and neuroimaging. These adult cases present with more diffuse features such as headache and changes in mental status, typically after herpes virus infection. A progressive or recurrent course is not uncommon, in contrast with the monophasic course of PVA described in children (Gilden et al. 2009). It has been reported that in adults VZV vasculopathy can involve both large and small arteries resulting in ischaemic or haemorrhagic strokes, and clinical presentation may also include aphasia, ataxia, hemisensory loss, hemianopsia or rarely monocular visual loss (Gilden et al, 2002; Hall et al, 1983; Venugopal, 2017). Adult patients also experience transient ischaemic attacks with protracted neurological symptomatology (Nagel et al, 2008). Nagel and colleagues have reported that 37% of adult patients with VZV vasculopathy do not have history of the characteristic varicella or zoster rash (Nagel et al, 2008). Rare associations of VZV vasculopathy include cranial neuropathies, vascular dissection, aneurysm, haemorrhage (subarachnoid or intracerebral) (Gilden et al, 2002). VZV vasculopathy has been reported to coexist with meningitis, myelitis or radicultits (Miyazaki et al, 2008).

The angiographic findings of VZV vasculopathy are more variable, often with multifocal vessel involvement (Figure 1.2). Cerebrospinal fluid (CSF) findings may be helpful diagnostically but are not always conclusive. CSF pleocytosis can

be present in up to two thirds of the cases but is not specific for VZV infection (Reis et al, 2014). VZV DNA is detected in CSF in a third of cases of adults with VZV vasculopathy. The presence of VZV antibodies in CSF appears to be a more sensitive diagnostic test in adults, being positive in >90% (Nagel et al. 2008), but there are still insufficient data in the paediatric population regarding this finding. Steroids and aciclovir are recommended in the treatment of adults with VZV vasculitis but are not yet routinely advocated in children with PVA.

A longitudinal study conducted at Great Ormond Street Hospital between 1990-2004 looked at the clinical features of children presenting with VZV- related AIS (Miravet et al. 2007). This study revealed a common pattern of presentation: patients tended to be younger children, between 6 months and 2 years of age, previously healthy, with a monophasic stroke clinical course. The median time from VZV infection and AIS was 4 months (Miravet et al. 2007). Figure 1.2. illustrates the clinical phenotype of VZV-associated AIS. These children demonstrate an arteriopathy with radiological features of a focal, unilateral, proximal occlusive arteriopathy, indistinguishable from FCA, most often involving the initial portion of the middle cerebral artery, typically causing a basal ganglia stroke.

In terms of laboratory investigations, perhaps surprisingly, extensive microbiological investigations or lumbar punctures in children with AIS are not yet part of routine clinical practice. Many of the published cases reported that VZV DNA is not detected in the CSF (Miravet et al. 2007), and data on VZV antibodies or other infectious biomarkers is scarce. More systematic screening using these

indices could provide more evidence of a direct causal role for the viral infection in AIS, however. A recent brief review paper (in French) by Monteventi and Fluss has summarized 26 published and 3 unpublished cases of VZV-related paediatric AIS (Monteventi et al. 2013). The clinical and radiological features were similar with the ones described in the UK study. Lumbar puncture with VZV DNA detection by PCR was performed in 14 of the 29 cases, and VZV DNA was detected in 6. The intrathecal production of anti-VZV IgG antibodies was analysed in only 8 cases, but was positive in 4 cases, of which 2 had concomitant presence of VZV DNA and intrathecal anti-VZV IgG. CSF examination was performed in only 11 cases and revealed moderate CSF pleiocytosis in 3 cases, and isolated increase in CSF protein in 2 cases.

It terms of the radiological course of VZV cerebral arteriopathy, the most common course in children is monophasic with subsequent resolution of the vascular stenosis (Figure 1.1.). However, the literature in children and in adults also describes improvement without complete resolution of arterial stenosis, and absence of a clear regression despite neurological improvement (Reis et al, 2014; Miravet et al, 2007; Bartolinin et al, 2011; Braun et al, 2009; Nagel et al, 2008). Progressive arteriopathy may also occur, with associated increased risk of recurrent stroke, especially in the first months after the acute episode (Miravet et al, 2007; Braun et al, 2009; Chabrier et al, 2013).

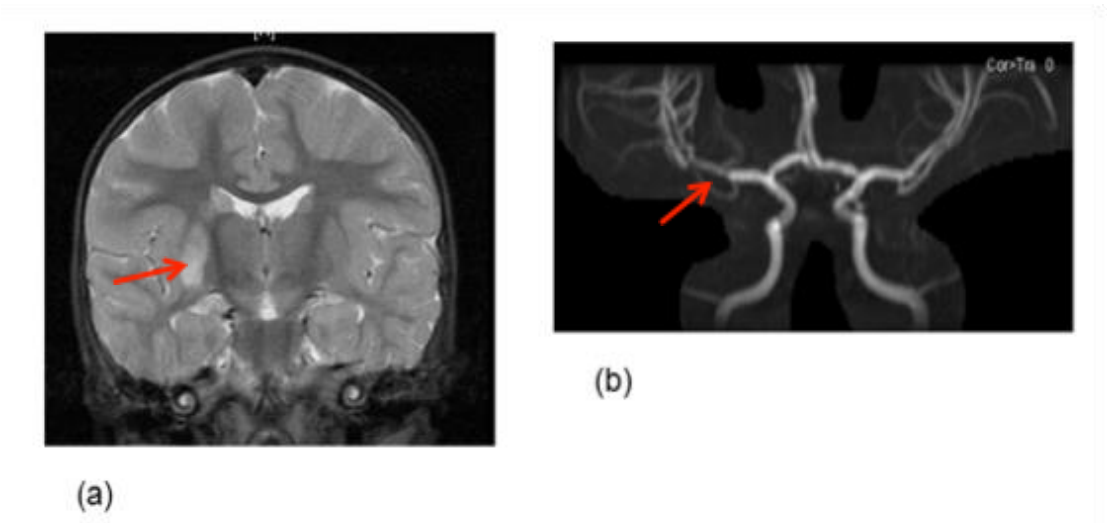

Figure 1.1. Radiological phenotype of post-varicella arteriopathy in childhood (Adapted from Moraitis and Ganesan, 2014)

This case illustrates the radiological phenotype of varicella-associated arterial ischaemic stroke (AIS). Images from a 17 month old boy who presented with an acute left hemiparesis, and history of chickenpox 8 months prior to the onset of the symptoms. Brain imaging (a) Coronal FLAIR images showing high signal in the basal ganglia (caudate and lentiform nuclei) on the right (arrowed). (b) 2D time of flight magnetic resonance imaging showing reduced flow in the distal right M1 segment of the middle cerebral artery (arrowed). No other AIS risk factors were identified despite extensive investigation, including echocardiography. He was considered to have post-varicella cerebral infarction and cerebral arteriopathy. He was treated with aspirin and followed-up until the age of 12 years with no recurrence and an excellent recovery with minimal residual left sided motor signs.

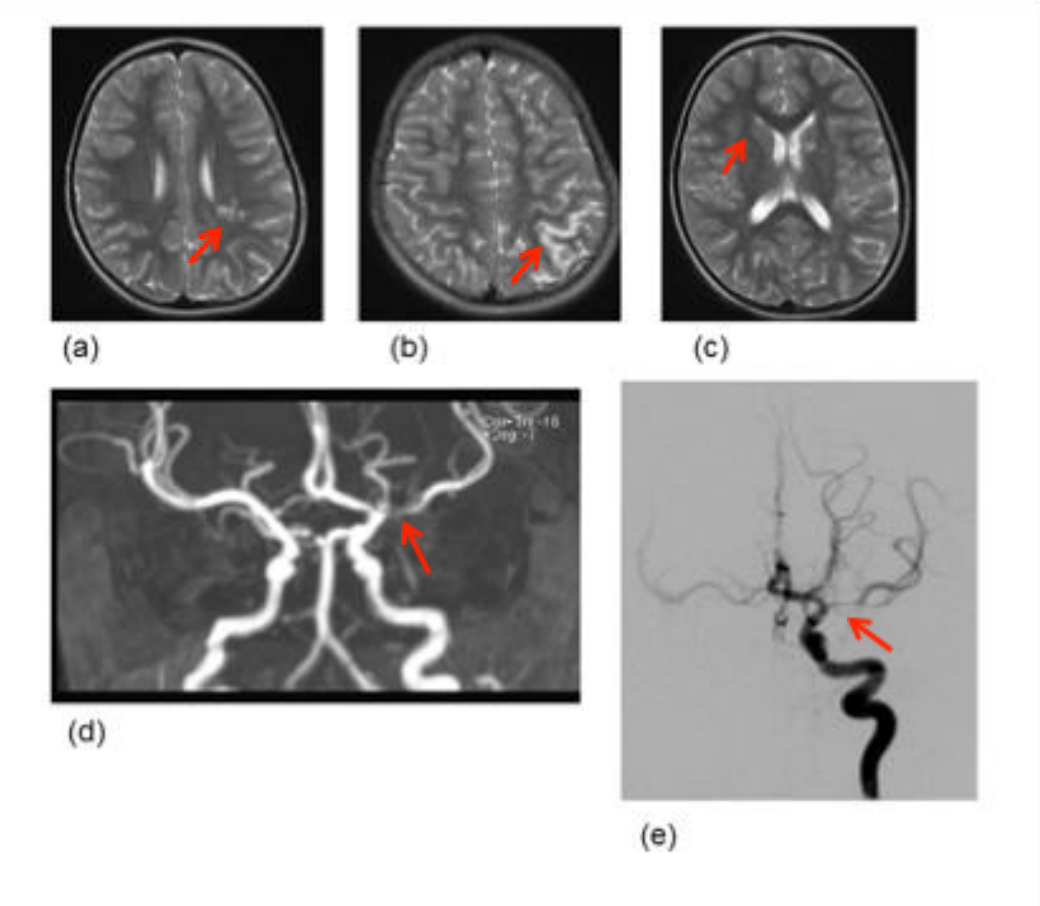

Figure 1.2. Radiological phenotype of varicella vasculitis in children (Adapted from Moraitis and Ganesan, 2014).

This case illustrates the clinical presentation and imaging findings of varicella vasculitis. Images from a 7 year old girl who presented with transient weakness of the right arm 3 months after chickenpox, and no previous neurological symptoms. Axial T2 weighted MRI scans ***(a-c)*** *show infarcts involving the right periventricular white matter and posterior borderzone region, which had restricted diffusion (a and b) and an additional lesion with free diffusion in the head of the left caudate (c), suggesting an older clinically undetected event. 2D time of flight MRA* ***(d)*** *showed a focal area of signal drop-out in the M1 segment of the left*

MCA. A lumbar puncture was performed, and CSF was acellular and negative for VZV DNA. A diagnosis of FCA was made and she was treated with aspirin. Three weeks later she presented with a further episode of transient right-sided weakness. Brain imaging did not show any further infarcts but catheter cerebral angiography ***(e)*** *demonstrated progression, with more severe and extensive stenosis of the L middle cerebral artery (MCA), and bilateral A1 stenoses and unilateral P1 stenosis. CSF examination was repeated; the CSF remained acellular, on this instance CSF was positive for VZV DNA low titer, and VZV IgG intrathecal production was demonstrated. She was treated with a short course of oral steroids and 3 months of aciclovir.*

1.2.1.9. The mechanism of Varicella zoster virus-related arteriopathy

The mechanism by which VZV causes vasculopathy is yet to be fully established. Recent adult studies have indicated that VZV-related arteriopathy could be caused by productive virus infection in cerebral arteries (Mayberg et al. 2011; Nagel et al. 2013). Mayberg and colleagues examined cerebral and temporal arteries from 3 patients with VZV-related disease histologically and by immunochemistry, during early or late disease, and compared the findings with a single control normal cerebral artery. VZV antigen was detected in the adventitia in the case with early disease, in contrast with the 2 cases with late disease, where VZV antigens were found in the arterial media and intima (Mayberg et al. 2011). These findings suggest that the virus spreads in the vascular wall with

point of entry via the adventitia possibly after transaxonal transport from ganglionic neurons after reactivation, and moves towards the media and intima in an “outside in” fashion. The authors also showed that the VZV-infected arteries displayed a thickened intima especially in the late disease cases, with cellular expression alpha-smooth muscle actin (α-SMA) and smooth muscle myosin heavy chain (SM-MHC) indicative of cells with a smooth muscle origin, or cells expressing a-SMA but not SM-MHC best characterized as myofibroblasts. In addition, the internal elastic lamina was disrupted.

In another study, the same research group analysed the inflammatory cell content and distribution in 6 normal arteries, and 2 VZV-infected arteries from subjects with early or late disease (Nagel et al. 2013). T cells, activated macrophages, and rare B cells were detected in the adventitia and intima of the VZV-infected arteries in both early and late disease. In the artery of early disease, adventitia contained numerous neutrophils and VZV antigen, and the hyperplastic intima displayed inflammatory cells in the vessels of vasa vasorum, findings suggestive of virus-induced inflammation and remodeling in the vessel wall. Intima and media of late VZV disease contained viral antigen, but not inflammatory cells. Taken together, the findings of the two above small adult studies support the theory that after reactivation and transaxonal spread from the ganglia to the arterial adventitia, VZV spreads transmurally to produce vascular remodeling in an inflammatory fashion. Studies in cats have identified afferent fibers from trigeminal and dorsal root ganglia to both intracranial and extracranial blood vessels (Langer et al. 1981), therefore suggesting that this could be a

possible anatomic pathway for transaxonal spread of virus from the ganglia following viral reactivation.

In paediatric cases in particular, the interval between acute infection and AIS in can be as long as 12 months, suggesting an ongoing silent process which could potentially have two mechanisms: 1. reactivation of latent VZV neuronal infection and subsequent infection of brain arteries from the external layer to the intima; and/or 2. an ongoing process of persistent silent infection in the brain arteries after the primary infection/ viraemia and direct invasion of the arterial wall by the virus.

Other mechanisms proposed include immune mediated vascular reaction secondary to distant infection (Bartolini et al, 2011; Ganesan and Kirkham, 1997); sympathetic stimulation due to the local irritant effect of the chickenpox lesions in the region of the superior cervical ganglion (Ganesan et Kirkham, 1997); thrombotic vascular occlusion by virus mediated direct endothelial damage (Losurdo et al, 2006; Ganesan et al, 1997); and acquired transient deficiencies of protein S and/or protein C (Losurdo et al, 2006; Alehan et al, 2002).

As far as the pathways involved in the pathogenesis of VZV vasculopathy are concerned, a recent study by Nagel and Gilden investigated a model of VZV persistence in cerebral arteries (Nagel et al. 2014). This study has shown inhibition of phosphorylated-STAT1 nuclear translocation and Mx1 antiviral protein expression in human brain vascular adventitial fibroblasts infected with

VZV, suggesting that VZV can interfere with the type I interferon pathway (an important anti-viral host response) as a mechanism of virus persistence in the brain arteries (Nagel et al. 2014).

The same group have shown differential regulation of matrix metalloproteinases in VZV-infected human brain vascular adventitial fibroblasts, suggesting that this mechanism could contribute to the aneurysm formation which has been reported in the context of VZV vasculopathy in adults (Nagel et al. 2014). A later study by the same research group showed that VZV infection of human brain vascular adventitial fibroblasts perineural cells downregulates the expression of programmed death ligand 1 (PD-L1) and MHC-I within 72 hours post infection. PD-L1 can be expressed on virtually all nucleated cells and suppresses the immune system by interacting with the programmed cell death protein receptor 1, found exclusively on immune cells (Jones et al, 2016). Therefore downregulation of PD-L1 may promote inflammation. This study provided insights into the mechanism by which inflammatory cells persist in VZV-infected arteries and therefore foster persistent inflammation in vessels, leading to pathological vascular remodeling during VZV vasculopathy (Jones et al, 2016).

An additional interesting aspect is highlighted by a number of studies showing that asymptomatic VZV reactivation occurs under stressful conditions, even in immunocompetent individuals (Mehta et al. 2004; Cohrs et al. 2008; Gilden et al. 2009; Papaevangelou et al. 2013). In a study which included children in the intensive care unit setting, Papaevangelou *et al.* detected VZV DNA more commonly in those who had subclinical primary VZV infection (Papaevangelou et

al. 2013). These results lead to the speculation that subclinical chickenpox could be associated with lower levels of viraemia and associated cellular immunity, therefore predisposing these children to greater risk of viral reactivation under stress. Similarly, the VIPS study identified a number of cases with herpesvirus-related AIS with serological evidence of acute infection in the absence of clinical symptoms (Elking et al. 2016). It is suggested therefore that VZV infection can be subclinical, but still contribute to childhood AIS where there is no previous history of VZV. This hypothesis, whilst attractive, currently lacks strong supporting evidence.

A contribution of the host genetic predisposition is also suspected but still unproven.

1.2.1.10. The structure of arteries: characteristics of systemic and cerebral arteries

The arterial wall consists of three layers: tunica intima, the innermost layer, comprised of endothelial cells, tunica media comprised of smooth muscle cells, elastin and collagen, and the outermost layer, tunica adventitia, composed of fibroblasts and collagen fibers (Figure 1.3). The intima is separated from the media by the internal elastic lamina, whilst the media is separated from the adventitia by the external elastic lamina (Tedgui, 1999). There are three types of arteries: the elastic arteries (aorta, pulmonary arteries) which receive blood

directly from the heart, muscular arteries which deliver blood to different parts of the body, and arterioles, which are small arteries which carry blood to capillaries. The muscular arteries, such as cerebral arteries have less elastic fibers and a well-defined tunica media compared to the elastic arteries. In contrast with the systemic arteries, cerebral arteries have no external elastic lamina (Lee. 1995). Also, unlike systemic arteries, cerebral arteries are poor in elastic fibers in the tunica media, and have a very thin adventitia (Cipolla. 2009). In addition, the tunica media of middle cerebral arteries has been reported to be relatively thinner compared other muscular arteries (Idowu. 2008).

The wall of the systemic arteries is nourished by diffusion of luminal blood to the the innermost arterial layers; and by a network of microvessels named vasa vasorum, supplying the outermost arterial layers. The vasa vasorum penetrates the adventitia and sometimes extends to the media. In contrast with systemic arteries, intracranial arteries generally lack vasa vasorum, apart from the proximal segments of the internal carotid artery where they are seen frequently with aging or atherosclerosis, and sometimes with other pathological processes (Portanova et al. 2013). A study in which human intracranial arteries from adults, children and newborns, and control systemic arteries were compared reported no vasa vasorum in children (Aydin et al. 1998). The lack of vasa vasorum in the intracranial arteries could be the result of structural features of cerebral arteries, such as thinner adventitia and media compared to extracranial arteries. These features could permit the vessel to be completely nourished by diffusion from luminal blood, with an additional contribution from the cerebrospinal fluid which

bathes the outermost layer (Portanova et al. 2013).

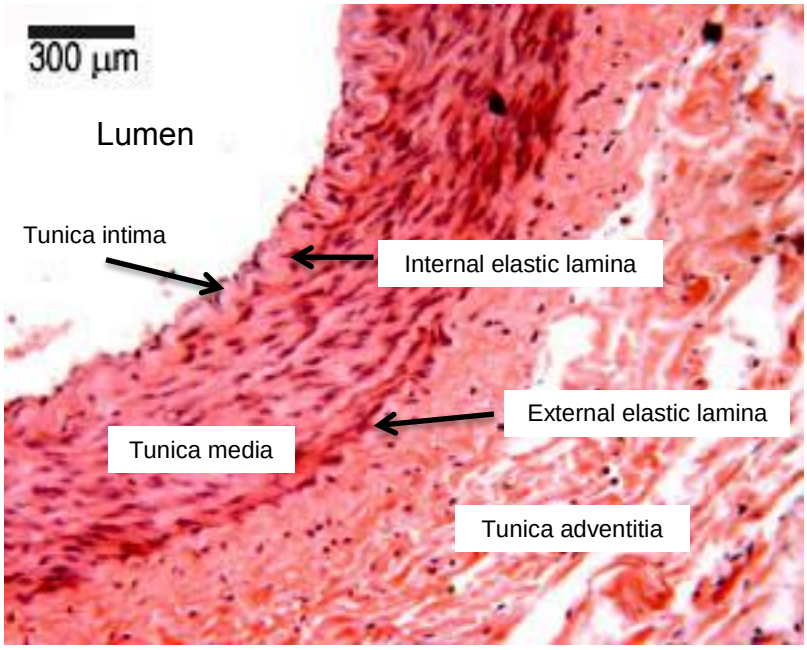

Adapted from: Histology Guide © Faculty of Biological Sciences University of Leeds

Figure 1.3. Histological aspects of the arterial wall. *Histology demonstrating the layers of a muscular artery. The arterial wall is composed of three layers: intima, media and adventitia, separated by two elastic membranes: internal elastic lamina and external elastic lamina. Cerebral arteries lack an elastic lamina.*

1.2.2. Varicella zoster virus and extracranial vasculopathy

In the past few years, the clinical spectrum of VZV vasculopathy has expanded to include not only intracranial vasculopathy, but also vasculopathy involving extracranial arteries presenting as giant cell arteritis (GCA) and granulomatous arteritis of the aorta. GCA is the most common systemic vasculitis in the elderly and presents with persistent headache, scalp tenderness and vision loss, as well as a history of jaw claudication, polymyalgia rheumatica, fever, night sweats, weight loss, fatigue and elevated inflammatory markers (Nagel et al, 2017).

The diagnosis of GCA is usually made based on clinical findings correlated with histopathological findings of temporal arteries biopsy which reveal the presence of transmural inflammation, medial smooth muscle cell damage, and multinucleated giant or epithelioid cells in non-contiguous skip lesions of temporal artery (GCA-pathology positive) (Nagel et al, 2017). However, in a number of cases the temporal artery biopsy is negative and the diagnosis and decision to treat is based on clinical suspicion (GCA- pathology negative) (Nagel et al, 2013). Treatment includes prompt initiation of corticosteroids to prevent vision loss. However up to 50% cases have been described to relapse after

discontinuation of therapy, or show progression to vision loss or stroke despite treatment (Nagel et al, 2017).

The aetiology of GCA is unclear, and previous studies have proposed as an early mechanism of disease progression the activation of vascular dendritic cells in the arterial wall possibly triggered by an unknown antigen (Ma-Krupa et al, 2014).

Recently, a series of studies done by a research group at the University of Denver, Colorado, using immunohistochemistry (IHC) and PCR performed on formalin-fixed, paraffin-embedded (FFPE) temporal arteries demonstrated the presence of VZV antigen or nucleic acid in the vessel walls of more than one hundred temporal arteries of patients with GCA-pathology positive. The analyses for the possible role of VZV in GCA pathogenesis were triggered by the similar changes at the histopathological level seen in patients with intracerebral VZV vasculopathy and GCA, and also by case reports describing an overlap between features of GCA and VZV vasculopathy (Salazar et al, 2011; Mathias et al, 2013; Nagel et al, 2013). These studies of virological analyses of temporal arteries from GCA-pathology positive and GCA-pathology negative patients detected VZV antigen in a significantly higher ($p=0.0001$) number of GCA-pathology positive arteries and GCA-pathology negative arteries compared to control normal temporal arteries: 73/104 (70%) GCA-pathology positive arteries, 58/100 (58%) GCA-pathology negative arteries, to 11/61 (18%) normal temporal arteries (Gilden et al, 2016; Nagel et al, 2013; Gilden et al, 2015). Adventitial inflammation and GCA pathology was observed in areas adjacent to the skip

areas were VZV antigen was detected, and no inflammation was seen in normal arteries containing VZV antigen (Nagel et al, 2013, Gilden et al, 2015). The presence of VZV in the normal temporal arteries was interpreted as most likely reflecting subclinical reactivation in some elder people.

Interestingly, similar to the studies of cerebral arteries, the presence of VZV antigen was detected in adventitia in most of the cases, followed by a lower frequency of detection in media and intima (Gilden et al, 2016). Taken together, these observations could support a viral spread from adventitia towards intima after transaxonal transport to the temporal arteries after reactivation from the ganglia.

In contrast, a recent small study investigated for the presence of VZV DNA by PCR in 11 snap frozen temporal arteries from 5 patients with GCA and compared with arteries from healthy controls. This study could not detect the presence of VZV in either temporal arteries from patients with GCA or healthy controls (Procop et al, 2017).

Aortitis (inflammation of the aorta) is characterized by granulomatous inflammation with inflammatory infiltrates composed of lymphocytes and plasma cells, along with epithelioid macrophages with or without multinucleated giant cells, as well as vessel wall damage (Stone et al, 2015). The same research group exploring VZV as an infectious trigger for GCA, also studied the potential role of VZV in the aortas of patients with pathologically verified granulomatous arteritis (Gilden et al, 2016). The rationale of the study was based on the

similarity of histopathological findings between intracerebral VZV vasculopathy, extracranial GCA, and large-vessel disease involving the aorta in granulomatous arteritis. Having identified VZV as involved in the pathogenesis of cerebral vasculopathy and GCA, the question was whether this infectious agent could be also the cause of the changes noted in granulomatous aortitis.

The Gilden lab used IHC and PCR to investigate the presence of the VZV antigen and VZV DNA in 11 FFPE aortas from patients with pathologically verified aortitis, and 18 FFPE control aortas obtained from intervening non-inflamed aortic repairs or routine autopsy (Gilden et al, 2016). The investigators detected abundant VZV antigen in all of 11 aortas that exhibited the characteristic pathology of granulomatous arteritis, and in 28% (5/18) control aortas from subjects with no symptoms or signs of aortitis ($p<0.0001$). VZV DNA was also present in most VZV antigen–positive aortas.

Consistent with the findings in the VZV cerebral vasculopathy and GCA, the VZV antigen was detected in the three aortic wall layers, with a predominance in the adventitia. Similarly to VZV cerebral arteriopathy and GCA, for granulomatous aortitis the mechanisms by which the VZV infects the arteries and trigger the abnormalities remain unknown. VZV infection of the aorta could follow viral reactivation of virus from latency from thoracic sensory ganglia and autonomic ganglia (Mahalingam et al, 1992; Nagel et al, 2014) and transaxonal spread to the aortic adventitia followed by transmural spread to the media and intima (Gilden et al, 2016).

In summary, all the histopathological and epidemiological studies highlighted in the above sections suggest a link between VZV and vasculopathy progression. However, the mechanisms are yet to be fully understood and therefore targets for slowing the progression of vasculopathy or even primary prevention are not yet identified.

1.3. Hypothesis and Aims

Epidemiological studies have suggested a link between VZV and childhood and adult AIS, however the mechanism of VZV arteriopathy is unknown.

Previous histological studies in adults suggest that direct viral invasion of cerebral, temporal arteries and possibly of aorta could cause changes in arterial caliber and contractility, produced in part by abnormal accumulation of smooth muscle cells and myofibroblasts causing thickened neointima and disruption of the tunica media.

The central hypothesis of this study is that the primary arterial target for VZV is the cell(s) residing in the adventitia (vascular fibroblasts). Following infection, changes/signals in these cells could promote vascular remodeling (VZV arteriopathy).

The **aims** of this project were to examine:

(i) whether following VZV infection *in vitro*, human brain vascular adventitial fibroblasts (HBVAF) differentiate into myofibroblasts with changes in their proliferating and migratory capacity;

(ii) whether VZV-infected HBVAF interact with endothelial cells or other nearby cells to promote progressive cerebral arteriopathy theorizing that the interaction could be partly mediated by the release of microvesicles (introduced in section 4.2.2.).

2 General methods and materials

This section contains predominantly materials and methods that are used in more than one chapter. Methods applicable to one chapter only will be discussed in detail in the relevant chapter.

2.1. Varicella zoster virus (VZV)

2.1.1. Virus strains

Infection experiments were carried out using the VZV virus strain THA, at passage 11 clinical isolate, of plaque forming units (pfu) 2x105/ml, generously provided by Professor Breuer, UCL. The virus was cultured and titred in MeWo cells (as described in a later section in this report).

In addition, the VZV-GFP23 (green fluorescent protein; GFP fused to the N terminus of ORF23) tagged strain at passage 13, pfu 4.6x105/ml, kindly provided by Professor Paul Kinchington, Pittsburgh, USA, was used in a series of experiments. The virus was cultured and titred using the same protocol as for the

untagged strain.

2.1.2. Viral proteins

Table 2-1. summarizes the viral proteins targeted with monoclonal antibodies or for GFP tagging in the series of experiments described in this report.

Table 2-1. Varicella zoster viral proteins

Protein	**Localization**	**Role**	**Category**	**Kinetics of expression** (Reichelt et al. 2009)
IE62	Tegument protein	Major viral protein, helps to regulate transcription early in infection; essential for virus replication.	Immediate-early	Nuclear localization at 2-4 hours post infection. Limited cytoplasmatic localization at 12 hours post infection.
gE	Membrane glycoprotein	Essential for virus replication and virus fusion.	Late	Cytoplasmic and membrane expression at 9-12 hours post infection.
gH	Membrane glycoprotein	Virus fusion and cell to cell spread	Late	Expression 12-24 hours post infection.
ORF 23	Nucleocapsid	Viral capsid assembly	Late	Expression at 9 hours

				post infection.

2.2. Cells

2.2.1. Human brain vascular adventitial fibroblasts (HBVAF) were purchased from Sciencell, Carlsbad, CA, USA. These cells are isolated from human brain, cryopreserved at passage one and delivered frozen. HBVAFs used in the series of experiments presented in this report were sub-cultivated and used at passages 2 to 5.

2.2.2. Human umbilical vein endothelial cells (HUVEC) were purchased from PromoCell (single donor, Heidelberg, Germany). They were used at passages 2-5.

2.2.3. Malignant melanoma cells (MeWo; Sigma-Aldrich) were kindly provided by Ms Helena Tutill, Research Assistant in the Breuer laboratory at UCL, Division of Infection and Immunity. MeWo cells are granular fibroblasts derived from a human melanoma by Professor C Grose in 1978. These cells multiply rapidly and have an unlimited life span. They are widely used for growth of VZV isolates. They were used to initiate the virus production at passage 46.

2.3. Tissue culture media

The following tissue culture media were used.

For HBVAF either complete media or quiescent media was used. The complete media comprised of basal fibroblast media supplemented with 2% fetal bovine serum (FBS), 1% fibroblast growth factor and 100x Penicillin/Streptomycin, (Sciencell, Carlsbad, CA, USA); media used to induce quiescence or for the absorption incubation during infection experiments contained basal fibroblast medium supplemented with 0.1% FBS, 100x Penicillin/Streptomycin and no growth factors.

For HUVEC: Endothelial Cell Growth Medium 2 (EGM-2, Promocell) comprised of basal endothelial growth medium supplemented with 2% FBS, 5ng/ml of epidermal growth factor, 10 ng/ml of basic fibroblast growth factor, 10 ng/ml of insulin growth factor, 0.5 ng/ml of Vascular Endothelial Growth Factor (VEGF), 1 µg/ml of ascorbic acid, 0.2 µg/ml of hydrocortisone and 90 µg/ml of heparin as per manufacturer's instructions.

For MeWo cells: Complete growth media consisting of Eagle's Minimum essential medium (MEM; Sigma-Aldrich) supplemented with 1% Non-Essential Amino Acids (NEAA) and 10% FBS, apart from the virus attachment incubation when MEM with 2% FBS was used.

2.4. Antibodies

The primary antibodies used for flow cytometry or immunohistochemistry in this study are listed in table 2-2. All antibodies were titrated by plotting a dilution curve against median fluorescence index, the relevant dilution for each antibody corresponding to the shoulder of the curve. Each antibody was also checked against an appropriate isotype-control antibody with the same protein concentration, as per manufacturers' recommendation.

Table 2-2. Primary antibodies for flow cytometry and immunohistochemistry

Specificity	Isotype	Conjugate	Clone number	Dilution/Application	Company
VZV gE	Goat IgG	Unconjugated	vN-20	1:200 flow cytometry	Santa Cruz Biotechnology
VZV IE62	Goat IgG	Unconjugated	vC-20	1:200 flow cytometry	Santa Cruz Biotechnology
VZV gH	Mouse IgG_1	Unconjugated	6A6	1:200 flow cytometry	Abcam
VZV (mixture)	Mouse Mixed	Unconjugated		1:2000 immunohistochemistry	Meridian Life Sciences
CD54	Mouse IgG_1	PE	LB-2	1:50 flow cytometry	BD PharminGen

Alpha-Smooth muscle actin	Mouse IgG_{2A}	APC	1A4	1:50 flow cytometry	R&D Systems
Alpha-Smooth muscle actin	Mouse IgG_{2A}	PERCP	1A4	1:50 flow cytometry	R&D Systems

Secondary antibodies used in this study are summarized in table 2-3.

Table 2-3: Secondary antibodies for flow cytometry and immunohistochemistry.

Antigen	**Conjugate**	**Host species**	**Target species**	**Dilution/ Application**	**Company**
Immunoglobulin	RPE	Goat	Mouse	1:50 flow cytometry	Dako
Immunoglobulin	FITC	Rabbit	Goat	1:50 flow cytometry	Dako
Immunoglobulin	Biotinylated	Goat	Mouse	1:1000 immunohistochemistry	Vector Labs

2.5. Protein(s) used for flow cytometry and immunohistochemistry

The following fluorochrome conjugated proteins were used:

1. Annexin V (PE or PERCP labeled; 1:50 dilution, for flow cytometry, BD)
2. Streptavidin (Alkaline Phosphatase labeled, 1:400, for immunohistochemistry, Jackson ImmunoResearch)

2.6. Cell preparation

2.6.1. HBVAF

In the experiments described in this report HBVAF were used after reaching quiescence, in order to closely replicate the state of the vascular adventitial fibroblasts *in vivo*. After establishing a new culture, the cells were subcultured when they were 80-90% confluent, and seeded at a density of 5000-10000 cells/cm^2 (depending on the requirements of the experiment) in basal fibroblast medium supplemented with 2% fetal bovine serum, 1% fibroblast growth factor

and 100x Penicillin/Streptomycin, (Sciencell, Carlsbad, CA,USA). Quiescence was achieved by shifting after 24h and for 7 days to basal fibroblast medium supplemented with 0.1% FBS, 100x Penicillin/Streptomycin and no growth factors, following published methods (Nagel et al. 2014). The medium was replenished every 48 hours.

2.6.2. HUVEC

The HUVECs were seeded at 5000 cells/cm^2 (recommended plating density by the manufacturer) in EGM-2 (PromoCell), and passaged after reaching 80- 90% confluency.

2.6.3 MEWO cells

MeWo cells were seeded at 2-4x10000 cells/cm^2, and sub-confluent cultures (70-80%) where split at a ratio of 1:2 to 1:4.

2.7. Cell subculture

When initiating a culture from cryopreserved cells, the vial was thawed in a 37^0C water bath and cells returned to culture in poly-L-lysine-coated culture vessel (T75 flask) as quickly as possible with minimal handling. The culture medium was refreshed the next day to remove residual DMSO and unattached cells, then every other day thereafter. To subculture the cells, the medium was aseptically removed from the flask and rinsed using a gently rocking motion with appropriate volumes of sterile Ca^{2+-} and Mg^{2+}-free DPBS (10 mls per T75 flask, 1 ml per well

in 12 well culture plates; Gibco Life Technologies, Paisley, Scotland, UK). DPBS was discarded, and appropriate volume of Trypsin/EDTA 0.025%/0.01% (3-5 mls per T75 flask, 300-500 µL per well in 12 well plate; PromoCell) added. HBVAF and HUVEC were detached at room temperature, while MeWo cells were incubated at 37^0C while observing the cells every 1-2 minutes.

The cells were examined under an inverted microscope, and when they rounded up and started to detach, I gently tapped the side of the vessel to loosen the remaining cells, and added Trypsin Neutralization Solution (0.05 % trypsin inhibitor, 0.1 % BSA); same volume as the volume of Trypsin/EDTA added; PromoCell) was added to the culture vessel and gently agitated. The cell suspension was carefully aspirated after gently pipetting up and down to obtain a single cell suspension, and transferred to a centrifugation tube. The cells were counted, and after adding appropriate volume of fresh growth medium they were seeded to new culture dishes at a split ratio of 1:2 -1:4 for MeWo cells, 1:3 for HUVEC and HBVAF, or appropriate seeding density for relevant experiments.

2.8. Cell counting

10µl of the cell suspension was mixed with 10µl of trypan blue. 10µl of this mix was placed in a Neubauer counting chamber. Unstained live cells were counted in the specified 25 box field and the total calculated according to the formula below:

unstained cells × dilution factor × 10^4 = viable cells/ml

2.9. Freezing cells

Processed cells were cryopreserved in liquid nitrogen for long-term storage. After counting, cells were centrifuged and re-suspended at a concentration of $2x10^6$/ml in freezing media (FBS supplemented with 10% v/v dimethyl sulphoxide from Sigma). One ml aliquots were transferred into individual cryovials which were placed into a freezing pot with isopropanol coolant for 24 hours at -80^0 C (allowing slow cooling) over night before transfer to liquid nitrogen storage.

2.10. Recovery of frozen cells

Cryopreserved cells were removed from liquid nitrogen and rapidly thawed in a 37^0C water bath. Cells were then transferred to a T75 flask in 15mls of fresh culture media at room temperature, and moved to a 37^0C 5% CO2 incubator.

2.11. Cytokines

Recombinant TNF-α (Sigma-Aldrich) at a concentration of 10 ng/mL was used for HUVEC treatment (positive control condition for upregulation of CD54 surface expression). Recombinant Human TGF-β1 (PeproTech, USA) at 5 ng/mL was

used for HBVAF stimulation. TGF-β1, the most abundant isoform of TGF-β, was originally identified for its ability to induce phenotypic transformation of fibroblasts. TGF-β is multifunctional cytokine that regulates cell proliferation, growth, differentiation and motility, as well as synthesis and deposition of the extracellular matrix, and it was used to induce HBVAF transdifferentiation to myofibroblasts.

2.12. Varicella zoster virus stock production

The THA strain of VZV was propagated in MeWo cells as described previously (Grose and Brunell. 1978; Eisfeld et al. 2007). A MeWo culture was initiated in MEM supplemented with 1% NonEssential Amino Acids (NEAA) and 10% FBS. Two T75 flasks of Mewo cells 60-70% confluent were taken, media removed, and the cells inoculated with 250 µL (approximately $25x10^5$pfu) in each flask. Briefly, the content of the virus vial was diluted into 5mls MEM with only 2%FBS, and 2.5 mls added to each flask. The inoculum was left on for 1hour at 37^0C, gently swirling the culture vessels every 15minutes to facilitate uniform distribution and virus attachment to the cells. After one hour, the media was topped up with 7.5mls MEM with 10%FBS and 1%NEAA, cells moved to 34^0C incubator, and cytopathic effect monitored daily. Edmond and colleagues have shown that incubation of MeWo and guinea-pig embryo cells with VZV at 36^0C and 32^0 results in higher yield of infection when propagated at 32^0C. This suggests that VZV may be a temperature-sensitive virus whose optimal temperature for growth

is below 36^0C, and that a shift in the incubation temperature would improve viral replication (Edmond et al. 1981).

Cytopathic effect or cytopathogenic effect (CPE) refers to the morphological changes in the host cell resulting from viral invasion. When cytopathic CPE was present in about 80% of cells (day 4-5 post infection), the culture media was decanted, cells scrapped and inoculated to 4 T175 flasks of 80% confluent MeWo cells, in 5 mls MEM 2% FBS for each flask. After one hour incubation at 37^0C, a volume of 20mls MEM supplemented with 10% FBS and 1% NEAA was added to each flask, and transferred to 34^0C incubator. When cytopathic effect was evident in 80% of cells (5 days post inoculation), the virus was ready to harvest. To harvest the cells, the media was removed, cells scraped and resuspended in a total of 8 mls freezing media for the 4 T175 flasks (freezing media is was comprised of 45% MEM, 45% FBS and 10% DMSO). 250 µL aliquots were transferred into individual cryovials which were placed into a freezing pot with isopropanol coolant for 24 hours at -80^oC overnight before transfer to liquid nitrogen storage.

Prior to freezing, the cells were treated with mitomycin C (0.05 mg/ml for 3 hours) to mitotically inactivate the Mewo cells to allow me to use cell associated virus in my experiments (Markus et al. 2011). Varicella zoster virus is highly cell associated in culture. Whilst cell free virus can be obtained by scraping that induces mechanical disruption of the cell monolayer and sonication followed by low speed centrifugation, these methods don't usually provide high titer of cell free virus (Carpenter et al. 2009; Grose et al. 1979; Weller et al. 1953), and the

virus obtained is highly unstable. (Harper et al. 1998). Therefore studies using cell free virus are extremely difficult to perform and were not chosen for this study.

2.12.1. Varicella zoster virus stock titration

After growing the VZV stock, the virus was titrated following an optimized protocol kindly provided by Dr Meleri Jones, at the time a Research fellow in Professor Breuer's laboratory at UCL, Division of Infection and Immunity.

In brief, MeWo cells were grown in one 24-well plate; when reaching 50% confluence, 10-fold dilutions of the virus from 10^{-1} to 10^{-6} were performed in MEM supplemented with 2% FBS. After removing the media culture, a volume of 100 µL per well was added in triplicates to enhance accuracy of the experiment, and the same volume of neat virus and media with no virus as negative control was also added in triplicates. The plate was incubated for 1 hour in a 37^0C incubator gently shaking it every 15 minutes, followed by topping up with 400 µL of MEM supplemented with 10% FBS and 1% NEAA, and moving it to a 34^0C incubator for 5 days. After 5 days the cell monolayer was rinsed once with 0.5 mL PBS per well, fixed in 4% Paraformaldehyde (PFA; 0.25 mL/well; Sigma-Aldrich) for 20 minutes, rinsed with PBS and proceeded to indirect immunohistochemical (IHC) staining to measure the viral pfu.

Methods for virus quantification can be divided into traditional methods and more modern methods. Traditional methods (virus plaque assay, fluorescent focus assay, tissue culture infective dose assay) are well-established methods that measure viral infectivity, but are time and labor intensive and can produce results that vary widely between replicates. Viral quantification based on the immunohistochemical staining for anti-VZV antibodies and automated reading of number of viral foci is quicker and improves the data reproducibility.

For IHC, the wells were emptied, 500 µL blocking solution (PBS + 10% FBS) was added to each well and the plate was incubated at room temperature for 30 minutes. The blocking solution was decanted and 250 µL primary antibody added to each well (mAb to VZV mixed; Meridian Life Sciences; 1:2000 dilution in PBS + 1%FBS), followed by incubation at room temperature for 60 minutes. The monolayer was washed twice by incubating for 5 minutes in 1 mL PBS per well, and 250 uL of Biotinylated anti-mouse IgG (H+L) affinity purified made in goat (1:1000 dilution in PBS + 1% FBS; VectorLabs) added per well and incubated at room temperature for 30 minutes. The cell monolayer was rinsed once with PBS as above, followed by a further 5 minutes incubation in 1 mL TBS per well (Tris buffered saline pH 7.6; Sigma-Aldrich) to obtain cleaner background. From this point onwards all the washing steps and antibody dilutions were performed with TBS. The TBS was decanted and the wells incubated at room temperature for 30 minutes in 250 µL per well of anti-mouse Alkaline Phosphatase-conjugated Streptavidin (1:400 dilution in TBS + 1%FBS; Jackson ImmunoResearch), washed twice in TBS, and 250 µL per well of Fast Red substrate was dispensed

and plate incubated at room temperature until the plaques became a strong red colour (approximately 5 minutes). Fast Red substrate was freshly prepared before use by dissolving 2mg Napthol AS-MX phosphate (Sigma-Aldrich) and 20 mg Fast Red TR salt (Sigma-Aldrich) to 10 mL 0.1M Tris (Trizma hydrochloride solution; pH 8; Sigma-Aldrich) by vortexing vigorously and passing through a 0.45µm syringe filter. When the plaques changed to a strong red colour, the reaction was stopped by filling the wells with distilled water, and wells emptied and air dried before counting the plaques.

Plaques were counted one week later using an automated ELISPOT reader. The AID ViruSpot Reader (Autoimmun Diagnostika) has full optical zoom integrated, permitting to read and interpret viral plaque assays in 6,12, 24, 48 or 96 well plates. To interpret the results, the number of plaques in each well were taken (to minimize error, only wells with between 20 and 100 plaques were included) and the average calculated. The average was then divided by the dilution factor to get the number of plaque forming units/100 µL neat virus, and multiplied by 10 to obtain pfu/mL neat virus. The pfu of the VZV THA strain I have grown and used in the experiments described in this report was therefore calculated to 200 000 pfu/mL.

2.12.2. Assessment of cellular changes in response to VZV infection using microscopy

As briefly mentioned earlier in this chapter, CPE refers to structural changes in host cells that are caused by viral invasion. Not all viruses are cytopathogenic, and the degree of CPE depends on the virus, the host cell type, multiplicity of infection (MOI) and other factors. In general, CPE is best observed in cultures infected at a low MOI where it develops gradually. In contrast, at a high MOI and depending on the virus used, the CPE can appear in the severe form including the destruction of the cell monolayer with cells relatively rapidly detaching from the culture vessel surface (Enders et al. 1954; Knipes and Howley. 2001). Culture dishes with VZV infected cells were observed every 1-2 days on Nikon TMS inverted microscope, in parallel with control mock infected cultures, to document the presence, degree and extent of cytopathic effect. In the same manner, the presence and extent of green fluorescence for experiments using the GFP tagged virus was assessed using a fluorescence microscope. Both CPE and green fluorescence were verified by two observers, myself and Dr Ying Hong, Research associate in our group.

2.13. Varicella zoster virus infection of HBVAF

VZV was propagated in culture using published methods, similar to the methods used for VZV propagation in MeWo cells (Grose and Brunell. 1978; Eisfeld et al. 2007).

2.13.1. HBVAF direct infection with mitotically inactivated MeWo cells associated VZV

Virus infection of cell cultures was achieved by incubating cells with a small volume of virus containing medium for certain time to allow relatively quick virus adsorption to the cells, prior to topping up with fresh media and continuing the incubation. In order to reach the target cell, the virus must traverse the distance to it. When inoculating virus to a cell monolayer, a series of factors are particularly important: the number of infectious viral particles added per cell (MOI), the concentration of viral particles in the total volume of media in which the virus is diluted during the attachment period, the length of time in which virus and cells and exposed to each other in a minimal volume of media, and the temperature during their interaction (Klasse et al. 2015).

HBVAF were seeded at 7000-10000 cells/cm^2 in appropriate culture vessels, in basal fibroblast media supplemented with 2% fetal bovine serum, 1% fibroblast growth factor and 100x Penicillin/Streptomycin (full media). When the culture reached 70-80% confluence, the media was removed and VZV was added at a MOI 0.002 (2000pfu per $1x10^6$cells) in a small volume of basal fibroblast media (the standard volume used for the virus attachment incubation in all the infection experiments was 2 mL/T75 flask, 700 µL/T25 flask, 300 µL/well in 6-well plate or 150 µL/well in 12-well plate) supplemented with only 0.1% FBS, 100xPenicillin/Streptomycin and no growth factors.

The culture dish was moved to a 37^0C incubator and gently swirled every 15

minutes; after one hour, the media was topped up to the recommended volume for each culture dish (15 mL for T75 flask, 5 mL for T25 flask, 2 mL/well in 6-well plate, 1 mL/well in 12-well plate), the culture vessel was moved to a 34^0C incubator, and CPE +/- fluorescence when the case was observed every 1-2 days to monitor the spread of the infection. The first signs of CPE appear at around 48 hours post infection in approximately 10% or less of the monolayer. After 6-7 days, when CPE/fluorescence was present in approximately 40% of the monolayer, the cells were harvested by trypsinization and used for HBVAF cell to cell infection.

The MOI of 0.002 was used based on prior infection optimization experiment. Serial 2-fold dilutions of the virus were used for infection, and the appearance/extent of CPE was observed, with additional confirmation of infection efficiency indicated by increase in percentage of cells expressing VZV gE and gH proteins (shown in Figure 2.1.).

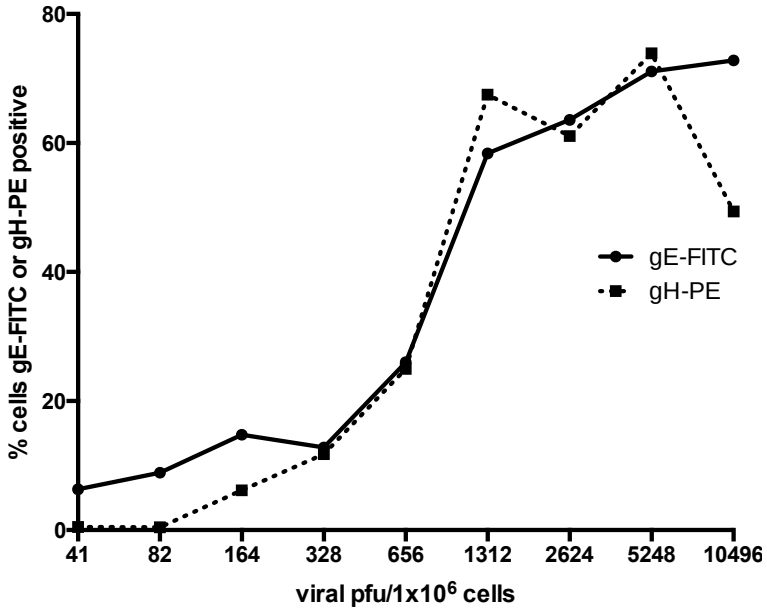

Figure 2.1. Flow cytometric analysis of VZV protein expression in virus-infected HBVAF shown at different serial dilutions of the virus.

This figures shows VZV gE and VZV gH protein expression on day 9 p.i. in HBVAF infected at different multiplicities of infection (MOI). Samples were stained in parallel with anti-VZV gE or anti-VZV gH antibodies and results are presented as percentage of positive cells (single experiment). A plaque forming units (pfu) of 2000 per 1x10^6 cells was selected to use in future experiments.

In the experiments described in this thesis, I have used HBVAF cell to cell infection as a more representative *in vitro* model of the *in vivo* infection. Following reactivation from latency in neurons, *in vivo* the virus already replicates when reaches the adventitial fibroblasts of the cerebral artery.

When directly infecting HBVAF with the VZV strains, for most of my experiments unless otherwise stated in the specific methods, my aim was not to specifically achieve a high infection efficiency in a short period of time. So I used a modest MOI to infect at a MOI which would permit the virus to gradually spread from cell to cell in less than 7 days and without being too low to allow the uninfected cells to multiply (HBVAF are rapidly growing cells) and overtake the culture limiting the propagation of the virus in the set time frame.

2.13.2. HBVAF cell to cell infection

HBVAF were seeded at 5000 cells/cm2 in 12-well or 6-well plates and quiescence induced by serum restriction and growth factors starvation as described in section 2.6.1. In parallel with the quiescent culture, proliferating HBVAF were directly infected with VZV-MeWo associated or uninfected MeWo (stock grown under the same experimental conditions as VZV- associated MeWo cells) referred to as mock-infection from here after. When resting HBVAF were fully quiescent (day 8), infected HBVAF (either VZV or mock) were inoculated to the quiescent culture at a ratio of 1 cell from the infected culture to 3 uninfected cells (Figure 2.2.).

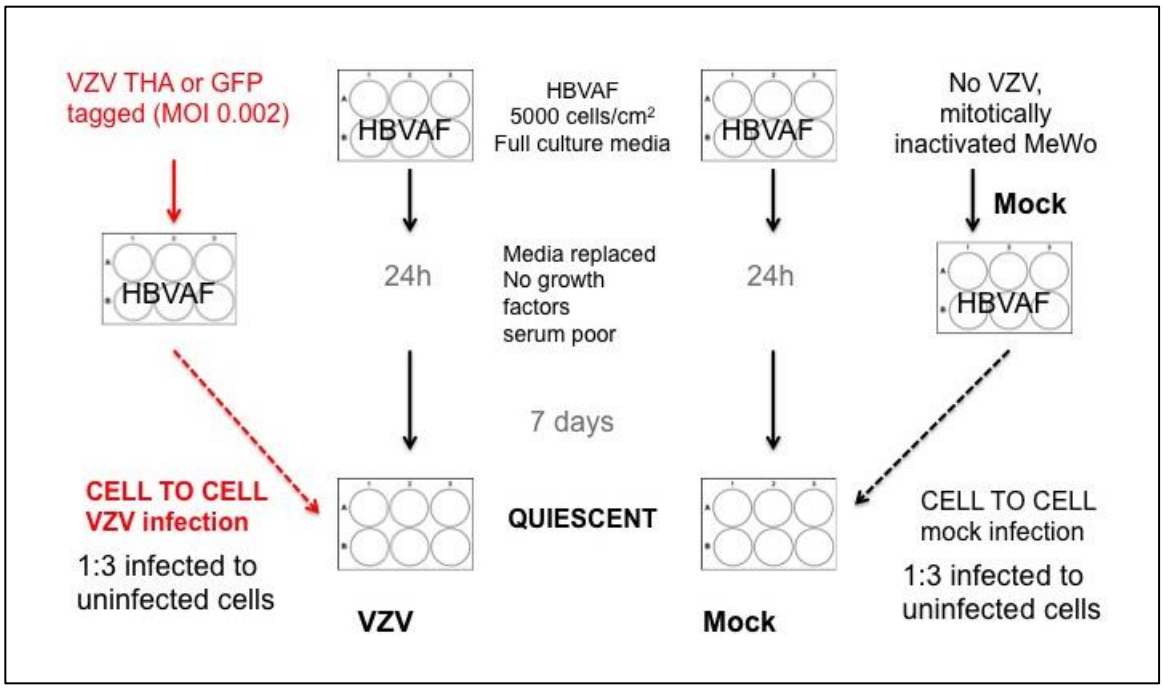

Figure 2.2. Schematic representation of experiments inducing VZV HBVAF cell to cell infection.

Extrapolating from the above ratio and taking into account the extent of CPE/fluorescence observed in the inoculum cells (approximately 40% on day 7 post infection), gives an estimate of 1 infected cell to 7.5 uninfected cells. Prior to infection, cells from 1 well of each condition were detached and counted to ensure ratio accuracy and minimize variation between experiments. The spread of infection and appearance of culture were monitored daily at a microscope and cells harvested at different time points post infection. In addition to observing the CPE, cells were stained with anti-VZV protein antibodies to assess infection efficiency (figure 2.3.).

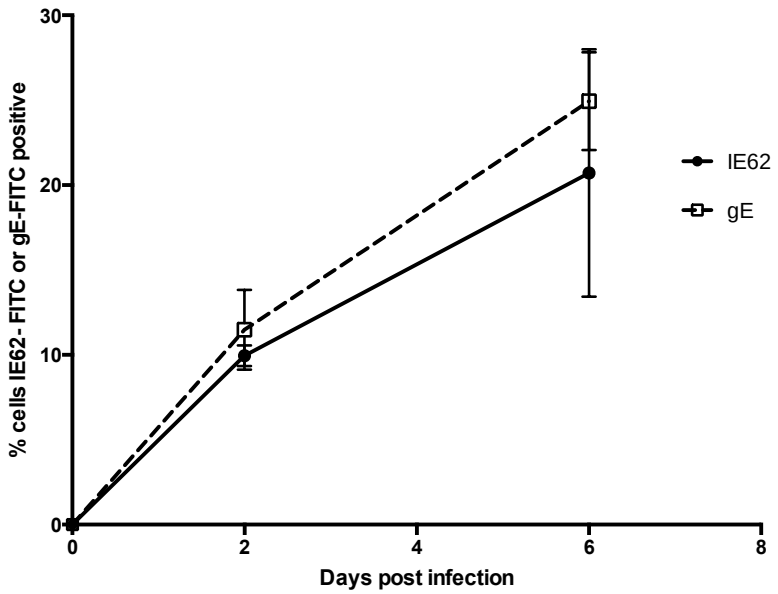

Figure 2.3. Time course of VZV protein expression in VZV infected HBVAF following cell to cell infection.

VZV IE62 and VZV gE protein expression in HBVAF infected cell to cell at a ratio

of 1:3 cells from infected culture to uninfected cells. Samples were stained in parallel with anti -VZV IE62 or anti-VZV gE antibodies at 2 d.p.i. and 6 d.p.i. and analysed by flow cytometry. The percentage of cells expressing VZV IE62 and VZV gE is presented as mean and SEM for n=3 independent experiments.

2.14. Statistical analysis

All vitro experiments were completed in triplicates at least and results are expressed as mean ± SEM. Statistical significance between experimental groups was determined using unpaired Student *t* tests. P-values of less than 0.05 (two sided) were regarded as significant. Statistical analysis was performed using GraphPad Prism (San Diego, CA) version 6.0h. Data are presented using GraphPad Prism (San Diego, CA).

3. Human brain vascular adventitial fibroblast differentiation, proliferation and migration in response to VZV infection

3.1. Summary

Background: Previous studies exploring vascular remodeling mechanisms in a number of vascular disorders have suggested an important role for vascular adventitial fibroblasts. Histological studies outlined in previous chapters have also indicated that cerebrovascular adventitial fibroblasts may also play a key role in vascular remodelling associated with VZV vasculopathy. To date however limited studies have examined the exact changes induced in these cells in response to VZV infection.

Objectives: The aim of this part of my study was to develop an in vitro model of VZV-induced HBVAF infection and study the changes in the proliferation, differentiation and migration of these cells in response to VZV.

Methods: Flow cytometry analysis of α-SMA, a marker of myofibroblast differentiation, and EdU expression, a marker of cell division of VZV-infected HBVAF compared to mock-infected HBVAF. Standard scratch assay was used to assess the migratoy capacity of HBVAF in response to VZV-infection.

Results: A significantly higher number of cells expressed α-SMA and Edu in the HBVAF cultures VZV-infected compared to the cultures mock-infected. A significantly higher number of cells migrated in the marked field in the HBVAF cultures infected by VZV, compared to the cultures mock-infected, as shown by the standard scratch assay.

Conclusions: In this chapter, I show for the first time in a series of *in vitro* experiments that VZV infection promotes HBVAF proliferation, transdifferentiation to myofibroblasts, and enhances their migratory capacity. Taken together, these findings provide insight into the mechanisms of vascular remodeling in the context of VZV related arteriopathy.

3.2. Introduction

3.2.1 Adventitial vascular fibroblast as regulators of vascular wall structure and function

The outermost layer of the arterial wall, the adventitia, exerts roles as an extracellular matrix (ECM) rich generator. The adventia is also a component of the vascular wall that contains conduits for nutrient supply and removal, the vasa

vasorum in addition to containing endothelial cells and pericytes, lymphatic vessels, trophic nerves, resident cells (mainly fibroblasts) but also immunomodulatory cells (dendritic and macrophages) and progenitor cells (Pugliese et al, 2015). It is recognized that the vascular adventitia is, indeed, the most heterogeneous layer of the vascular wall.

Previous studies in other vascular conditions have shown that the adventitia responds to pathological changes in the microenvironment by initiating a cascade of processes leading to vascular remodeling. In humans and animal models of pulmonary hypertension (PH), in response to hypoxia, the adventitia undergoes substantial thickening due to a remarkable increase in collagen and ECM protein deposition, expansion of the vasa vasorum, proliferation of resident fibroblasts, as well as recruitment of circulating immune and progenitor cells (Pugliese et al, 2015; Mitzner et al, 2014). The highly proliferatory phenotype of the adventitial vascular fibroblasts in PH has prompted associations with cancer pathology due to similarities in the abnormal cell growth that favors the emergence of an apoptosis-resistant phenotype (Mc Murtry et al, 2005).

Growing experimental evidence now suggests that, in response to vascular stresses, including hypoxia and mechanical stress, the adventitial vascular fibroblast is the first cell in the adventitia to become activated. Cells subsequently release molecules that can directly affect nearby smooth muscle cells tone and growth, cause upregulation of contractile and ECM proteins, as well as lead to enhancement of recruitment of inflammatory cells (Wilcox et al, 2001; Li et al,

2011). These studies have also provided evidence that hypoxia induced changes in adventitial fibroblasts lock these into an activated phenotype and perpetuate chronic vascular inflammation most likely through epigenetic mechanisms (Li et al, 2011; Wang et al, 2014; El Kasmi et al, 2014).

In turn these activated fibroblasts have either direct or indirect effects on the overall vascular function and structure and this mediated by the secretion of a variety of cytokines, chemokines, growth factors, and proteins (Stenmark et al, 2013). Several signaling pathways have been suggested as important regulators of hypoxia-induced proliferation of adventitial fibroblasts in PH. These include activation of Gαi and Gαq family members, perhaps in a ligand-independent fashion, with subsequent stimulation of PKC and mitogen-activated protein (MAP) kinase family members, as well as activation of PI3K, and synergistic interaction with Akt, mTOR, and p70 ribosomal protein S6 kinase (Stenmark et al, 2013).

Another appealing aspect of the model of vascular remodeling of PH is the marked increase in the numbers of myofibroblasts observed the adventitia not only in the model of hypoxia-induced PH, but also in other vasculopathies (Wilcox et al, 2011). These myofibroblasts originate from activation and differentiation of fibroblasts in response to a variety of stimuli. Myofibroblasts are usually identified by expression of α-SMA not present in undifferentiated fibroblasts. Myofibroblasts have been shown to be implicated in tissue remodeling due to their ability to perform multiple physiologic functions in

response to change in the local environment. Some of these functions include: production of collagen and other extracellular matrix proteins (elastin, fibronectin), as well as matricellular proteins including tenascin-C and osteopontin; and production of a variety of growth factors, cytokines, and reactive oxygen species that have paracrine effects on the nearby cells (Stenmark et al, 2013). Myofibroblasts also exhibit marked contractile effects.

In summary, the current growing body of experimental data mainly in relation to PH demonstrates that the adventitia acts as a key regulator of vascular wall function and structure in an "outside-in" manner. Resident adventitial fibroblasts have been shown to be the first cellular target to be activated and reprogrammed ultimately influencing the constitution of the arterial wall, initiating and perpetuating chronic vascular inflammation.

Given that the previous literature on the histology of VZV infected arteries from affected humans also suggests that there are similar vascular remodeling processes contributing to the cerebral arteriopathy, it is possible that VZV infection of adventitial cells might lead to cerebrovascular wall remodeling in a similar manner.

3.3. Aims

In this chapter the hypothesis that VZV is capable of directly infecting HBVAF and inducing changes to the HBVAF phenotype such as increased differentiation, proliferation and enhanced migratory capacity, was investigated.

3.4. Methods

3.4.1. Fluorescent activated cell sorting for HBVAF differentiation and proliferation

3.4.1.1. Surface and intracellular marker identification

To analyse HBVAF for expression of VZV gE/gH surface proteins and VZV IE62 or α-SMA intracellular proteins, quiescent HBVAF (plated in 12-well plates) were harvested by trypsinisation, transferred to Eppendorf tubes, washed in PBS 500 µL/well and pelleted by centrifugation at 3500g for 3 minutes. The supernatant was removed, the cell pellet dislodged and incubated for 5 minutes at room temperature in 1% BSA in PBS. The cells were pelleted by centrifugation at 3500g for 3 minutes, supernatant removed, and the unconjugated antibodies to the surface markers were added at the respective dilutions (listed in table 2-2) in 1% BSA in PBS 50 µL per tube. The cells were incubated with the primary antibodies for 20 minutes at room temperature in the shaker. At the end of the incubation the cells were washed in 1% BSA in PBS as described above, and the secondary antibodies were added in 1% BSA in PBS 50 µL/tube (dilutions listed in table 2-3) and incubated for 20 minutes at room temperature, in a shaker, protected from light. The cells were washed twice in 1%BSA in PBS and fixed by

incubating with 4% Paraformaldehyde 100 uL/tube for 15 minutes at room temperature. The cells were washed in 1% BSA in PBS and incubated for 15 minutes at room temperature, protected from light, in 100 uL/tube permeabilisation solution (1:10 dilution in 1% BSA in PBS; Invitrogen). The antibodies to intracellular molecules (VZV IE62, unconjugated or conjugated antibody to alpha-SMA) were added to the permeabilisation solution at relevant dilutions (listed in table 2-2) and incubated for 20 minutes at room temperature. The cells were washed in the permeabilisation and wash reagent and the secondary antibodies were added at relevant dilutions in permeabilisation and wash reagent, 50 µL/tube, and incubated at room temperature for 20 minutes. The cells were washed twice in permeabilisation and wash reagent, pelleted by centrifugation, and further steps completed for the proliferation assay prior to fixation in 500 µL/tube CellFix (BD; 10x concentrate diluted in deionized water) and flow cytometric analysis.

3.4.1.2. Proliferation assay

Cell proliferation in response to VZV infection was assessed with flow cytometry using Click-iT Plus EdU flow cytometry assay kit Alexa Fluor 647 picolyl azide (Invitrogen). EdU is a nucleoside analog to thymidine and is incorporated into DNA during active DNA synthesis. Detection is based on a click reaction a copper catalyzed covalent reaction between an azide and an alkyne. In this application, the alkyne is found in EdU, while the azide is coupled to Alexa Fluor® 647 dye. Standard flow cytometry methods are used for determining the

percentage of proliferating cells in the population. The EdU assay allows for detection of the incorporated EdU using mild conditions without requiring DNA denaturation, and was multiplexed with intracellular and surface staining as described in the above subsection.

The cells were stimulated with full media and labeled with 1 µL/well of EdU solution (prepared by adding 20 mg EdU to 8 mL PBS) 16 hours and 2 hours prior to harvesting the cells, respectively. It is recommended that the length of the incubation time with EdU and incubation conditions are decided subject to the cell type, growth rate and proliferation parameters of interest. In this case, I was interested in the population of highly proliferative cells, and therefore a shorter stimulation period with full medium was desired. The 2 hours incubation time with EdU was determined after optimization experiments, where I compared the detection rate of proliferating cells using 2 hours or 4 hours incubation time. There was no significant increase in the detection rate of proliferating cells, and therefore I selected the 2 hour incubation time (Figure 3.1.).

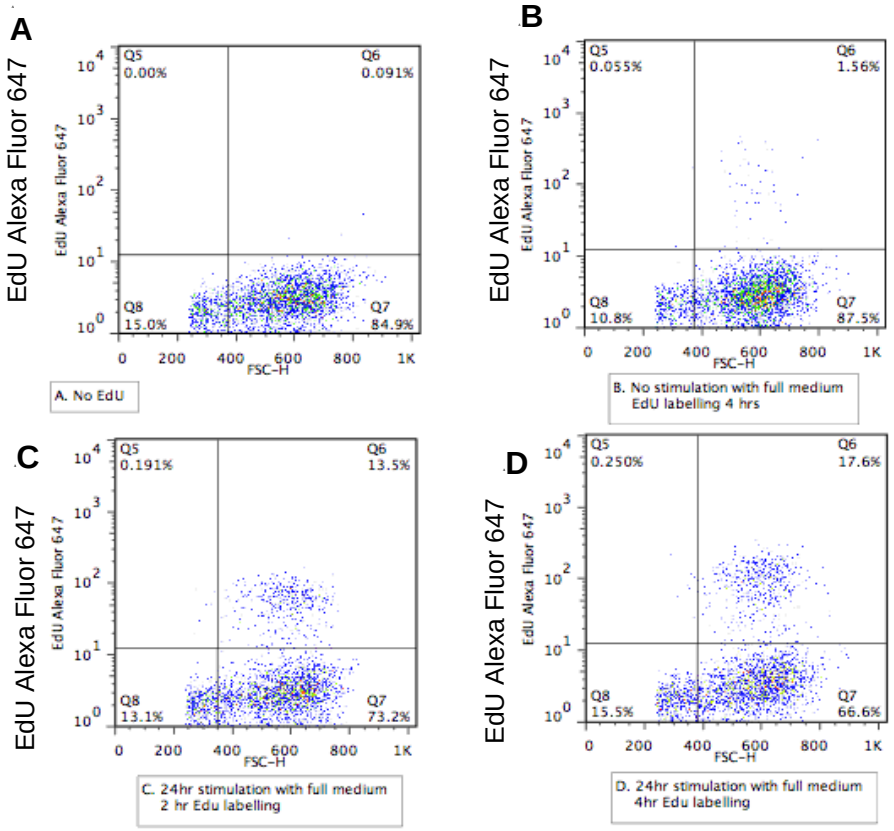

Figure 3.1. Flow cytometric plots for detection of proliferating HBVAF using Click-iT Plus EdU flow cytometry assay.

*Figure **(A)** shows quiescent unstained HBVAF. Figure **(B)** shows minimal proliferation in the quiescent population not stimulated with full media. There was increased proliferation rate for quiescent HBVAF stimulated with full media for 24 hours and labeled with EdU 2 hours **(C)** prior to harvest. There was no significant increase in the detection rate of proliferating cells when increasing the incubation time with EdU to 4 hours **(D).***

Further to staining for the VZV proteins and α-SMA, the cells were washed twice, permeabilised by adding 100 µL/tube saponin-based permeabilisation reagent, 200 µL/tube of EdU reaction cocktail added and mixed well. The samples were incubated with the reaction cocktail for 30 minutes at room temperature, washed, and fixed in 500 µL CellFix (BD) per sample prior to flow cytometric analysis.

The EdU reaction cocktail was prepared as per manufacturer's instructions, including: PBS, copper protectant, fluorescent dye picolyl azide and buffer additive.

3.4.1.3. Flow cytometry data analysis

Flow cytometric data were collected on a FACS Calibur flow cytometer. $10x10^3$ events were collected for each condition and cells gated based on their forward scatter properties. A representative set of flow cytometric plots, and the gating strategy are shown in figure 3.2. Unstained samples were used to identify positivity, and samples stained with only secondary antibodies were used as negative controls. Data were analysed using FlowJo (Treestar Inc, Ashland, OR).

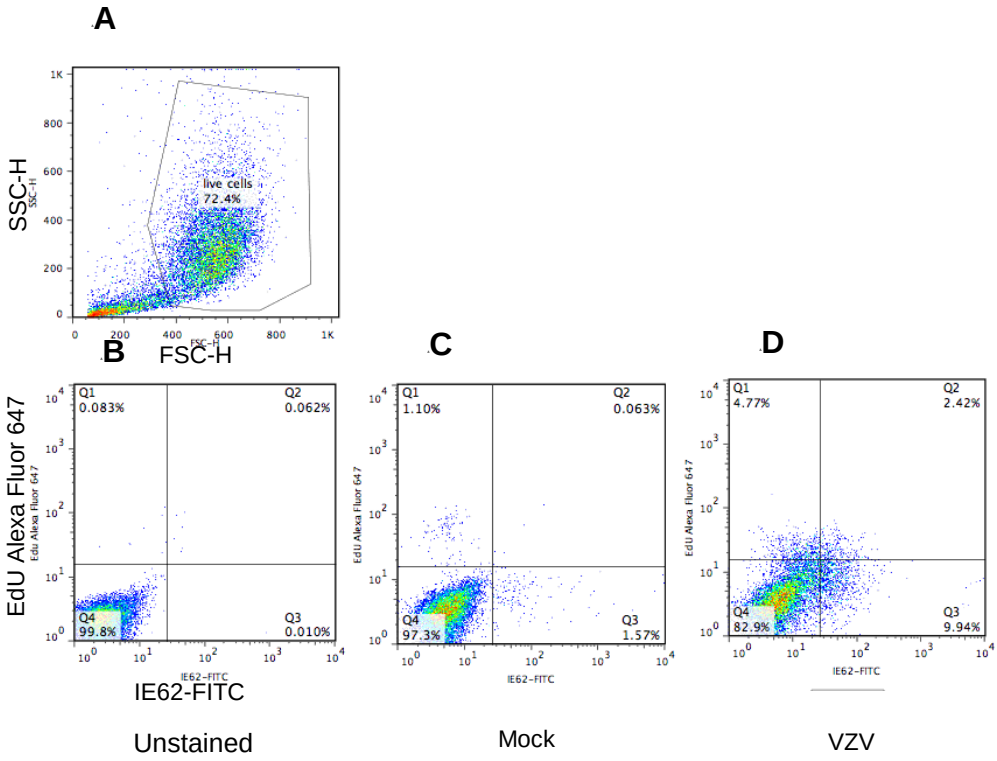

Figure 3.2. Flow cytometry for EdU and VZV IE 62 detection in HBVAF. *HBVAF were stained for EdU Alexa Fluor 647 and VZV IE62-FITC. The live cells were gated initially on their FSC and SSC characteristics* ***(A).*** *Unstained samples were used to identify positivity for EdU or IE62-FITC* ***(B).*** *Cells positive for EdU Alexa Fluor 647 and/or VZV IE62 were then identified in mock infected and VZV-infected HBVAF (****C,D*** *respectively).*

3.4.2. Scratch assay

A number of assays are used to investigate cell migration including: *in vitro* scratch assay, transwell assay, electric cell impedance sensing, and a microfluidics-based system assay. The in vitro scratch assay is probably the simplest method: it is inexpensive, and mimics to some extent the cell migration *in vivo*. It also has the advantage of being particularly suitable for microscopy, live imaging and study of the regulation of migration by cell-cell interaction (Liang et al. 2007).

HBVAF migratory capacity was assessed using the scratch assay method, following published methods in Nature Protocols by Liang and colleagues (Liang et al. 2007).

In summary, the method involved generating a scratch in a cell monolayer with a pipette tip, recording images at the start and at regular intervals during cell migration to close the scratch, and quantifying the migration rate of the cells by comparing the images.

The assay was performed in 12-well plate using quiescent HBVAF mock-infected or VZV infected at approximately 80% confluence. Additional wells with quiescent HBVAF were treated with TGF-beta (5ng/mL; Peprotech) and used as a positive control. Prior to performing the scratch, the cells were treated with mitomycin C (0.01 mg/ml for 2 hours) to inhibit mitosis of the cells and allow us to distinguish migration from proliferation (Di J et al, 2015).

In brief, the media was removed, and the external surface of the bottom of the well was etched with a razor blade with the aid of a ruler, creating 3 parallel symmetric horizontal lines – to produce reference marks so that the same field is obtained when acquiring the images.

The cell monolayer was scraped using a P200 sterile pipette tip in a vertical line which meets the external horizontal marks at the center of the well. It is important to produce scratches of approximately same width between control and the assessed population, to minimize any possible variation in results due to the different size of the scratches. It is particularly important to achieve smooth edges of the scratch and this can be generally achieved by increasing the speed of scraping. In addition, in the case of fibroblasts which are cells that start growing in layers when reaching full confluence, ideally the scratch is performed when the cells are close to confluence but not overcrowded. Moreover, for the VZV infected wells, it is important that the CPE is not severe when the scratch is completed because unscratched parts of the cell monolayer would detach. With this in mind, after optimization experiments I chose to perform the scratch assay at 2 days post infection (at the infection ratio I used, CPE not severe), based on literature showing that the expression of α-SMA in TGF-beta stimulated fibroblasts peaks at 72 hours post treatment (Grotendorst et al. 2014), therefore the cells differentiated to myofibroblasts would possess migratory activity. I also based this decision on my own results of differentiation experiments shown in a later section of this thesis.

Following the scratch, the wells were gently washed twice in 1 mL PBS to remove cell debris and smoothen the edges of the scratch, fresh media supplemented with 0.1% FBS and antibiotics added (not full media, to minimize proliferation). Baseline photos of the marked field were taken and the plate moved to a 37^0C incubator and examined periodically.

The length of the incubation time for the scratch assay was determined empirically for the cell type used. Generally, the time frame for incubation should be selected to allow the population under the quickest migration condition to just reach the complete closure of the area. In my experiments, the migration rate was extremely low in the first 12 hours, and complete closure was achieved at approximately 36-40 hours.

During the incubation, the plate was taken under a phase-contrast microscope, a reference point aligned and subsequent images of the same fields as baseline taken. Migration was quantified by counting the cells that crossed into the scratch area from the reference point defined at baseline.

3.5. Results

3.5.1. HBVAF are permissive to Varicella zoster virus infection *in vitro*

No animal model exists for stroke caused by VZV vasculopathy, therefore in this study I have used primary human cerebrovascular cells i.e. HBVAF to infect with VZV.

First, I needed to confirm the ability of VZV to infect HBVAF in my *in vitro* model. Since VZV is highly cell associated, and cell free virus difficult to produce, I infected HBVAF cultures with MeWo cells infected with either VZV (strain THA) or GFP- expressing VZV. MeWo cells were treated with mitomycin C to block cell division before using them to infect HBVAF cultures (Markus et al. 2011). This approach prevented MeWo cells from overgrowing the HBVAF and still allowed efficient cell-mediated viral infection of the cells of interest. Quiescent HBVAF were then co-cultured with VZV-infected fibroblasts as per above.

As mentioned earlier in this thesis, CPE refers to the morphological changes in the host cell resulting from viral invasion. Not all viruses are cytopathogenic; however, VZV has been shown to produce CPE in various permissive cells (Grose et al. 1979; Harper et al. 1998).

The culture dishes with VZV infected cells were observed every 1-2 days on an inverted microscope and fluorescence microscope (Figure 3.3.) in parallel with control mock-infected cultures, to document the presence, degree and extent of CPE and fluorescence. Healthy HBVAF are flat, adherent, spindle-shaped cells. In response to VZV infection, the appearance of the monolayer changed, with

foci of HBVAF characterized by alteration of the cell shape specifically rounding. CPE was present in HBVAF infected with VZV as early as day 2 post infection (p.i.) at the MOI 0.002 or cell to cell ratio used, and extended gradually in a concentric manner from the initial foci. Such changes were not present in mock infected cultures.

At high MOI the CPE involved destruction of the cell monolayer, with cells detaching from the culture vessel surface (figure 3.3). Similar results were observed in separate experiments using GFP tagged VZV too.

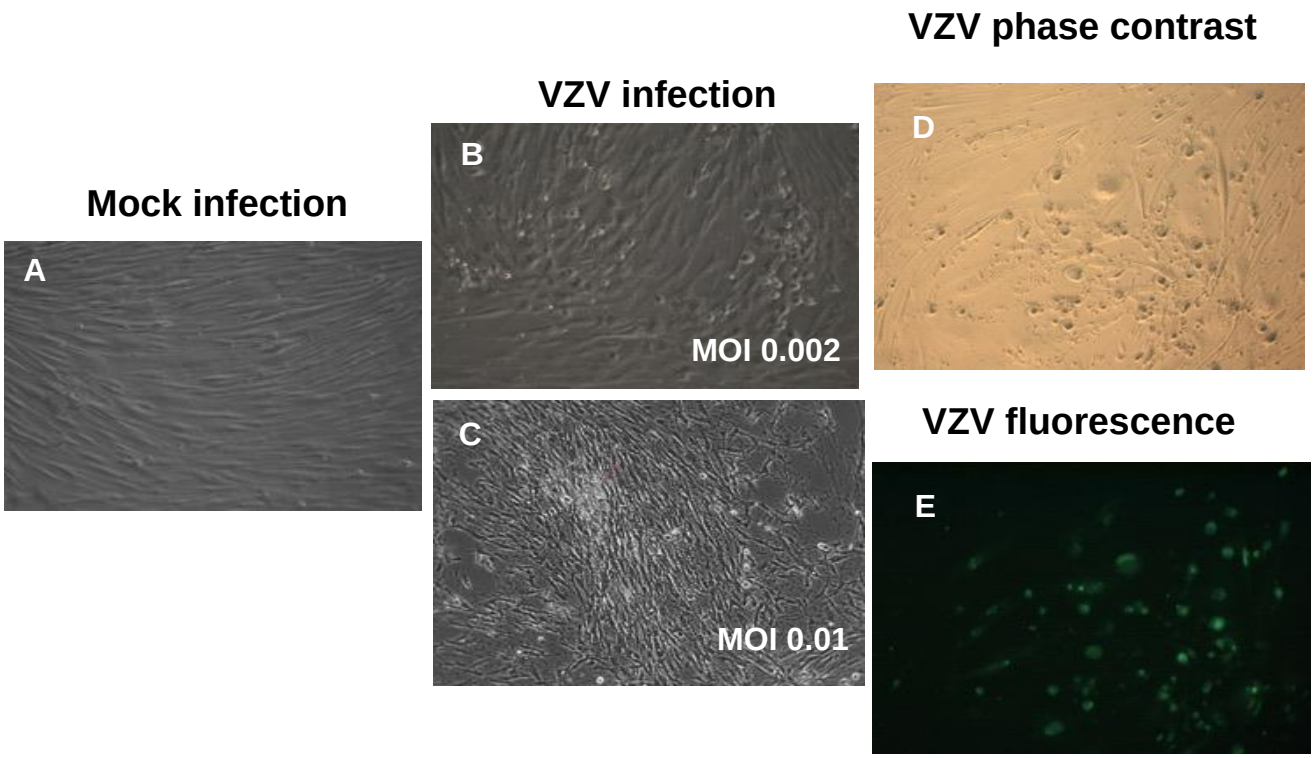

Figure 3.3. HBVAF are susceptible to infection by VZV in vitro. *Phase contrast microscopy images (100x magnification) of human brain vascular adventitial fibroblasts (HBVAF) inoculated with VZV-infected THA strain or mock-infected.* ***(A).*** *Mock infection on day 3 post infection (d.p.i.). show no cytopathic effect (CPE)* ***(B)*** *CPE in VZV infected*

HBVAF at a multiplicity of infection (MOI) 0.002, day 3 p.i. ***(C)*** *Severe cytopathic effect with cell lysis and destruction of the monolayer present 2 d.p.i. in VZV-infected HBVAF at MOI 0.01.* ***(D,E)*** *Phase contrast and fluorescence microscopy images (200x magnification) of HBVAF co-cultured with VZV GFP ORF23 infected HBVAF at a ratio of 1:3 infected to uninfected cells, obtained on day 6 post infection. Figure D. shows morphological changes of infection in phase contrast microscopy, and Figure E. shows in the same field green fluorescence representing GFP ORF 23 tagged infected HBVAF.*

Next, I looked at VZV related protein expression (IE62, gH, GFP ORF23) using flow cytometry. At 48 hours post cell to cell infection, a mean of 9.95% (SEM 0.43%) and 11.42% (SEM 1.66%) of VZV-infected HBVAF expressed VZV IE62 protein (immediate-early protein) and VZV gH protein (late protein), respectively (n=3 experiments). At 6 days post infection, 20.71% (SEM 5.15%) of VZV-infected HBVAF expressed VZV IE62 protein, 24.94% (SEM 2.03%) expressed VZV gH protein (Figure 3.4, n=3 experiments). No expression of VZV proteins was detected in mock-infected HBVAF. These data provide further confirmatory evidence that HBVAF are permissive to VZV infection *in vitro.*

I was also interested to examine whether the detection of cells expressing VZV gH proteins correlates well with the detection of VZV GFP ORF23 using flow cytometry, as in my experiments I have used both these methods to identify the infected cells. A good correlation between the detection rate of infected cells using VZV gH and VZV GFP ORF23 expression was identified (Figure 3.4)

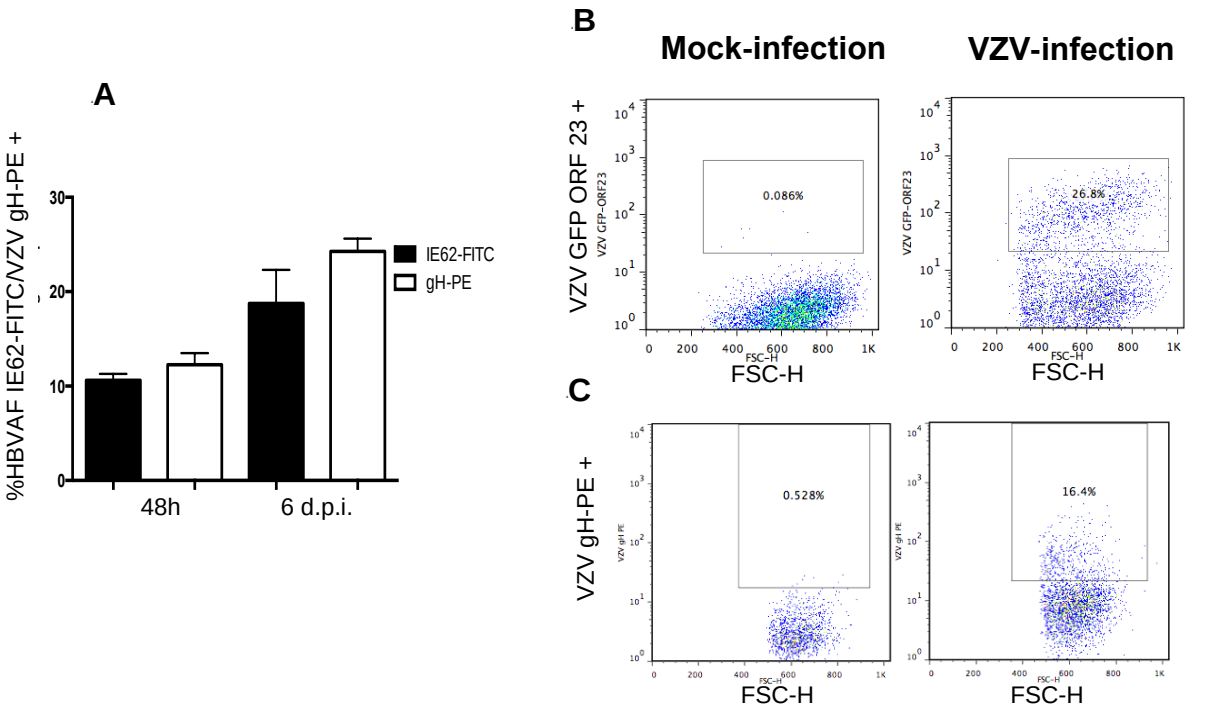

Figure 3.4. Flow cytometric analysis of GFP VZV ORF23, VZV gH and VZV IE62 protein expression on VZV-infected HBVAF. (A) *Infection efficiency in VZV cell to cell viral propagation in HBVAF. VZV IE62 and VZV gH protein expression in HBVAF infected cell to cell at a ratio of 1:3 cells infected to uninfected cells. Samples were stained in parallel with anti-VZV IE62 (immediate early viral protein) or anti-VZV gH (late viral protein) antibodies at 48h .p.i. and 6 d.p.i. . The percentage of cells expressing VZV IE62 and VZV gH (shown as mean and SEM; n=3) was analysed by flow cytometry. At 48 hours post cell to cell infection, a mean of 9.95% (SEM 0.43%) and 11.42% (SEM 1.66%) of VZV-infected HBVAF expressed VZV IE62 protein and VZV gH protein, respectively (n=3 experiments). At 6 days post infection, 20.71% (SEM 5.15%) of VZV infected HBVAF expressed VZV IE62 protein, 24.94% (SEM 2.03%) expressed*

*VZV gH protein **(B,C)** Representative flow cytometric plot of GFP ORF23 (B) and VZV gH protein expression (C) in mock-infected and VZV-infected on day 6 post infection. In the VZV-infected population, 28.86% of HBVAF express gH protein, and 35.7% express GFP ORF23, demonstrating a good correlation between the detection rate of infected cells using VZV gH and VZV GFP ORF23 expression.*

3.5.2. HBVAF activation and differentiation in response to VZV infection

In order to confirm my hypothesis that resident cerebrovascular fibroblasts in response to VZV infection differentiate into myofibroblasts and therefore may be the source of myofibroblast induced changes seen on histology of VZV infected arteries in humans (Nagel et al. 2013), I then studied the potential of VZV to activate HBVAF and induce myofibrolast differentiation.

The fibroblasts present within the ECM of the connective tissue of vascular adventitia constitutively express vimentin and fibroblast- specific protein 1, however no fibroblast specific marker has been identified as yet. In response to a variety of stimuli generated when tissue injury occurs, normal fibroblast can acquire an activated phenotype and differentiate into myofibroblasts. Myofibroblasts are a form of fibroblastic cells that have differentiated partially towards a smooth muscle phenotype, and possess contractile and migratory activity by using in particular alpha-smooth muscle actin, a cytoskeletal protein found in smooth muscle cells (Hinz et al. 2007).

A-smooth muscle actin is a widely used as a marker of myofibroblasts. Alpha-smooth muscle actin expression in VZV- and mock-infected HBVAF was therefore investigated by flow cytometry.

There was a significant fold percentage increase detected in HBVAF expressing α-SMA following VZV infection compared to mock infection, 9.79 fold (SEM 2.80 fold) and 19.53 fold (SEM 3.38 fold) for VZV-infected, compared with 1.24 fold change (SEM 0.56 fold) and 8.24 fold (SEM 1.37 fold) in mock-infected cells, $p=0.04$ and $p=0.03$ at 48 hours and 6 d.p.i. respectively (Figure 3.5). Fold increase in the percentage of α-SMA positive cells was calculated compared to resting quiescent fibroblast expression analysed on the day of infection, and was expressed as mean and SEM for n=3 independent experiments.

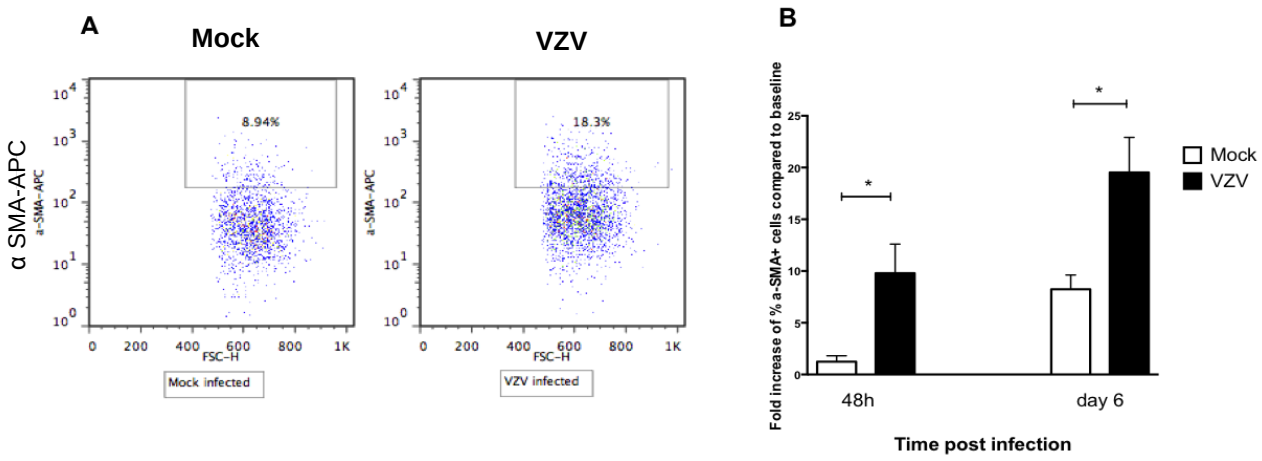

Figure 3.5. VZV induces HBVAF differentiation to myofibroblasts. (A) *Representative flow cytometry plots demonstrating expression of α-SMA in mock and VZV-infected cells on day 6 post infection.* ***(B)*** *Detection of α-SMA in HBVAF infected by VZV presented as fold increase in the percentage of α-SMA positive cells for mock infected and VZV-infected cultures compared to resting baseline expression on HBVAF. The VZV-infected cultures exhibited significantly higher increase in the percentage of cells expressing α-SMA suggesting myofibroblast differentiation of these cells compared to mock-infected cells, at 2 days post infection (p=0.04) and 6 days post infection (p=0.03), n=3 experiments. Unpaired t test; *P<0.05, **P< 0.001, ***P< 0.001.*

Two subsets were identified in terms of α-SMA in the VZV-infected HBVAF: one subset co-expressing VZV proteins and α-SMA, and one subset of cells expressing α-SMA but not VZV proteins (figure 3.6). Even when taken individually, the latter percentage was higher than the total percentage of α-SMA+ in the mock-infected cultures.

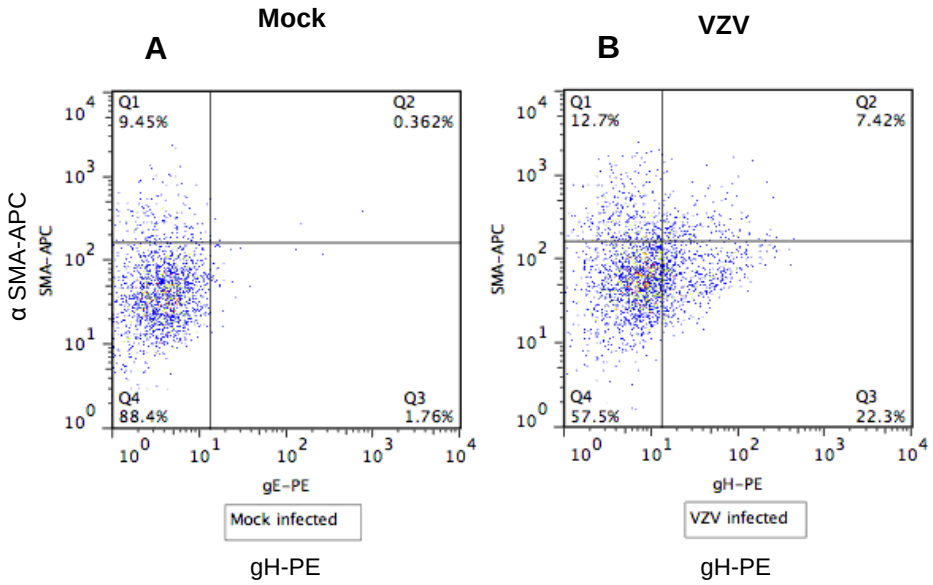

Figure 3.6. Co-staining of HBVAF for detection of α-SMA and VZV gE proteins. *Representative flow cytometry plots demonstrating co-expression of α-SMA and VZV gH in VZV-infected HBVAF on day 6 post infection.*

3.5.3. HBVAF proliferation in response to VZV infection

The proliferative responses of HBVAF were assessed using EDU expression by flow cytometry. VZV infection also enhanced the proliferative potential of HBVAF in vitro as assessed using EDU expression.

There was a significant increase in the percentage of EdU+ cells observed in VZV-infected cultures compared to mock-infected cultures expressed as fold change in relation to resting quiescent HBVAF EdU expression: 18.38 fold (SEM 3.22 fold) and 25.38 fold (SEM 3.37 fold) in VZV-infected cultures, compared with 1.72 fold (SEM 0.35 fold) and 3.31 fold (SEM 0.09 fold) in mock-infected cultures (p=0.03 and p=0.01) at 48 hours and 6 d.p.i., respectively, (Figure 3.7).

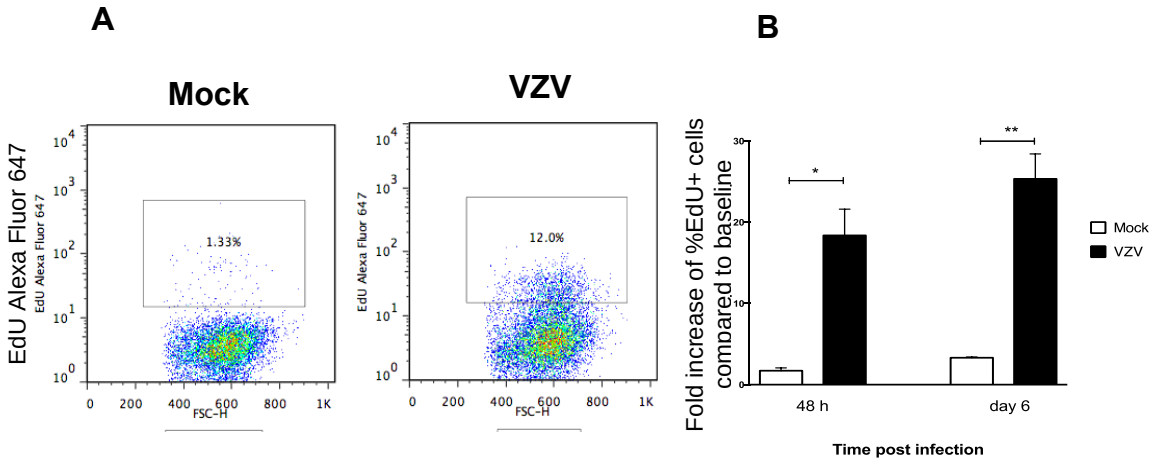

Figure 3.7. VZV infection enhances HBVAF proliferation (A) *Representative flow cytometric plots demonstrating expression of EdU in mock- and VZV-infected cells at 48 hours post infection* ***(B)*** *Detection of EdU in HBVAF infected by VZV presented as fold increase in the percentage of EdU positive cells for mock-infected and VZV-infected populations compared to compared to resting quiescent fibroblasts analysed on the day of infection. The VZV-infected cultures exhibited significantly higher increase in the percentage of proliferating cells compared to mock-infected cultures: 18.38 fold (SEM 3.22 fold) and 25.38 fold*

*(SEM 3.37 fold) in VZV-infected cultures, compared with 1.72 fold (SEM 0.35 fold) and 3.31 fold (SEM 0.09 fold) in mock-infected cultures (p=0.03 and p=0.01, unpaired t test) at 48 hours and 6 d.p.i., respectively (n=3 experiments). *P<0.05, **P< 0.001, ***P< 0.001.*

Similarly to the findings with regards to the α-SMA, two subsets were also identified in terms of and EdU expression in the VZV-infected HBVAF: one subset co-expressing VZV proteins and EdU, and one larger subset of cells expressing a-SMA or EdU but not VZV proteins (figure 3.2. C,D) .

3.5.4. Migratory capacity of human brain adventitial fibroblasts in response to Varicella zoster virus infection

Next, I explored whether the migratory capacity of HBVAF had changed in response to VZV infection, using the standard scratch assay.

Scratch assay was performed on culture monolayers of mock-infected and VZV-infected HBVAF on day 2 post infection. Cells treated with TGF-β were used as positive control. The number of cells which migrated into the scratch area from the reference marks at baseline was quantified at 17 hours post scratch. Increased cell migration into the marked field was observed in the HBVAF cultures VZV-infected compared to mock-infected (Figure 3.8): a mean of 136.70 (SEM 21.47) cells migrated into the marked area in the VZV-infected cultures,

compared to 48.33 cells (SEM 7.12) in the mock-infected cultures (n=3 experiments, p=0.01,). These results showed that in response to VZV-infection, the HBVAF acquire increased migratory capacity. This is in keeping with the previous results which demonstrated enhanced differentiation in the VZV-infected populations. As discussed earlier in this thesis, the presence of α-SMA confers to the fibroblast increased contractile function, therefore increased migration capacity.

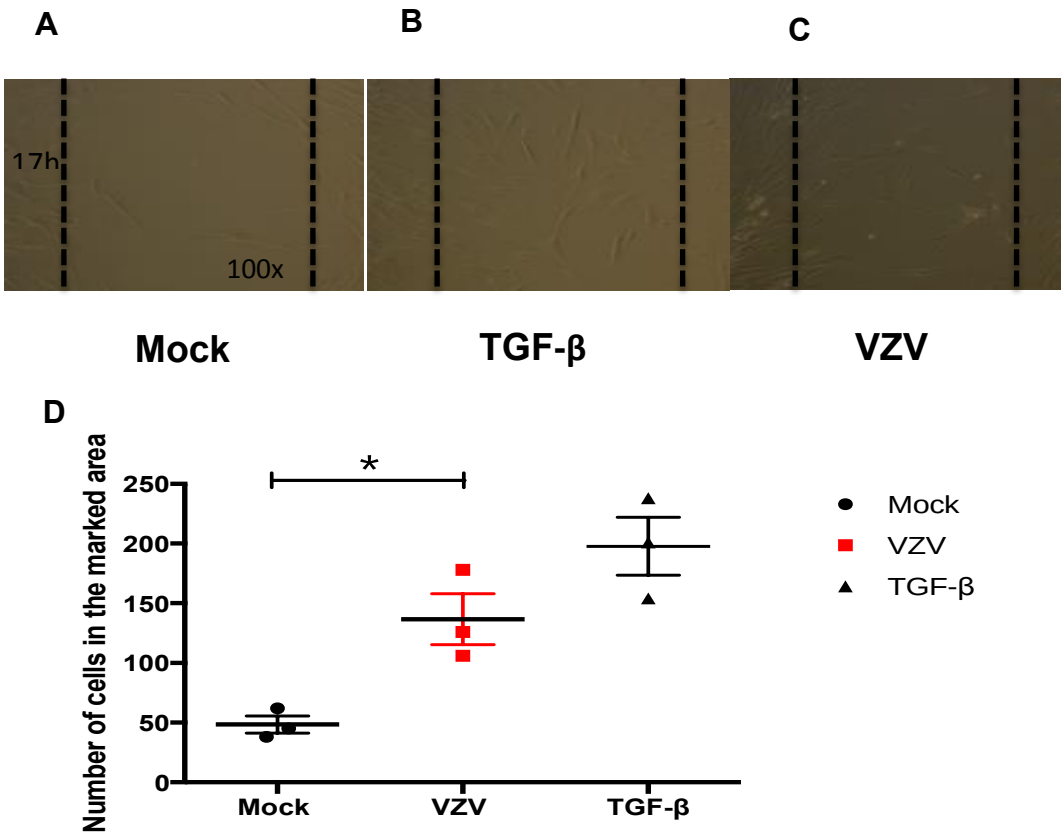

Figure 3.8. Migratory potential of HBVAF in response to VZV infection. *A scratch assay was performed on culture monolayers of mock-infecte.* ***(A)*** *and VZV-infected HBVAF* ***(C)*** *on day 2 post infection. Cells treated with TGF-β were used as positive control* ***(B).*** *The number of cells which migrated into the scratch area from the reference marks at baseline was quantified at 17 hours post scratch. Increased cell migration into the marked area was observed in the HBVAF cultures VZV-infected compared to mock-infected culture.* ***(D)*** *A mean of 136.70 (SEM 21.47) cells migrated into the marked area in the VZV-infected cultures, compared to 48.33 cells (SEM 7.12) in the mock-infected cultures (n=3 experiments, p=0.01). Unpaired t test. *P<0.05, **P< 0.001, ***P< 0.001.*

3.6. Discussion

I was able to show that HBVAF are permissive to VZV infection *in vitro*, and following infection a number of changes in HBVAF were observed. At the start of this project, only a single conference abstract had reported work on VZV-infected HBVAF. While my studies were ongoing, Nagel et al. published on some additional work on HBVAF in two studies (Nagel et al. 2015; Nagel et al. 2014). My results now also confirm the susceptibility of HBVAF to VZV infection.

My work suggests for the first time that VZV can trigger changes in HBVAF that could be of relevance to vascular remodeling: increased HBVAF proliferation, cellular activation and differentiation to myofibroblasts, and increased migratory activity. There was a significant difference between the number of proliferating cells and cells expressing α-SMA in the population infected with VZV, compared to mock infection. Interestingly, two subsets were identified in terms of α-SMA and EdU expression in the VZV-infected HBVAF: one subset co-expressing VZV proteins and α-SMA or EdU, and one larger subset of cells expressing α-SMA or EdU but not VZV proteins. This indicates two subgroups of cells in the infected population: one subgroup of HBVAF VZV-infected and differentiated to myofibroblasts or proliferating cells, and one larger subgroup of uninfected cells which were activated and differentiate to myofibroblasts or have increased proliferation. This possibly reflects an alteration in the differentiation and proliferation behavior of nearby uninfected cells through paracrine effects from VZV-infected cells.

A number of studies on arterial hypertension have indicated a role for fibroblasts in vascular remodeling processes. Adventitial fibroblasts have been shown to proliferate (Arribas et al. 1997; Das et al. 2000; Chatelain et al. 1988), and some differentiate towards myofibroblasts (Chatelain et al. 1988). Activated fibroblasts have been found in the neointima of injury-induced lesions (Siow et al. 2003; Shi et al. 1996), suggesting migration of fibroblasts from the adventitia towards the lumen. The findings of the migration experiments described here also show that cells in the VZV-infected population migrated at a higher rate than mock-infected cells. This is in keeping with the experiments of cell differentiation that also showed a higher rate of differentiated cells (hence capable to migrate) in the VZV-infected population compared to mock-infected cells.

In conclusion, the results of this chapter support a possible “outside in” model of cerebral arteriopathy in response to VZV infection. VZV infection promotes HBVAF differentiation into myofibrolasts, and contributes to enhancement of their migratory capability. Myofibroblast accumulation can directly contribute to changes in the tone and structure of the vessel wall under pathophysiologic conditions (Das et al, 2002). In addition, myofibroblasts could also migrate and accumulate in the media and intima thus further enhancing the vascular pathologic remodeling in the context of VZV vasculopathy. These changes could lead to occlusion of blood flow and ischaemic stroke.

A limitation of this model arises from the fact that it is an *in vitro* and not *in vivo* model. Numerous efforts have been made to develop adequate animal models of VZV infection, but these models remain limited (Haberthur et al, 2013). The rhesus macaque model of Simian varicella virus infection recapitulates key clinical and virological features of VZV infection, however reactivation has not yet been experimentally induced in the rhesus macaque model (Haberthur et al, 2013).

Also, background cellular changes and positive selection of adherent cells that survive are also potential limitations of my *in vitro* findings. In addition, an important question yet to be answered is what the therapeutic implications of these findings could be, and the relevant clinic impact, especially in terms of possible prevention or regression of the vascular changes shown.

Taken in the context of the past histological studies of VZV-infected brain arteries my data now support the previously speculated important role of brain adventitial fibroblasts as a portal of entry for VZV. These processes could contribute to arterial remodeling, and the remaining work of this thesis concentrated on investigating the potential mechanism for the pathogenesis of VZV cerebral arteriopathy. It is important to add that despite by best efforts, I have not been able to obtain and use human brain arteries from paediatric or adult patients with VZV vasculopathy. BRAIN UK is a network of National Health System and academic centres working together to provide CNS tissue for research. BRAIN UK provides a matching service for researchers requiring human tissue from

disorders affecting the brain and neuromuscular system. No relevant tissue from adults or children was found in the BRAIN UK brain bank following my application, and no brain arteries from children with VZV related arteriopathy were found in the Histopathology department at GOSH.

4. Microparticles and their role in Varicella zoster virus vasculopathy

4.1. Summary

Background: Previous studies in several vascular disorders have shown that fibroblast activation in response to mechanical stretch or hypoxia upregulates chemokine production and triggers inflammatory pathways *in vitro*, contributing to vascular remodeling (Lindner et al. 2014; Stenmark et al. 2006; Stenmark et al. 2006). The interplay between various cell types occurs either through direct cell contact (gap junctions or adhesion molecules) or via paracrine and autocrine effect (Stastna et al, 2012). Microparticles (MP) are membrane vesicles rich in phosphatidylserine, with important functions in intercellular communication, and have been shown to be elevated in a number of vascular disorders including systemic vasculitis and paediatric AIS (Hong et al, 2012, Eleftheriou et al, 2012). There is limited knowledge however regarding the potential interplay between vascular cells in the context of cerebral vascular remodeling, and whether MP play a role in facilitating these processes.

Objectives: The aim of this study was to assess the functional significance of the brain adventitial fibroblast activation in the context of VZV-infection demonstrated in the previous chapter, particularly in relation to potential paracrine effects on endothelial cells.

Methods: Endothelial activation and endothelial dysfunction, two processes that interact to trigger an inflammatory and prothrombotic phenotype in endothelial cells, were assessed using flow cytometry for expression of CD54 and reactive oxygen species (ROS). The secretome (containing the MP population) of VZV-infected HBVAF was evaluated using flow cytometry, mass spectrometry and electron microscopy. A particular focus was relinquished to the role of MP in the fibroblast to endothelial communication in the particular context of VZV vasculopathy, their potential to transport viral the pathogen, and the implications of this.

Results: There was activation in cultured HUVEC as indicated by upregulation of CD54 and increased ROS, induced by both conditioned media and MP from VZV-infected HBVAF. Further experiments revealed that VZV-infected HBVAF release proinflammatory cytokines and chemokines (IL-6, IL-8, TNF-a, IL-10, MCP-1). The possibility that some of these effects on endothelial cells could be mediated by MP release was examined. MP released by the VZV-infected HBVAF were found to express viral proteins by proteomic analysis and flow cytometry which showed increased expression of VZV gH protein and VZV GFP ORF23 when the GFP-tagged virus strain was used to infect. Transmission electron microscopy of MP released by HBVAF in response to VZV infection evidenced the pathogen cloaked in the MP. I also showed that MP induced lytic infection when incubated with healthy HBVAF.

Conclusions: Signals from infected HBVAF interact with HUVEC and contribute to endothelial activation and dysfunction, of relevance to the biology of VZV associated AIS.

4.2. Introduction

4.2.1. The interplay between endothelial activation and endothelial dysfunction in vascular disease

The endothelium, the innermost layer of the arterial wall, plays an intricate role in vascular biology being involved in vascular haemostasis, neutrophil recruitment, mediation of the vascular tone, hormone trafficking, and fluid filtration (Gimbrone et al, 1997). With a strategic anatomic position between blood and tissues, the endothelium is a dynamic interface exposed to various biochemical and also biomechanical stimuli originating from the circulating blood and/or nearby cells.

The healthy luminal endothelium is a relatively non-adhesive and non-thrombogenic surface, while specialized adhesive molecules present at the lateral cell–cell junctions influence the transendothelial permeability and the migration of leukocytes from the blood into the body tissues (Gimbrone et al, 1997). In health, at the basal aspect of the endothelium, transmembrane integrins and associated intracellular proteins link the extracellular matrix to cytoskeletal elements, providing stability and plasticity to the vascular lining

(Gimbrone et al, 1997). In disease, these interactions have been shown to undergo significant changes.

Studies at cellular and molecular levels support two paradigms of endothelial activation: biochemical and biomechanical, with the biochemical model probably more extensively studied (Liao KJ, 2013). Humoral factors, such as cytokines and bacterial products such as gram-negative endotoxins were shown to act directly on cultured endothelial cells and modulate their phenotype by modifying their adhesive properties for blood leukocytes resulting in enhanced firm attachment and transmigration of leukocytes in various in vitro model systems (Bevilacqua et al, 1986; Pober et al, 1985, Gimbrone et al, 1997). The two paradigms of endothelial dysfunction and endothelial activation have been shown to intersect and play complex roles in the pathogenesis of a number of diseases such as atherosclerosis, hypercholesterolemia, coronary artery disease, hypertension, diabetes, vascular injury and repair (De Caterina et al, 1995). Endothelial activation is defined by the increased expression of cell-surface adhesion molecules, such as Intercellular Adhesion Molecule-1 (CD54; ICAM-1), vascular cell adhesion protein 1 (VCAM-1; CD106), PECAM-1 (CD31) and endothelial leukocyte adhesion molecule (E-selectin; CD63E) that subsequently facilitate extravasation of leukocytes from the blood vessels to inflammatory sites in the peripheral tissues (Haraldsen et al. 1996; Liao et al. 1997). In brief, increased endothelial expression of these molecules is a marker of vascular inflammation, vascular permeability, and endothelial activation.

In addition, proinflammatory cytokines such as TNF-α and interleukin-6 have been shown to induce activation of endothelial cells since 1980s (Bevilacqua et al, 1986). Moreover, biomechanical stimuli such as fluid shear stress and hydrostatic pressure lead to endothelial activation (Gimbrone et al, 1997). The humoral factors (cytokines, growth factors, bacterial products) that lead to the activation of endothelial cells can originate from the blood, and/or are released locally from endothelial cells or other nearby cells and can act in an autocrine or paracrine manner.

Endothelial dysfunction is defined by a lack of Nitric Oxide (NO). NO has been shown to be a vascular protective factor that limits activation of the endothelial cells and prevents leukocyte adhesion to the vessel wall (Kubes et al, 1991; Liao et al, 1995).

Endothelial dysfunction and endothelial activation are linked (Figure 4.1.). Endothelial dysfunction has been shown to induce endothelial cell activation in the absence of cytokines. In a study by De Caterina and colleagues, suppression of basal endothelial NOS activity by l-NG-arginine methyl ester led to increased VCAM-1 expression and increased monocyte adhesion, indicating that endogenous endothelium-derived NO could basally inhibit endothelial cell activation (DeCaterina et al, 1995). Kuhlencordt and colleagues have shown that mice with a deletion of eNOS develop atherosclerosis and vascular inflammation (Kuhlencordt et al, 2001). These results also suggested that vascular areas with

turbulent and not laminar blood flow which would have less endothelium-derived NO, would be more prone to endothelial cell activation (Liao KR, 2013).

NO and ROS dynamically interplay to maintain the vascular homeostasis. ROS production and NO generation are closely linked and high levels of ROS lead to low NO bioavailability, as observed in endothelial cells exposed to irregular flow (Hsyue-Jen Hsieh et al, 2014).

ROS are oxygen metabolites that are highly active in terms of oxidative modifications of cellular macromolecules including proteins, lipids, and polynucleotides (Wang et al, 2013). ROS have both physiological and pathological functions. Homeostatic ROS maintain an optimal environment for the biochemical cellular activities. When ROS are produced in excess or when the endogenous antioxidant capacity is lowered, increased oxidation elicits harmful effects, resulting in “oxidative stress”. There is now an increasing body of evidence linking oxidative stress and malignancy, ischaemic injury, neurodegenerative disorders, and chronic inflammatory processes (Halliwell et al, 2001; Moskovitz et al, 2001; Valko et al, 2007; Newsholme et al, 2007; Chinta et al, 2008; Wells et al, 2009).

In summary, a healthy endothelium not only arbitrates endothelium-dependent vasodilation, but also inhibits thrombosis, vascular inflammation, and hypertrophy. It displays a vasodilatory phenotype consisting of high levels of vasodilators such as NO and low levels of ROS, an anti-coagulative phenotype

consisting of low levels of plasminogen activator inhibitor, von Willebrand factor, and P-selectin. Minimal inflammation may be present, as indicated by low levels of soluble VCAM-1, ICAM-1, E-selectin, TNF-α, and IL-6 (Rajendran et al, 2013). In contrast, a dysfunctional endothelium is characterized by impaired vasodilation, increased oxidative stress, and a procoagulant and pro-inflammatory phenotype with decreased vascular repair capacity.

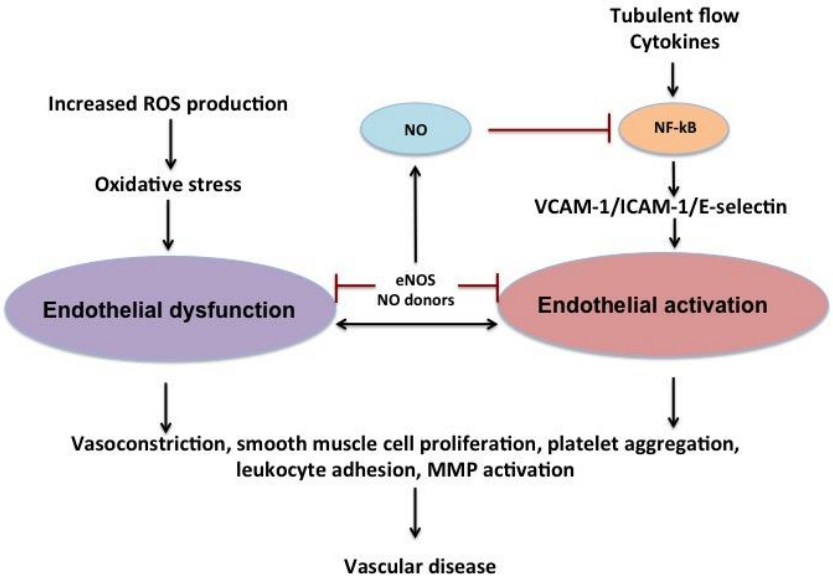

***Figure 4.1**. **The role of endothelial activation and endothelial dysfunction in vascular disease. (Adapted from Liao KJ, 2013).** Oxidative stress mediates endothelial dysfunction. Proinflammatory cytokines, and turbulent flow are important mediators of endothelial cell activation via the activation of the transcription factor, NF-κB. NO reduces endothelial cell activation through inhibition of NF-κB. Loss of NO increases the endothelial cell activation. Endothelial activation can lead to endothelial dysfunction, and both processes*

lead to vascular disease by increasing vasoconstriction, smooth muscle cell proliferation with vascular remodeling, platelet aggregation, leukocyte adhesion, low density lipoprotein oxidation, and activation of matrix metalloproteinases.

4.2.2. Cellular microparticles

Cells release into the extracellular environment diverse types of membrane vesicles of endosomal and plasma membrane origin called extracellular vesicles (EV) (Raposo et a, 2013). This generic term of EV has been used to describe all forms of secreted vesicles: exosomes, microvesicles, MP, apoptotic bodies and other subsets (Burger et al, 2015). Definitions of EV subsets vary between studies and there is currently no consensus regarding the nomenclature (Gould et al, 2013).

MP have been described as a heterogeneous in size (100-1000 nm) population of membrane vesicles rich in phosphatidylserine, that are released from cells through budding of the plasma membrane (ectocytosis) upon conditions of stress, injury, cellular differentiation, senescence, or apoptosis (Mause et al. 2010; Torrecilhas et al. 2012; Horstman et al. 1999). The above characterization enable differentiation from exosomes, vesicles of less than 100 nm in size, which are stored in multivesicular bodies in the cytoplasm to be released from cells

when these endosomal compartments fuse with the plasma membrane (Simons et al. 2009).

In the recent years, the term of microvesicles has also been introduced, referring to EV released from the cells by blebbing of the plasma membrane as described for MP but with a smaller size below 200 nm (Souza et al, 2015). The distinction between microvesicles and MP is subtle, and other authors refer to the MP as microvesicles (Burger et al, 2015). In this thesis I used the term MP to describe the EV with a size above 100 nm as confimed microscopically or by flow cytometry data which detects larger particles above 300 nm.

The normal cell membrane has two layers rich in phosphatidylserine and phosphatidylethanolamine, which are supported by enzymes flippase, floppase and scramblase (Mause et al, 2010). When MP are formed, flippase is inactivated and floppase and scramblase are activated, leading to a loss of the normal architecture of the membrane and producing an outward facing phosphatidylserine enriched layer (Zahra et al, 2011; Bern MM, 2017; Beyer et al, 2010).

MP express antigens indicative of their parental cells. They have been detected in plasma and other body fluids in various physiological and disease states. Their contents depend on their cells of origin and can include tissue factor, mRNA, microRNA, double stranded DNA, P-selectin glycoprotein ligand-1 (PSGL-1), growth factors, adhesion integrins, protease inhibitors, and ceramides (Bern MM, 2017; Ratajczak et al, 2006; Hunter et al, 2008).

Of note, it has been suggested that MP released upon cellular activation or apoptosis of the same cell type differ in terms of numbers and phenotype (Jimenez et al. 2003). Their number and their size distribution have been shown to be influenced by gender, age, and disease (Gustafson et al, 2015; Rautou et al, 2013).

MP contribute to a number of physiologic pathways, the complexity of which is still being investigated. Although originally regarded as inactive cellular debris, in the recent years a number of studies have highlighted the role of MP as vectors of biological information and protagonists of intercellular communication. This intercellular communication leads to activation of receptors on the target cell via presentation of membrane-expressed molecules, or direct transfer of MP components including proteins, lipids or genetic information to the target cell, potentially leading to cell activation, phenotypic changes and reprogramming of cell function (Mause et al. 2009; Kahn et al, 2017; Muralidharan-Chari et al, 2010). Some cytoplasm is engulfed during MP release by membrane blebbing, and so the MP have been shown to also carry cytokines and chemokines, growth factors, enzymes, and signaling proteins (Garcia et al, 2005; Dean et al, 2009; Mause et al, 2010).

As described above, in both physiological conditions and disease, MP can induce in the target cell profound changes, and the responding cell can in turn release molecules, which can act locally or systemically. The ability of MP and exosomes

to deliver molecules to target cells introduces the compelling possibility of their use for drug delivery, but also for the pathogenesis of diseases, including (of relevance to this thesis) the potential for MP to be mediators/vehicles for viral propagation.

There is very limited knowledge of the role of MP and/or exosomes in infectious diseases. MP released from cells in response to an infection can originate from either the pathogen or host cell. Gram negative bacteria and mycobacteria have been shown to release outer-membrane vesicles which can convey pathogen molecules ultimately serving as antigens to induce host defense and immunity. Bacteria can also release membrane vesicles that act as agonists of innate immune receptors and serve as regulators of host defense and mediators of immune evasion (Schwechheimer et al, 2015; Prados-Rosales et al, 2011; Prados-Rosales et al, 2014). Less is known of the vesicles released from the host cells in response to infection.

Exosomes are the most studied cellular particles that are used by viruses. It has been shown that in response to viral exposure cells release exosome populations with distinct molecular profiles (Meckes et al, 2013). Exosomes released from virus-infected cells have been studied in HIV and some herpesviruses, and more recently hepatitis C virus (HCV), hepatitis A virus, human papilloma virus. HIV induces release of MP from infected cells (Kadiu et al. 2012). Epstein-Barr virus-infected B cells have been shown to secrete exosomes that contain virally

encoded miRNA (Pegtel et al, 2010). A role of exosomes in the transfer of infectious agents between cells has been postulated, however this has still not been extensively demonstrated. Ramakrishnaiah and colleagues have shown that exosomes contain viral envelope proteins and viral genomes and facilitate transmission of HCV between human hepatoma Huh7.5 cells (Ramakrishnaiah et al, 2013). Hepatitis A (HAV), a non-enveloped virus, was shown to be released from cells surrounded by host-derived membranes which protected the virus from antibody-mediated neutralization (Feng et al, 2013). These enveloped HAV viruses resembled exosomes. Encapsulation of viral genomes by hijacking the host cell membranes may be a strategy of the virus to protect itself from antibody-mediated neutralization. Studies on herpes simplex virus (HSV) exosomes, have shown that these particles contain viral tegument proteins and can increase the infectivity of viral DNA (Meckes DG, 2015).

A strong case for cellular vesicles having a role in facilitating viral infections is that the particles released by virus-infected cells have modified physiological characteristics, and interfere with, rather than trigger, antiviral immunological responses (Robbins et al, 2014; Meckes DG, 2015; van Dongen et al, 2016).

Studies in mice have suggested that the signalling of cellular vesicles could function not only locally, but also extend systemically (Batra et al, 2015; Peinado et al, 2012).

In vasculitides, MP have been shown to induce endothelial changes and contribute directly to the vasculopathy aetiopathogenesis (Hong et al. 2012).

Therefore these studies suggest that MP are important mediators of vascular pathology, and may also contribute to viral infection propagation. The role of MP in the mechanism of VZV related arteriopathy thus far have not been explored.

4.3. Hypothesis

In this chapter the hypothesis explored was that VZV-infected HBVAF interact with nearby cells such as endothelial cells through MP, and trigger inflammatory responses.

4.4. Methods

4.4.1. Fluorescence activated cell sorting of HBVAF-derived microparticles

4.4.1.1. Isolation of MP from HBVAF

MP were harvested from HBVAF culture supernatants by sequential centrifugation according to published methods, as follows: culture supernatants were collected in sterile Eppendorf tubes and centrifuged at 3500g at 4^{o}C for 5 minutes to remove detached cells. The supernatant was collected and further centrifuged at 5000g and 4^{o}C for 5 minutes to remove cell debris, prior to a last centrifugation step at 15000g, 4^{o}C, for 60mins. The supernatant was carefully decanted and aliquoted in sterile Eppendorf tubes using a 200 µl pipette, for use in experiments as described in a later section. This is referred to as the MP free

fraction of the supernatant, or the soluble fraction. The MP pellets, usually invisible, were left in a small amount of approximately 20 µL in the tube and used immediately for staining for flow cytometry in HBVAF infection experiments or HUVEC stimulation experiments as described in the relevant sections.

4.4.1.2. Preparation of monoclonal antibodies and labelling of MP with Annexin V

The labelling of MP was achieved as follows: 5 µL of a 1 in 5 dilution Annexin V conjugated with phycoerythrin (PE; BD Pharmingen) or PERCP (BD, Pharmingen) in Annexin V buffer (Annexin V buffer diluted as per instructions 1/10 in distilled water) was added to each Eppendorf tube. 5 µL of cell marker unconjugated antibodies: goat anti-gE VZV monoclonal antibody (Santa Cruz Biotechnology) or mouse anti-gH VZV monoclonal antibody (Abcam) 1 in 20 dilution in Annexin V buffer were also added when required, according to the experiment plan. All antibodies were titrated to ascertain their optimal working dilution, and used at final dilutions listed in table 2-2 in the general methods section. Forty µL of gently aliquoted MPs were incubated with the Annexin V and antibodies when required for 20 minutes at room temperature in the dark with gentle shaking.

For the experiments in which VZV-GFP ORF23 strain was used and no co-staining with the above VZV monoclonal antibodies was performed, the incubation was then terminated by adding 200 µl of Annexin V buffer to each well, and the samples transferred to small FACS tubes prior to flow cytometry. If

staining with unconjugated antibodies was performed, one additional washing step in Annexin V buffer was required, followed by 20 minutes incubation of the pellets at room temperature in the dark with 50 µL of respective secondary antibody FITC or PE conjugated (final dilutions as listed in Table 2-3).

4.4.1.3. Flow cytometric analysis of MP

Flow cytometry is the most commonly used method for MP analysis. The advantages of flow cytometry include that large MP numbers may be analysed rapidly, size gating provides a way for excluding cellular debris from the analysis, and that numerous antigen markers can be detected simultaneously on a single MP. Annexin V has been used in numerous studies to identify the MP as they bind phosphatidylserine, a negatively charged phospholipid exposed on the plasma membrane during vesiculation (Thiagarajan ET AL, 1990). Lactadherin has also been used as a probe to detect the MP by flow cytometry, as it is reported to be sensitive to phosphatidylserine and is compatible with calcium chelators such as EDTA (Latham et al, 2015). However, reports have also described that some phosphatidylserine-low MP do not bind annexin V or lactadherin, therefore raising concerns for the use of these labels in MP detection and analysis (Latham et al, 2015). Other disadvantages of MP identification by standard flow cytometry are that this method offers a lower detection limit of only 300–500 nm, and is unable to distinguish coincident events.

All analysis was performed on a FACScalibur flow cytometer (Becton Dickinson). MP samples were run at medium flow rate for 30 seconds.

A representative set of flow cytometric plots, and the gating protocol are shown in figure 4.2. When analysing FACSCalibur flow cytometry plots of MP, size was defined using forward scatter. MP were defined first as <1μm in diameter when compared to 1μm diameter polystyrene beads (Sigma, UK), and then positive for Annexin V. 1μm diameter polystyrene beads were used to define the MP gate, with anything classed as a MP if it showed forward scatter less than these beads, but to exclude the first forward scatter channel containing maximal noise. 3μL of the bead stock was diluted in 2mL sterile filtered PBS, then 10μL of this working solution was diluted in 190μL sterile filtered PBS. This sample was acquired for 15-20s. The same protocol was performed using 0.3μm diameter polystyrene beads to show the size resolving capability of the flow cytometer used.

Data were analysed using FlowJo (Treestar Inc, Ashland, OR).

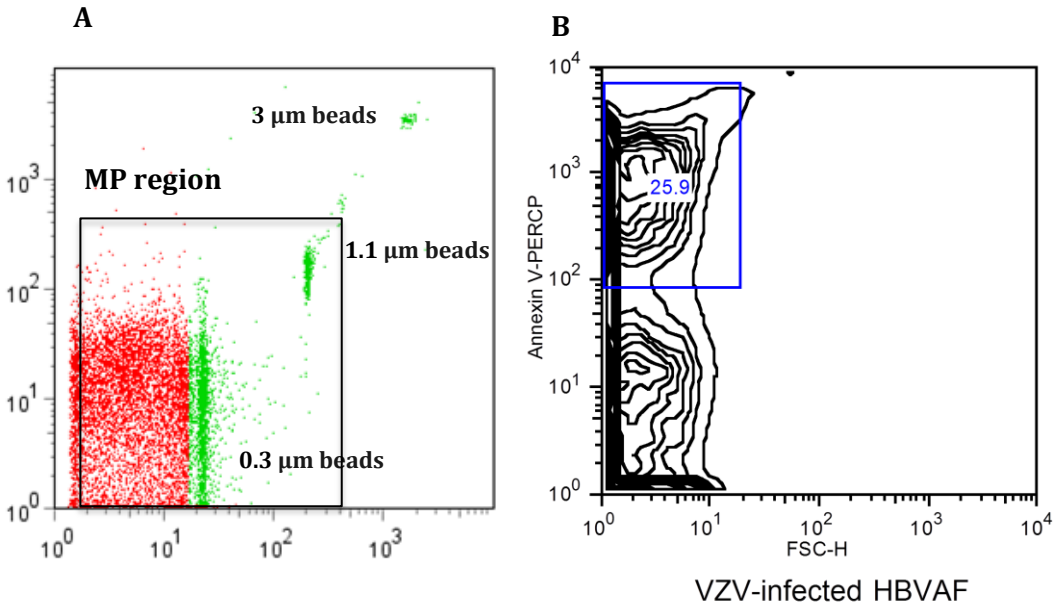

Figure 4.2. Flow cytometric detection of MP released from HBVAF. (A) *Figure indicates that 0.3, 1.1 and 3 µm beads are distinguishable from the background noise within the system. The HBVAF MP gate was defined by forward-scatter characteristics corresponding with a size < 1.1 µm and positive annexin V labeling.* ***(B).*** *Annexin V is a protein and not an antibody and thus no isotype control antibody exists. The threshold for annexin V binding was therefore determined by using the fluorescence threshold established for MP in the absence of labeled annexin V. Representative flow cytometry plot showing release of MP from VZV-infected HBVAF as annexin V-PERCP positive events.*

In order to enumerate the MP, a suspension of 3µm diameter polystyrene beads (Sigma, UK) was run in addition. The beads were provided in a stock at

6.667x10^9/mL. 6µL of bead stock was diluted in 2mL sterile filtered PBS, giving the working solution (2x10^7/mL). 10µL of working solution was diluted in 190µL sterile filtered distilled H_2O, giving a total of 200,000 beads. The absolute number of Annexin V binding MP per mL of media was then determined by using the proportion of beads counted and the exact volume of media from which the MP were analysed, as described by Brogan et al. (Brogan et al. 2004). The equation to calculate the absolute number of MP is shown in figure 4.3.

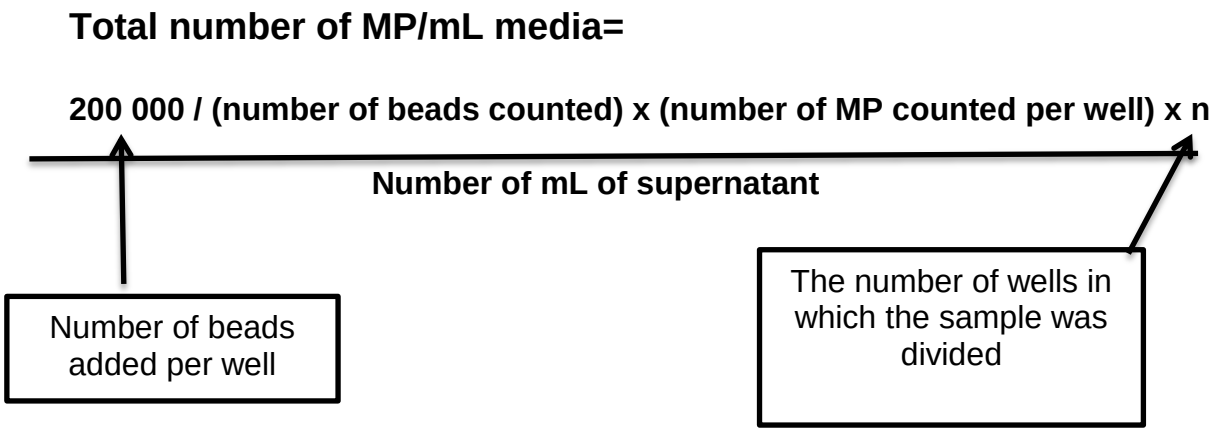

Figure 4.3. Conversion equation for calculation of MP number per mL of media from flow cytometer counts.

4.4.2. Quantification of soluble cytokines and chemokines in HBVAF culture supernatants

The Meso Scale Discovery (MSD) electrochemiluminescence assay was used for measurement of the cytokine levels released in the culture supernatants from mock- infected and VZV-infected HBVAF, at several time points post infection. MSD provides a plate pre-coated with capture antibodies, and the user adds the sample and a solution containing detection antibodies conjugated with electrochemiluminescent labels over the course of one or more incubation periods. Analytes in the sample bind to the capture antibodies, to then recruit the detection antibodies. An MSD buffer is then added to the wells to create the appropriate chemical environment for electrochemiluminescence. The plates are loaded to the reader, where a voltage applied to the plate electrodes causes the captured labels to emit light. The reader measures the intensity of emitted light.

The assay was performed according to the manufacturer's instructions. Samples were collected at different times post infection, stored in -80C freezer and processed in batches. All standards and samples were measured in duplicate. The cytokines measured were IL-6, IL-8, IL-10, TNFα and MCP- 1. In brief, samples were defrosted to room temperature and 25 µl was added to the appropriate well of the MSD plate, and incubated at room temperature in the shaker for 2 hours. 25 µl of the appropriate detection antibody was added to each well, and plates incubated for 1 hour at room temperature. Plates were washed,

and 150 µl per well of 2x MSD Read Buffer diluted in deionised water was added to the plates. Plates were analysed within 30 minutes of the addition of Read Buffer on the MSD imager.

4.4.3. Fluorescence activated cell sorting for human umbilical vein endothelial cell activation and dysfunction in response to Varicella zoster virus infection

4.4.3.1. Production of HBVAF culture conditioned media

Media was collected in sterile Eppendorf tubes from VZV- and mock-infected HBVAF at approximately 48 hours post infection, centrifuged at 3500g at 4^{o}C for 5 minutes to remove detached cells, the supernatant collected and further centrifuged at 5000g, 4^{o}C for 10 minutes to remove cell debris. The samples were stored in -80C freezer and used within 1 month.

4.4.3.2. HBVAF conditioned media fractionation

Samples of conditioned media prepared as above were thawed and further centrifuged at 15000 g, 4^{o}C, for 60mins, in 1.5 mL sterile Eppendorf tubes. The supernatant was carefully decanted and aliquoted in Eppendorf tubes using a 200 µl pipette, and the MP pellet left in approximately 20 µl. Next, the pellet was diluted in 0.5 mL of fresh media and used immediately in HUVEC stimulation experiments as outlined in the next section.

4.4.3.3. HUVEC incubation with conditioned media/MP /MP-free fractions harvested from VZV -infected HBVAF culture

HUVEC (PromoCell, Heidelberg, Germany) at passage 4 were seeded at 5000 cells/cm^2 in EGM-2 (PromoCell), and 12-well plates. When reaching confluence, the media was removed and cells washed twice in 1 mL PBS. 0.5 mL of full conditioned media, or MP fraction diluted in 0.5 mL fresh basal HBVAF media, or 0.5 mL of MP fraction free conditioned media from VZV- or mock-infected HBVAF. The media was collected at approximately 48 hours post infection (at the start of day 3 post infection), and was added to the relevant HUVEC culture wells. The MP pellets and MP free fractions were separated from equal volumes of conditioned media collected from quiescent fibroblasts seeded at the same density. When incubating with MP, for each HUVEC well from the 12 well plate, I added the MP pelleted from the supernatant of a 6 well plate. The media was topped up with 0.5 mL fresh EGM-2 (1:1 ratio conditioned media to fresh media) and plates moved to 37^{o}C incubator. Next, the cells were harvested by trypsinization and used for the above mentioned flow cytometry experiments.

4.4.3.4. Fluorescent activated cell sorting for human umbilical vein endothelial cell CD54 expression

HUVEC (passage 2, PromoCell, Heidelberg, Germany) were incubated for 6 hours with conditioned media from mock-infected or VZV-infected HBVAF and the surface expression of CD54 was analysed by flow cytometry after staining with anti CD54-PE antibody (BD PharminGen, dilution listed in table 2-2). HUVEC treated with TNF-α (100 ng/mL) were used as positive control. Unstained samples were used to identify positivity, and samples stained with only secondary antibody were used as negative controls. A minimum of $10x10^3$ cells per sample were acquired. Results were analyzed with FlowJo 10.0.8 software.

4.4.3.5. Reactive oxygen species detection by Flow Cytometry.

2', 7'-Dichlorodihydrofluorecin (H_2DCF-DA) is a widely used probe for detecting intracellular H_2O_2 and oxidative stress. H_2DCF-DA diffuses into the cell where esterases cleave the acetate group and the resulting molecule is trapped into the cell where intracellular ROS products such as Nitric Oxide, peroxyl products and peroxyl radicals oxidises H_2DCF to the fluorescent compound dichlorofluorescein (DCF; Jakubowski et al. 1997). This can be detected in the FL1 channel of the flow cytometer. This dye is often used to measure the general level of oxidative stress inside the cell, (Amir et al. 2008). It is important to keep in mind that there are several limitations in terms of the interpretation of the results: the oxidation reaction may be accelerated by peroxidases and inhibited by glutathione levels (Garcia-Ruiz et al. 1997), cytochrome c, a heme protein that is released from the mitochondria to the cytosol during apoptosis can oxidise Dichlorodihydrofluorecin directly via a perodidase-type mechanism to form DCF (Kalyanaraman et al,

2012). Indeed the accumulating DCF may also oxidise H2DCF amplifying the signal (Johnson et al, 2010).

ROS production was studied in HUVEC at approximately 70% cell confluence plated at $2x10^4$ in 12-well plates and cultured for 3-4 days. The culture medium was removed, and HUVEC were incubated in the dark for 30 minutes with 10 μM H_2DCF-DA (Molecular Probes, USA). Next, they were washed twice in serum free basal media to remove extracellular H_2DCF-DA, and incubated for 1 hour with conditioned media harvested from mock- or VZV-infected cultures prior to flow cytometry analysis. Caution was taken to minimize light exposure during the experiment because H_2DCF-DA is susceptible to photo-oxidation (therefore increasing DCF fluorescence) or photo-bleaching (loss of DCF fluorescence) (Wang et al, 2013).

Cells treated with 200 μM H_2O_2 and 0.1 μM tBHP were used as positive controls. Cells without labeling were used as negative control.

4.4.4. Qualitative mass spectrometric analysis of the proteomic profile of MP released by HBVAF in response to VZV infection

4.4.4.1. Sample preparation

HBVAF were cultured in T225 flasks in basal fibroblast medium supplemented with 2% FBS 1% fibroblast growth factor and 100x Penicillin/Streptomycin, (Sciencell, Carlsbad, CA,USA). Quiescence was achieved by shifting after 24

hours and for 7 days to basal fibroblast medium supplemented with 0.1% FBS, 100x Penicillin/Streptomycin and no growth factors. Quiescent fibroblasts were infected cell to cell with fibroblasts infected with VZV GFP ORF23 or mock-infected as described in the general methods, by adding one T75 flask of infected cells to the T225 flasks. At the time of cell to cell infection, around 75% green fluorescence was present in the infected flasks, indicating that more than half of the culture monolayer was infected. Each of the two conditions, VZV-infected or mock-infected HBVAF was prepared in triplicates in a total of 6 samples.

The proteomic profiling of the cells secretome is difficult to study *in vitro* due to contamination issues by serum proteins such as FBS that is a critical component of most cell culture media. With this in mind, when designing the methods for this experiment's samples preparation, a challenge that I anticipated was to minimize the media FBS content for cells that would already be in a stressful environment due to infection. In addition, because MP are small particles compared to cells, and therefore a large pellet is required to enable extraction of enough protein for the mass spectrometry analysis, I decided to avoid repeated media changes in order to not lose any MP released. Not changing media and maintaining the infected cells in FBS free media could cause great damage to the cells. Published studies showed that a stringent wash treatment of the cells prior to changing the media to serum free media for 24 hours prior to sample collection allowed the confident identification of a larger portion of the secretome by liquid chromatography tandem-mass spectrometry (LC–MS/MS) (Pellitteri-Hahn et al, 2006). However, these studies were not conducted on infected cells.

I therefore concluded that it would be particularly challenging to maintain the infected cells in FBS-free media while infection is propagating. HBVAF were cultured after cell to cell infection in quiescent media with reduced 0.1%FBS, with a focus to infect them at a high MOI to facilitate viral spread in a shorter period of time rather than maintain them in culture for 6-7 days without changing the media.

At 24 hours after cell to cell infection, the media was removed, and the cells were washed twice in PBS, and once in serum-free media, followed by replacement of the media with serum-poor media. The cultures were monitored daily using fluorescence microscopy for the extent of infection. On day 4 post infection, 80% fluorescence was present in the flasks of VZV-infected cells, concurrently with CPE. The supernatants were collected and the MP pelleted as described previously. The pellets were washed twice and transferred fresh to the mass spectrometry facility in 20-30 µl PBS.

4.4.4.2. Liquid chromatography tandem-mass spectrometry

Mass spectrometry has emerged as the primary tool for protein identification and is the cornerstone of proteomics. In brief, the protein identification process using mass spectrometry is presented in Figure 4.4., from Cottrell et al, 2011.

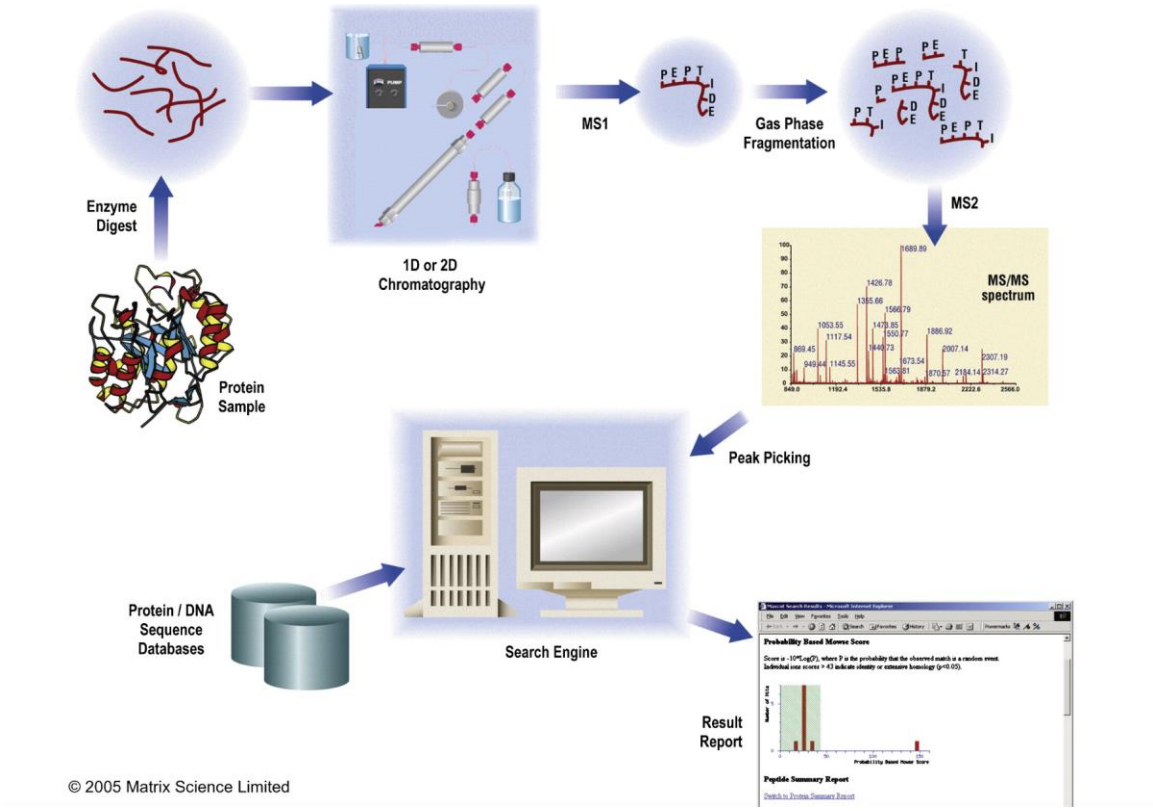

Figure 4.4. Basic schematic representation of a typical experimental workflow for protein identification and characterisation using liquid chromatography tandem-mass spectrometry (LC-MS/MS) (From J Cottrell, 2010). *An enzyme, often trypsin, digests the proteins from the sample to peptides. One or more chromatography are used to regulate the flow of peptides into the mass spectrometer. 1D or 2D gel electrophoresis may also be used for separation followed by a single step of chromatography. Peptides are selected one at a time using the first stage of mass analysis (MS1). Each isolated peptide is then induced to fragment, and the second stage of mass analysis (MS2) used to capture an LC-MS/MS spectrum. Individual peptide sequences are identified.*

Then the set of peptide sequences is used to deduce which proteins may have been present by comparing with databases of known proteins.

Liquid chromatography tandem-mass spectrometry (LC-MS/MS) was performed on triplicate samples of MP from VZV-infected and control mock-infected HBVAF with assistance from Mr Ivan Doykov, Research Assistant in the Mass Spectrometry Unit at University College of London and Great Ormond Street Hospital. In-gel digestion of proteins was performed according to published methods (Mills et al, 2001). All analyses were performed as described previously (Heywood et al, 2012) using a nano-Acquity UPLC and QTOF Premier mass spectrometer (Waters Corporation, Manchester, UK). Data were analysed using ProteinLynx Global Server (PLGS) version 2.4 (Waters Corporation, Manchester, UK) with a downloaded Uniprot Human Proteome database. Search settings allowed a minimum three ion matches per peptide, seven ion matches and three peptides matches per protein. At the center of all protein identification methods is the scoring system. Mass spectrometry data arisen from the unidentified protein are compared with theoretical data from known proteins, and a score is assigned according to how well the two sets of data compare. Any score above an arbitrary confidence threshold, usually 95%, is termed a “hit” (McHugh and Arthur, 2008). The top such hit is expected to identify the unknown protein. If there are no scores above this threshold (“no hits”), then the protein remains unidentified. The limiting factor on all protein identification algorithms is the

compromise between false positives and false negatives (McHugh and Arthur, 2008). It is essential to keep false positives to a minimum during protein identification because identifying the wrong protein, and at the same time, it is desirable to identify as many proteins as possible to achieve the greatest benefit from the experimental data. The capacity of a tool to identify a protein is termed its sensitivity, and its capacity to discriminate between true positives from false positives is termed its specificity. Sensitivity and specificity are incorporated in the confidence level, a numerical threshold above which proteins are defined as identified.

In this study, only proteins with a PLGS confidence score > 95% confidence, “definite hits” were considered. Viral protein identification including number of peptides and coverage from the LC-MS/MS analysis for each protein are provided in the results section.

4.4.5. Transmission electron microscopy (TEM) of MP and MP-free pellets

For the electron microscopy experiments, the supernatant collected after isolation of the MP pellets was subjected to a further ultracentrifugation step, to isolate the smallest particles with diameter under 100 nm. The volume of supernatant used to concentrate the pellets was approximately 12 mL for each sample, collected from T75 flasks of HBVAF cultures mock-infected or VZV GFP ORF23-infected displaying green fluorescence on approximately 50% or more of the culture dish, on day 6 post infection. The MP free supernatants were

transferred in ultracentrifugation clear tubes, and the volume was topped up with PBS to 38.5 mL which is the maximum volume required by each tube. The tubes were transferred to an Optima XPN (Beckman Coulter) preparative ultracentrifuge with a SW 32 Ti Rotor, swinging bucket, and centrifuged at 131 000 g, 4^{o}C for 1 hour. The supernatant was discarded gently, and the pellets left in approximately 100 µl PBS, transferred to Eppendorf tubes and transported on ice to the electron microscopy facility where they were negatively stained within 1 hour.

The samples were kindly prepared by uranyl acetate negative-staining in assistance by Mark Turmaine, Experimental officer in the Electron microscopy facility at University College of London, using standard published methods (von der Malsburg et al, 2011). An aqueous solution of 2% uranyl acetate was prepared using uranyl acetate dehydrate powder (Merck, KGaA, Darmstadt, Germany) dissolved in double distilled water. A 20 µL sample drop was placed on a 400-mesh carbon-coated grid for 2 minutes at room temperature. Excess sample was gently removed with a filter paper. The sample was rinsed by swiping the grid on a drop of PBS, excess solution was blotted. To negatively stain the sample, the grid was placed, film side down, on a fresh 20 µL drop of 2% uranyl acetate for 2 minutes, followed by blotting and air drying.

Next, the samples were analysed using a JEOL JEM-1010 electron microscope, using its room temperature sample holder. As the manufacturer describes, JEOL JEM-1010 is a highly integrated compact transmission electron microscope with

advanced features and functions. The operating voltage ranges from 40kV to 100kV which is ideal for life science as well as material science applications. JEM-1010 is a high-contrast TEM because of low operating voltage and the design of the objective pole piece. In addition, it is equipped with a camera for digital image acquisition. The images were acquired at magnifications between 60000 and 135000x.

The samples were analysed fresh, to avoid artifacts described in the literature associated with sample freezing, such a perturbed architecture due to the development of ice crystals.

The samples I studied on the transmission electron microscope were: MP pellets from mock-infected HBVAF used as control; MP pellets from VZV-infected HBVAF; and pellets obtained after ultracentrifugation from mock-infected or VZV-infected HBVAF.

4.4.6. HBVAF incubation with MP harvested from infected cultures

For the infection experiments using MP/MP-free fraction harvested from HBVAF culture supernatants (either VZV- or mock-infected), the healthy quiescent fibroblasts were prepared as described in the general methods chapter, in a 6-well plate.

Supernatants were collected from HBVAF cultures infected similarly to the samples for proteomic analysis, with inoculum cells from cultures with extended green fluorescence. When approximately 70-80% of the cells displayed green

fluorescence, supernatants were removed and MP and MP free fractions were separated from conditioned media by sequential centrifugation as described previously. MP pellets were washed twice in quiescent fibroblast media before being added to the healthy cells. MP and MP-free fractions were used fresh in the same experiments. In brief, the principle of infection was the same: after removing the media, the resting cells were incubated with the inoculum for 1 hour in a 37^{o}C incubator in a minimum volume of media to promote the adsorption of the MP or free virus particles if present in the MP-free fraction, gently shaking the plates every 15 minutes. For the 1 hour incubation time, the MP pellet was diluted in 300 µL of basal media supplemented with 0.1% FBS and antibiotics, and from the MP free fraction 1 mL was added per well in the 6-well plate. For each well of a 6 well plate I added the MP pelleted from the media of a T25 flask. At the end of the 1 hour attachment incubation time, the media was topped up to 1 mL per well, plates moved to a 34^{o}C incubator, 16 hours later the media was topped up to 2 mL, and CPE and fluorescence observed daily. The controls used were HBVAF mock-infected, and HBVAF infected cell to cell. In additional experiments, HBVAF were incubated as above in the presence or absence of heparin 10 µg/ml (Sigma-Aldrich). Previous studies showed that heparin inhibits VZV and HSV infection in cultures, by interfering with the viral attachment (Zhu et al, 1995; Nahmias et al, 1964).

4.4.7. Circulating MP in children with VZV-related AIS

4.4.7.1. Patients

Children > 28 days old presenting to Great Ormond Street Hospital with VZV-related AIS between October 2013 and February 2017 were recruited to the study. Patients were identified by the Neurology team and recruited during the acute AIS episode and blood samples were collected. VZV-related AIS was defined as AIS occurring within 12 months post Varicella infection.

Informed consent was obtained from all parents/guardians and participants with local ethics approval.

4.4.7.2. Healthy controls and disease controls

Blood samples were obtained from healthy adult volunteers, staff from within the Infection, Inflammation and Immunity Programme at the Institute of Child Health, University College London (UCL).

A disease control group was included comprising of children with a new presentation of AIS and cerebral arteriopathy of other aetiology. These patients were identified at presentation to the neurology services at Great Ormond Street Hospital.

4.4.7.3. Isolation of MP from platelet poor plasma

One to 3 mls of whole blood was collected into bottles containing 3.2% trisodium citrate (Becton Dickinson). Platelet poor plasma (PPP) was obtained by

immediate centrifugation of the whole blood at 5000g for 5 minutes twice. Plasma was then stored at –80^{o}C analysis. Prior to analysis PPP was thawed rapidly in a 37^{0}C water bath. Exact volumes of plasma (200-400µl) were then centrifuged at 17000 g for 60 minutes and the supernatant decanted to obtain the MP pellet. The MP were then reconstituted in Annexin V binding buffer (BD PharMingen, UK), divided into 40 µl aliquots and plated onto the wells of a 96 well U-bottomed plate prior to staining with Annexin V and anti-VZV protein antibodies.

4.5. Results

4.5.1. Assessment of endothelial cell activation in response to stimulation with conditioned media derived from VZV-infected HBVAF

HUVEC activation was measured by endothelial surface expression of CD54. After incubation of HUVEC for 6 hours with conditioned media from mock-infected or VZV-infected HBVAF (collected at 48 hours post infection), I analysed the surface expression of CD54 by flow cytometry.

The conditioned media contains a soluble fraction comprising of peptides and proteins including cytokines and chemokines, and a pelletable unsoluble fraction comprising of protein aggregates and extracellular particles. I postulated that if an effect of the conditioned media on HUVEC was identified, it is highly likely that the soluble fraction of it was responsible. With this in mind, I selected the 48-hour time point for collection of culture supernatants based on previously published

work suggesting that cytokine release peaks relatively quickly, often within hours to 24 hours after stimulating a cell population (Carlquist et al. 1994). In general, the intracellular production of cytokines is detected earlier than the cytokine secretion. The kinetics of cytokine production depends on the cell type and stimulus. VZV-infected cultures are a mixture of cells at different stages of infection, and VZV is propagated gradually in the cell cultures from cell to cell. Therefore, in terms of cytokine release as a first point to start, I theorized that if every single infected cell peaked in the secretion of cytokines at around 24 hours or less, and the virus propagates gradually, it is likely that a more representative peak would be beyond the 24-hour time-point when infection would have spread. Therefore a time point of 48 hours for collection of culture supernatants seemed reasonable for these experiments.

The results are presented in Figure 4.5. There was a significant difference in the CD54 median fluorescence intensity (MFI) between HUVEC treated with conditioned media derived from VZV-infected or mock-infected populations: 9.93 (SEM 1.34) for co-incubation with supernatants from mock-infected cells compared with 21.44 (SEM 2.75) for VZV-infected, p=0.002, n=9 independent experiments (Figure 4.5, B).

In summary, I detected upregulation of CD54 expression in cultured HUVEC treated with conditioned media derived from VZV-infected cultures.

.

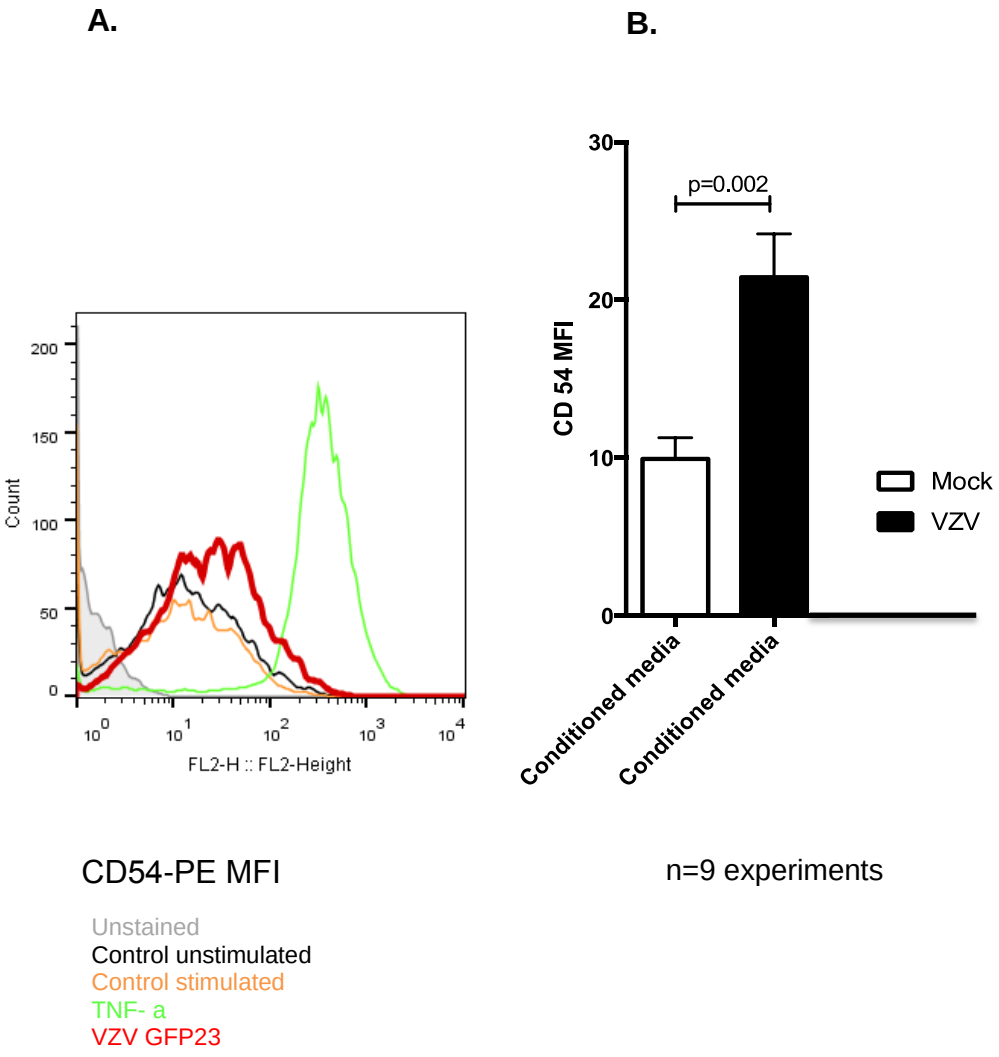

Figure 4.5. Effect of conditioned media from VZV-infected HBVAF on HUVEC CD54 expression.

Human umbilical vein endothelial cells (HUVEC) were incubated for 6 hours with equal volumes of conditioned media from mock-infected or VZV-infected HBVAF (collected at 48 hours post infection) and the expression of CD54 adhesion molecule was analysed by flow cytometry. ***(A)*** *Flow cytometry histogram*

demonstrating increased CD54 expression in HUVEC treated with conditioned media collected from VZV-infected HBVAF (shown in red) compared to HUVEC treated with conditioned media collected from mock-infected HBVAF (shown in orange). ***(B)*** *Data are expressed as mean and SEM (n=9); there was a significant difference in CD54 expression on HUVEC stimulated with conditioned media from VZV-infected HBVAF compared to HUVEC stimulated with conditioned media from mock-infected HBVAF (p=0.002, determined using unpaired t test).*

4.5.2. Assessment of endothelial cellular oxidative stress in response to stimulation with conditioned media derived from VZV-infected HBVAF

Having shown that media derived from VZV-infected HBVAF induce HUVEC activation with enhanced expression of CD54, I went on to investigate if this could also trigger endothelial dysfunction. Cellular oxidative stress was assessed by measuring the production of ROS. 2',7'-dichlorodihydrofluorescein diacetate (H_2DCF; DCFH-DA) is a well-established compound to detect intracellular peroxylated proteins, which are a marker of the overall level of oxidative stress within the cell.

Upon cleavage of the acetate groups by intracellular esterases and oxidation, the nonfluorescent cell-permeant H_2DCFDA is converted to the highly fluorescent 2',7'-dichlorofluorescein (DCF), which is detected by flow cytometry. In this thesis

ROS were detected by flow cytometric detection of DCF. The methods are outlined in section 4.4.3.

There was a significant difference in the DCF MFI between HUVEC treated with conditioned media derived from VZV-infected or mock-infected populations, in relation to untreated HUVEC: 8.48% (SEM 0.18 %) for co-incubation with supernatants from VZV-infected cells compared with 5.60% (SEM 0.62 %) for mock- infected (p=0.01, n=3 experiments, unpaired t test) (Figure 4.6.).

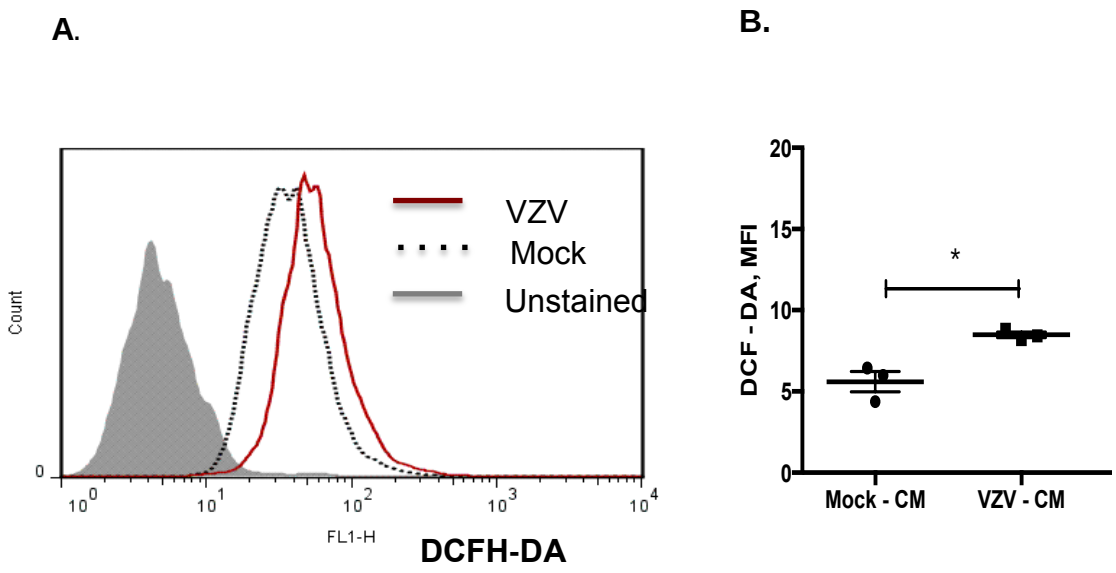

Figure 4.6. Conditioned media harvested from VZV-infected HBVAF induces ROS production in endothelial cells. *HUVEC were loaded with DCFH-DA and exposed for 60 minutes to conditioned media derived from VZV or mock-infected HBVAF, or H_2O_2 and tBHP (positive controls). Oxidation-dependent fluorescence of DCF was determined by flow cytometry, and the*

results are expressed as mean and SEM of DCF median fluorescence intensity (MFI). ***(A)*** *Flow cytometry histogram demonstrating increased DCF median fluorescence intensity (MFI) in HUVEC treated with conditioned media collected from VZV-infected HBVAF (solid black line) compared HUVEC treated with conditioned media collected from mock-infected HBVAF (dotted black line).* ***(B)*** *There was a significant difference in DCF MFI on HUVEC stimulated with conditioned media from VZV-infected HBVAF compared to HUVEC stimulated with conditioned media from mock-infected HBVAF: 8.48 (SEM 0.18) and 5.60 (SEM 0.62), respectively (p=0.01, n=3 experiments, unpaired t test). *P<0.05, **P< 0.001, ***P< 0.001*

4.5.3. Assessment of the soluble factors in conditioned media harvested from VZV-infected HBVAF

Next, I wondered what could be mediating these effects on endothelial cells. Could it be the soluble factors of the media? Could the insoluble fraction also have a contribution?

4.5.3.1. Quantification of proinflammatory cytokine and chemokine secretion released by VZV-infected HBVAF

To address this, first I profiled the cytokine production from VZV-infected HBVAF.

I examined the pattern of cytokine release by VZV infected fibroblasts to establish whether VZV infection promotes release of proinflammatory cytokines and chemokines that in turn could contribute to the pathogenesis of cerebral arteriopathy through a modification in the phenotype of endothelial cells as shown in the above results sections.

Conditioned media collected at 48 hours, 4 days and 6 days post infection from mock-infected and VZV-infected HBVAF was fractionated as described in the methods section of this chapter, and the soluble fraction was analysed using the MSD cytokine assay, assessing: IL-8, IL-6, IL-10, TNF-α and MCP-1. 48 hours post infection, VZV-infected HBVAF released several cytokines/chemokines (Figure 4.7.). that could contribute to the pathogenesis of cerebral arteriopathy either through exerting a paracrine effect on vascular endothelial cells triggering a switch in their phenotype to a proinflammatory one, or through a paracrine effect on other nearby HBVAF or other cells, such as vascular smooth muscle cells. IL-6 and TNF-α are cytokines known to promote leucocyte adhesion to endothelial cells (Luckett and Galluci. 2007; Galluci et al. 2006; Galluci et al. 2007; Fredi et al. 2005; Wung et al. 2005). IL-8 is known to enhance fibroblast migration and endothelial cell proliferation, activation (Dunlevy and Couchman. 2002). MCP-1 promotes leucocyte adhesion and inflammation, and compensatory IL-10 is suppressive of vascular remodelling (Viedt et al. 2002).

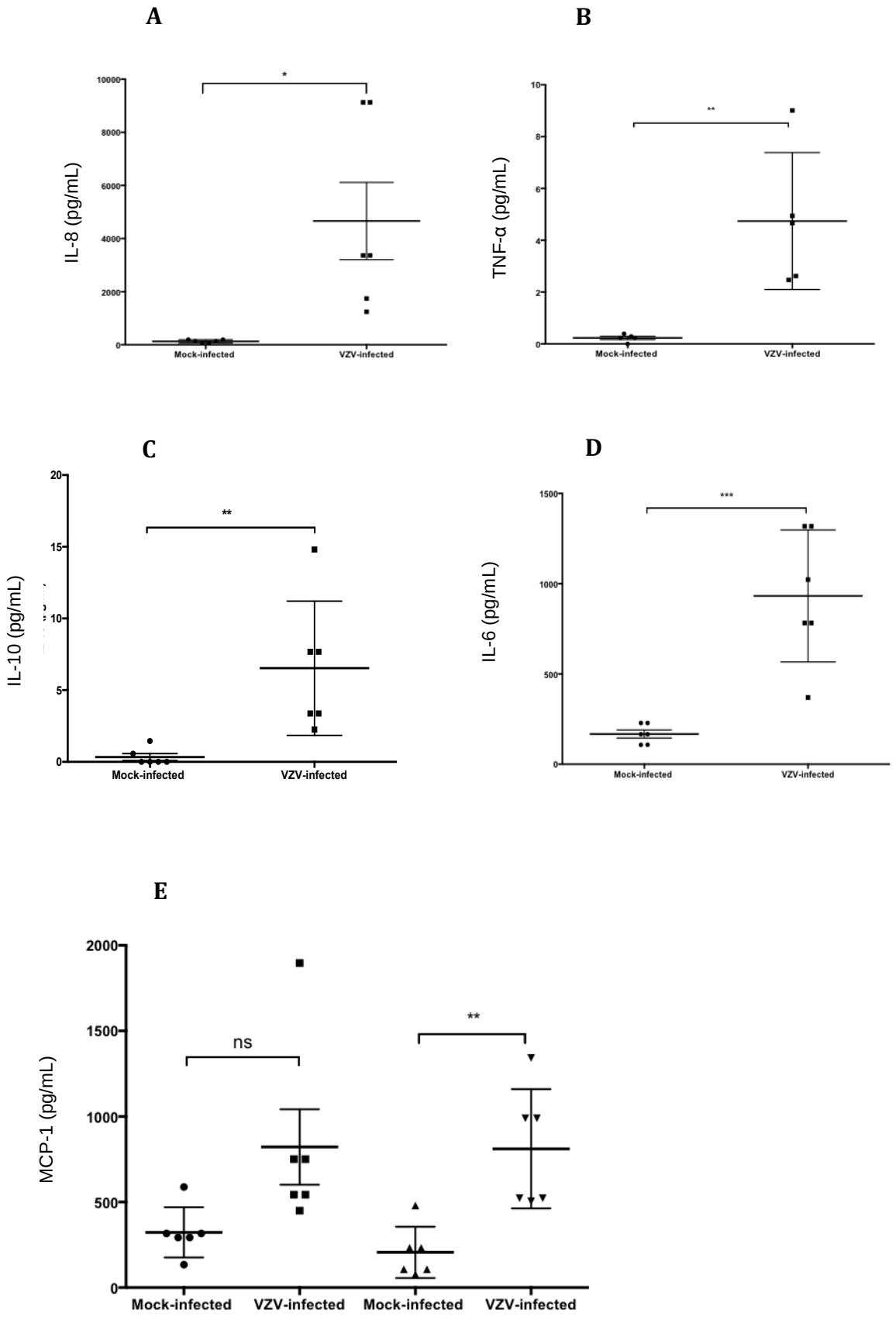
A
IL-8 (pg/mL)
10000
8000
6000
4000
2000
0
*
Mock-infected
VZV-infected
B
TNF-α (pg/mL)
10
8
6
4
2
0
**
Mock-infected
VZV-infected
C
IL-10 (pg/mL)
20
15
10
5
0
**
Mock-infected
VZV-infected
D
IL-6 (pg/mL)
1500
1000
500
0
***
Mock-infected
VZV-infected
E
MCP-1 (pg/mL)
2000
1500
1000
500
0
ns
**
Mock-infected
VZV-infected
Mock-infected
VZV-infected

Figure 4.7. Analysis of cytokine and chemokine levels released by VZV-infected and mock-infected HBVAF, 48 hours post infection.

*Data are presented as mean and SEM of n=6 experiments. At 48 hours post infection, the levels of cytokines were significantly higher for IL-8 (Figure A; p=0.01), IL-6 (Figure B; p=0.0005), IL-10 (Figure C; p=0.09), TNF-a (Figure D; p=0.005). Figure E shows the analysis of MCP-1 levels at 48 hours and 4 days post infection; the MCP-1 levels in the fraction of the media from VZV-infected HBVAF were higher at 48 hours compared to mock-infected HBVAF, without reaching statistical significance (p=0.05). At 4 days post infection, the MCP-1 levels were significantly higher in the VZV-infected population (p=0.002). Unpaired t test. *P<0.05, **P< 0.001, ***P< 0.001 ns P>0.5*

The mean and SEM of cytokine levels of 6 experiments, as well as the results of statistical analyses used to compare the levels of cytokines secreted by VZV-infected and mock-infected HBVAF are listed in table 4-1.

Table 4-1. Comparison of mean cytokine levels secreted by VZV-infected HBVAF and mock-infected HBVAF.

Cytokine	Cells	Time post infection	Level (mean, pg/mL)	SEM	Statistical significance for comparison between VZV and mock-infected cells
IL-8	VZV	48h	4661	1454	p=0.01
	Mock		131.7	24.92	
IL-6	VZV	48h	932.3	149.2	p=0.0005
	Mock		167.3	22.1	
IL-10	VZV	48h	6.52	1.91	p=0.09
	Mock		0.33	0.24	
TNF-a	VZV	48h	4.73	1.18	p=0.005
	Mock		0.23	0.06	
MCP-1	VZV	48h	822.1	220.6	p=0.05 (*ns*)
	Mock		323.3	59.94	
	VZV	4 days	811.4	142.2	p=0.002

	Mock		206.1	61.18	

A time course of cytokine release from mock- and VZV-infected HBVAF was also examined (Figure 4.8.). The highest levels of cytokines were present in the fraction of the media collected at 48 hours post infection.

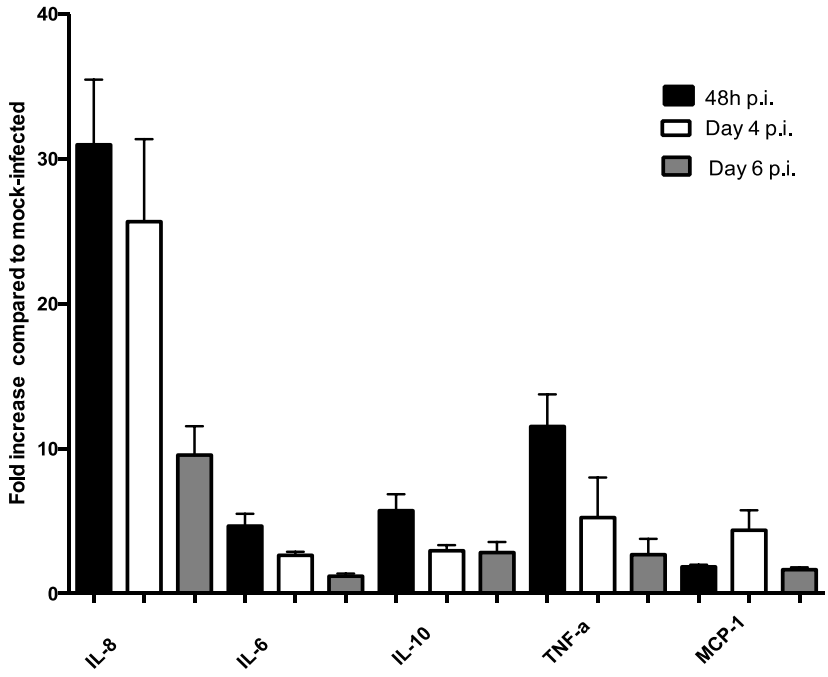

Figure 4.8. Time course of cytokine secretion in VZV-infected HBVAF.

Fold increase in the levels of IL-8, IL-6, IL-10, TNF-α and MCP-1 cytokines and chemokines secreted by VZV-infected HBVAF compared to mock-infected HBVAF at 48 hours, 4 days and 6 days post infection. Fold increase is expressed as mean and SEM of n=6 experiments for 48 hours and 4 days post infection, and n=3 experiments for 6 days post infection time point. Conditioned media was

stored in -80C freezer and samples analysed in batches using the Meso Scale Discovery cytokine assay. The maximal signal was identified at 48 hours.

Assessment of the pelletable factors in conditioned media harvested from VZV-infected HBVAF

Studies in cancer have shown that both soluble factors and the extracellular vesicles secreted by the tumour cells work together to establish metastatic disease. Jung and colleagues used the rat pancreatic adenocarcinoma as a model system and have demonstrated that the exosomes are the driving force of metastasis, but they required the help of the soluble factors (Jung et al, 2009). Aliotta and colleagues have demonstrated that extracellular vesicles are capable of inducing pulmonary vascular remodeling and also of reversing the pulmonary vascular responses in monocrotaline-induced pulmonary hypertension in mice (Aliotta et al, 2013; Aliotta et al, 2016).

I therefore next hypothesized that some of the phenotypic modulation of HUVEC could be part-mediated by MP release. To test this hypothesis I explored whether VZV induces MP release from infected fibroblasts, and the possibility that fibroblast MP contribute to endothelial cell activation.

4.5.4. Flow cytometry study of MP derived from HBVAF

4.5.4.1. HBVAF release MP in response to VZV infection

Supernatants from mock- and VZV-infected HBVAF were collected on day 6, and subjected to differential centrifugation as described in methods section of this chapter. to separate MP with size between 0.1 and 1μm. After isolation, the pellets were used immediately for staining with Annexin V (AnV) and analysed by flow cytometry. HBVAF derived MP were defined as particles less than 1.1 μm in size and binding AnV (Figure 4.2.)

The flow cytometry analysis confirmed MP release from VZV- and mock-infected HBVAF. The supernatants from cultured VZV-infected cells contained a significantly higher number of AnV+ particles per mL compared to control mock-infected cultures (Figure 4.9.): 70.16 x 10^4 (SEM 87.2 x 10^3), and 7.02 x 10^4 (SEM 1.3 x 10^3), respectively (n=3, p=0.001, unpaired t test).

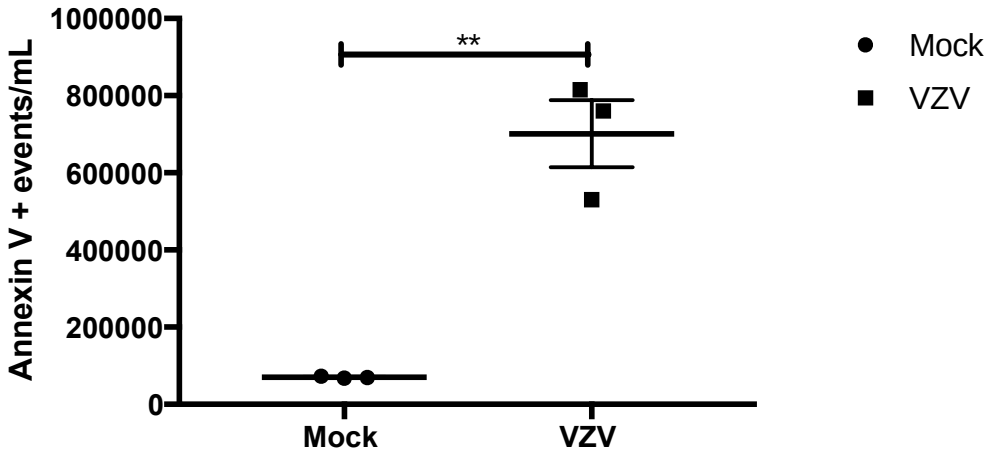

Figure 4.9. Enumeration of MP in culture supernatants of infected fibroblasts. *Culture supernatants collected on day 6 post infection with VZV or mock from HBVAF were subjected to centrifugation to separate the MP pellets. The pellets were stained with Annexin V-PERCP protein-fluorochrome and analysed by flow cytometry. In order to enumerate the MP, a suspension of 3μm diameter polystyrene beads was run in addition, and MP were defined as AnV + particles of less than 1μm in size. The supernatants of VZV-infected HBVAF contained a significantly higher number of MP compared to the supernatants of mock-infected HBVAF: 70.16 x 10^4 (SEM 87.2 x 10^3), and 7.02 x 10^4 (SEM 1.3 x 10^3), respectively (n=3, p=0.001, unpaired t test). *P<0.05, **P< 0.001, ***P< 0.001*

4.5.4.2. Study of endothelial activation and cellular oxidative stress in response to stimulation with MP derived from VZV-infected HBVAF

Having previously shown that media derived from VZV-infected HBVAF induce HUVEC activation and dysfunction, and having also confirmed the release of MP from infected HBVAF, I wished to further investigate the potential functional role of MP, and in the first instance to ascertain whether they could also induce endothelial changes.

As in the previous experiments of HUVEC stimulation with conditioned media, I now used MP suspended in media to stimulate HUVEC as outlined in the methods section of this chapter. Cellular oxidative stress was assessed by measuring the production of ROS, and endothelial activation was measured by assessing expression of CD54 using flow cytometry. The analysis showed that at 6 hours post incubation with MP, there was a significant difference in the CD54 MFI between HUVEC treated with MP isolated from VZV-infected or mock-infected populations: 8.04 (SEM 0.51) for co-incubation with MP from mock-infected cells compared with 15.70 (SEM 2.31) for VZV- infected, p=0.04, n=5 experiments (Figure 4.10). In addition, HUVEC treated for 30 minutes with MP derived from VZV-infected cells displayed an increased ROS production as demonstrated by a significantly increase in the mean DCF MFI (13.06, SEM 2.12), compared to HUVEC treated with MP isolated from mock-infected HBVAF (5.09, SEM 0.38), n=3 experiments, p=0.02 determined using t test (Figure 4.11).

With the knowledge derived from previous experiments that conditioned media contains cytokines and chemokines known to have effects on endothelial CD54 upregulation and increased oxidative stress, I wished to establish whether the MP pellets used to treat the HUVEC could possibly be contaminated by the cytokines from the media, and therefore confounding the results. In the next experiment, MP pellets harvested from supernatants of VZV-infected cells were separated, washed twice and next re-suspended in a small volume of fresh culture media as per methods used in the HUVEC stimulation experiment.

TNF-α, IL-6 and IL-8 were next measured using the MSD cytokine assay, and the results are presented in Figure 4.12. As controls I used conditioned media, and the fraction of the conditioned media obtained after centrifugation of MP. The levels of TNF-α, IL-6 and IL-8 were undetectable in the suspension of MP therefore excluding contamination of the pellets from the conditioned media.

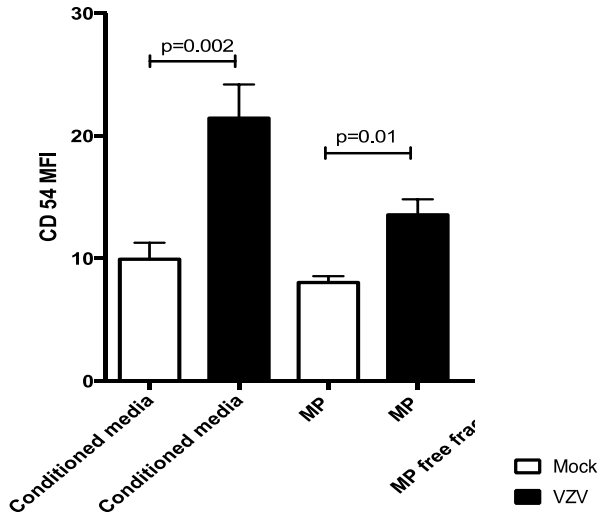

Figure 4.10. *MP* ***from VZV-infected HBVAF induce CD54 upregulation in HUVEC.*** *The MP fraction was harvested from conditioned media of VZV- and mock-infected HBVAF at 48 hours post infection by centrifugation, washed twice and incubated with HUVEC for 6 hours at 37^{o}C, in parallel with the control MP free fraction of the conditioned media, and with full conditioned media. The expression of CD54 adhesion molecule was analysed by flow cytometry. A significant increase in the mean CD54 MFI was detected by flow cytometry in the HUVEC treated with VZV-infected HBVAF derived MP compared to mock-infected HBVAF derived, with a mean CD54 MFI 8.04 (SEM 0.51) for co-incubation with MP from mock-infected cells compared with 15.70 (SEM 2.31) for VZV- infected (p=0.04, n=5 experiments, unpaired t test). *P<0.05, **P< 0.001, ***P< 0.001*

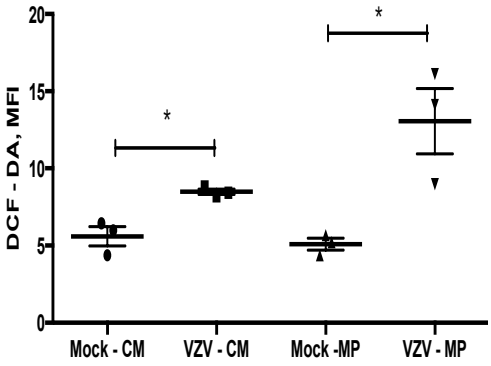

Figure 4.11. MP harvested from VZV-infected HBVAF stimulate ROS production in endothelial cells. *HUVEC were loaded with DCFH-DA and exposed for 60 minutes to MP and control MP-free fractions and full conditioned media derived from either VZV- or mock-infected HBVAF, or H2O2 and tBHP (positive controls). Oxidation-dependent fluorescence of DCFH-DA was determined by flow cytometry, and the results are expressed as mean and SEM of DCFH-DA MFI (n=3 experiments). There was a significant increase in the DCFH-DA MFI in HUVEC treated with MP harvested from VZV-infected HBVAF compared to HUVEC treated with MP harvested from mock-infected HBVAF: 13.06 (SEM 2.12) and 5.09 (SEM 0.38), respectively (n=3 experiments, p=0.02 determined using unpaired t test.*

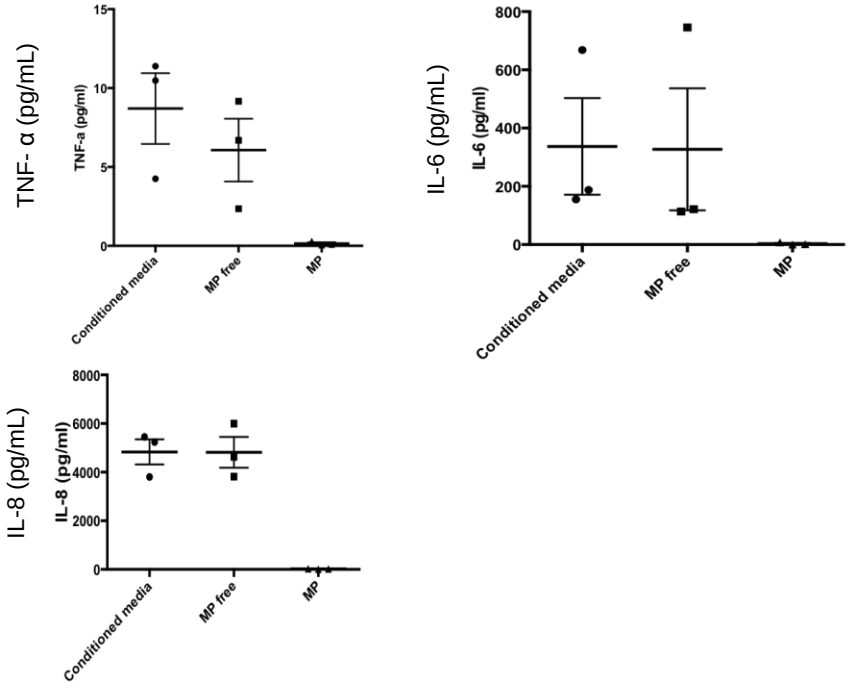

Figure 4.12. Study to assess for potential cytokine contamination of MP pellets isolated from culture supernatants of VZV-infected HBVAF.

No cytokine contamination was observed in the MP pellets obtained from culture supernatants of VZV-infected HBVAF. MP pellets isolated from culture supernatants of VZV-infected HBVAF at 48 hours post infection were washed twice in phosphate buffered saline and resuspended in fresh culture media. Cytokine levels (IL-6, IL-10, TNF-α) were analysed by electrochemiluminescence in three conditions: control conditioned media, the fraction of the conditioned media obtained after isolation of the MP pellet, and in the MP pellets samples prepared as above. The levels of IL-6, IL-8 and TNF-α in the MP samples were very low, suggesting no cytokine contamination (summary of n=3 experiments, data presented as mean and SEM). Mean IL-6 levels: conditioned media 336.9

pg/ml (SEM 287.5 pg/ml), MP pellets 3.19 pg/ml (SEM 3.93 pg/ml). Mean IL-8 levels: conditioned media 4830 pg/ml (SEM 894.9 pg/ml), microparticle pellets 23.3 pg/ml (SEM 9.59 pg/ml). Mean TNF-α levels: conditioned media 8.70 pg/ml (SEM 3.88 pg/ml), microparticle pellets 0.14 pg/ml (SEM 0.13 pg/ml).

In order to gain insight into the possible mechanisms by which HBVAF MP can alter the phenotype of endothelial cells in first instance and also contribute to the development of vasculopathy, I investigated the intriguing possibility that MP harbor VZV.

4.5.4.3. Flow cytometry analysis of MP derived from VZV-infected HBVAF

Emerging evidence suggests a role of extracellular vesicles in the transfer of pathogen-derived antigens and virulence factors. However, it is still unclear whether the release of extracellular vesicles from infected cells contributes to immune control and clearance of infection by the host or it could be a strategy employed by the pathogens for immune evasion.

As a first step towards ascertaining if the VZV was associated with the MP released from HBVAF, I used flow cytometry to analyse MP harvested from mock and VZV-infected cells for VZV protein detection. The MP were pelleted from equal volumes of media collected from mock and VZV-infected HBVAF seeded at the same densities. The analysis revealed that of the particles of size < 1000 nm pelleted from VZV-infected supernatants, a mean of 5.4 % (SEM

0.6032 %) co-expressed AnV and VZV GFP-ORF23 compared to a mean of 0.3082% (SEM 0.0572%) in the particles collected from mock-infected supernatants in n=5 experiments, p=0.001 (Figure 4.13, A). MP were enumerated and the absolute number per mL of culture supernatant was calculated. The culture media collected from VZV-infected cells contained a mean of 37.8 x 10^3 (SEM 4.7 X 10^3) MP, compared with 0.2 x 10^3 (SEM 0.004 x 10^3), p=0.001. This finding suggested that MP contained VZV proteins as indicated by detection of VZV GFP ORF23 viral protein.

The relatively low detectable percentage of VZV protein-expressing MP might reflect the fact that the total MP population is a mixture of MP released by the infected cells and by the uninfected cells, as not all the cells in the culture were infected at the time of the analysis. The uninfected cells may release MP in response to activation by the cytokines secreted by the infected cells, therefore diminishing the relative percentage of MP VZV+. However, when calculated, the absolute numbers of MP per mL released in response to VZV infection expressing viral antigens was increased 2-fold compared to the total number of MP/mL released by the uninfected cells.

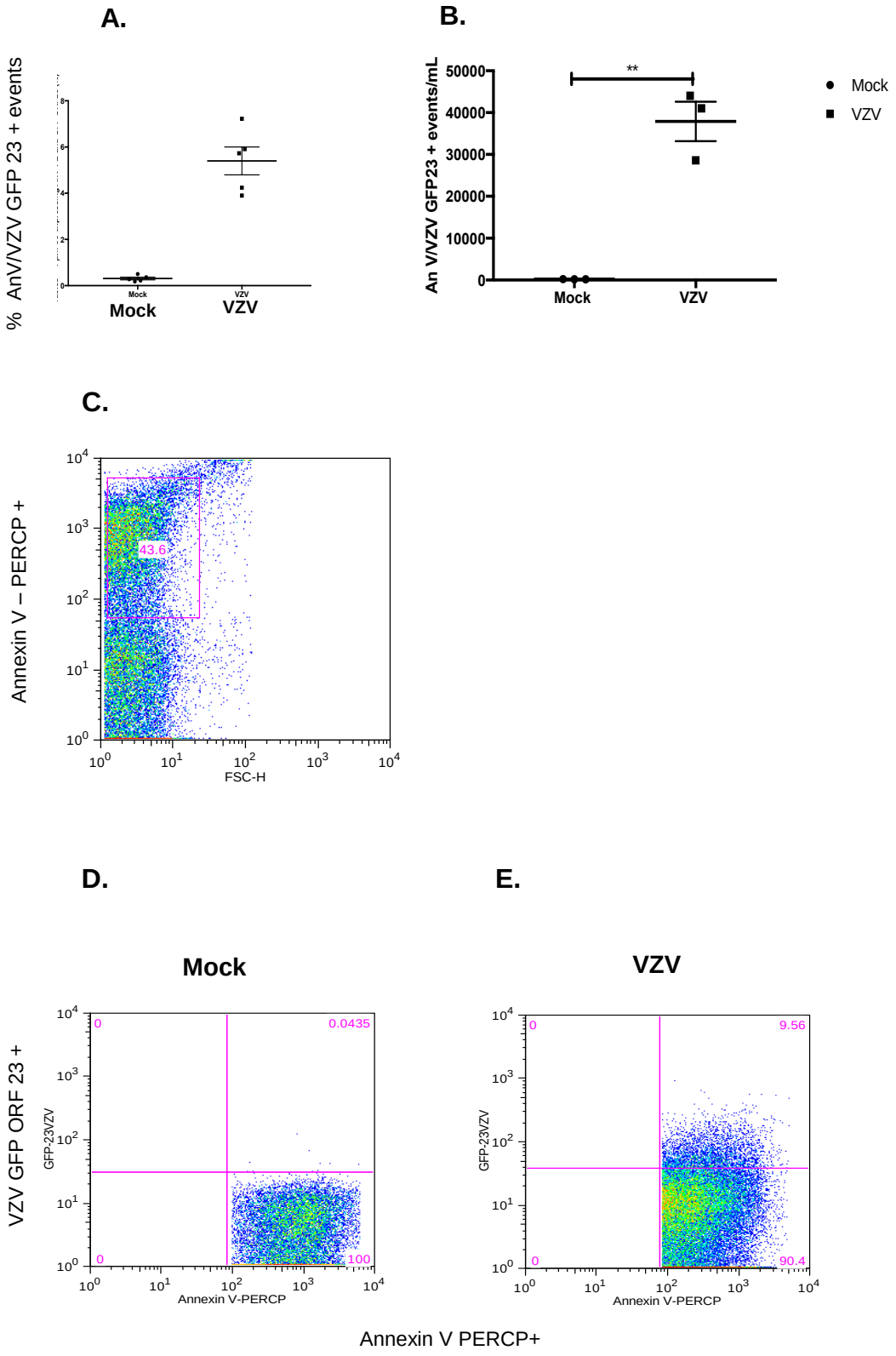
A.
% AnV/VZV GFP 23 + events
Mock
VZV
B.
An V/VZV GFP23 + events/mL
**
Mock
VZV
C.
Annexin V – PERCP +
43.6
FSC-H
D.
Mock
VZV GFP ORF 23 +
GFP-23VZV
0.0435
100
Annexin V-PERCP
E.
VZV
GFP-23VZV
9.56
90.4
Annexin V-PERCP
Annexin V PERCP+

Figure 4.13. MP released from VZV-infected HBVAF harbour viral proteins. ***(A)*** *Microparticles were harvested by sequential centrifugation from supernatants collected from mock- or GFP-ORF23 VZV-infected HBVAF and analysed using flow cytometry. A mean of 5.4 % (SEM 0.6032 %) of particles of size < 1000 nm collected from VZV-infected supernatants co-expressed AnV and GFP-ORF23 compared to a mean of 0.3082% (SEM 0.0572%) in the particles collected from mock-infected supernatants, n=5 experiments, p=0.001.* ***(B)*** *The absolute number of MP VZV GFP+ per mL of culture supernatant was calculated. The culture media collected from VZV-infected cells contained a mean of 37.8 x 10^3 (SEM 4.7 X 10^3) MP, compared with 0.2 x 10^3 (SEM 0.004 x 10^3), p=0.001.*

(C) *Flow cytometry dot plot demonstrating release of MP from VZV-infected HBVAF and the gating strategy. Representative flow cytometry plots of VZV GFP ORF23/Annexin V co-expression in MP harvested from mock* ***(C)*** *and VZV-infected HBVAF* ***(D)*** *at 4 days post infection with VZV GFP ORF23, demonstrating detection of VZV GFP ORF23 in the events Annexin V positive harvested from VZV- infected cells. *P<0.05, **P< 0.001, ***P< 0.001*

4.5.5. Mass spectrometric analysis of MP derived from VZV-infected HBVAF

MP are comprised by a plasma membrane surrounding a small amount of cytosol and contain a subset of cellular proteins. The proteome of MP may provide important pieces of information with regard to the condition of the original parent cells, such as what stimulated the cells and how the cells responded.

To confirm the presence of VZV proteins in the MP derived from the infected HBVAF, a mass spectrometric analysis was carried out to determine their protein composition.

72 proteins were identified in the MP pellets harvested from VZV-infected HBVAF, and 85 proteins in the pellets from mock-infected HBVAF. Also identified were 41 proteins unique to control MP from mock-infected cells, and 54 proteins unique to MP from VZV-infected cells. 31 proteins were detected as overlapping between the two experimental conditions (Figure 4.14.).

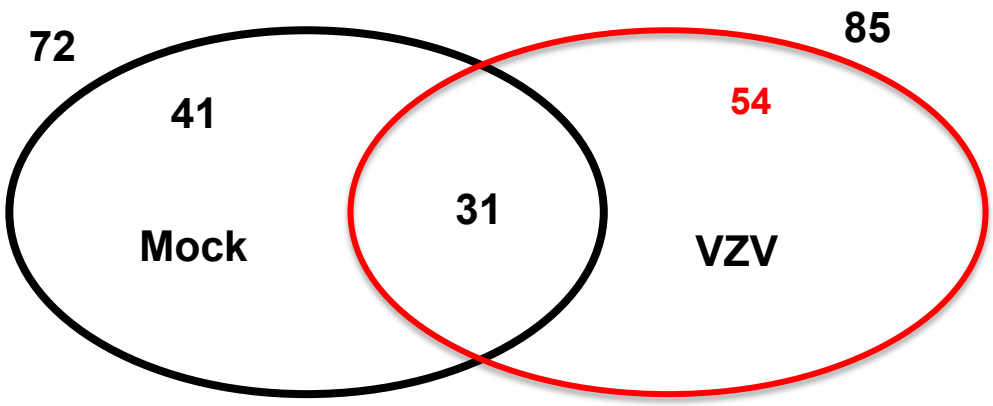

Figure 4.14. Venn diagram of number of proteins identified in MP from control mock-infected HBVAF and MP from VZV-infected HBVAF. *A total of 157 proteins were identified between the triplicates, of which 41 were unique to control MP, 54 were unique to MP derived from VZV-infected cells, and 31 were common between the two conditions. Proteins were identified in each MP population by liquid chromatography–mass spectrometry (LC/MS-MS) methods (n = 3 independent samples MP collected from mock-infected supernatants; n = 3 independent samples MP from VZV-infected supernatants).*

As shown in Table 4-2, the qualitative proteomic analysis of MP confirmed the presence of 10 VZV proteins in 3 independent samples collected from VZV-infected HBVAF. Viral proteins were not present; nor were they identified in the MP populations derived from 3 control mock-infected samples.

The 10 viral proteins identified in the pellets derived from the infected cells originated from all of three virion components: envelope (glycoprotein E,

glycoprotein I, glycoprotein B), tegument (IE62, VP22, UL47, cytoplasmic envelopment protein 2, serine/threonine-protein kinase UL13 homolog, tegument protein VP16 homolog), and nucleocapsid (major capsid protein) (Zerboni et al, 2014). These proteins are known to be abundant and possess important regulatory functions. For instance the IE62 is a major viral trans-activating factor encoded by ORF62 (Kinchington et al, 1992). gE is the most abundant envelope glycoprotein and together with glycoprotein I have been shown to boast a role essential for the spread of the infection (Howard et al, 2014). Lastly the tegument protein VP16 homolog encoded by ORF10 is an activator of lytic infection (Kinchington et al, 1992).

Table 4-2. Viral proteins identified in microparticle pellets derived from Varicella zoster virus-infected human brain vascular adventitial fibroblasts by mass spectrometry

Protein accession	**Protein name**	**Gene**	**Function**	**Localization**	**Peptides number (median)**	**Coverage (median)**
P09272	Tegument protein VP22	ORF 9	Participates in both the accumulation of viral mRNAs and viral protein translation at late time of infection. Modulates the RNase activity of the virion host shutoff protein ORF17 probably to ensure necessary levels of key cellular mRNAs and proteins. Plays a role in microtubule reorganization that occurs after viral infection by stabilizing microtubule network.	Tegument One of the most abundant tegument protein (about 2000 copies per virion) .	17 (range 13-24) *detected in 3 samples*	56.29% (range 51.32% - 77.48%)
P09310	Immediate-early protein 62	ORF62	Transcriptional transactivator. May interact with and recruit specific components of the general transcription machinery to viral promoters and stabilize their formation for transcription initiation. Negatively regulates its own transcription. This immediate early (IE) protein may be necessary in virion for viral pathogenesis	Tegument	38 (25-65) *detected in 3 samples*	32.98% (29.39% - 59.47%)

	Major viral transcription factor ICP4 homolog					
P09259	Envelope glycoprotein E	gE ORF68	Envelope glycoprotein that binds to the potential host cell entry receptor IDE. In epithelial cells, the heterodimer gE/gI is required for the cell-to-cell spread of the virus, by sorting nascent virions to cell junctions. Once the virus reaches the cell junctions, virus particles can spread to adjacent cells extremely rapidly through interactions with cellular receptors that accumulate at these junctions. Implicated in basolateral spread in polarized cells. In neuronal cells, gE/gI is essential for the anterograde spread of the infection throughout the host nervous system. Together with US9, the heterodimer gE/gI is involved in the sorting and transport of viral structural components toward axon tips (By similarity).By similarity The heterodimer gE/gI serves as a receptor for the Fc part of host IgG. Dissociation of gE/gI from IgG occurs at acidic pH. May thus be involved in anti-VZV antibodies bipolar bridging, followed by intracellular endocytosis and degradation, thereby interfering with host IgG-mediated immune responses (By similarity).	Envelope	14 (12-16) *detected in 2 samples*	37.96% (33.87% - 42.05%)
P09258	Envelope glycoprotein I	gI	In epithelial cells, the heterodimer gE/gI is required for the cell-to-cell spread of the virus, by sorting nascent virions to cell junctions.	Envelope	11.5 (7-16) *detected in 2*	25.56% (17.51% - 33.62%)

			Once the virus reaches the cell junctions, virus particles can spread to adjacent cells extremely rapidly through interactions with cellular receptors that accumulate at these junctions. Implicated in basolateral spread in polarized cells. In neuronal cells, gE/gI is essential for the anterograde spread of the infection throughout the host nervous system. Together with US9, the heterodimer gE/gI is involved in the sorting and transport of viral structural components toward axon tips (By similarity).By similarity The heterodimer gE/gI serves as a receptor for the Fc part of human IgG. Dissociation of gE/gI from IgG occurs at acidic pH. May thus be involved in anti-VZV antibodies bipolar bridging, followed by intracellular endocytosis and degradation, thereby interfering with host Ig-mediated immune responses (By similarity)		*samples*	
P09263	Tegument protein UL47 homolog	ORF11	Tegument protein that can bind to various RNA transcripts. Plays a role in the attenuation of selective viral and cellular mRNA degradation by modulating the activity of host shutoff RNase ORF17/VHS. Plays also a role in the primary envelopment of virions in the perinuclear space, probably by interacting with two nuclear egress proteins ORF24 and ORF27	Tegument Major tegument protein of the virion. Undergoes nucleocytoplasmic shuttling during infection. Localizes to the major sites of transcription in the	31 *detected in 1 sample*	36.62%

				infected cell nucleus.		
P09257	Envelope glycoprotein B	gB	Envelope glycoprotein that forms spikes at the surface of virion envelope. Essential for the initial attachment to heparan sulfate moieties of the host cell surface proteoglycans. Involved in fusion of viral and cellular membranes leading to virus entry into the host cell. Following initial binding to its host receptors, membrane fusion is mediated by the fusion machinery composed at least of gB and the heterodimer gH/gL. May be involved in the fusion between the virion envelope and the outer nuclear membrane during virion egress.	Envelope	22 (18-26) *detected in 2 samples*	24.81% (20.09% 0 29.54%)
P09293	Cytoplasmic envelopment protein 2	ORF44	Plays a critical role in cytoplasmic virus egress. Participates in the final step of tegumentation and envelope acquisition within the host cytoplasm by directly interacting with the capsid. Upon virion binding to target cell, a signaling cascade is triggered to disrupt the interaction with the capsid, thereby preparing capsid uncoating.	Tegument Localizes in the host nucleus up to 18 hours post-infection, but at later times localizes to punctate, cytoplasmic structures.	5 *detected in 1 sample*	24.79%
P09245	Major capsid protein	MCP	Self-assembles to form an icosahedral capsid with a T=16 symmetry, about 200 nm in diameter, and consisting of 150 hexons and 12 pentons (total of 162 capsomers). Hexons	capsid	25 *detected in 1*	29.15%

			form the edges and faces of the capsid and are each composed of six MCP molecules. In contrast, one penton is found at each of the 12 vertices. Eleven of the pentons are MCP pentamers, while the last vertex is occupied by the portal complex. The capsid is surrounded by a layer of proteinaceous material designated the tegument which, in turn, is enclosed in an envelope of host cell-derived lipids containing virus-encoded glycoproteins.		*sample*	
P09296	Serine/threonine-protein kinase UL13 homolog	ORF47	Multifunctional serine/threonine kinase that plays a role in several processes including egress of virus particles from the nucleus, modulation of the actin cytoskeleton and regulation of viral and cellular gene expression. Regulates the nuclear localization of viral envelopment factor proteins 24 and 27, by phosphorylating the protein kinase ORF66, indicating a role in nuclear egress. Disrupts host nuclear lamins, including LMNA and LMNB1. Phosphorylates the viral Fc receptor composed of glycoproteins E (gE) and I (gI) (By similarity). Phosphorylation of glycoprotein E (gE) by UL13 alters its subcellular localization, from the host early endosome to the plasma membrane. Participates in the transcriptional regulation of cellular and viral mRNAs mainly by phosphorylating the viral transcriptional regulator IE63	Tegument	7.5 *detected in 1 sample*	20% (16.86% - 23.14%)
	Tegument protein VP16	ORF10	Transcriptional activator of immediate-early (IE) gene products (alpha genes). Acts as a key activator of lytic infection by initiating the	Tegument	8 *detected in 1*	26.10%

	homolog		lytic program	Host nucleus	*sample*	

Moreover, MP as vesicles transferring biological signals and information should contain proteins playing a role in essential biological processes. Among the proteins, for example, there were proteins (Tubulin alpha-1AC, actin cytoplasmic 1) involved in cell adhesion, cell junction or leukocyte trans-endothelial migration, which are key proteins in the processes of endothelial high permeability and capillary leak. Human Annexin A2 was one of the top proteins identified in all samples, both mock-infected and VZV-infected. Information from UniProt Knowledgebase reveals that Annexin A2 may cross-link plasma membrane phospholipids with actin and the cytoskeleton and be involved with exocytosis, and that it positively regulates the vesicle fusion. Reflecting this role, HBVAF MP with Annexin A2 will tend to fuse with other cells and may have play biological roles. In addition, it was confirmed that annexin A2 is capable of assembling plasminogen and has a positive effect on vascular fibrinolysis (Dasah et al, 2009; He et al, 2010).

Research on platelet MP has shown that the mechanism of production and release of MP concerns the alteration of the cytoskeleton (Hugel et al, 2005). Three proteins associated with cytoskeletal structure (vimentin, actin cytoplasmic 1 and tubulin β chain) were identified amongst the top hits in my dataset. Human fibronectin was another protein present amongst the top hits in all samples. Fibronectins are involved in cell adhesion, cell motility, opsonization, wound healing, and maintenance of cell shape (UniProt KnowledgeBase).

Interestingly, amongst the proteins identified exclusively in the MP derived from VZV-infected HBVAF were the human histones H4, H3 and H2. Noubouossie et al have recently shown that single histone proteins such as Human histone H3 and H4 purified from normal human neutrophils induce thrombin generation in a platelet-dependent manner and promote coagulation activation (Noubouossie et al, 2017). This finding suggested that therapeutic strategies could be directed against specific structures such as histone proteins.

4.5.6. Transmission electron microscopy study of MP shed by VZV-infected HBVAF

To gather morphological information on the structure of MP released from VZV-infected HBVAF and investigate whether they harbor VZV virions as suggested by flow cytometry and mass spectrometry findings, I next progressed to direct imaging of the MP pellets using transmission electron microscopy (TEM).

Due to their nanometric size, MP are at the lower limit of resolution for confocal or fluorescence microscopy, which cannot detect the details of these particles, but can (in the best case scenario) detect larger particles above 200 nm. TEM and scanning electron microscopy (SEM) have both been used to visualise MP (Heijnen et al, 1999; Coombes et al, 1999; Pisitkun et al, 2004). However, TEM is the only technique which delivers clear images of viruses due to their small size. TEM has been used in clinical virology for discovery of many viruses and the diagnosis of various viral infections, although over time has gradually been replaced by PCR in routine clinical practice. In research, TEM continues to contribute to studies of viral assembly and investigations of virus—host cell interactions (Roingeard P, 2008).

MP pellets were prepared for microscopy as outlined in the methods of this chapter, and in addition the MP free supernatants were subjected to ultracentrifugation to obtain control pellets possibly containing viral particles. Samples were transferred to the electron microscopy facility on ice and examined

fresh, after negative staining. Negative staining is an easy and rapid method for examining the structure of individual organelles and viruses at the electron microscopy level. However, the method does not allow a high resolution examination of samples. Also, because negative staining involves deposition of heavy atom stains, structural artefacts such as flattening of spherical structures are common. The staining and drying procedures in preparing the specimens probably alter much of the particles dimensions (Issman et al, 2013). Nevertheless, negative staining is a very useful technique because it requires no specialized equipment other than that found in a regular TEM laboratory.

MP pellets were collected from culture supernatants of VZV- and mock-infected HBVAF following sequential centrifugation as previously published and detailed in the methods. In addition, the conditioned media removed after pelleting the MP and prior to the MP washing step was collected and subjected to a further ultracentrifugation step to collect the structures with a size below 100 nm, and the pellets were analysed fresh unfixed by TEM for the presence of free virions. In summary, three materials were visualized using TEM: MP derived from VZV-infected HBVAF, control MP derived from mock-infected HBVAF, and control pellets of structures below 100 nm obtained from the supernatants of VZV-infected HBVAF.

Overall, 80 electron micrographs were examined from 3 sets of infection cycles. Most of the particles were collapsed donut shaped, with dimensions of 100–400 nm (Figure 4.15 A). As expected in light of the flow cytometry findings, the

material collected from mock-infected HBVAF had a lower number of MP compared to the material collected from VZV-infected HBVAF, and this was evident in all the electron micrographs obtained at 93000x magnification, where more MP were captured in each field. A very low number of VZV particles were identified in the material obtained after ultracentrifugation, however the TEM study of these few particles enabled me to familiarize with the EM appearance of the virus and also establish a control for the identification of the virus in the MP material. In these images, the viral particles had a diameter of around 80 nm, and on close inspection had the appearance of a hexagon with surface projections. No envelope was seen, therefore it is possible that these structures are viral nucleocapsids.

The EM MP material obtained from VZV-infected HBVAF contained a majority of MP with an appearance identical to that of the MP visualized in the control samples. In addition, in these samples, a group of MP were identified with entrapment of virus inside MP membrane coats (Figure 4.15, B,C). The viral particles were discernible in the MP structures partially penetrated by the stain.

In summary, the ultrastructural analysis of MP released by VZV-infected HBVAF revealed that a fraction of them contained virus cloaked in MP. VZV particles were observed by electron microscopy with negative staining using uranyl acetate closely associated with pelleted MP. With regards to this finding, my next question was whether VZV could take advantage of MP to facilitate its spread.

These experiments, however, are not without limitations. Other than negative staining of the MP, the generation of ultra-thin sections and TEM analysis could have provided additional extremely valuable details. In an initial attempt to pellet the MP on filters and generate sections, the analysis proved very challenging as many MP were lost, and sectioning the filter proved difficult.

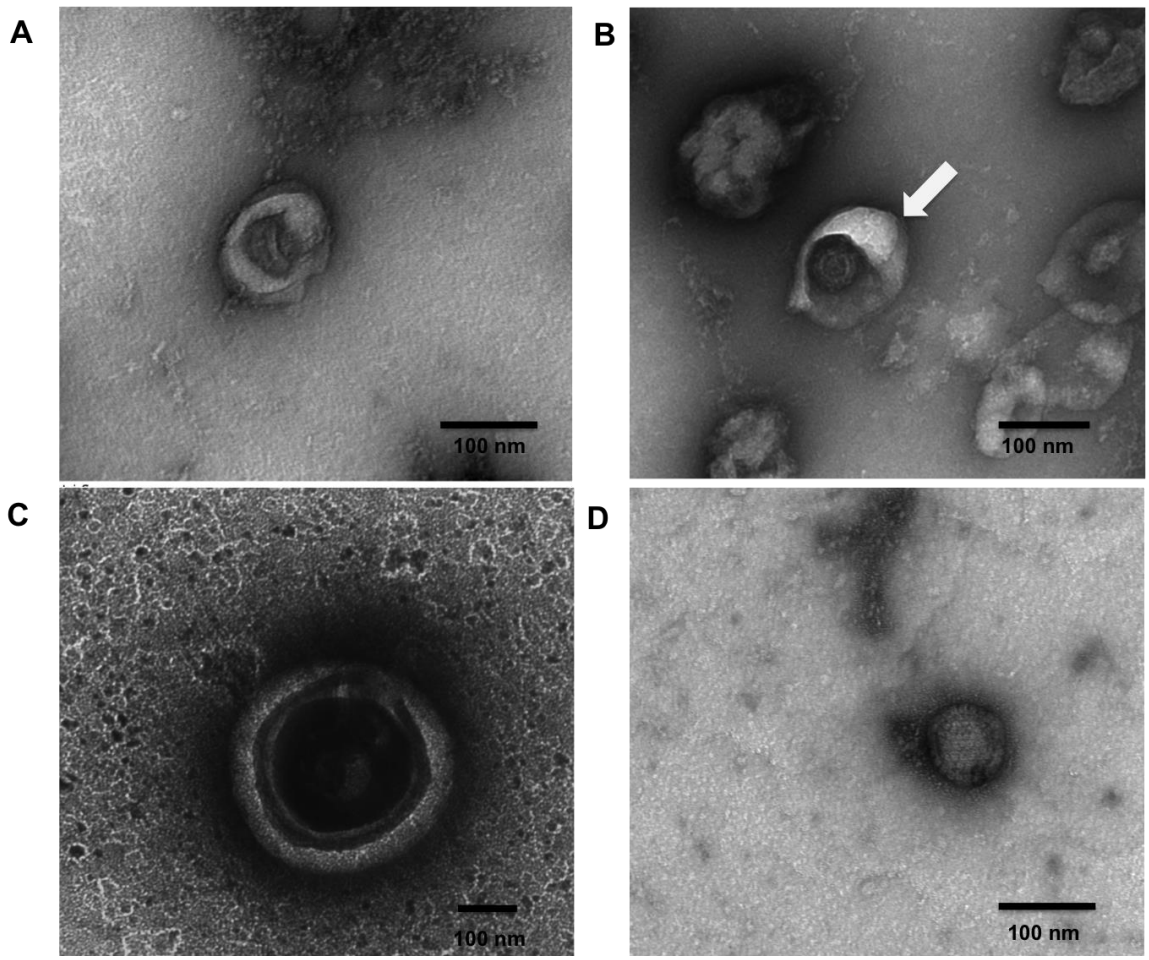

Figure 4.15. Representative transmission electron micrographs of MP in mock or VZV-infection experiments

MP pellets were collected from culture supernatants of VZV- and mock-infected HBVAF following sequential centrifugation to remove apoptotic bodies and cell debris, and further centrifuged at 15000G with one washing step. The conditioned media collected after centrifugation of MP was subjected to ultracentrifugation, and the pellets were examined for the presence of VZV particles. The TEM images were obtained with the JEOL 1010 microscope at 135000 X Mag (A,B,D) and 95000 X Mag (C). Scale bar 100nm.

Figure A *shows the appearance of a MP shed by mock-infected HBVAF. The staining and drying likely altered the MP dimensions, and they appear collapsed, donut shaped, with a diameter of approximately 100 nm as shrinkage may have occurred.* ***Figure B*** *represents an MP (arrow) harvested from VZV-infected HBVAF and closely associated with a viral particle. The MP is likely penetrated by the stain therefore making the presence of VZV virions distinguishable.* ***Figure C****. MP with a diameter of 400 nm reveals a central spherical structure of approximately 80 nm diameter likely with surface spikes, surrounded by a membrane which is possibly the viral envelope.* ***Figure D.*** *Very few free viral particles were identified in the pellets obtained after ultracentrifugation of conditioned media collected after pelleting the MP, of which the nanostructure was studied and images obtained as control. Representative TEM image of a free VZV particle measuring approximately 80 nm in diameter, partially penetrated by the stain, with the appearance of a hexagon with surface projections (viral nucleocapsid). No envelope was identified outlining the nucleocapsid.*

4.5.7. Productive infection of HBVAF by MP from VZV-infected cells

To investigate the functional role of MP in the transmission of infection, I isolated MP from VZV-infected cells and incubated them with naive HBVAF cells. The experiments were performed using MP derived from HBVAF cultures infected with GFP VZV ORF23 or VZV wild type. Infection was assessed by flow cytometry, looking at the expression of GFP ORF23 or VZV IE23 protein when infected with the wild type virus, in addition to monitoring for cytopathic effect and green fluorescence.

As shown in Figure 4.16, 4-6 days after exposure to VZV-positive MP, HBVAF stained positive for VZV IE62 protein by flow cytometry, in addition to displaying cytopathic effect and/or green fluorescence when infected with MP derived from cultures infected with GFP VZV ORF23-tagged virus. When the cultures were visualized within hours post infection, no fluorescence was seen. On day 2 post infection, a few small areas of green fluorescence were identified, and within the next 3-4 days the fluorescence in the areas previously identified started spreading locally suggesting that the infected cells spread the infection to the nearby cells. In addition, new small but discernible areas of fluorescence became visible at distance from the ones previously identified, suggesting that these areas could possibly be secondary focuses of infection. On day 6 post infection, I estimated the green fluorescence as less than 10% of the culture dish area.

The flow cytometry analysis showed that on day 6 post infection, a mean of 4.94% (SEM 1.1) cells expressed GFP ORF 23 in the cultures incubated with MP derived from VZV-infected HBVAF, compared to 0.23% (SEM 0.06) in the cultures incubated with MP derived from mock-infected HBVAF; summary of 5 experiments, p=0.005 (Figure 4.16).

The small percentage of infected cells found was not unexpected. The extent of *in vitro* VZV infection is dose-dependent; we know that the larger the dose of the inoculated virus is introduced, the more extensive infection it elicits. When incubating the cultures with MP pellets derived from VZV-infected HBVAF (therefore mixed population of MP shed by infected and uninfected cells), the viral pfu could not be estimated and therefore the MOI was unknown. From the previous experiments, approximately 5% of MP expressed viral proteins and similarly less than 10% of the MP visualized by TEM contained virus cloaked in their membranes. Therefore it is likely that a larger inoculum of MP pellets (therefore associated with a higher number of viral particles) might have produced a more extensive infection.

In additional experiments I incubated the MP collected from VZV-infected HBVAF with healthy HBVAF in the presence or absence of heparin, an inhibitor viral attachment to the cells, as described in the methods of this chapter. These experiments showed no difference in the infection efficiency between HBVAF cultures infected with MP in the presence or the absence of heparin.

In conclusion, I demonstrated that MP can facilitate productive infection in HBVAF in addition to entrapping viral particles.

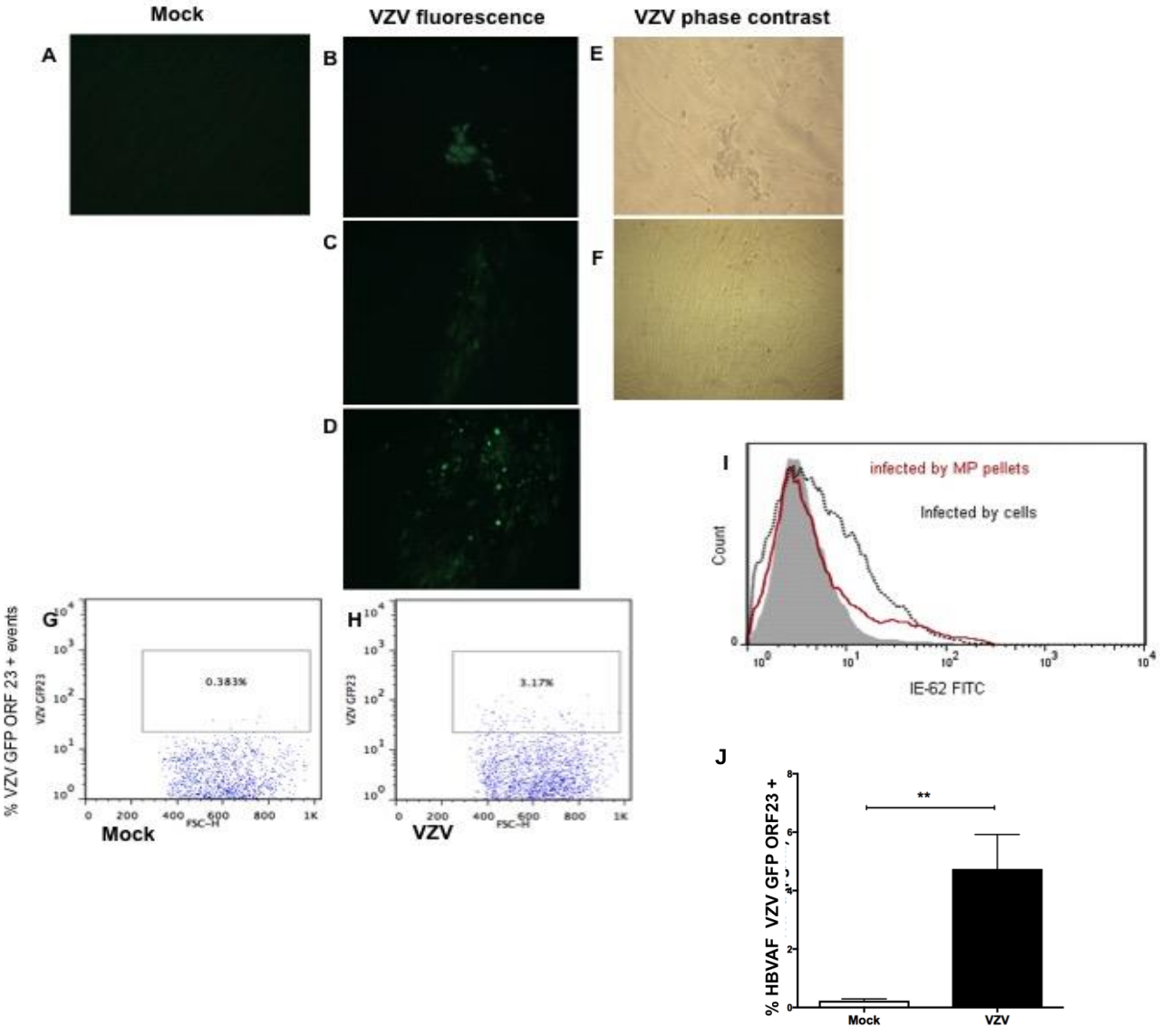
Mock
VZV fluorescence
VZV phase contrast
A
B
C
D
E
F
G
H
I
J
% VZV GFP ORF 23 + events
0.383%
3.17%
Mock
VZV
infected by MP pellets
Infected by cells
Count
IE-62 FITC
% HBVAF VZV GFP ORF23 +
**
Mock
VZV

Figure 4.16. MP derived from VZV-infected HBVAF can facilitate infection of healthy cells. (A-I). *Phase contrast and fluorescence microscopy images (200x magnification) of quiescent HBVAF co-cultured with MP harvested on day 5 post infection (p.i.) from VZV GFP ORF23 infected HBVAF (images obtained on day 6 p.i.). The MP free media obtained after the separation of MP fraction was incubated with HBVAF under the same experimental conditions and used as a control.* ***Figures B, C and D*** *demonstrate green fluorescence representing GFP ORF 23 tagged VZV-infected HBVAF, while* ***Figures E and F*** *show in the same fields' cytopathic effect in phase contrast microscopy, confirming infection. No fluorescence was detected in HBVAF incubated with MP harvested from mock-infected HBVAF, or MP free fractions of conditioned media from mock or VZV-infected HBVAF (Figure A).* ***(G-I).*** *Flow cytometry plots of VZV GFP ORF23 expression at 4 days post infection in quiescent HBVAF incubated with MP derived from supernatants of mock-infected HBVAF* ***(G),*** *VZV infected HBVAF* ***(H).*** *VZV GFP ORF23 positive cells were detected in the population incubated with MP harvested from VZV-infected HBVAF, and no VZV GFP ORF 23 positive cells were identified in the population incubated with mock-derived MP.* ***(I).*** *Histogram demonstrating comparable VZV IE62 expression levels in HBVAF infected with MP collected from VZV infected HBVAF (red) and by cell to cell infection (black dotted line).* ***(J)*** *The graph summarises the results of 5 flow cytometry experiments which investigated the expression of VZV GFP ORF23 in HBVAF incubated with MP from mock- or VZV-infected cultures. The cells were analysed on day 6 post infection; a mean of 4.94% (SEM 1.18%) cells expressed VZV GFP ORF 23 in the cultures incubated with MP derived from VZV-infected HBVAF, compared to*

*0.23% (SEM 0.06) in the cultures incubated with MP derived from mock-infected HBVAF; summary of 5 experiments, p=0.005. *P<0.05, **P< 0.001, ***P< 0.001*

4.5.8. Circulating MP in plasma from children with VZV-related AIS

Low levels of circulating MP in blood help maintain homeostasis, whereas increased MP generation of cell-derived MP is linked to many pathological conditions such as cardiovascular, rheumatic, diabetes, arterial ischaemic stroke and other (Eleftheriou et al, 2012; Thulin et al, 2016; Deng et al, 2016). Subpopulations of MP are promising biomarkers for improving risk prediction, as well as monitoring treatment.

Punyadee *et al* demonstrated that MP provide a novel biomarker to predict severe clinical outcomes of Dengue virus infection (Punyadee et al, 2016). In this study, elevated levels of red blood cell-derived MP directly correlated with disease severity, whereas a significant decrease in platelet-derived MP was associated with a bleeding tendency.

In a preliminary study MP were analysed by flow cytometry for the presence of VZV gH protein, in children with VZV-related AIS, children with other arteriopathies and healthy adult controls. VZV-related AIS was defined as AIS occurring within 12 months post Varicella infection. Acute phase plasma samples from 3 children with VZV-related AIS, 5 children with other arteriopathies were analysed, together with 10 samples from adult controls. The median time from Varicella to AIS was 8 months (range 5-11 months). Two patients had monophasic disease with MCA stenosis, and one had involvement of MCA and

posterior cerebral artery (PCA) with recurrence of symptoms shortly after the initial presentation. All samples were stored in the -80C freezer prior to analysis. MP were identified according to their standard size and AnV labeling as described in methods, and duplicates of each sample were prepared and analysed.

The samples were thawed, MP isolated and stained for the detection of AnV and VZV gH protein as outlined in the methods section.

Circulating MP levels in the plasma of children with VZV-related AIS or other arteriopathies and healthy adult controls were compared. Total AnV+ MP were higher in the 3 children with stroke recurrence, at 491 x 10^3 /mL (n=3) compared to those children with AIS in the context of other arteriopathies 362.01 x 10^3 /mL (n=5) and healthy controls 97.33 x 10^3 /mL (n=10); p=0.14 and p=0.07, respectively, by Mann Whitney test (Figure 4.17).

When co-stained for the detection of VZV gH, a significantly higher number of AnV/gH MP were present in plasma from children with VZV-related AIS 14.48 x 10^3 (n=3), compared to children with other arteriopathies 1.54 x 10^3 (n=5) or healthy adult controls 0.87 x 10^3 (n=10); p=0.03 and p=0.007, respectively, Mann Whitney test.

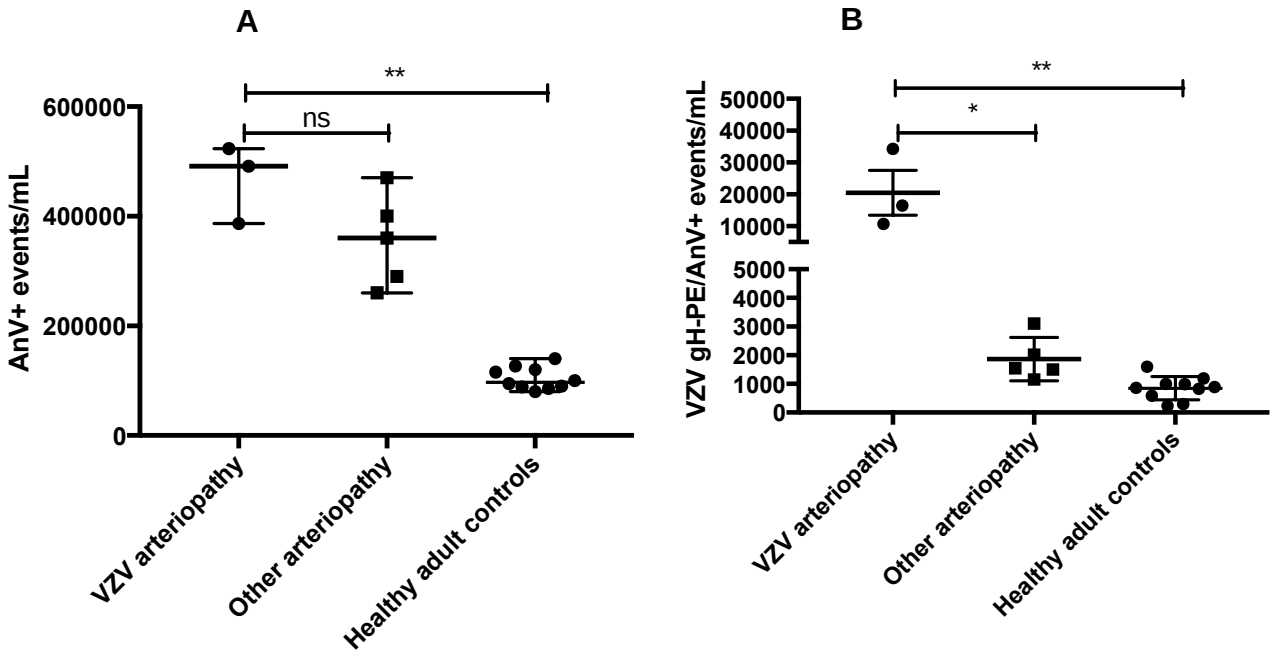

Figure 4.17. Circulating MP in children with VZV-related AIS. (A)*Total Annexin V+ microparticles (MP) were elevated in children with VZV related AIS compared to those with other arteriopathies (p=0.14) and healthy adult controls (p=0.07)* ***(B)*** *A significantly higher number of AnV/gH + events were detected in the group of children with VZV-related AIS compared to children with other arteriopathies (P=0.03) and healthy adult controls (p=0.007).*

**P<0.05, **P< 0.001, ***P< 0.001 with Mann Whitney test.*

4.6. Discussion

To determine whether VZV infection induces changes in HBVAF that in turn affect neighbouring cells such as endothelial cells, I undertook a number of experiments and was able to demonstrate that conditioned media from mock-infected or VZV-infected HBVAF (collected at 48 hours post infection) induced upregulation of CD54 expression and ROS production in cultured HUVEC. Next, I showed that VZV-infected HBVAF released several cytokines/chemokines that could contribute to the pathogenesis of cerebral arteriopathy. I then explored whether some of these effects could be part mediated by MP release; flow cytometry analysis of MP released by VZV-infected HBVAF revealed that they express VZV proteins, and the presence of viral antigens in MP was also confirmed by mass spectrometry. These MP were also able to induce infection when co-incubated with healthy HBVAF, and TEM confirmed the presence of viral particles associated with MP in supernatants harvested from VZV-infected cells.

The cytokine secretion profiling of infected HBVAF strongly indicated an increased secretion of proinflammatory cytokines by the VZV-infected cells, with potential implications for cell-to-cell interactions. It has been shown that myofibroblasts exhibit a secretory phenotype, and are capable of producing

proinflammatory chemokines and prostaglandins (Eyden et al. 2001). IL-6 has been shown to modulate fibroblast differentiation and motility in dermal fibroblasts from IL-6-deficient mice in a number of studies (Luckett and Galluci. 2007; Galluci et al. 2006; Galluci et al. 2007) possibly by inhibition of matrix metalloproteinases (MMP) function, and the induction of TGF-beta genes. Another study demonstrated that IL-6 influences cardiac fibroblast proliferation in a paracrine manner (Fredi et al. 2005). IL-6 signaling also increases the expression of endothelial leukocyte adhesion molecules like CD54 further promoting leukocyte accumulation (Wung et al. 2005). In a small study. Tang XL *et al.* showed that IL-6 upregulates the expression of tissue factor on HUVEC, with potential implications on coagulation disorders (Tang et al. 2006). IL-6 also induces smooth muscle cell migration and proliferation (Nabata et al, 1990), which could contribute to myofibroblast accumulation in the thickened intima of VZV-infected cerebral arteries. In addition, IL-8 is a potent chemoattractant for neutrophils, leukocytes, and has been shown to reduce the focal adhesions and promote a motile behavior in primary fibroblasts. Moreover, TNF- α stimulates IL-8 secretion in fibroblasts (Dunlevy and Couchman. 2002). This could explain the observation regarding abundance of neutrophils in cerebral arteries in early VZV vasculopathy (Nagel et al, 2013) and in the CSF of patients with VZV inflammatory brainstem disease (Haug et al, 2010).

In a recently published study, Jones et al. measured the levels of cytokines and matrix metalloproteinases in the CSF of adult patients with confirmed VZV-

related vasculopathy, and found that the levels of IL-8, IL-6 and MMP-2 were significantly elevated compared to the levels detected in healthy controls or patients multiple sclerosis (Jones et al, 2016). My results in this experimental *in vitro* set up are also in keeping with their findings in these human studies. In addition, levels of IL-8 were recently shown to be elevated in the circulation of patients with GCA during corticosteroid taper or active GCA. Also MMP-2 was shown to be elevated in temporal artery biopsies and in the aorta of patients with GCA, a disease that has recently emerged as a possible extracranial VZV vasculopathy (Nagel et al, 2013). So all these studies show a similar cytokine profile in human studies to the specific cytokine profile I identified in my *in vitro* experiments in association with VZV-induced HBVAF activation and differentiation.

Notably, infected HBVAF may be interacting with neighboring uninfected HBVAF or endothelial cells, and change their profiles towards inflammation and vascular remodeling, perhaps unsurprising since fibroblasts in general are known to exert immunomodulatory influence in a paracrine fashion. Smith *et al.* defined fibroblasts as “sentinel cells”, capable of switching to a proinflammatory phenotype by secreting proinflammatory cytokines and controlling leukocyte infiltration (Smith et al. 1997). Paracrine inflammatory signalling from infected HBVAF may therefore stimulate endothelial cells to intensify inflammation through the production of cytokines/chemokines and upregulation of adhesion molecules such CD54.

Endothelium is also an important active participant in inflammation as well as the target of inflammatory triggers. In healthy resting states, endothelial cells prevent leukocyte adhesion and “unwanted”, unnecessary inflammatory responses. However, external triggers can initiate the expression of adhesion molecules on endothelial cells, mediating leukocyte recruitment and adhesion to the arterial wall. Monocyte chemotactic protein-1 (MCP-1) is a chemokine that regulates the migration and infiltration of monocytes and macrophages into the site of inflammation. In addition, MCP-1 has been shown to increase proliferation and IL-6 production by vascular smooth muscle cells (Viedt et al. 2002), which could be relevant in the context of vascular remodeling. MCP-1 can also stimulate collagen expression and upregulate TGF-β expression in fibroblasts, with potential implications for fibroblast differentiation (Gharaee- Kermani et al. 1996), and hence, in this context, arterial inflammation and remodelling. Taken together, these data suggest that VZV-infected HBVAF can switch to a proinflammatory phenotype and trigger endothelial activation through a paracrine fashion, in line with other studies that have reported that fibroblasts induce inflammatory responses in a paracrine manner.

The aforementioned inflammatory mediators are of course are not the only relevant cytokines that may contribute to the pathogenesis of VZV related cerebral arteriopathy. Type I and type II interferons; and macrophage inflammatory protein 1-alpha (MIP-1-α) are also likely to be highly relevant in the

crosstalk between endothelium and fibroblasts in other disease states (Steinhauser et al. 1998; Zimmerman et al. 1999; Maiellaro et al. 2007; McGettrick et al. 2009; McGettrick et al. 2009).

Having demonstrated that the conditioned media from VZV-infected HBVAF elicits a switch to a pathological proinflammatory phenotype in HUVEC, the next step was to examine individually, the relative contribution of the soluble and insoluble fractions of this conditioned media. Of particular interest was to characterize the role of HBVAF-derived MP in the communication between the VZV-infected HBVAF and endothelial cells.

Very few studies had examined the role of MP as potential mediators of infection propagation. Kadiu *et al* demonstrated that MP and exosomes facilitate transfer of HIV and viral components from infected macrophages to nearby uninfected cells (Kadiu et al. 2012). In other studies, constituents of Mycobacterium tuberculosis and Toxoplasma gondii were located within exosomes after microbial infection (Sweet et al. 2008; Singh 2011; Bhatnagar et al. 2007; Schorev and Bharnagar. 2008; Schorev et al. 2008).

As MP have been shown to transfer important biological information from cell to cell, I considered exploring their possible role in the crosstalk between VZV-infected HBVAF with endothelial cells. I therefore explored whether some of the effects I could see detect in HBVAF could be part-mediated by MP release. I

was able to show, for the first time, that supernatants from cultured VZV cells contained a significant number of AnV+ MP compared to control. MP released by VZV-infected HBVAF were shown to stimulate CD54 upregulation and ROS production in endothelial cells.

One other particularly interesting and novel observation I have made is that MP released by VZV-infected HBVAF are associated with viral particles that are capable to productively infect healthy cells. This could suggest an entirely new model of VZV cell to cell viral dissemination, of considerable relevance to the pathogenesis of cerebral arteriopathy and other VZV-associated vasculopathies, but also of primary VZV infection and virus propagation as well.

VZV is recognized as a highly cell-associated virus in culture, which expresses a range of glycoproteins that have a role in cell–cell fusion and syncytia formation (gH/gL complex, gE, gB), regarded as the hallmark of cell-to-cell transmission of virus. Studies have suggested that fusion-induced VZV cell-to-cell spread is significantly affected by a variety of factors including cell type. Cole and Grose demonstrated that there was a significant difference between syncytia formation in cultures of human foreskin fibroblasts, and epidermal cells isolated from human neonatal foreskins in which a highly fusogenic strain of VZV was propagated under the same experimental conditions. Very little fusion occurred in the fibroblast population in contrast with the epidermal cells (Cole and Grose. 2003). In addition, Reichelt and colleagues have shown that in human embryonic lung fibroblasts VZV infection was initiated without cell-cell fusion (and amplified

later on by cell-to-cell fusion), a mechanism that the authors attributed to the transfer of extracellular virions on surfaces of uninfected cells in proximity to the infected cell, possibly promoted by VZV gE protein which enhances the junction formation between the plasma membranes (Reichelt et al. 2009). In this study, they labeled with different fluorescent dyes the inoculum infected cells and healthy output cells, and tracked the events on confocal microscopy and electron microscopy.

It was important to establish whether the infective potential I could detect was truly due to MP associated virus, and not free virus. As VZV is highly cell-associated, often free virus is not released in the culture media. I showed that when analysed on TEM, the pellets obtained after ultracentrifugation from media of the VZV-infected HBVAF which was MP depleted, contained barely a few virus particles. It is important to also emphasize that MeWo cells do not release free virus in the culture media. Also, cell-free VZV released from MeWo cells by mechanical disruption of the monolayer includes many defective particles unable to infect permissive cells (Carpenter et al. 2009).

In contrast, media from VZV infected neuronal cultures has been shown to initiate productive infection in susceptible cells, dependent on infectious viral dose (Gowrishankar et al. 2007; Markus et al. 2011; Lee et al. 2012; Sloutskin et al. 2013). Therefore, I specifically explored the question whether the MP pellets

used to inoculate the monolayer of healthy HBVAF could be contaminated with free VZV.

Firstly, the VZV enveloped particle has been reported to have a diameter of 80–120 nm, and 1.21g/mL particle density, similar to the characteristics of cellular exosomes (approximately 50-100nm diameter and 1.19g/mL particle density). In contrast, MP are larger particles with a diameter between 100-1000 nm (Abendroth et al. 2010; Zerboni et al. 2014; György et al. 2011). The speeds of centrifugation I used to pellet MP from culture were between 15000- 20000g, and thus were extremely unlikely to have pelleted any free virus. Exosomes and free viruses require much higher ultracentrifugation forces, typically forces of 100,000–200,000g (György et al. 2011). Based on the methodology I used to separate MP pellets, it seemed unlikely that any significant amount of free virus (if HBVAF capable of releasing free virions in culture) was pelleted with the MP. Even if that were to be the case, extracellular VZV virions are very unstable and often defective, lacking capsid thus significantly impairing infective capacity (Carpenter et al. 2009).

Interestingly, in the initial neuron VZV infection studies, when using cell-associated infection productive infection was observed, whereas using cell-free virus preparation as inoculum resulted in non-productive infection (Pugazhenthi et al. 2011; Yu et al. 2012). Later studies reported on successful infection of neurons using cell-free VZV using a significantly higher viral dose (Gowrishankar

et al. 2007; Markus et al. 2011; Lee et al. 2012; Sloutskin et al. 2013). Whilst neuronal cells are of course different cells from HBVAF and endothelium, and hence have different susceptibility to VZV infection, these studies in general suggest that a high dose of infectious extracellular virus is required to achieve productive infection in permissive cells.

Markus *et al* showed by transmission electron microscopy that neurons infected with VZV displayed virions adjacent to the external aspect of the cell membrane. Based on this finding, they investigated whether these virions were released into the culture media, and if they retained their capacity to infect other cells (Makus et al. 2011). In their experiments, culture media (which was subjected to centrifugation at 3000g for 15 minutes to remove the cell debris) was used successfully to infect MeWo cells or human foreskin fibroblasts, but this required a very high dose of concentrated culture medium containing large numbers of free virus in order to do so.

In my experiments, I achieved infection by adding MP pellets to uninfected cells, with very few (if any) free virus. Therefore, if MP pellets were contaminated by free virus the dose was very low and unlikely to produce infection, strongly suggesting that it was indeed the MP component that was responsible for viral transfer. In addition, as a control for these experiments, I used the MP free fraction of conditioned media from GFP tagged VZV to try to infect healthy HBVAF: no infected cells were observed this way. This could mean that no free complete virions are released into the media from VZV infected HBVAF.

However, there are some caveats to this: infection with cell-free virus is highly dose dependent (as detailed above), and in these control experiments I deliberately did not attempt to concentrate the MP free fraction of media (since I was trying to compare infectivity directly with experimental conditions using MP fractions). I was able to therefore conclude that even if intact free virus was present, the virion dose was too low to cause infection.

To finally prove that infection in these experiments was the result of the MP fraction, in additional experiments I incubated the MP harvested from VZV-infected HBVAF with healthy HBVAF in the presence or absence of heparin, an inhibitor of cell free virus entry to the cells (Markus et al. 2011). These experiments showed no difference in the infection efficiency between HBVAF cultures infected with MP in the presence or the absence of heparin, thereby proving beyond doubt that the productive infection was mediated by MP-VZV complexes, and not free VZV.

Flow cytometry analysis of MP revealed that they contain VZV proteins as demonstrated by co-staining for Annexin V/GFP ORF23 and Annexin V/gH. In addition, the presence of viral antigens in MP was confirmed by mass spectrometry. The qualitative proteomic profiling revealed the presence of 10 VZV proteins with important functions in the MP pellets derived from VZV-infected HBVAF that were absent in the control mock-infected MP.

Lastly, the electron microscopy studies I performed demonstrated that a group of MP were identified with entrapment of virus inside MP membrane coats, providing further evidence to support the notion that VZV employs MP released in response to infection to propagate the infection. These MP-virus complexes may also exert further pathological effects that remain to be established, and open up a new chapter in the VZV life-cycle that could be fruitful for future study regarding the pathogenesis of disease in humans.

In the context of VZV vasculopathy, this novel finding could have immediate implications for disease pathogenesis. VZV could use MP to disseminate and accelerate infection, perhaps evading detection by the immune system by being packaged in the MP by host cellular membrane, thus facilitating viral propagation within the host. Moreover, HBVAF may exploit this pathway to transmit virus locally within brain arteries to neighbouring cells, contributing to the remodelling observed in VZV vasculopathy.

In support of this, another promising, albeit preliminary observation, is my discovery of MP expressing viral proteins in the plasma of paediatric patients with VZV-related cerebral vasculopathy and stroke. The diagnosis of VZV vasculopathy is often confirmed by the presence of intrathecal production of VZV antibodies or VZV PCR of the CSF following lumbar puncture, an invasive procedure that carries potential complications. MP-VZV complexes could therefore represent a potential novel diagnostic biomarker for this disease. These

interesting findings would certainly warrant further investigation, but require validation in a larger prospective cohort of patients.

It would also be interesting to characterize the cellular of origin of these circulating MP-VZV complexes, using combinations of flow cytometry, proteomics, and electron microscopy as described in this chapter. For example, further electron microscopy analysis of these particles may identify if they only express viral proteins/whole virus on the surface, or alternatively if viral components are completely packaged within the MP. If the latter as the case, this could have implications for dissemination of infection to distant sites, as described above.

An important limitation in relation to the clinical component of the results in this chapter was that there was limited clinical information available regarding past VZV infection in the healthy adult controls recruited. In addition, due to lack of availability and therefore purely on a practical basis, no child healthy control samples were available for use in these experiments. Therefore this is an immediate and obvious avenue for future study before beginning to contemplate the potential for this approach as a biomarker for VZV arteriopathy. Extremely low numbers of VZV gH+ MP were found in the plasma of adult controls; this could reflect a low level of subclinical reactivation in healthy individuals, an interesting concept which could be further investigated in larger patient numbers including children, and with carefully documented VZV infection histories.

In conclusion, signals from infected HBVAF interact with endothelial cells and alter important patho-physiological endothelial cell properties, of relevance to the biology of VZV associated AIS. Moreover, a novel mechanism of paracrine VZV propagation of inflammation or infection has been described which could be highly relevant in this disease context, and may have implications for other VZV associated diseases of humans.

5. Analysis of the gene expression profile in human brain vascular adventitial fibroblasts in response to Varicella zoster virus infection

5.1. Summary

Background: Viral infection depends on a complex interplay between host and viral factors. Viruses have acquired mechanisms by which they efficiently evade the host defences in order to propagate. Virus cellular entry, and the way the virus then interacts with the host often requires multiple signaling pathways, often of individual cell type specificity.

Objective: The aim of this part of my study was to ascertain gene expression profile changes that associate to the phenotypic changes of HBAVF observed *in vitro* in response to VZV infection, and also identify possible pathways that allow VZV cellular entry and virus propagation in these cells.

Methods: Transcriptional changes in cultured HBVAF following VZV infection were compared to those seen in mock-infected HBVAF using RNA-sequencing (RNAseq).

Results: I present here the results of experiments that demonstrate significant changes in the transcriptomic profile of HBVAF in response to VZV infection, with the expression of a total of 6911 altered genes (up- or down-regulated). Of the top genes found to be altered, preliminary analyses identified *AREG, FMO2, and*

CKS2 as interesting candidates for further work given their involvement in fibroblast activation. More than 60 pathways were identified as significantly altered.

Conclusions: Further work will be needed to validate these findings using RT-qPCR and to ascertain the contribution of these differences to the virus-host interaction in the context of pathogenesis of VZV vasculopathy.

5.2. Introduction

The interaction between viruses and host cells is an intricate process, which can vary between different cell types due to the different composition of cell components such as the membrane, cellular organelles, and other factors. Microarrays, and more recently RNAseq, in which mRNA transcription patterns can be determined simultaneously for thousands of genes, have emerged as a new method for evaluating virus-host cell interactions (Browne et al, 2001; Chang et al, 2000; Cuadras et al, 2002; Jones et al, 2003; Markus et al, 2014). RNAseq uses next-generation sequencing to reveal the presence and quantity of RNA in a biological sample at a given moment in time. Both RNAseq and microarrays are established tools for transcriptome analysis. RNAseq has now become the gold standard for whole-transcriptome gene expression quantification. With the advent of next generation DNA sequencing technologies, RNAseq has become feasible and affordable. RNAseq first sequences complementary DNA (cDNA) in short fragments and this is followed by mapping

of such short sequence fragments (reads) against reference genome expression data.

RNAseq provides advantages over microarray based approaches (Everaert et al, 2015; Zhao et al, 2015):

1. higher sensitivity for the detection of very low or very high abundance transcripts, lower technical variation and higher levels of reproducibility
2. no limitation by prior knowledge about the content of the transcriptome is required, thus providing an unbiased view on the ensemble of transcripts in a sample
3. excellent detail about transcriptional features, such as novel transcribed regions, alternative splicing and allele-specific expression

Microarrays are subject to cross-hybridisation bias while RNA-seq is considered unbiased. However, RNAseq sequencing technology is more expensive than microarray and analysis is more complex (Zhao et al, 2015).

Like other viruses, VZV must subvert the internal antiviral defences of differentiated human cells by co-opting the cell machinery and resources to make viral gene products and produce lytic infection. This process takes place through complex interactions with the host. Little is known about the effects of VZV infection on host cells at a molecular level. However recent studies have started to add to our knowledge, showing that VZV radically modifies the transcription of cellular genes upon infection (Jones and Arvin, 2003, 2005, 2006). The

transcriptional changes seen in lytic VZV infection of T cells, human foreskin fibroblasts and neurons have been studied and partly delineated (Jones and Arvin, 2003; Markus et al, 2014), however no studies have examined the transcriptional changes in HBVAF in response to VZV.

It has been shown that VZV decreases cell surface expression of major histocompatibility complex class I (MHC-I) molecules in T cells and fibroblasts by causing their retention in the Golgi complex (Abbendroth et al, 2001). VZV also interferes with the Jak/Stat signal transduction pathway, inhibiting cell surface expression of MHC-II in response to gamma interferon (Abbendroth et al, 2000). The signaling pathways triggered by viruses in the host cells appear complex. Delineation of these pathways and mechanisms for virus entry and use of the host cell are important areas of study, however, as this may reveal targets for drug development as specific anti-viral treatments.

5.3. Aims

The aim of this part of my study was to identify the gene expression profile changes observed in HBVAF in response to VZV infection. This approach could help establish pathways that facilitate virus entry and propagation, and could explain some of the phenotypic changes I observed *in vitro* (chapter 3), and ultimately may broaden our understanding of the pathogenesis of VZV-related vasculopathy.

5.4. Methods

5.4.1. Cell preparation for RNA extraction

HBVAF at passage 3 were infected with VZV GFP ORF23 or mock-infection cell to cell as described in the general methods, in 6 well plates. As in the proteomic experiments, a higher virus dose was used. On day 5 post infection and when CPE and green fluorescence were present in 80% of the cultures VZV-infected, Trizol was added and the cells saved in -80^{0}C freezer.

5.4.2. RNA extraction

A RNA free zone with RNase was established. RNA was isolated following the below protocol. Media was removed from cells and 1ml of TRIzol (Life technologies) was added per 5-10x10^6 cells, and pipetted to lysed the cells. This was incubated at room temperature for 5 minutes. The samples in TRIzol were stored at -80°C for RNA extraction.

For RNA extraction, 0.2mL chloroform was added per 1mL TRIzol, and this was shaken vigorously for 15s and incubated for 2-3min at room temperature. This was followed by centrifugation at 12 000g for 15 min at 2-8°C. The upper colourless aqueous phase was transferred to a fresh tube. RNA was precipitated by mixing with isopropanol, 0.5ml/original 1ml TRIzol and incubated at 4°C overnight, to increase the yield of RNA relative to the standard protocol. Next, the samples were centrifuged at 12 000g for 10 min. The RNA pellet forms a gel like

pellet on the bottom and side of the tube. This was washed with 75% ethanol, at least 1mL to each 1mL of starting reagent, by vortexing and spinning at 7500g for 5 min at 2-8°C. The pellet was air dried for approximately 10 min and dissolved in RNase free water by pipetting. This was incubated for 10 min at 55-60°C, quality control done using nanodrop, stored at -80^{o}C overnight and samples transferred the next day to the UCL Pathogen Genomics laboratory for the RNA sequencing.

5.4.3. cDNA library preparation, quality control and RNA sequencing

UCL Pathogen Genomics team assisted with the sequencing, quality control and read alignment. In brief, the library prep protocol used the KAPA Stranded mRNA-Seq kit (Illumina, UK). to process the samples. As per technical data provided by the manufacturer, the KAPA Stranded mRNA-Seq Kit is designed for both manual and automated next generation sequencing library construction from 100 ng – 4 µg of intact, total RNA. The protocol is applicable to a wide range of RNA-seq applications, including gene expression. This kit provides all of the enzymes and buffers required for mRNA enrichment, cDNA synthesis, and library construction and amplification.

An input of 500ng and 12 cycles of PCR was used. Libraries were validated using the DNA D1000 TapeStation kit and were quantified using the Qubit dsDNA HS assay. Libraries were then normalised and pooled to 4nM, and loaded onto the sequencer at 1.8pM. The samples were sequenced on an Illumina NextSeq 500. PhiX control was loaded at 1%.

5.4.4. Read alignment, count conversion and gene set enrichment analysis

Dr Cristina Venturini, bioinformatician postdoctoral fellow at UCL Pathogen Genomics, assisted with generating the read count table and differential gene expression analysis.

Data was de-multiplexed using bcl2fastq v 2.17. Paired end reads were mapped to the Ensembl human transcriptome reference sequence (Homo sapiens GRCh38 (v 84). Mapping and generation of read counts per transcript were done using Kallisto (Everaert et al, 2017). Tximport was used to import the mapped counts data and summarise the transcripts-level data into gene level as described by Soneson and colleagues (Soneson et al, 2015).

5.4.5. Statistical analysis

Further analyses were run using DESeq2 (Anders et al, 2010; Love et al, 2014) and the SARTools packages developed at PF2 - Institute Pasteur. Normalization and differential analysis were carried out according to the DESeq2 model and package. Normalization and differential analysis were carried out according to the DESeq2 model by use of negative binomial generalized linear model. The estimates of dispersion and logarithmic fold changes incorporate data-driven prior distributions. SARTools is an R pipeline based on DESeq2 which was used

to generate lists of differentially expressed genes and diagnostic plots for quality control.

Gene expression heatmaps were generated using the MEV software suite (http://www. tm4.org/mev.html) with assistance from Ebun Omoyinmi, Senior research associate at UCL. Functional classification of genes was performed using the xGR online database (http://galahad.well.ox.ac.uk:3020).

5.5. Results

5.5.1. Description of raw data

The total read counts were expected to be similar within similar experimental conditions. The total read counts sometimes vary significantly between replicates for several reasons, including: different rRNA contamination levels between samples (even between experimental replicates), and slight differences between library concentrations, since they may be difficult to measure with high precision. The number of reads was over 10×10^5 for each of the samples, and the total number of reads was similar between the triplicates of each of the two conditions (Figure 5.1.) confirming good quality in my hands.

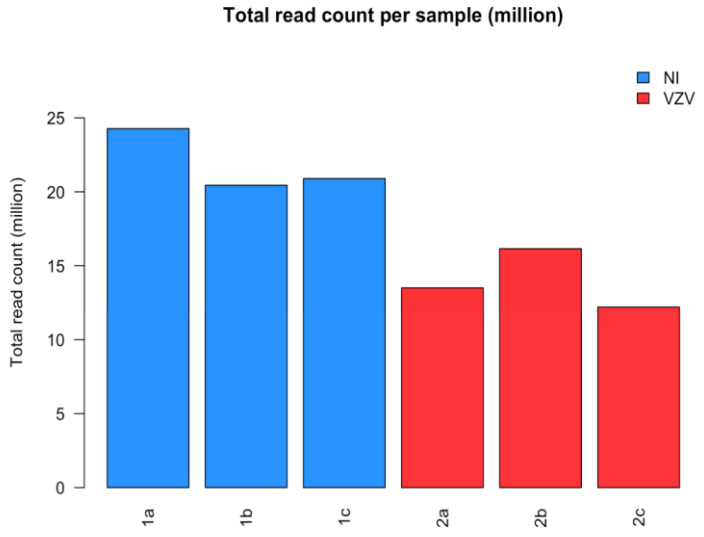

Figure 1: Number of mapped reads per sample. Colors refer to the biological condition of the sample.

Figure 5.1 Total number of mapped and counted reads for each sample for gene expression profiles of HBVAF: VZV- or mock-infected. *Colors refer to the experimental condition of the sample: Blue, mock-infected HBVAF; red, VZV-infected HBVAF. The number of reads was over 10 x* 10^5 *for each of the samples, and the total number of reads was similar between the triplicates of each of the two conditions.*

5.5.2. Principal component analysis

Commonly, variability in transcriptomic analyses stems from experimental differences between samples processed. One way of visualizing experimental sample variability is to look at the first components of the principal component

analysis (PCA), as shown on the figure 5.2. The PCA revealed that the principal component (PC1) separated samples based on two separate experimental conditions (VZV and mock infection) in my experiments, meaning that experimental variability was the main source of variance my data set.

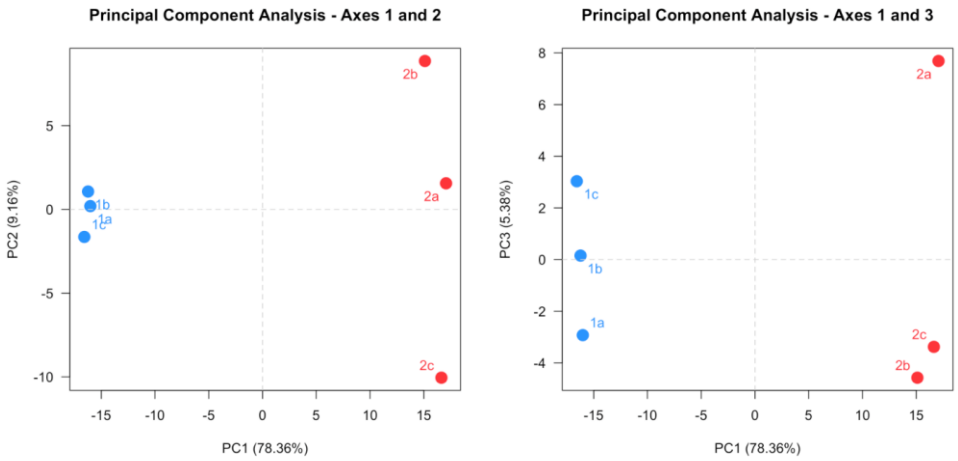

Figure 5.2. Principal Component Analysis, with percentages of variance associated with each axis for gene expression profiles of HBVAF: VZV- or mock-infected. *Colors refer to the biological condition of the sample: Blue, mock-infected HBVAF; red, VZV-infected HBVAF. In this figure, the first principal component (PC1) separates the samples from the different biological conditions, meaning that the biological variability is the main source of variance in these data.*

5.5.3. Data normalization

Normalization aims at correcting systematic technical biases in the data, in order to make read counts comparable across samples. The normalization proposed by DESeq2 relies on the hypothesis that most genes are not differentially expressed. The software computes a scaling factor for each sample. Normalized read counts are obtained by dividing raw read counts by the scaling factor associated with the sample they belong to. Scaling factors around 1 mean (almost) no normalization is performed. Scaling factors lower than 1 will produce normalized counts higher than raw ones, and the other way around. Boxplots are often used as a qualitative measure of the quality of the normalization process, as they show how distributions are globally affected during this process. We expect normalization to stabilize distributions across samples. Figure 5.3. shows boxplots of raw (left) and normalized (right) data respectively.

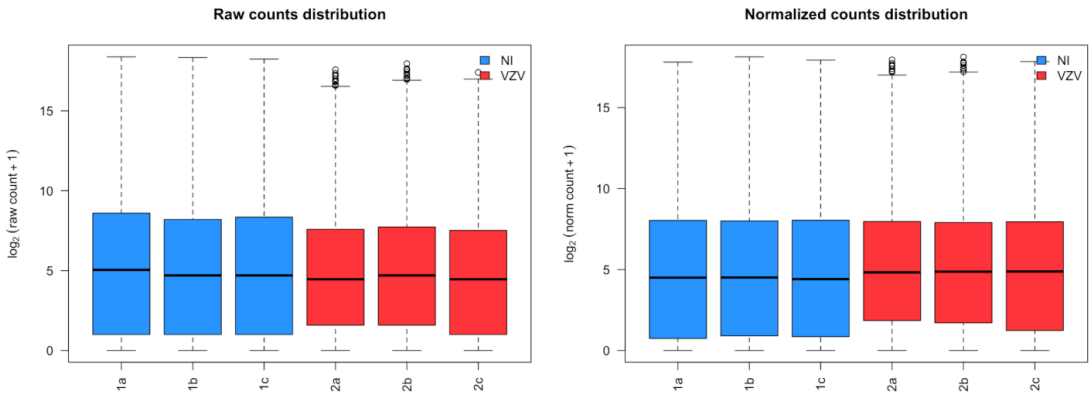

Figure 5.3. Boxplots of raw and normalized read counts for gene expression profiles in HBVAF VZV- or mock-infected. *Colors refer to the experimental condition of the sample: Blue, mock-infected HBVAF; red, VZV-infected HBVAF. Raw data is presented in the boxplot on the left, and normalized data on the boxplot on the right.*

5.5.4. Visualisation of RNAseq results

A p-value adjustment is performed to take into account multiple testing and control the false positive rate to a chosen level *α*. For this analysis, a false discovery rate (FDR) p-value adjustment was performed (Benjamini et al, 2001) and the level of controlled false positive rate was set to 0.05. This means the generated list of significant hits has in expectation at most 5 % false positives.

Figure 5.4. shows the volcano plots for the comparisons performed and differentially expressed features are still highlighted in red. The volcano plot represents the log of the adjusted P value as a function of the log ratio of differential expression. A volcano plot typically plots some measure of effect on

the x-axis (typically the fold change) and the statistical significance on the y-axis (typically the -log10 of the p value). Genes whose expression is highly dysregulated are far to the left and right sides, while highly significant changes appear higher on the plot.

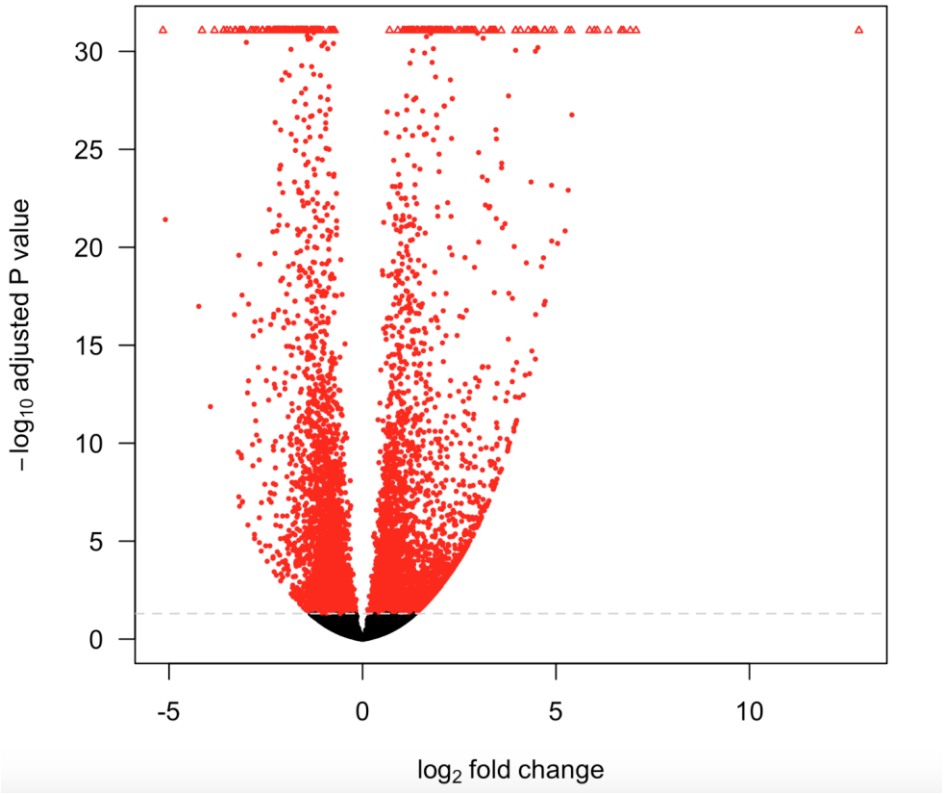

Figure 5.4. Volcano plot of the comparison between gene expression profiles of HBVAF: VZV- or mock-infected. *Red dots represent significantly differentially expressed features.*

Full results of the raw data with lists of differentially expressed features were provided in a spreadsheet.

5.5.5. Overview of transcriptomic data analysis

With a FDR cutoff of 0.05, a total of 6911 differentially expressed genes were identified across the comparison of interest. Of the total of 6911 altered genes, the expression of 3465 (50%) was up-regulated, and 3446 (50%) were down-regulated. When filtering the data to include only the genes with cutoffs cutoff of 2-fold changes with a significance of 0.05, the expression of 3364 genes was modified in VZV-infected HBVAF, with 481 (14%) of genes up-regulated and 2887 (86%) genes down-regulated, therefore a skew towards downregulation.

Given the high number of differentially expressed genes, I focused my attention on the top 20 highly differentially expressed genes in VZV-infected HBVAF relative to mock-infected HBVAF. A zoomed heatmap including only the top 20 differentially expressed genes was generated, to illustrate the expression pattern between the two conditions (Figure 5.5.).

Of these genes, 16 were identified with up-regulation of expression in VZV-infected HBVAF: *IL11, TFPI2, NR4A1, TMSB4XP6, AREG, STC1, DEDD2, HSPA1B, MT2A, H2AFX, HSPA1A, CKS2, AHSA1, CXCL8, NAMPT, MT1L; 4 genes were identified with down-regulation: FMO2, CORIN, CCDC80, TIMP2*. (Table 5-1)

Table 5-1. List of top 20 altered genes identified with altered expression in VZV-infected HBVAF by RNAseq

Gene	Description	Summary	Up- or down-regulated
IL11	Interleukin 11	Encodes protein member of the gp130 family of cytokines. This cytokine is shown to stimulate the T-cell-dependent development of immunoglobulin-producing B cells. Supports support the proliferation of hematopoietic stem cells and megakaryocyte progenitor cells.	Up
TFPI2	Tissue Factor Pathway Inhibitor 2	Encodes a member of the Kunitz-type serine proteinase inhibitor family. May play a role in the regulation of plasmin-mediated matrix remodeling. Inhibits factor VIIa/tissue factor, factor Xa, plasmin, trypsin, chymotryspin and plasma kallikrein. Gene identified as a tumor suppressor	

		gene in several types of cancer.	
NR4A1	Nuclear Receptor Subfamily 4 Group A Member 1	Encodes a member of the steroid-thyroid hormone-retinoid receptor superfamily. Expression is induced by phytohemagglutinin in human lymphocytes and by serum stimulation of arrested fibroblasts. The encoded protein acts as a nuclear transcription factor. Translocation of the protein from the nucleus to mitochondria induces apoptosis.	Up
TMSB4XP6	Thymosin Beta 4, X-Linked Pseudogene 6	Pseudogene	Up
AREG	Amphiregulin	Encodes protein member of the epidermal growth factor family. It is an autocrine growth factor as well as a mitogen for astrocytes, Schwann cells and fibroblasts. It is related to epidermal growth factor and transforming growth factor	Up

		alpha.	
STC1	Stanniocalcin 1	Encodes a secreted, homodimeric glycoprotein that is expressed in a wide variety of tissues. The protein may play a role in the regulation of renal and intestinal calcium and phosphate transport, cell metabolism, or cellular calcium/phosphate homeostasis.	Up
DEDD2	Death Effector Domain Containing 2	Encodes protein which may regulate the trafficking of caspases and other proteins into the nucleus during death receptor-induced apoptosis.	Up
HSPA1B	Heat Shock Protein Family A Member 1B	Encodes protein which works in conjuction with other heat shock proteins, to stabilize existing proteins against aggregation and mediate the folding of newly translated proteins in the cytosol and in organelles	Up

		during cellular stress	
MT2A	Metallothionein 2A	Proteins encoded interacts with the protein encoded by the homeobox containing 1 gene in some cell types, controlling intracellular zinc levels, affecting apoptotic and autophagy pathways.	Up
H2AFX	H2A Histone Family Member X	Encodes a histone with central role in transcription regulation, DNA repair, DNA replication and chromosomal stability.	Up
HSPA1A	Heat Shock Protein Family A (Hsp70) Member 1A	Encodes protein which works in conjuction with other heat shock proteins, to stabilize existing proteins against aggregation and mediate the folding of newly translated proteins in the cytosol and in organelles during cellular stress. In case of rotavirus A infection, serves as a post-attachment receptor for the virus to facilitate	Up

		entry into the cell. and degradation.	
CKS2	CDC28 Protein Kinase Regulatory Subunit 2	Encodes protein which inds to the catalytic subunit of the cyclin dependent kinases and is essential for their biological function.	Up
AHSA1	Activator Of HSP90 ATPase Activity 1	Protein coding GO annotations related to this gene include chaperone binding and ATPase activator activity.	Up
CXCL8	Interleukin 8	Encodes IL8 protein, chemotactic factor that attracts neutrophils, basophils, and T-cells, but not monocytes. It is also involved in neutrophil activation. It is released from several cell types in response to an inflammatory stimulus.	Up
NAMPT	Nicotinamide Phosphoribosyltransferase	Encodes protein of the nicotinic acid phosphoribosyltransferase family, thought to be	Up

		involved in many important biological processes, including metabolism, stress response and aging.	
MT1L	Metallothionein 1L	Psueodogene	Up
FMO2	Flavin Containing Monooxygenase 2	Encodes a flavin-containing monooxygenase family member. Emerging roles in atherosclerosis and cardiovascular disease, aging, neurodegenerative diseases, and metabolic pathways (Rossner et al, 2017)	Down
CORIN	Corin, Serine Peptidase	Encodes serine-type endopeptidase involved in atrial natriuretic peptide hormone processing. Converts through proteolytic cleavage the non-functional propeptide natriuretic peptide hormone into the active hormone, regulating blood pressure in heart and promoting natriuresis,	Down

		diuresis and vasodilation. Role in female pregnancy by promoting trophoblast invasion and spiral artery remodeling in uterus.	
CCDC80	Coiled-Coil Domain Containing 80	Encodes protein Promotes cell adhesion and matrix assembly.	Down
TIMP2	TIMP Metallopeptidase Inhibitor 2	Encodes natural inhibitors of the matrix metalloproteinases, involved in degradation of the extracellular matrix. Encoded protein may be critical to the maintenance of tissue homeostasis by suppressing the proliferation of quiescent tissues in response to angiogenic factors, and by inhibiting protease activity in tissues undergoing remodelling of the extracellular matrix.	Down

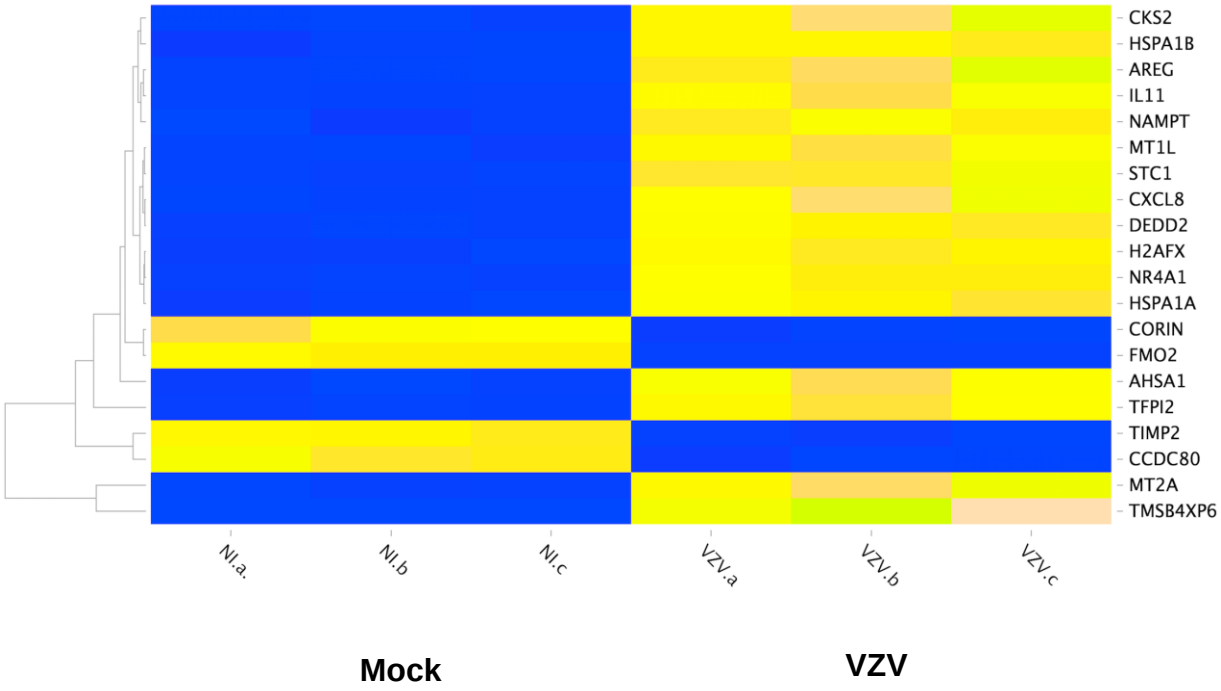

Figure 5.5. Heatmap illustrating hierarchical clustering analysis of the top 20 significantly altered genes in VZV-infected and mock-infected HBVAF. *Clustering analysis was performed with meV. The blue colour represents down-regulated genes and the yellow up-regulated genes. In the heatmaps, each column represents a sample and each row represents a gene. The 3 columns on the left represent triplicates of mock-infected HBVAF, and the 3 columns on the right triplicates of experiments for VZV-infected HBVAF. The figure demonstrates that there is virtually no overlapping patterns between the two conditions. Genes with significant increase (>2fold) in expression in VZV-infected HBVAF: IL11, TFPI2, NR4A1, TMSB4XP6, AREG, STC1, DEDD2, HSPA1B, MT2A, H2AFX, HSPA1A, CKS2, AHSA1, CXCL8, NAMPT, MT1L; genes with significant decrease (fold<0.5): FMO2, CORIN, CCDC80, TIMP2.*

A table with the summary of the 20 differentially expressed genes and the read counts for comparison is presented below (Table 5-2).

Table 5-2. Top differentially expressed genes with read counts in VZV-infected HBVAF by RNAseq

NAME	Mock a	Mock b	Mock c	VZV a	VZV b	VZV c
FMO2	3083	3226	3231	85	82	88
IL11	127	115	107	4697	5363	4524
TFPI2	451	608	576	14421	15841	14083
NR4A1	184	213	182	2912	3129	3128
TMSB4XP6	0	0	0	30349	26459	42389
AREG	81	104	107	4626	5033	3626
STC1	126	104	125	2548	2532	2159
DEDD2	163	184	171	1657	1724	1788
HSPA1B	701	830	869	5751	5748	6011
MT2A	4281	3653	3676	33858	38859	30714
CCDC80	15306	17119	16815	3154	3498	3490
H2AFX	336	342	420	3174	3384	3241
TIMP2	14543	14621	15043	5494	5393	5593
HSPA1A	479	536	576	3326	3460	3669
CKS2	595	656	528	6431	7476	5529
CORIN	2980	2550	2593	104	152	172
AHSA1	1604	1829	1686	8055	9325	8174
CXCL8	65	43	38	1629	1957	1508
NAMPT	1062	900	977	4764	4381	4712
MT1L	349	361	312	2131	2343	2051

A common approach to interpreting gene expression data is gene set enrichment analysis based on the functional annotation of the differentially expressed genes. This is useful for finding out if the differentially expressed genes are associated with a certain biological process or molecular function. For the gene set enrichment analysis, I have used XGR, a web-based free software for enhanced interpretation of genomic summary data. The basic concepts behind XGR is that the user provides an input list of genes and XGR, available as both an R

package and a web-app and is then able to run enrichment, network, similarity, and annotation analyses based on this input. The analyses themselves are run using a combination of ontologies, gene networks, gene/SNP annotations, and genomic annotation data (built-in data). The output comes in various forms, including bar plots, directed, circos plots, and network relationships. Furthermore, the web-app version provides interactive tables, downloadable files, and other visuals. As part of XGR, enrichment analysis (or 'Enricher') which I have used, is based on conventional statistical tests (Fisher's exact test, hypergeometric or binomial test) to identify enriched ontology terms using either built-in or custom ontologies.

I provided separately the list of genes the expression of which was down-regulated or up-regulated, and I chose the ontology option of "Canonical/KEGG/REACTOME/BioCarta pathways to analyse this. The software analyses the input data and displays the results as table and barplots. The top enrichments found as up-regulated or down-regulated are presented in Figures 5.6 and 5.7, respectively.

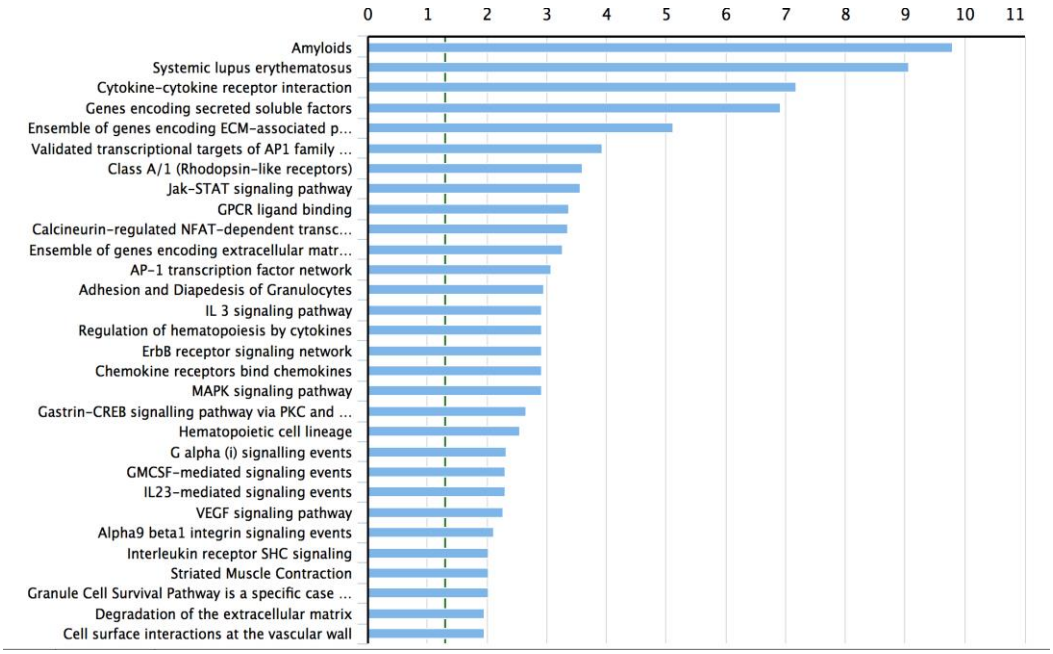

Figure 5.6. Top pathways that were found to be significantly upregulated in VZV-infected HBVAF. *This plot displays the top enrichments. Where a vertical line indicates the FDR cutoff at 0.05. This plot displays the top enrichments down-regulated. Where a vertical line indicates the FDR cutoff at 0.05. Enrichment analysis (or 'Enricher') was used in XGR to identify enriched ontology terms with the input of a list of up-regulated genes (>2fold). The "Canonical/KEGG/REACTOME/BioCarta pathways was chosen. The software analysed the input data and displayed the result is displayed as barplot.*

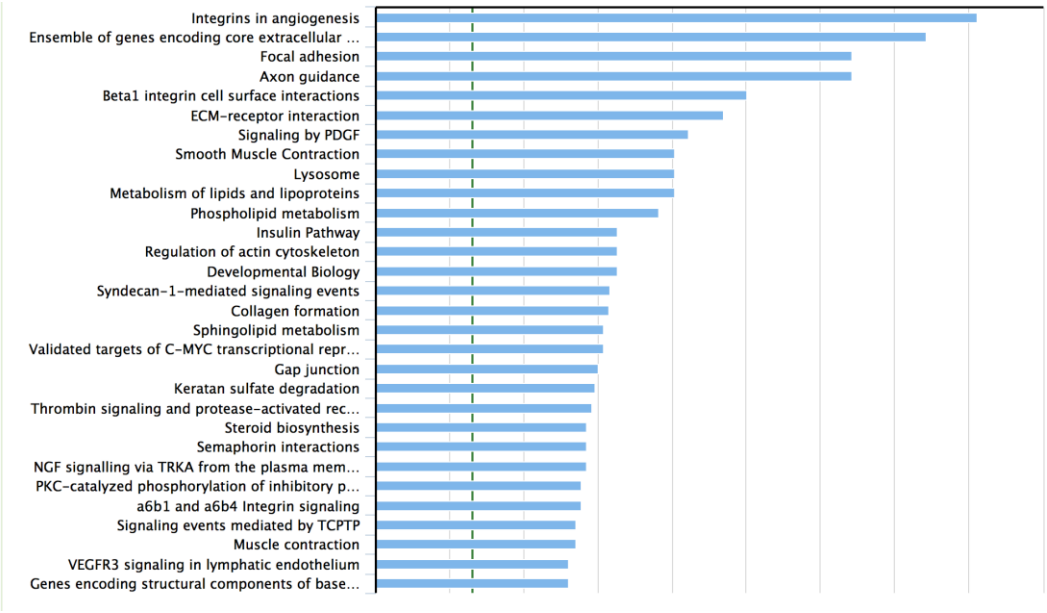

Figure 5.7. Top pathways that were found to be significantly down-regulated in VZV-infected HBVAF. *This plot displays the top enrichments down-regulated. Where a vertical line indicates the FDR cutoff at 0.05. Enrichment analysis (or 'Enricher') was used in XGR to identify enriched ontology terms with the input of a list of down-regulated genes (<0.5fold). The "Canonical/KEGG/REACTOME/BioCarta pathways was chosen. The software analysed the input data and displayed the result is displayed as barplot.*

The top pathways that were found to be significantly enriched are presented in table 5-3.

Table 5-3. Top pathways that were found to be significantly altered in VZV-infected HBVAF.

Pathway	Up- or down-regulation	Genes	Number of genes overlapping
Amyloids	Up	APOA1, H2AFX, H2AFZ, H3F3B, HIST1H2AB, HIST1H2AE, HIST1H2BB, HIST1H2BC, HIST1H2BD, HIST1H2BE, HIST1H2BF, HIST1H2BG, HIST1H2BH, HIST1H2BJ, HIST1H2BK, HIST1H2BN, HIST1H2BO, HIST1H3A, HIST1H3B, HIST1H3D, HIST1H3E, HIST1H3H, HIST1H3J, HIST1H4D, HIST1H4E, HIST1H4H, HIST1H4J, HIST2H2AA3, HIST2H2AA4, HIST2H2BE, HIST2H3A, HIST2H3C, HIST3H2BB, HIST4H4, IAPP, LYZ, TGFBI	37
Systemic lupus erythematosus	Up	C3, C8G, FCGR2A, H2AFJ, H2AFX, H2AFZ, H3F3B, HIST1H2AB, HIST1H2AE, HIST1H2AG, HIST1H2AH, HIST1H2AI, HIST1H2AL, HIST1H2AM, HIST1H2BB, HIST1H2BC, HIST1H2BD, HIST1H2BE, HIST1H2BF, HIST1H2BG, HIST1H2BH, HIST1H2BJ, HIST1H2BK, HIST1H2BN,	47

		HIST1H2BO, HIST1H3A, HIST1H3B, HIST1H3D, HIST1H3E, HIST1H3H, HIST1H3J, HIST1H4D, HIST1H4E, HIST1H4H, HIST1H4J, HIST2H2AA3, HIST2H2AA4, HIST2H2AB, HIST2H2BE, HIST2H3A, HIST2H3C, HIST3H2A, HIST3H2BB, HIST4H4, IL10, SNRPB, SNRPD1	
Integrins in angiogenesis	Down	ADGRA2, CDKN1B, COL11A1, COL12A1, COL14A1, COL15A1, COL16A1, COL1A1, COL1A2, COL3A1, COL4A5, COL5A1, COL5A2, COL6A1, COL6A2, COL6A3, COL8A1, COL8A2, CSF1, EDIL3, FN1, ILK, IRS1, ITGAV, MFGE8, PI4KA, PI4KB, PIK3C2A, PIK3CA, PIK3R1, PTPN11, PXN, ROCK1, TGFBR2, TLN1, VCL	36
Ensemble of genes encoding core extracellular	Down	ABI3BP, AEBP1, ASPN, BGN, BMPER, CHAD, CILP, COL11A1, COL12A1, COL14A1, COL15A1, COL16A1, COL1A1, COL1A2, COL21A1, COL3A1, COL4A2, COL4A5, COL5A1, COL5A2, COL6A1, COL6A2, COL6A3, COL8A1, COL8A2, CRIM1, CTHRC1, DCN, DPT, ECM1, ECM2, EDIL3, EFEMP1, EFEMP2, ELN, EMILIN1, FBLN1, FBLN2, FBLN5, FBN1, FBN2, FN1, GAS6, HSPG2, IGFBP3, IGSF10, INTS6L, LAMA2, LAMA4, LAMB1,	83

		LAMB2, LAMC1, LTBP2, LTBP3, LTBP4, LUM, MATN2, MFAP2, MFAP4, MFGE8, MGP, MXRA5, NID1, NID2, NTN4, OGN, OMD, PAPLN, PCOLCE, PODN, POSTN, PRELP, PXDN, RSPO2, SPARC, SPARCL1, SPON2, SVEP1, THBS1, THBS2, THBS3, THSD4, WISP2	
Focal adhesion	Down	ACTB, ACTN1, ACTN4, AKT2, AKT3, ARHGAP35, BIRC2, CAPN2, CAV1, CAV2, CCND2, CDC42, CHAD, COL11A1, COL1A1, COL1A2, COL3A1, COL4A2, COL5A1, COL5A2, COL6A1, COL6A2, COL6A3, DOCK1, EGFR, ERBB2, FLNA, FLNC, FN1, ILK, ITGA1, ITGA11, ITGA4, ITGA8, ITGAV, ITGB1, ITGB8, JUN, LAMA2, LAMA4, LAMB1, LAMB2, LAMC1, MET, MYL9, MYLK, PARVA, PDGFC, PDGFD, PDGFRA, PDGFRB, PIK3CA, PIK3R1, PIK3R2, PIP5K1C, PPP1CA, PPP1CB, PRKCA, PXN, RAF1, RAP1A, RAP1B, RAPGEF1, ROCK1, ROCK2, SHC2, SOS1, SOS2, THBS1, THBS2, THBS3, TLN1, VCL, VEGFB, VEGFD	75
Axon guidance	Down	ABL1, ALCAM, AP2B1, AP2M1, ARHGAP35, ARHGEF12, CACNB3, CAP2, CDC42, CLTC, CNTNAP1, COL1A1, COL1A2, COL3A1, COL4A2,	83

		COL4A5, COL5A1, COL5A2, COL6A1, COL6A2, COL6A3, CRMP1, DLG1, DNM1, DOCK1, DPYSL2, DPYSL3, EGFR, ERBB2, EVL, EZR, FGFR1, GFRA1, GPC1, ITGA1, ITGAV, ITGB1, LAMB1, LAMC1, LIMK1, MET, MSN, MYH10, MYH9, MYL6, MYL9, MYO10, NCK2, NEO1, NRAS, NRCAM, NRP2, NTN4, PIP5K1C, PLXNA1, PLXNB1, PLXNC1, PLXND1, PRNP, RAF1, RDX, RGMA, RHOC, ROBO1, ROBO2, ROCK1, ROCK2, RPS6KA2, RPS6KA4, RRAS, SCN2A, SCN7A, SDCBP, SEMA5A, SHTN1, SOS1, SOS2, SPTBN1, SRGAP1, TLN1, TRIO, WASL, YWHAB	
Beta 1 integrin cell surface interactions	Down	CD81, COL11A1, COL1A1, COL1A2, COL3A1, COL4A5, COL5A1, COL5A2, COL6A1, COL6A2, COL6A3, FBN1, FN1, ITGA1, ITGA11, ITGA4, ITGA8, ITGAV, ITGB1, LAMA2, LAMA4, LAMB1, LAMB2, LAMC1, NID1, THBS1, THBS2, VCAM1	28

These results are preliminary and further research/analysis into these pathways will be necessary. Further PCR validation of the expression of these proposed interesting candidate genes is required.

5.6. Discussion

The enrichment analysis identified a high number of differentially expressed genes in the VZV-infected HBVAF compared to mock-infected, with over 6000 altered genes. The analysis of this dataset is complex. In a preliminary analysis I have identified the top 10 genes whose expression was altered in HBVAF in response to VZV infection. With a candidate gene approach based of a brief literature review, I identified *AREG, FMO2, and CKS2* as important candidate genes to study further.

Amphiregulin (AREG), an epidermal growth factor receptor (EGFR) ligand, is implicated in tissue repair and fibrosis and mediates its biologic function through the EGFR (Shoyab et al, 1978; Kimura et al, 1990). AREG is expressed in multiple cell populations, including fibroblasts, epithelial cells, leukocytes, dendritic cells, keratinocytes, group 2 innate lymphoid cells and Tregs (Zaiss et al, 2015). *AREG* functions to orchestrate immunity, inflammation and tissue repair, and mediates resistance to helminth infection (Zaiss et al., 2015).

AREG is also known to modulate cell proliferation, apoptosis and migration in different cell types (Berasain et Avila, 2014) and to play an essential role in the pathogenesis of TGFβ1-induced pulmonary fibrosis (Zhou et al, 2012). AREG expression is also associated with increased fibroblast proliferation and motility by inducing telomerase reverse transcriptase (Ding et al, 2016). AREG deficiency

in knockout (KO) mice significantly diminished pulmonary fibrosis (Zhou et al, 2012).

The findings outlined above demonstrate that activated fibroblasts upregulate expression of AREG causing increased cells proliferation, and fibroblast differentiation to myofibroblasts. This therefore makes *AREG* a top candidate for further studies in light of the HBVAF phenotypical changes observed in chapter 3 of this thesis. A myriad of factors are known to regulate fibroblast proliferation, motility and activation, and the role of the specific factors such as AREG remain largely unknown with respect to their significance in the context of individual conditions such as VZV vasculopathy.

Flavin-containing monooxygenase 2 (FMO2) is part of the 5 FMOs, primarily studied as a xenobiotic metabolizing enzyme with a prominent role in drug metabolism. Endogenous functions of *FMO2* are less well understood, but a growing body of recent evidence suggests a role of FMO in atherosclerosis and cardiovascular disease, aging, neurodegenerative diseases, and metabolic pathways (Rossner et al, 2017). The nature of FMO involvement in these diseases remains largely undefined, and FMO2 is the less studied of the 5 Flavin-containing monooxygenases. In this analysis, *FMO2* was identified as the most significant downregulated gene, and the emerging roles of the FMO make this gene an interesting candidate to be further evaluated in the context of VZV-related vasculopathy.

Cyclin-dependent kinase subunit 2 (*CKS2*), has been identified as a cancer gene and is implicated in the processes of cell cycle and cell proliferation, so therefore is another interesting gene for the pathogenesis of VZV vasculopathy. The *CKS2* upregulation observed in cancers is most likely due to its ability to promote cancer cell growth, invasion and migration. The effects gene expression of *CKS2* may have on other regulatory genes, might be relevant in the context of VZV vasculopathy.

Other host cell genes have been identified as significantly altered in response to VZV infection in this study, such as: *IL11, TFPI2, NR4A1, TMSB4XP6, STC1, DEDD2, HSPA1B, MT2A, H2AFX, HSPA1A, AHSA1, CXCL8, NAMPT, MT1L, CORIN, CCDC80, TIMP2*, although their significance remains to be fully established in this context.

To obtain better insight into the molecular mechanisms underlying different changes demonstrated in this model, I started analyzing the gene set for identification of possible pathways that might have a contribution. The preliminary analysis suggest that over 50 pathways are altered in response to VZV infection of HBVAF, likely reflecting a combination of the alteration of cellular environment by the virus and also potential compensatory mechanisms which in turn affect other pathways. The analysis is complex and ongoing.

KEGG systemic lupus erythematosus pathway, currently marked as specific to systemic lupus erythematosus and lung cancer, amyloids, cytokine-cytokine receptor interaction, genes encoding secreted soluble factors were the most significantly upregulated pathways.

Transcripts related to integrins in angiogenesis, ensemble of genes encoding core extracellular associated proteins including ECM-affiliated proteins, ECM regulators and secreted factors, focal adhesions and axon guidance pathways were detected with the most significant downregulation.

JAK-STAT and mitogen-activated protein kinases (MAPK) signaling pathways were also detected as affected.

The MAPK pathway is exploited by a number of viruses to manipulate the host cellular environment for optimal virus replication, cell transformation, and prevention of apoptosis HIV, influenza virus, human hepatitis viruses, rotavirus activate MAPK to enhance virus replication (XueQiao et al, 2012). Human herpesviruses, such as Epstein-Barr virus (EBV), herpes simplex virus (HSV), or Kaposi's sarcoma-associated herpesvirus, target the MAPK pathway for cell transformation, prevention of apoptosis, or induction of reactivation (XueQiao et al, 2012). VZV has been shown to activate the MAPK pathway (Rahaus et al, 2005; Rahaus et al, 2006).

The activation of JAK STAT signaling by interferons leads to the upregulation of hundreds of interferon stimulated genes for which, many have the ability to rapidly kill viruses within infected cells. VZV has been shown to interact with and inhibit the interferon-stimulated JAK-STAT signaling (Verweij et al, 2015). Nagel and colleagues have detected decreased levels of beta interferon (IFN-β,) STAT1, and STAT2 transcripts as well as STAT1 and STAT2 protein were decreased in VZV-infected HBVAF (Nagel et al, 2014). In this study, IFN-α transcript levels were increased but no IFN-α was detected, suggesting that phosphorylated STAT1 did not translocate to the nucleus, resulting in impaired downstream expression of interferon-inducible antiviral Mx1. This pathway analysis highlighted the JAK STAT pathway as significantly upregulated in response to VZV infection. These findings now require validation with RT-qPCR.

6. Analysis of gene expression profile changes in HUVEC in response to activation by MP derived from VZV-infected HBVAF

6.1. Summary

Background: In previous chapters I showed that in the context of VZV infection MP derived from HBVAF can activate HUVEC and induce a proinflammatory phenotype.

Objectives: The aims of this part of my study were to: (i) identify the changes at gene expression level in HUVEC that could underlie the phenotypical changes observed in the HUVEC in response to incubation with MP from VZV-infected HBVAF or conditioned media alone (i.e MP removed), and (ii) establish other possible pathways involved in the interaction of MP derived from VZV infected HBVAF and endothelial cells.

Methods: Transcriptional changes following 6 hours incubation of HUVEC with MP or media from VZV-infected HBVAF were compared to those in HUVEC incubated with MP from mock-infected HBVAF using RNAseq, to gain insight into the direct effects of these components on endothelial function.

Results: The first steps of the analysis focused on the transcriptomic profile of HUVEC following incubation with MP. Preliminary results showed changes in the gene expression profile of several genes, with changes in the expression of a total of 100 genes (up- or down-regulated when using FDR<0.05), and in the

expression of 55 genes when using a more stringent FDR<0.01. Of the genes whose expression was found to be altered, *ADAMTS18* and *LAMP3* were identified as biologically relevant candidates to further study, considering their established general role in vasculopathy pathogenesis. A number of additional pathways were identified to also be altered, the significance of which remains to be established.

Conclusion: Further work will be needed to validate these preliminary findings using RT-qPCR and provide more in depth analysis of this rich dataset.

6.2. Introduction

Within the complex pathological picture of this model of vascular remodeling associated with VZV-vasculopathy, the interaction of HBVAF and endothelial cells appears to play an important role, and MP appear as key players.

As described in an earlier chapter, the regulation of endothelial barrier and function is essential for maintaining circulatory homeostasis and the physiological function of blood vessels and different organs. The dysregulation of the endothelial barrier represent a key event in the development of a variety of disease processes, such as ischaemia–reperfusion injury, diabetic vascular complications and tumor metastasis (Kumar et al, 2009).

In this thesis, I have shown that the dysregulation of vascular endothelial cells induced by MP derived from HBVAF in response to VZV infection could play a role in the development of a VZV vasculopathy. MP can trigger important cellular processes via delivery of virus and other molecules to the endothelial cells. However, transcriptional regulation of vascular endothelial cells by these MP is not understood and it could reveal important pathways implicated in this interaction.

6.3. Aims

The aim of this part of my study was to (i) identify the changes at gene expression level in HUVEC that could underlie the phenotypical changes observed in the HUVEC in response to incubation with MP from VZV-infected HBVAF or conditioned media alone (i.e MP removed), and (ii) establish other possible pathways involved in the interaction of MP derived from VZV infected HBVAF and endothelial cells.

6.4. Methods

HUVEC at passage 4 were prepared and incubated for 6 hours with conditioned media or MP collected from VZV- or mock-infected HBVAF on day 3 post infection, as described in section 4.4.6. Each condition was prepared in triplicates, therefore a total of 12 samples was used: HUVEC treated with

conditioned media from VZV- or mock-infected HBVAF, and HUVEC incubated with MP pellets harvested from VZV- or mock-infected HBVAF (figure 6.1).

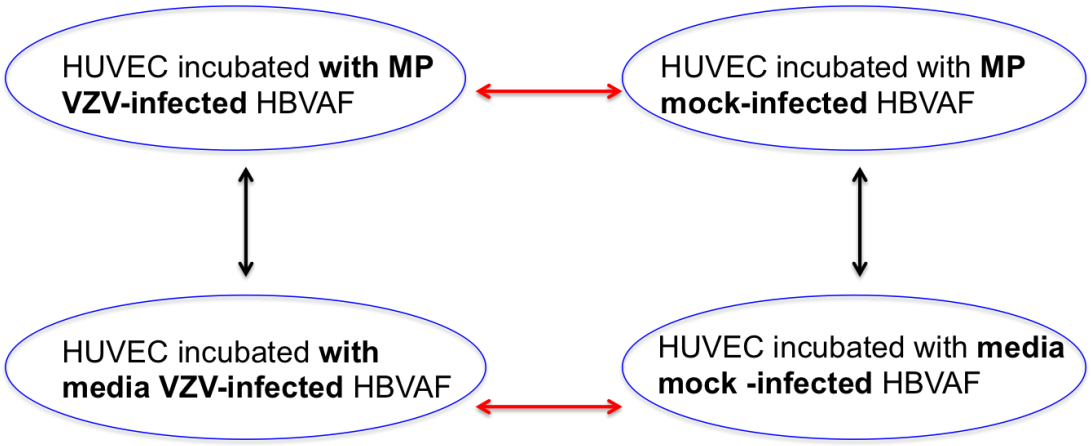

Figure 6.1. Schematic summary of RNAseq experiments examining gene expression profile changes in HUVEC incubated with MP or conditioned media derived from VZV-infected HBVAF: grouped samples and comparisons are highlighted.

The methods for RNA extraction, cDNA library preparation, quality control and RNA sequencing, read alignment, count conversion and gene set enrichment analysis and statistical analysis were identical to the ones described in section 5.4 and used for the HBVAF RNAseq analysis.

6.5. Results

6.5.1. Description of raw data

The number of reads was over 10 x 10^5 for each of the samples, and the total number of reads was similar between the triplicates of each of the two conditions (Figure 6.2.) confirming good quality in my samples.

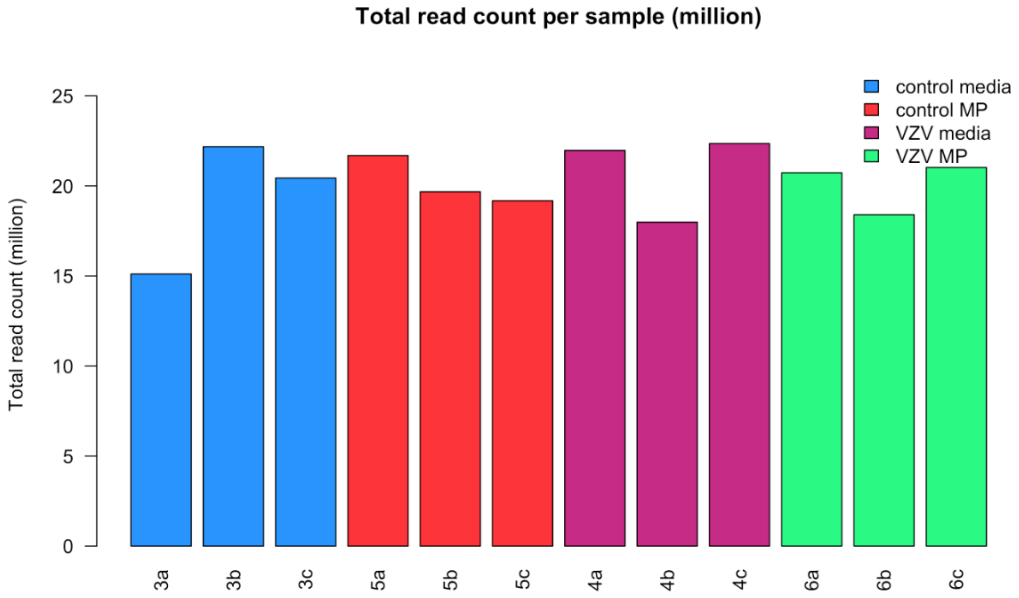

Figure 6.2. Total number of mapped and counted reads for each HUVEC sample processed following incubation with MP or conditioned media. *Colors refer to different experimental conditions of the sample: Blue, mock-infected media; red, mock-infected MP; purple, VZV-infected media; green, VZV-*

infected MP. The number of reads was over 15 x 10^5 for each of the samples, and the total number of reads was similar between the triplicates of each of the two conditions.

6.5.2. Principal component analysis

The main variability within samples in this experiment is expected to come from experimental differences between the processed samples. As discussed previously, one way of visualizing experimental variability is to look at the first principal components of the PCA, as shown on the figure 6.3. Samples from different experimental conditions cluster together with the exception of one outlier, which was identified with lower quality of RNA compared to the other samples.

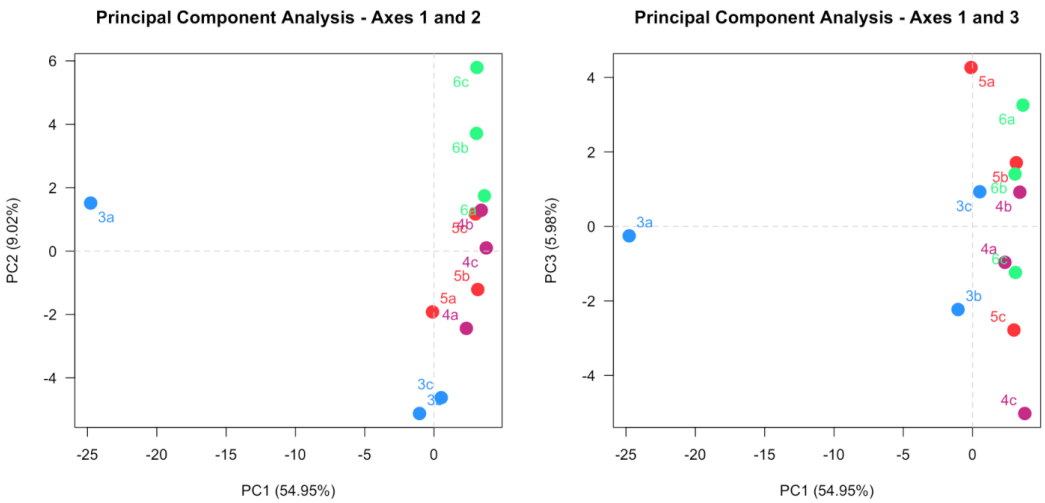

Figure 6.3: Principal Component Analysis, with percentages of variance associated with each axis for HUVEC gene expression profiles examined under different conditions. *Colors refer to the experimental condition of the sample: Blue, mock-infected media; red, mock-infected MP; purple, VZV-infected media; green, VZV-infected MP. In this figure, samples from different biological conditions cluster together with the exception of one outlier (sample incubated with mock-infected media, which was identified with lower quality of RNA compared to the other samples).*

6.5.3. Data normalization

Normalization aims at correcting systematic technical biases in the data, in order to make read counts comparable across samples. We expect normalization to

stabilize distributions across samples. Figure 6.4. shows boxplots of raw (left) and normalized (right) data respectively.

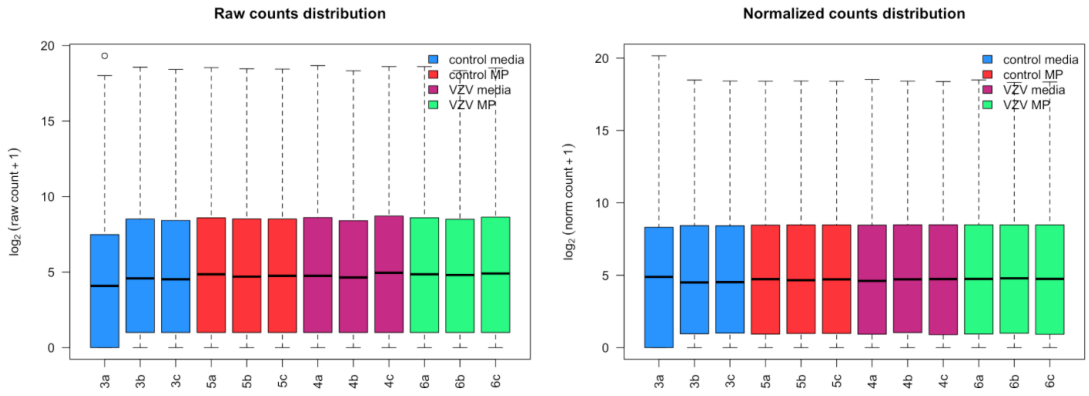

Figure 6.4. Boxplots of raw and normalized read counts for HUVEC gene expression profiles examined under different conditions. *Colors refer to the biological condition of the sample: Colors refer to the biological condition of the sample: Blue, mock-infected media; red, mock-infected MP; purple, VZV-infected media; green, VZV-infected MP. Raw data is presented in the boxplot on the left, and normalized data on the boxplot on the right.*

6.5.4. Visualisation of the RNAseq results

Figure 6.5. shows the volcano plots for the six possible comparisons performed between the 4 conditions, and differentially expressed genes are still highlighted in red. The volcano plot represents the log of the adjusted P value as a function

of the log ratio of differential expression. A volcano plot typically plots some measure of effect on the x-axis (typically the fold change) and the statistical significance on the y-axis (typically the -log10 of the p value). Genes whose expression is highly dysregulated are far to the left and right sides, while highly significant changes appear higher on the plot.

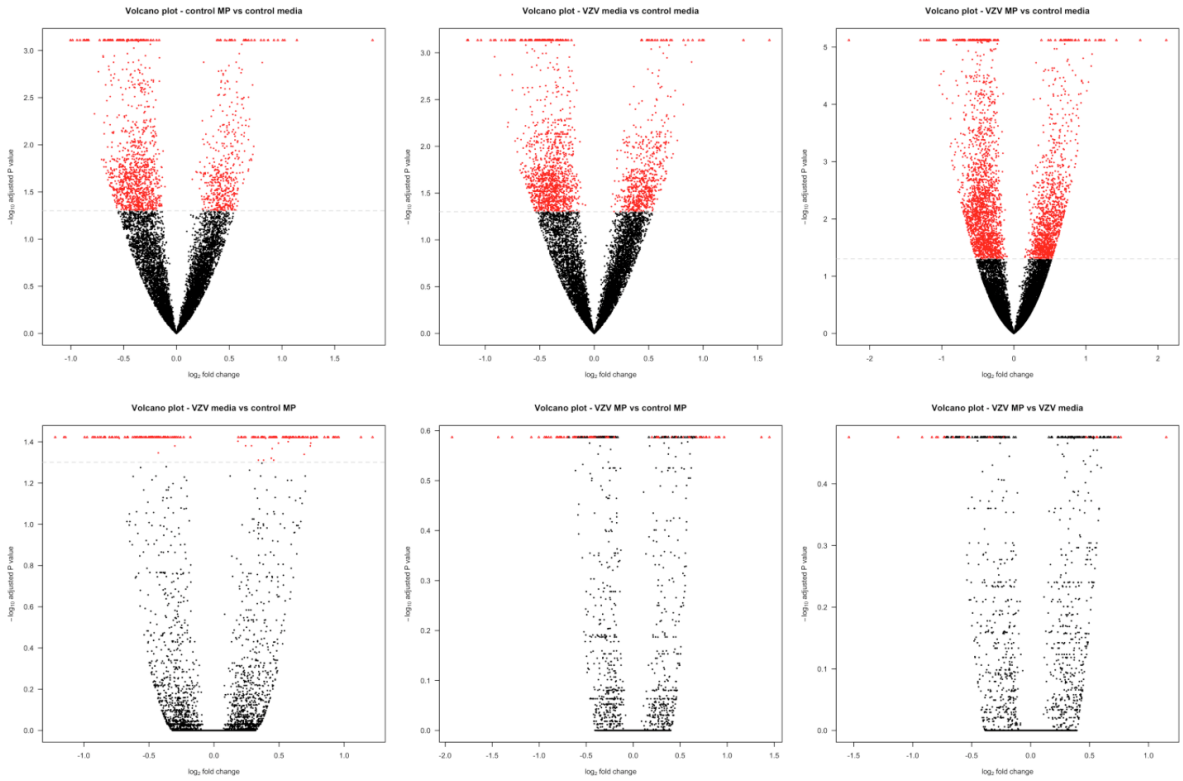

Figure 6.5. Volcano plot of the comparison between gene expression profiles of HUVEC incubated with conditioned media or MP derived from VZV-infected HBVAF. *Red dots represent significantly differentially expressed features. The 6 plots were generate for the possible comparisons between the 4*

conditions: VZV MP to mock MP, VZV MP to VZV media, VZV MP to control MP, VZV MP to mock media, mock MP to mock media, mock MP to VZV media,

Full results with lists of differentially expressed features were provided in a spreadsheet.

6.5.5. Overview of the transcriptomic analysis

With an FDR cutoff of 0.05, the total number of differentially expressed genes were identified, as summarized in table 6-1. The expression of 1992 genes was altered in response to HUVEC treatment with culture media derived from VZV-infected HBVAF, when compared to media derived from mock-infected HBVAF, with expression of 1305 genes up-regulated (65.5%) and expression of 687 genes down-regulated (34.5%). This comparison revealed the most striking differences. Transcriptomic changes of a smaller extent where identified in response to incubation with MP, with 62 genes up-regulated and 38 genes down-regulated. The expression of 43 genes (55% up-regulated, 44% down-regulated) was found to be altered in the HUVEC incubated with MP derived from VZV-infected HBVAF compared to those treated with conditioned media.

Table 6-1. Number of genes differentially expressed in response to incubation of HUVEC with MP or culture media from VZV-infected HBVAF

	Total number	Up	Down
VZV MP vs Mock MP	100	62	38
VZV media vs mock media	1992	1305	687
VZV MP vs VZV media	43	24	19

Using a more stringent FDR cutoff of 0.01, the number of genes whose expression was altered reduced to 614 altered in response to HUVEC treatment with culture media derived from VZV-infected HBVAF, when compared to media derived from mock-infected HBVAF; expression of 55 genes in response to incubation with MP; and expression of 18 genes in the HUVEC incubated with MP derived from VZV-infected HBVAF compared to those treated with conditioned media (Figure 6.6).

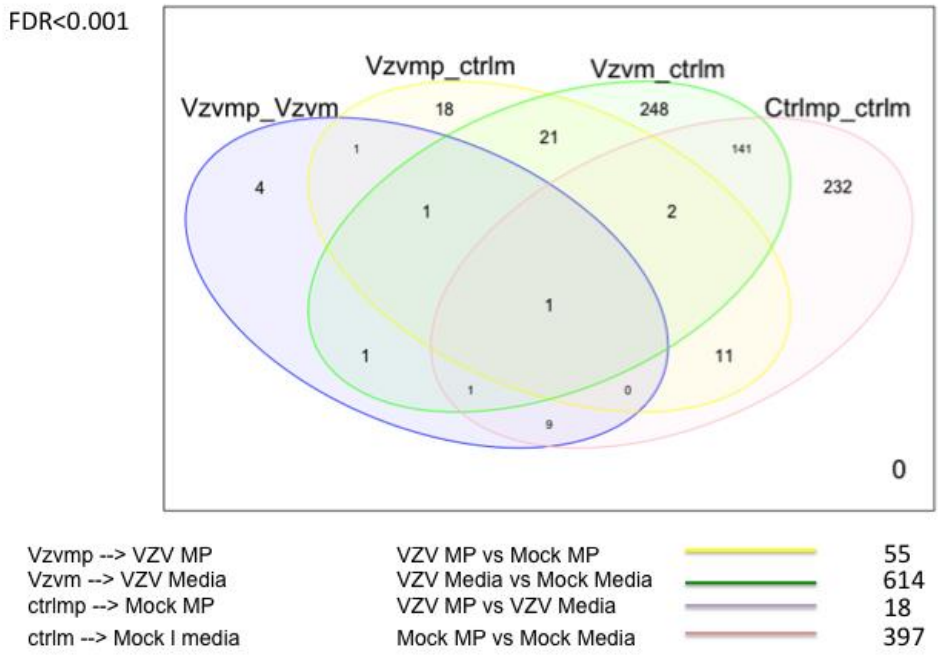

Figure 6.6. Number of significant differentially expressed genes across 4 comparisons*. The Venn diagram indicates the number of significant (FDR<0.001) differentially expressed genes across the four key comparisons and the overlap between each set of genes.*

Future work will complete this analysis, starting with a comparison of the transcriptomic profile of HUVEC incubated with MP. A preliminary analysis has shown that expression of 55 genes was dysregulated in HUVEC in response to incubation with MP derived from VZV-infected HBVAF, when being more stringent and using an FDR<0.01. Of these genes, I have identified ADAM metallopeptidase with thrombospondin type 1 motif 18 (*ADAMTS18*) and lysosome-associated membrane protein 3 *(LAMP3)* genes as possible

candidates to study further, both found to have increased expression in response to stimulation of HUVEC with VZV infected cell-derived MP.

ADAMTS18 is a plasma metalloprotease that interacts with thrombin. A recent conference abstract at the European Society for Paediatric Infectious Diseases meeting in 2017 highlighted this gene as playing a key role in the coagulopathy of meningococcal disease (abstract ESP17-1368**,** Klobassa et al, ESPID 2017).

LAMP3 was first identified as a cell surface marker of mature dendritic cells specifically expressed in lung tissues, endothelial cells (Kobayashi et al, 2000). Recent studies demonstrated that LAMP3 plays a critical role in several cancers, is regulated by hypoxia, and also has a potential role in cardiac remodeling in the context of cardiomyopathy. *LAMP3* is also considered a possible novel therapeutic target for pathological cardiac remodeling (Ding-Sheng Jiang, 2016). This could make *LAMP3* an attractive regulating gene to study further in the setting of VZV-vasculopathy vascular remodeling.

A heatmap of differentially expressed genes was generated including the altered genes with FDR<0.05, to illustrate the expression pattern between the four conditions (Figure 6.7.).

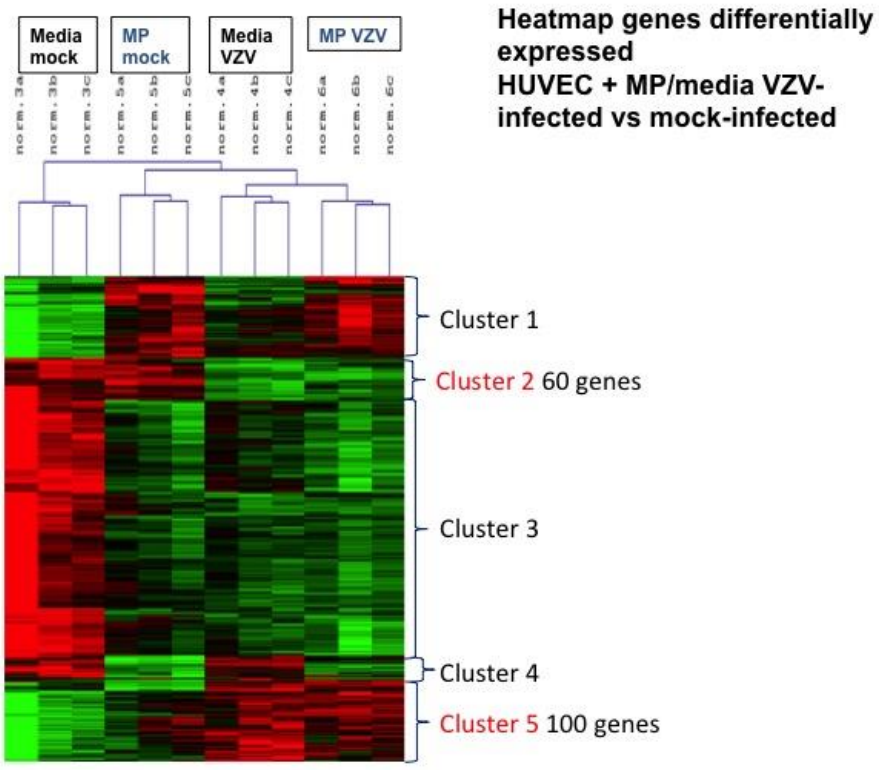

Figure 6.7. Heatmap illustrating hierarchical clustering analysis of the significantly altered gene expression in endothelial cells incubated with MP or media from VZV - and mock-infected HBVAF. *Cluster analysis was performed with meV. The green colour represents down-regulated genes and the red colour up-regulated genes (FDR<0.05). In the heatmap, each column represents a sample and each row represents a gene. Each experimental condition is represented triplicates, making a total of 12 columns for 4 conditions as marked on the figure. The replicates are similar. Focusing on the comparison between HUVEC treated with MP from VZV- or mock-infected human brain fibroblasts, the figure demonstrates that the less degree of overlapping patterns is identified in cluster 2 and cluster 5. Cluster 2 contains 60 genes, and cluster 5 contains 100 genes.*

For the gene set enrichment analysis I used XGR and I have provided the list of genes that appear down-regulated or up-regulated (FDR<0.05) in clusters 2 and 5 between HUVEC treated with MP, and I have chosen the ontology option of “Canonical/KEGG/REACTOME/BioCarta” to identify possible pathways altered. The top enrichments found as altered (up-regulated or down-regulated) are presented in Figures 6.8 and 6.9, respectively. The significance of these findings remains to be explored in further analyses, an area of future work.

Term Name	Z-score	P-value	FDR	# of genes overlapped	Genes
Genes encoding proteins affiliated structurally or functionally to extracellular matrix proteins	2.54	0.0074	0.0095	3	ANXA1, ANXA3, CLEC2B
Ensemble of genes encoding extracellular matrix and extracellular matrix-associated proteins	3.6	0.00042	0.00079	12	BMP2, BMP4, ANXA1, HBEGF, TNFSF18, TNFSF4, FST, RSPO3, ESM1, CYR61, ANXA3, CLEC2B
BMP receptor signaling	6.45	0.000037	0.00019	3	BMP2, BMP4, FST
Cytokine-cytokine receptor interaction	2.58	0.0068	0.0092	4	BMP2, TNFSF18, TNFSF4, TNFRSF12A
Gastrin-CREB signalling pathway via PKC and MAPK	2.21	0.013	0.016	3	EDN1, ANXA1, HBEGF
Signaling by GPCR	-0.0686	0.4	0.42	4	EDN1, ANXA1, HBEGF, RHOB
p53 signaling pathway	4.86	0.00024	0.00054	3	GADD45B, BBC3, DDB2
Direct p53 effectors	4.31	0.00037	0.00076	4	JUN, BBC3, DDB2, DKK1
Pathways in cancer	2.11	0.015	0.018	4	JUN, BMP2, BMP4, FOS
Regulation of nuclear beta catenin signaling and target gene transcription	4.39	0.00046	0.00079	3	JUN, DKK1, CYR61
Signaling events mediated by Hepatocyte Growth Factor Receptor (c-Met)	4.39	0.00046	0.00079	3	JUN, EGR1, SNAI1
Differentiation Pathway in PC12 Cells; this is a specific case of PAC1 Receptor Pathway.	8.42	0.0000016	0.000016	4	JUN, EGR1, TUBA1A, EGR2
Presenilin action in Notch and Wnt signaling	6.12	0.000053	0.0002	3	JUN, FOS, DKK1
AP-1 transcription factor network	8.34	6.4e-7	0.000016	5	JUN, FOS, EDN1, EGR1, CYR61
Calcineurin-regulated NFAT-dependent transcription in lymphocytes	8.22	0.000002	0.000016	4	JUN, FOS, EGR1, EGR2
Immune System	-0.0826	0.4	0.42	4	JUN, FOS, EGR1, USP18
ErbB1 downstream signaling	5.13	0.00011	0.00036	4	JUN, FOS, EGR1, ZFP36
MAPK signaling pathway	1.64	0.033	0.037	3	JUN, FOS, GADD45B

Figure 6.8. Pathways that were found to be significantly altered in HUVEC incubated with MP from infected HBVAF- cluster 2. *The "Canonical/KEGG/REACTOME/BioCarta pathways was chosen. Those terms with FDR<0.05 are highlighted in dark green.*

Term Name	Z-score	P-value	FDR	# of genes overlapped	Genes
Synthesis of PIPs at the plasma membrane	7.2	0.000016	0.00036	3	PIP4K2B, PIK3C2A, PIK3C2B
Cell death signalling via NRAGE, NRIF and NADE	4.82	0.00026	0.0014	3	ARHGEF18, SQSTM1, ABR
Ubiquitin mediated proteolysis	3.95	0.00066	0.0024	4	ANAPC1, WWP2, MID1, UBE2O
Endocytosis	3.17	0.0024	0.0067	4	ARRB1, HSPA1B, PIP4K2B, RAB11FIP5
Signaling by Rho GTPases	3.18	0.0027	0.0067	3	ARHGEF18, SRGAP2, ABR
Phospholipid metabolism	2.99	0.0034	0.0074	4	PIP4K2B, PIK3C2A, PIK3C2B, SLC44A1
Metabolism of lipids and lipoproteins	1.65	0.035	0.064	5	NCOA1, PIP4K2B, PIK3C2A, PIK3C2B, SLC44A1
Axon guidance	1.55	0.038	0.064	3	SRGAP2, SPTBN1, NRP2
Developmental Biology	1.41	0.051	0.081	4	NCOA1, SRGAP2, SPTBN1, NRP2

Figure 6.9. Pathways that were found to be significantly altered in HUVEC incubated with MP from infected HBVAF - cluster 5. *The "Canonical/KEGG/REACTOME/BioCarta pathways was chosen. Where those terms with FDR<0.05 are highlighted in dark green.*

6.6. Discussion

In this chapter I present a preliminary analysis of gene expression profile changes in HUVEC in response to MP derived from infected HBAVFs. These data need further analyses, but may provide broader and deeper insights into transcriptional regulation of vascular endothelial function in response to MP derived from the VZV-infected brain vascular fibroblasts.

RNAseq analysis identified that the expression of a large number of genes was altered in response to VZV infection but with small fold changes. The Venn diagram generated based on the altered gene expression using a stringent FDR

of <0.001 showed that there was very little overlap between the 4 key experimental conditions examined: HUVEC treated with MP or media derived from VZV-infected or mock-infected HBVAF.

The heatmap showed that the detected gene expression changes in replicates were similar. The initial steps of the analysis focused on the comparison between the gene expression profile of HUVEC stimulated with MP. The heatmap showed that 2 clusters of genes appeared up- or down-regulated in response to MP from VZV-infected cells. When these clusters of genes were analysed through XGR for gene ontology and pathway analysis, 22 pathways were highlighted. These findings now require validation by RT-qPCR. More in-depth analysis of other pathways and genes of interest is also required to fully understand the importance of the wealth of data I generate herein.

This preliminary analysis also suggests that altered expression of *LAMP3* and *ADAMTS18* may contribute to the development of pathological changes leading to vascular remodeling in the context of VZV-related AIS.

There are limitations of RNAseq and it is important that the results of the are interpreted in this context. Several issues have been described to cause difficulties in accurately estimating gene expression using RNAseq (Han et al, 2015; Hirsch et al, 2015). It is important to note that the preparation and fragmentation of RNA and the library construction can be biased. Small

transcripts can be more difficult to count due to the standard size selection implemented during construction of RNAseq libraries (Han et al, 2015). In some cases two different genes have overlapping transcripts and it is difficult to determine to which gene the read should be assigned (Hirsch et al, 2015). Also, there are related issues in precisely estimating the abundance of different transcripts from the same gene (Trapnell et al.,2010).

7 General discussion and future directions

Primary VZV infection typically results in varicella, followed by establishment of viral latency in neurons of the cranial nerve, dorsal root and autonomic ganglia along the entire neuraxis, as well as of the adrenal glands (Nagel et al., 2017). The virus reactivates from one of more ganglia, travels peripherally to skin and produces herpes zoster in the corresponding dermatome. During reactivation, VZV could also travel centrally via the anatomical pathways described above, to produce other neurological and ocular diseases with or without associated rash. One such disease is VZV vasculopathy, first described in 1919 (Baudouin and Lantuejoul, 1919) and referred to cases of varicella or zoster temporally associated with stroke, particularly when zoster occurred in the ophthalmic division of the trigeminal nerve. Since the first description, growing epidemiological evidence strongly linked VZV with AIS, but the mechanisms remained unclear until 2011 when a research group very active in neurovirology research led by Don Gilden and Maria Nagel carried out of body of work examining the histology of cerebral arteries from adult patients with VZV vasculopathy. They were able to detect the presence of VZV DNA, and also VZV antigen detected by immunohistochemical analyses in the vascular adventitia of cerebral arteries from patients at the early stages of their disease. VZV DNA and antigens were detected in media and intima of cerebral arteries from patients at a

later stage of their disease (Mayberg et al, 2011). These findings suggested that VZV vasculopathy was due to productive virus infection of arteries, with the adventitia as a likely port of entry for the virus to the cerebral circulation. Recently, the clinical spectrum of VZV vasculopathy has expanded to include extracranial vasculopathy presenting as GCA, the most common systemic vasculitis in the elderly, and granulomatous aortitis (Gilden et al, 2015; Gilden et al, 2016). The pathogenesis of these conditions remains unknown but it has been suggested that viral triggers such as VZV may play a role, and that the adventitia is the portal for viral entry, similar to VZV-related vasculopathy.

In 2013 when I started the work on this project, only a single conference abstract by Nagel et al described work that attempted to elucidate the mechanisms of VZV-related AIS. Since then, this research group published the results of a number of small research studies contributing to our knowledge of the pathogenesis of this disease.

In 2014, Nagel and Gilden investigated a model of VZV persistence in cerebral arteries (Nagel et al. 2014). They demonstrated inhibition of phosphorylated-STAT1 nuclear translocation and Mx1 antiviral protein expression in HBAVF infected with VZV, suggesting that VZV can interfere with the type I interferon pathway as a mechanism of virus persistence in the brain arteries (Nagel et al. 2014). In the same year, this group demonstrated differential regulation of matrix metalloproteinases in varicella zoster virus-infected HBAVF, suggesting that this mechanism could contribute to the aneurysm formation which has been reported

in the context of VZV vasculopathy in adults (Nagel et al. 2014).

In 2016, the Nagel group showed that VZV infection of HBVAF and perineural cells downregulates the expression of programmed death ligand 1 (PD-L1) and MHC-I within 72 hours post infection, and promotes inflammation (Jones et al, 2016). This latest study provided insights into the mechanism by which inflammatory cells persist in VZV-infected arteries, and therefore foster persistent inflammation in vessels leading to pathological vascular remodeling during VZV vasculopathy.

Other than the work of this very active research group, not much is available in the literature on the mechanisms on VZV-related vasculopathy. Earlier studies proposed immune mediated vascular reaction secondary to distant infection (Bartolini et al, 2011; Ganesan and Kirkham, 1997); sympathetic stimulation due to the local irritant effect of the chickenpox lesions in the region of the superior cervical ganglion (Ganesan et Kirkham, 1997); thrombotic vascular occlusion by virus mediated direct endothelial damage (Losurdo et al, 2006; Ganesan et al, 1997); and acquired transient deficiencies of protein S and/or protein C (Losurdo et al, 2006; Alehan et al, 2002).

In this thesis, I attempted to provide the first comprehensive insight into the mechanisms of VZV vasculopathy, creating a hypothetical model and identifying HBVAF as the key player.

My results support an “outside in” model of cerebral arteriopathy in response to VZV infection, with vascular remodeling processes that could lead to arterial obstruction triggered by the activated HBVAF in response to viral infection. I was able to also show a proinflammatory switch of the endothelium in response to soluble and insoluble stimuli released by the infected fibroblasts (figure 7.1.).

I also identified a key role for MP released by the infected adventitial fibroblasts in facilitation cross talk between HBVAF and endothelial cells. I showed for the first time that MP induce endothelial activation and ROS production and also carry virus that can productively infect neighbouring cells. I examined in detail the proteins contained in the MP and that could mediate this process. In addition, preliminary work examined the changes in the transcriptomic profile of HBVAF and endothelial cells in response to VZV infection.

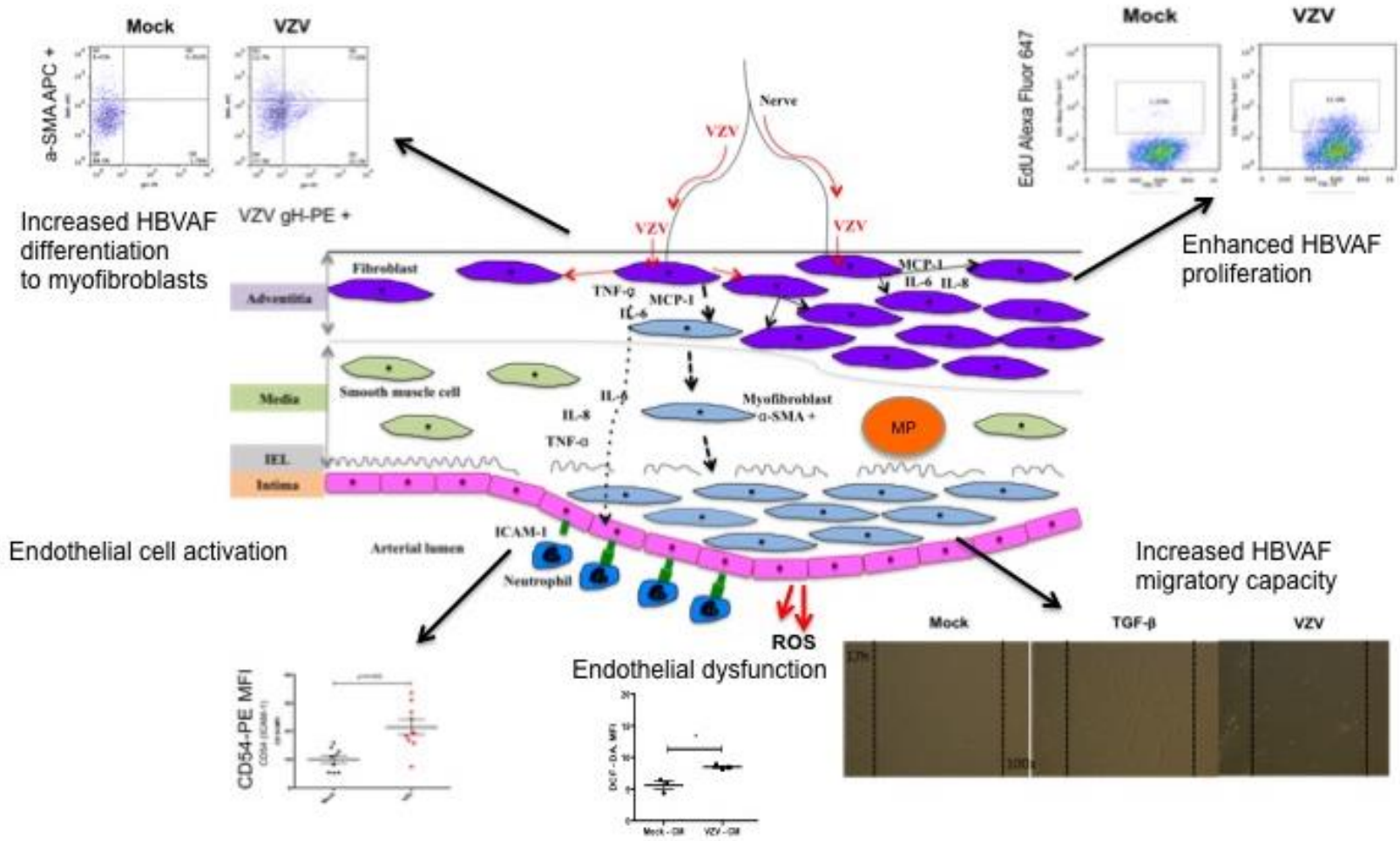

Figure 7.1. VZV-induced changes in HBVAF: an in vitro model of cerebral arteriopathy.

In more detail in my proposed model, VZV infection activates HBVAF and triggers differentiation of HBVAF into myofibrolasts, causing proliferation of these cells and enhancing their migratory capability. Myofibroblasts derived from HBVAF could then theoretically migrate and accumulate in the innermost layers of the vascular wall inducing changes in the caliber of the artery and leading to occlusive vasculopathy, as seen in AIS. In addition, I showed that HBVAF show an increased proliferative potential in response to infection, and this could further worsen the pathological arterial remodeling.

The infected and differentiated fibroblasts could migrate through the arterial wall spreading the infection by direct infection, or as shown here for the first time, by release of MP containing viral particles. It is also possible, as suggested by my in vitro model, that these activated HBVAF and myofibroblats exert paracrine effects on other nearby cells due to their potential to release cytokines. These results from my *in vitro* experiments are in keeping with the histological findings from studies examining VZV-infected brain arteries (Mayberg et al, 2011).

I also examined the effects that infected HBVAF could have on endothelium, and demonstrated that the can cause endothelial activation and dysfunction via cytokine and MP release. The cytokine secreting profile of VZV-infected HBVAF included several proinflammatory cytokines such as IL-8, IL-6, TNF- α and MCP-1. All these cytokines can act in an autocrine fashion further enhancing the migration of differentiated myofibroblasts, or in a paracrine fashion exacerbating

the pathological proliferation, differentiation and migration of other nearby fibroblasts. These chemokines and cytokines may also act as chemoattractants for other inflammatory cells such as neutrophils and other leukocytes (Luckett and Galluci. 2007; Galluci et al. 2006; Galluci et al. 2007; Fredi et al. 2005; Gharaee- Kermani et al. 1996; Nabata et al, 1990). Nagel et al showed that the neutrophils are abundant in cerebral arteries in early VZV vasculopathy (Nagel et al, 2013). Jones et al have recently measured the levels of cytokines and matrix metalloproteinases in the CSF of adult patients with confirmed VZV-related vasculopathy, and found the levels of IL-8, IL-6 and MMP-2 were significantly elevated compared to the levels detected in healthy controls or patients with multiple sclerosis (Jones et al, 2016). These additional publications provide support from human studies to my proposed *in vitro* model.

Of particular and novel interest was to explore the potential role of HBVAF-derived MP in the communication between the VZV-infected HBVAF and endothelial cells and other neighboring HBVAF, in the wider context of emerging evidence suggesting that MP can carry pathogens such as HIV, Dengue, Mycobacterium tuberculosis, and Toxoplasma gondii (Kadiu et al. 2012; Sweet et al. 2008; Singh 2011; Bhatnagar et al. 2007; Schorev and Bharnagar. 2008; Schorev et al. 2008). I showed that VZV-infected HBVAF released AnV+ MPs and that these MP stimulated CD54 upregulation and ROS production in endothelial cells, compatible with endothelial activation and stress.

One particularly interesting and novel observation I made is that MP released by VZV-infected HBVAF harbor viral particles which are capable of inducing lytic infection in healthy fibroblasts. This could suggest an additional model of VZV cell-to-cell viral propagation, which may be of relevance to the pathogenesis of cerebral arteriopathy, and to other conditions. This is an exciting finding which I plan to further investigate in experiments (outside this PhD), for example by further studying the ultrastuctural characterization of MP derived from VZV-infected HBVAF using TEM ultrathin sections.

I have shown that MP contain/are associated with viral particles through a number of different experiments: 1) flow cytometric detection of VZV proteins within the MP population; 2) protein profiling of MP with mass spectrometry confirming the presence of viral proteins within the MP; 3) EM images showing the viral particles were associated with MP and lack of presence of free virus: and 4) MP were able to induce infection in healthy fibroblasts confirmed with CPE and detection of viral antigens.

Excitingly, I was also able to detect VZV antigens in circulating MP obtained from the plasma of paediatric patients with VZV-related cerebral vasculopathy and stroke, not present in children with other vasculopathies, nor in adult controls. These pilot data would support a larger prospective biomarker study of children with VZV associated vasulopathy and AIS. MP VZV+ could be an attractive non-

invasive diagnostic or prognostic biomarker that might in the future eliminate the need for invasive tests as such sampling of CSF, or brain biopsy.

It would also be of considerable interest to establish the cellular origin of these circulating MP. They could be released from fibroblasts, endothelial cells, or also infected T-cells during the viraemia phase.

The recruitment of appropriate controls, both healthy and disease including patients with acute chickenpox is also needed to establish the specificity of my findings. Electron microscopic analysis of MP particles isolated from patients with VZV-related AIS in the acute phase could be done after sorting VZV+ MP to confirm if these particles truly carry the VZV virus *in vivo.*

Finally, in the last part of my PhD, I started a study exploring the transcriptomic profile of VZV-infected HBVAF and also of HUVEC activated by MP derived from VZV-infected HBVAF. This analysis has generated a huge amount of data which will form the basis of many future studies. Preliminary analyses identified *AREG, FMO2, and CKS2* as interesting candidate genes to study further in VZV-infected HBVAF.

LAMP3 and *ADAMTS18* were identified in the series of RNAseq experiments of HUVEC as interesting candidates to study further. Validation studies with qPCR of the expression of all these identified genes is now needed to confirm the

results of RNAseq. In addition, I generated data that could be used for further molecular studies in my proposed model of VZV vasculopathy, although it is too early to speculate on the potential translatable benefit for patients at this stage.

8 Publications from this thesis

Moraitis E, Ganesan V. Childhood infections and trauma as risk factors for stroke. Curr Cardiol Rep. 2014 Sep;16(9):527.

9 References

Abend NS, Beslow LA, Smith SE, Kessler SK, Vossough A, Mason S, Agner S, Licht DJ, Ichord RN. 2011. Seizures as a presenting symptom of acute arterial ischemic stroke in childhood. *J Pediatr*, 159(3):479-83

Abendroth A, Lin I, Slobedman B, Ploegh H, Arvin AM. 2001. Varicella-zoster virus retains major histocompatibility complex class I proteins in the Golgi compartment of infected cells. *J. Virol,* 75:4878–4888

Abendroth A, Slobedman B, Lee E, Mellins E, Wallace M, Arvin AM. 2000. Modulation of major histocompatibility class II protein expression by varicella-zoster virus. *Virol,* 74:1900–1907

Abendroth A, Arvin A, Moffat J. 2010. Varicella zoster virus, New York, *Springer*

Adams HP Jr, Biller J. 2015. Classification of subtypes of ischemic stroke: history of the trial of org 10172 in acute stroke treatment classification. *Stroke,* 46(5): e114-7

Adams HP Jr, Woolson RF, Biller J, Clarke W. 1992. Studies of Org 10172 in patients with acute ischemic stroke. TOAST Study Group. *Haemostasis,* 22(2): 99-103

Aho K, Harmsen P, Hatano S, Marquardsen J, Smirnov VE, Strasser T. 1980. Cerebrovascular disease in the community: results of a WHO collaborative study. *Bull World Health Organ*, 58.113–130

Alehan F, Boyvat F, Baskin E, Derbent M, Ozbek N. 2002. Focal cerebral vasculitis and stroke after chickenpox. *Eur J Paediatr Neurol,* 6: 331–3

Aliotta JM, Pereira M, Amaral A, Sorokina A, Igbinoba Z, Hasslinger A, El-Bizri R, Rounds SI, Quesenberry PJ, Klinger JR. 2013. Induction of pulmonary hypertensive changes by extracellular vesicles from monocrotaline-treated mice. *Cardiovasc Res,* Dec 1; 100(3): 354-62

Aliotta JM, Pereira M, Wen S, Dooner MS, Del Tatto M, Papa E, Goldberg LR, Baird GL, Ventetuolo CE, Quesenberry PJ, Klinger JR. 2016. Exosomes induce and reverse monocrotaline-induced pulmonary hypertension in mice. *Cardiovasc Res,* 110(3):319-30

Amarenco P, Bogousslavsky J, Caplan JR, Donnan GA, Hennerici MG. 2009. Classification of stroke subtypes. *Cerebrovasc. Dis*, 27, pp. 493-501

Ambagala AP, Cohen JI. 2007. Varicella-Zoster virus IE63, a major viral latency protein, is required to inhibit the alpha interferon-induced antiviral response. *J Virol,* Aug; 81(15): 7844-51

Amir Y, Edward O-A, Utpal B. 2008.A protocol for in vivo detection of reactive oxygen species. *Proto. Exch.*

Amlie-Lefond C, Sébire G, Fullerton HJ. 2008. Recent developments in childhood arterial ischaemic stroke. *Lancet Neurol*., 7, (5) 425-35

Amlie-Lefond C, Bernard TJ, Sébire G, Friedman NR, Heyer GL, Lerner NB, DeVeber G, Fullerton HJ; International Pediatric Stroke Study Group. 2009. Predictors of cerebral arteriopathy in children with arterial ischemic stroke: results of the International Pediatric Stroke Study. *Circulation*, 119, (10) 1417–23

Arribas SM, Hillier C, Gonzalez C, McGrory S, Dominiczak AF, McGrath JC. 1997. Cellular aspects of vascular remodeling in hypertension revealed by confocal microscopy. *Hypertension*, 30 1455–64

Arvin AM, Gilden D. 2013. Varicella-Zoster Virus. In: Howley PM, Knipe DM, editors. Fields Virology. Vol. 2. Philadelphia: Lippincott Williams and Wilkins Press pp. 2015–2184

Askalan R, Laughlin S, Mayank S, Chan A, MacGregor D, Andrew M, Curtis R, Meaney B, deVeber G. 2001. Chickenpox and stroke in childhood: a study of frequency and causation. *Stroke*, 32, (6), 1257–62

Aviv RI, Benseler SM, DeVeber G, Silverman ED, Tyrrell PN, Tsang LM,

Armstrong D. 2007. Angiography of primary central nervous system angiitis of childhood: conventional angiography verses magnetic resonance angiography at presentation. *AJNR Am J Neuroradiol,* 28, 9–15

Aydin F. 1998. Do human intracranial arteries lack vasa vasorum? A comparative immunohistochemical study of intracranial and systemic arteries. Acta Neuropathol. 1998, 96, (1), 22-8

Baird AE, Warach S. 1998. Magnetic resonance imaging of acute stroke. *J Cereb Blood Flow Metab*, 18, (6) 583-609

Barna M. 2013. Ribosomes take control. *Proc Natl Acad Sci U S A,* 110(1): 9–10

Bartolini L, Gentilomo C, Sartori S, Calderone M, Smioni P, Laverda AM. 2011. Varicella and Stroke in Children Good Outcome with steroids. *Clin Appl Thromb Hemost*, 17: E127–30

Batra SK, Jarnagin WR, Schwartz RE, Matei I, Peinado H, Stanger BZ, Bromberg J, Lyden D. 2015. Pancreatic cancer exosomes initiate pre- metastatic niche formation in the liver. *Nat Cell Biol,* 17:816 – 826

Benjamin EJ, Blaha MJ, Chiuve SE, Cushman M, Das SR, Deo R, de Ferranti SD, Floyd J, Fornage M, Gillespie C, Isasi CR, Jiménez MC, Jordan LC, Judd SE, Lackland D, Lichtman JH, Lisabeth L, Liu S, Longenecker CT, Mackey RH, Matsushita K, Mozaffarian D, Mussolino ME, Nasir K, Neumar RW, Palaniappan L, Pandey DK, Thiagarajan RR, Reeves MJ, Ritchey M, Rodriguez CJ, Roth GA, Rosamond WD, Sasson C, Towfighi A, Tsao CW, Turner MB, Virani SS, Voeks

JH, Willey JZ, Wilkins JT, Wu JH, Alger HM, Wong SS, Muntner P; American Heart Association Statistics Committee and Stroke Statistics Subcommittee.2017. Heart Disease and Stroke Statistics-2017 Update: A Report From the American Heart Association. *Circulation*, 7; 135(10): e146-e603

Berasain C, Avila MA. 2014. Amphiregulin. Semin Cell Dev Biol, 28:31-41

Bevilacqua MP, Pober JS, Wheeler ME, Cotran RS, Gimbrone MA Jr. 1985. Interleukin-1 acts on cultured vascular endothelium to increase the adhesion of polymorphonuclear leukocytes, monocytes and related leuko- cyte cell lines. *J. Clin. Invest, 76:2003*–2011

Bernard TJ, Manco-Johnson MJ. 2012. Towards a consensus-based classification of childhood arterial ischemic stroke. *Stroke*, 43, (2) 371-7

Beyer C, Pisetsky DS. 2010. The role of microparticles in the pathogenesis of rheumatic diseases. *Nat Rev,* 6: 21–29

Bhatnagar S, Shinagawa K, Castellino FJ, Schorey JS. 2007. Exosomes released from macrophages infected with intracellular pathogens stimulate a proinflammatory response in vitro and in vivo. *Blood,* 110, 3234–3244

Braun KP, Bulder MM, Chabrier S, Kirkham FJ, Uiterwaal CS, Tardieu M, Sébire G. 2009. The course and outcome of unilateral intracranial arteriopathy in 79 children with ischaemic stroke. *Brain*, 132, (Pt 2), 544–57

Breuer J, Pacou M, Gauthier A, Brown MM. 2014. Herpes zoster as a risk factor for stroke and TIA: a retrospective cohort study in the UK. *Neurology,* 82, (3)

206–12

Breuer J, Whitley R. 2007. Varicella zoster virus: natural history and cur- rent therapies of varicella and herpes zoster. *Herpes,* 14(Suppl 2):25–29

Browne EP, Wing B, Coleman D, Shenk T. 2001. Altered cellular mRNA levels in human cytomegalovirus-infected fibroblasts: viral block to the accumulation of antiviral mRNAs. *J. Virol,* 75:12319–12330

Bryan RN, Levy LM, Whitlow WD, Killian JM, Preziosi TJ, Rosario JA. 1991. Diagnosis of acute cerebral infarction: comparison of CT and MR imaging. *AJNR Am J Neuroradiol*, 12, (4) 611-20

Calabrese LH, Mallek JA. 1988. Primary angiitis of the central nervous system. Report of 8 new cases, review of the literature, and proposal for diagnostic criteria. *Medicine (Baltimore)*, 67, (1) 20–39

Carlquist JF, Edelman L, Bennion DW, Anderson JL. 1999. Cytomegalovirus induction of interleukin-6 in lung fibroblasts occurs independently of active infection and involves a G protein and the transcription factor, NF-kappaB. *J Infect Dis,* 179, (5) 1094-100

Chabrier S, Kossorotoff M, Darteyre S. 2013. Place des antithrombotiques dans l'accident vasculaire cerebral de l'enfant. *Presse Med*, 42: 1259–66

Chabrier S, Rodesch G, Lasjaunias P, Tardieu M, Landrieu P, Sébire G. 1998. Transient cerebral arteriopathy: a disorder recognized by serial angiograms in children with stroke. *J Child Neurol,* 13, (1) 27-32

Chang YE, Laimins LA. 2000. Microarray analysis identifies inter- feron-inducible genes and Stat-1 as major transcriptional targets of human papillomavirus type 31. J. Virol, 74:4174–4182

Chatelain RE, Dardik BN. 1988. Increased DNA replication in the arterial adventitia after aortic ligation. *Hypertension, 11* 130–4

Chinta SJ, Andersen JK. 2008. Redox imbalance in Parkinson's disease. *Biochim Biophys Acta*, 1780:1362–1367

Cipolla MJ. 2009. The cerebral circulation, San Rafael (CA), Morgan & Claypool Life Sciences.

Cohen JI. 2010. The varicella-zoster virus genome. *Curr Top Microbiol Immunol,* 342:1–14

CohenJ, Straus S, and Arvin A. 2007. Varicella-zoster virus replication, pathogenesis, and management, 5th ed., vol. 2. Lippincott Williams & Wilkins, Philadelphia, PA

Cohrs RJ, Mehta SK, Schmid DS, Gilden DH, Pierson DL. 2008. Asymptomatic reactivation and shed of infectious varicella zoster virus in astronauts. *J Med Virol,* 80(6) 1116–22

Cole NL, Grose C. 2003. Membrane fusion mediated by herpesvirus glycoproteins: the paradigm of varicella-zoster virus. *Rev Med Virol*, 13, (4), 207-22

Combes V, Simon AC, Grau GE, Arnoux D, Camoin L. 1999. In vitro generation of endothelial microparticles and possible prothrombotic activity in patients with lupus anticoagulant. *J Clin Invest*,104: 93–102

Cravioto K, Feigin I. 1959. Noninfectious granulomatous angiitis with a predilection for the nervous system. *Neurology*, 9(3): 599-609

Cuadras MA, Feigelstock DA, An S, Greenberg HB. 2002. Gene expression pattern in Caco-2 cells following rotavirus infection. *. Virol*, 76:4467–4482

Danchaivijitr N, Cox TC, Saunders DE, Ganesan V. 2006. Evolution of cerebral arteriopathies in childhood arterial ischemic stroke. *Ann Neurol*, 59, (4) 620–6

Das M, Dempsey EC, Reeves JT, Stenmark KR. 2002. Selective expansion of fibroblast subpopulations from pulmonary artery adventitia in response to hypoxia. *Am J Physiol Lung Cell Mol Physiol* 282(5): L976-86

Das M, Dempsey EC, Bouchey D, Reyland ME, Stenmark KR. 2000. Chronic hypoxia induces exaggerated growth responses in pulmonary artery adventitial fibroblasts: potential contribution of specific protein kinase c isozymes. *Am J Respir Cell Mol Biol*, 22 15–25

Dassah M, Deora AB He K and Hajjar KA. 2009. The endothelial cell annexin A2 system and vascular fibrinolysis. *Gen Physiol Biophys*, 28:F20–28

Dean WL, Lee MJ, Cummins TD, Schultz DJ, Powell DW. 2009. Proteomic and functional characterisation of platelet microparticle size classes. *Thromb Haemost*, 102: 711–718

DeCaterina R, Libby P, Peng HB, Thannickal VJ, Rajavashisth TB, Gimbrone MA Jr, Shin WS, Liao JK. 1995. Nitric oxide decreases cytokine-induced endothelial

activation. Nitric oxide selectively reduces endothelial expression of adhesion molecules and proinflammatory cytokines. *J Clin Invest*. Jul; 96(1): 60-8

DeHavenon A, Mossa-Basha M, Shah L, Kim SE, Park M, Parker D, McNally JS. 2017. High-resolution vessel wall MRI for the evaluation of intracranial atherosclerotic disease. *Neuroradiology*, 59(12): 1193-1202

DeVeber G. 2000. The Canadian Pediatric Ischemic Stroke Study Group: Canadian Paediatric Ischemic Stroke Registry: analysis of children with arterial ischemic stroke [abstract]. *Ann Neurol,* 48, 514

DeVeber G, Roach ES, Riela AR, Wiznitzer M. 2000. Stroke in children: recognition, treatment, and future directions. *Semin Pediatr Neurol,* 7, (4), 309-17

DeVeber G. 2003. Risk factor for stroke: little folks have different strokes! *Ann Neurol*, 53, 149–54.

Di J, Huang H, Qu D, Tang J, Cao W, Lu Z, Cheng Q, Yang J, Bai J, Zhang J. 2015. Rap2B promotes proliferation, migration, and invasion of human breast cancer through calcium-related ERK1/2 signaling pathway. Sci Rep, 5:12363

Ding L, Liu T, Wu Z, Hu B, Nakashima T, Ullenbruch M, Gonzalez De Los Santos F, Phan SH. 2016. Bone Marrow CD11c+ Cell-Derived Amphiregulin Promotes Pulmonary Fibrosis. *J Immunol,* 197(1): 303-12

Dunlevy JR, Couchman JR. 1995. Interleukin-8 induces motile behavior and loss of focal adhesions in primary fibroblasts. *J Cell Sci,* 108, (Pt 1) 311-21

Earley CJ, Kittner SJ, Feeser BR, Gardner J, Epstein A, Wozniak MA, et al.

1998. Stroke in children and sickle-cell disease: Baltimore–Washington Cooperative Young Stroke Study. *Neurology,* 51, 169–76

Edmond BJ, Grose C, Brunell PA. 1981. Varicella-zoster virus infection of diploid and chemically transformed guinea-pig embryo cells: factors influencing virus replication. *J Gen Virol*. 1981, 54, 403-7

Eisfeld AJ, Yee MB, Erazo A, Abendroth A, Kinchington PR. 2007. Downregulation of class I major histocompatibility complex surface expression by varicella-zoster virus involves open reading frame 66 protein kinase-dependent and -independent mechanisms. *J Virol,* 81, (17), 9034-49

El Kasmi KC, Pugliese SC, Riddle SR, Poth JM, Anderson AL, Frid MG, Li M, Pullamsetti SS, Savai R, Nagel MA, Fini MA, Graham BB, Tuder RM, Friedman JE, Eltzschig HK, Sokol RJ, Stenmark KR. 2014. Adventitial fibroblasts induce a distinct pro inflammatory/profibrotic macrophage phenotype in pulmonary hypertension. *J Immunol,* 193(2): 597-609

Elbers J, Benseler SM. 2008. Central nervous system vasculitis in children. *Curr Opin Rheumatol,* 20, (1) 47–54

Eleftheriou D. Ganesan V. 2009. Controversies in childhood arterial is- chemic stroke and cerebral venous sinus thrombosis. *Expert Rev Cardiovasc Ther*, 7, (7) 853–61

Elkind MS, Hills NK, Glaser CA, Lo WD, Amlie-Lefond C, Dlamini N, Kneen R, Hod EA, Wintermark M, deVeber GA, Fullerton HJ; VIPS Investigators. 2016.

Herpesvirus Infections and Childhood Arterial Ischemic Stroke: Results of the VIPS Study. *Circulation.* 133(8): 732-41

Enders JF. 1954. Cytopathology of virus infections: particular reference to tissue culture studies. *Annu Rev Microbiol*, 1954, 8, 473-502

Eyden B. 2001. The myofibroblast: an assessment of controversial issues and a definition useful in diagnosis and research. *Ultrastruct Pathol,* 25 39–50

Fang H, Knezevic B, Burnham KL, Knight JC. 2016. XGR software for enhanced interpretation of genomic summary data, illustrated by application to immunological traits. *Genome Med,* Dec 13;8(1): 129

Feng Z, Hensley L, McKnight KL, Hu F, Madden V, Ping L. 2013. A pathogenic picornavirus acquires an envelope by hijacking cellular membranes. *Nature*, 496: 367–371

Ferro JM, Massaro AR, Mas JL. 2010. Aetiological diagnosis of ischaemic stroke in young adults. Lancet Neurol, 9(11): 1085-96

Fredj S, Bescond J, Louault C, Delwail A, Lecron JC, Potreau D. 2005. Role of interleukin-6 in cardiomyocyte/cardiac fibroblast interactions during myocyte hypertrophy and fibroblast proliferation. *J Cell Physiol,* 204, (2) 428-36

Fox CK, Johnston SC, Sidney S, Fullerton HJ. 2012. High critical care usage due to pediatric stroke: results of a population-based study. *Neurology*, 79, (5), 420-7

Fullerton HJ, Wintermark M, Hills NK, Dowling MM, Tan M, Rafay MF, Elkind MS, Barkovich AJ, deVeber GA; VIPS Investigators. 2016. Risk of Recurrent Arterial

Ischemic Stroke in Childhood: A Prospective International Study. *Stroke,* 47, (1) 53–59

Fullerton HJ, Wu YW, Sidney S, Johnston SC. 2007. Risk of recurrent childhood arterial ischemic stroke in a population-based cohort: the importance of cerebrovascular imaging. *Pediatrics*, 119, 495–501

Fullerton HJ, Wu YW, Zhao S, Johnston SC. 2003. Risk of stroke in children: ethnic and gender disparities. *Neurology,* 61, (2) 189-94

Fullerton HJ, Hills NK, Elkind MS, Dowling MM, Wintermark M, Glaser CA, Tan M, Rivkin MJ, Titomanlio L, Barkovich AJ, deVeber GA; VIPS Investigators. 2015. Infection, vaccination, and childhood arterial ischemic stroke: Results of the VIPS study. Neurology. 85, (17) 1459-66

Gadian DG, Calamante F, Kirkham FJ, Bynevelt M, Johnson CL, Porter DA, Chong WK, Prengler M, Connelly A. 2000. Diffusion and perfusion magnetic resonance imaging in childhood stroke. *J Child Neurol*, 15, (5) 279-83

Gallucci RM, Lee EG, Tomasek JJ. 2006. IL-6 modulates alpha-smooth muscle actin expression in dermal fibroblasts from IL-6-deficient mice. *J Invest Dermatol,* 126, (3) 561-8

Ganesan V. 2010. Neuroimaging of childhood arterial ischaemic stroke. *Dev Med Child Neurol,* 52, (11), 983

Ganesan V, Chong WK, Cox TC, Chawda SJ, Prengler M, Kirkham FJ. 2002.

Posterior circulation stroke in childhood: risk factors and recurrence. *Neurology,* 59, (10), 1552-6

Ganesan V, Cox TC, Gunny R. 2011. Abnormalities of cervical arteries in children with arterial ischemic stroke. *Neurology*, 76, (2) 166– 71

Ganesan V, Hogan A, Shack N, Gordon A, Isaacs E, Kirkham FJ. 2000. Outcome after ischaemic stroke in childhood. *Dev Med Child Neurol,* 42, 455–61

Ganesan V, Kirkham FJ. 1997. Mechanisms of ischaemic stroke after chickenpox. *Arch Dis Child*, 76: 522–5

Ganesan V, Prengler M, McShane MA, Wade AM, Kirkham FJ. 2003. Investigation of risk factors in children with arterial ischemic stroke. *Ann Neurol*, 53, (2), 167-73

Ganesan V, Prengler M, Wade A, Kirkham FJ. 2006. Clinical and radiological recurrence after childhood arterial ischemic stroke. *Circulation,* 114, (20) 2170-7

Garcia BA, Smalley DM, Cho H, Shabanowitz J, Ley K, Hunt DF. 2005. The platelet microparticle proteome. *J Proteome Res*, 4: 1516–1521

Garcia-Ruiz C, Colell A, Mari M, Morales A, Fernandez-Checa JC. 1997. Direct effect of ceramide on the mitochondrial electron transport chain leads to generation of reactive oxygen species, *Journal of Biological Chemistry*, vol. 272, no. 17, pp. 11369- 11377

Gharaee-Kermani M, Denholm EM, PhanSH. 1996. Costimulation of fibroblast

collagen and transforming growth factor beta1 gene expression by monocyte chemoattractant protein-1 via specific receptors. *J Biol Chem,* 271 17779 – 17784

Gilden D, Cohrs RJ, Mahalingam R, Nagel MA. 2009. Varicella zoster virus vasculopathies: diverse clinical manifestations, laboratory features, pathogenesis, and treatment. *Lancet Neurol.,* 8, (8), 731-40.

Gilden D, Cohrs RJ, Mahalingam R, Nagel MA. 2009. Varicella zoster virus vasculopathies: diverse clinical manifestations, laboratory features, pathogenesis, and treatment. *Lancet Neurol,* 8(, 8) 731–40

Gilden DH, Lipton HL, Wolf JS, Akenbrandt W, Smith JE, Mahalingam R, Forghani B. 2002. Two patients with unusual forms of varicella zoster virus vasculopathy. *N Engl J Med*, 347:1500–1503

Gilden DH, Mahalingam R, Cohrs RJ, Kleinschmidt-DeMasters BK, Forghani B. 2002. The protean manifestations of varicella-zoster virus vasculopathy. *J Neurovirol*, 8(Suppl 2): 75–9

Gilden D, Nagel MA, Mahalingam R, Mueller NH, Brazeau EA, Pugazhenthi S, Cohrs RJ. 2009. Clinical and molecular aspects of varicella zoster virus infection. *Future Neurol,* 4, (1) 103–17

Mahalingam R, Wellish MC, Dueland AN, Cohrs RJ, Gilden D. 1992. Localization of herpes simplex virus and varicella zoster virus DNA in human ganglia. *Ann Neurol*, 31:444–8

Gilden D, White T, Khmeleva N, Katz BJ, Nagel MA. 2016. Blinded search for varicella zoster virus in giant cell arteritis (GCA)-positive and GCA-negative temporal arteries. *J Neurol Sci*, 364:141-3

Gimbrone MA Jr, Nagel T, Topper JN. 1997. Biomechanical activation: an emerging paradigm in endothelial adhesion biology. *J Clin Invest,* Apr 15; 99(8):1809-13

Giroud M, Lemesle M, Gouyon JB, Nivelon JL, Milan C, Dumas R. 1995. Cerebrovascular disease in children under 16 years of age in the city of Dijon, France: a study of incidence and clinical features from 1985 to 1993. *J Clin Epidemiol,* 48, 1343–8. Grose C. 1990. Glycoproteins encoded by varicella-zoster virus: biosynthesis, phosphorylation, and intracellular trafficking. *Annu Rev Microbiol*, 44, 59–80

Grose C, Brunel PA. 1978. Varicella-zoster virus: isolation and propagation in human melanoma cells at 36 and 32 degrees C. *Infect Immun.*, 19, (1), 199-203.

Grose C, Perrotta DM, Brunell PA, Smith GC. 1979. Cell-free varicella-zoster virus in cultured human melanoma cells. *J Gen Virol,* 43, (1), 15-27.

Grotendorst GR1, Rahmanie H, Duncan MR. 2004. Combinatorial signaling pathways determine fibroblast proliferation and myofibroblast differentiation. *Faseb J.*, 18, (3), 469- 79

Golomb MR, Fullerton HJ, Nowak-Gottl U, Deveber G. 2009. Male predominance in childhood ischemic stroke: findings from the International Pediatric Stroke

Study. *Stroke,* 40, 52–57

Gowrishankar K, Slobedman B, Cunningham AL, Miranda-Saksena M, Boadle RA, Abendroth A. 2007. Productive varicella-zoster virus infection of cultured intact human ganglia. *J. Virol*, 81, (12) 6752-6

Gray F, Bélec L, Lescs MC, Chrétien F, Ciardi A, Hassine D, Flament-Saillour M, de Truchis P, Clair B, Scaravilli F. 1994. Varicella-zoster virus infection of the central nervous system in the acquired immune deficiency syndrome. *Brain*, 117(Pt 5): 987-99

Grünewald K, Desai P, Winkler DC, Heymann JB, Belnap DM, Baumeister W, Steven AC. 2003. Three-dimensional structure of herpes simplex virus from cryo-electron tomography. *Science*, 21; 302(5649): 1396-8

Gustafson CM, Shepherd AJ, Miller VM, Jayachandran M. 2015. Age and sex specific differences in blood-borne microvesicles from apparently healthy humans. Biol Sex Differ. 6(11):10

György B, Szabó TG, Pásztói M, Pál Z, Misják P, Aradi B, László V, Pállinger E, Pap E, Kittel A, Nagy G, Falus A, Buzás EI. 2011. Membrane vesicles, current state-of-the-art: emerging role of extracellular vesicles. *Cell Mol Life Sci,* 68, (16), 2667-88

Haberthur K, Messaoudi I. 2013. Animal Models of Varicella Zoster Virus Infection. *Pathogens,* Jun; 2(2): 364–382

Hall S, Carlin L, Roach ES, McLean WT Jr. 1983. Herpes zoster and central retinal artery occlusion. *Ann Neurol,* 13:217–218

Halliwell B. 2001. Role of free radicals in the neurodegenerative diseases: therapeutic implications for antioxidant treatment. *Drugs Aging*, 18:685–716

Han Y, Gao S, Muegge K, Zhang W, Zhou B. 2015. Advanced Applications of RNA Sequencing and Challenges. *Bioinformatics and Biology Insights*, 9(Suppl 1): 29-46.

Haraldsen G., Kvale D., Lien B., Farstad I. N., Brandtzaeg P. 1996. Cytokine-regulated expression of E-selectin, intercellular adhesion molecule-1 (ICAM-1), and vascular cell adhesion molecule-1 (VCAM-1) in human microvascular endothelial cells. *J. Immunol,* 1, 2558–2565

Harper DR, Mathieu N, Mullarkey J. 1998. High-titre, cryostable cell-free varicella zoster virus. *Arch Virol*, 143, (6), 1163-70

Harson R, Grose C. 1995. Egress of varicella-zoster virus from the melanoma cell: a tropism for the melanocyte. *J Virol,* Aug; 69(8):4994-5010

Hassoun PM, Mouthon L, Barberà JA, Eddahibi S, Flores SC, Grimminger F, Jones PL, Maitland ML, Michelakis ED, Morrell NW, Newman JH, Rabinovitch M, Schermuly R, Stenmark KR, Voelkel NF, Yuan JX, Humbert M. 2009. Inflammation, growth factors, and pulmonary vascular remodeling. *J Am Coll Cardiol,* 54(1 Suppl):S10-9

Haug A, Mahalingam R, Cohrs RJ, Schmid DS, Corboy JR, Gilden D. 2010. Recurrent polymorphonuclear pleocytosis with increased red blood cells caused by varicella zoster virus infection of the central nervous system: Case report and review of the literature*. J Neurol Sci*, 292(1-2):85-8

He KL, Sui G, Xiong H, Broekman MJ, Huang B, Marcus AJ, Hajjar KA. 2010. Feedback regulation of endothelial cell surface plasmin generation by PKC dependent phosphorylation of annexin A2. *J Biol Chem*, 286:15428–15439

Heijnen HFG, Schiel AE, Fijnheer R, Geuze HJ, Sixma JJ. 1999. Activated platelets release two types of membrane vesicles: Microvesicles by surface shedding and exosomes derived from exocytosis of multivesicular bodies and-granules. *Blood*, 94: 3791–3799

Heywood W, Mills K, Wang D, Hogg J, Madgett T., Avent ND. 2012. Identification of new biomarkers for Down's syndrome in maternal plasma. *J Proteome,* 75(9):2621–2628

Hinz B. 2007. Formation and function of the myofibroblast during tissue repair. *J Invest Dermatol*, 127, (3), 526-37

Hirsch CD, Springer NM, Hirsch CN. 2015. Genomic limitations to RNA sequencing expression profiling. *Plant J,* 84(3):491-503.

Hong Y, Eleftheriou D, Hussain AA, Price-Kuehne FE, Savage CO, Jayne D, Little MA, Salama AD, Klein NJ, Brogan PA. 2012. Anti-neutrophil cytoplasmic antibodies stimulate release of neutrophil microparticles. *J Am Soc Nephrol*, 23, (1), 49-62

Horstman LL, Ahn YS. 1999. Platelet microparticles: a wide-angle perspective. *Crit Rev Oncol Hematol,* 30, 111–142

Howard VJ. 2013. Reasons underlying racial differences in stroke incidence and

mortality. Stroke, 44(6 Suppl 1):S126-8

Howard PW, Wright CC, Howard T, Johnson DC. 2014. Herpes Simplex Virus gE /gI Extracellular Domains Promote Axonal Transport and Spread from Neurons to Epithelial Cells. *J Virol*, 88(19): 11178–11186

Hsieh HJ, Liu CA, Huang B, Tseng AH, Wang DL. 2014. Shear-induced endothelial mechanotransduction: the interplay between reactive oxygen species (ROS) and nitric oxide (NO) and the pathophysiological implications. *J Biomed Sci.* 13;21:3

Hugel B, Martínez MC, Kunzelmann C, Freyssinet JM. 2005.Membrane microparticles: two sides of the coin. *Physiology (Bethesda),* 20:22–27

Humbert M, Morrell NW, Archer SL, Stenmark KR, MacLean MR, Lang IM, Christman BW, Weir EK, Eickelberg O, Voelkel NF, Rabinovitch M. 2004. Cellular and molecular pathobiology of pulmonary arterial hypertension. *J Am Coll Cardiol,* 43(12 Suppl S):13S-24S

Hunter MP, Ismail N, Zhang X, Aguda BD, Lee EJ, Yu L, Xiao T, Schafer J, Lee ML, Schmittgen TD, Nana-Sinkam SP, Jarjoura D, Marsh CB. 2008. Detection of microRNA expression in human peripheral blood microvesicles*. PLoS One*, 3: e3694

Idowu OE. 2008. *Int. J. Morphol., 26, (4)*, 1023-1027

Ishimaru H, Ochi M, Morikawa M, Takahata H, Matsuoka Y, Koshiishi T, Fujimoto T, Egawa A, Mitarai K, Murakami T, Uetani M. 2007. Accuracy of pre and post contrast time of flight MR angiography in patients with acute ischaemic stroke. *AJNR Am J Neuroradiol,* 28, 923–926

Issman L, Brenner B, Talmon Y, Aharon A. 2013. Cryogenic transmission electron microscopy nanostructural study of shed microparticles. *PLoS One*, 26;8(12):e83680

Jabs A, Okamoto E, Vinten-Johansen J, Bauriedel G, Wilcox JN. 2007. Sequential patterns of chemokine and chemokine receptor-synthesis following vessel wall injury in porcine coronary arteries. *Atherosclerosis*, 192 75–84

Jakubowski W, Bartosz G.1997. Estimation of oxidative stress in Saccharomyces cerevisae with fluorescent probes. *Int J Biochem Cell Biol.* Nov;29(11):1297-301

Jiang DS, Yi X, Huo B, Liu XX, Li R, Zhu XH, Wei X. 2016. The potential role of lysosome-associated membrane protein 3 (LAMP3) on cardiac remodelling. *American Journal of Translational Research*, *8*(1), 37–48

Jimenez JJ, Jy W, Mauro LM, Soderland C, Horstman LL, Ahn YS. 2003. Endothelial cells release phenotypically and quantitatively distinct microparticles in activation and apoptosis. *Thromb Res*, 109, 175–180.

Jones BP, Ganesan V, Saunders DE, Chong WK. 2010. Imaging in childhood arterial ischaemic stroke. Neuroradiology, 52,(6) 577-89

Jones JO, Arvin AM. 2006. Inhibition of the NF-kappaB pathway by varicella-zoster virus in vitro and in human epidermal cells in vivo. *J Virol,* 80:5113–5124

Jones JO, Arvin AM. 2003. Microarray analysis of host cell gene transcription in response to varicella-zoster virus infection of human T cells and fibroblasts in vitro and SCIDhu skin xenografts in vivo*. J Virol,* 77:1268–1280

Jones JO, Arvin AM. 2005. Viral and cellular gene transcription in fibroblasts infected with small plaque mutants of varicella-zoster virus. *Antiviral Res,* 68:56–65

Jones D, Blackmon A, Neff CP, Palmer BE, Gilden D, Badani H, Nagel MA. 2016. Varicella-Zoster Virus downregulates Programmed Death Ligand 1 and Major Histocompatibility Complex Class I in human brain vascular adventitial fibroblasts, perineurial cells, and lung fibroblasts. *J Virol*, 90(23):10527-10534

Jung T, Castellana D, Klingbeil P, Cuesta Hernández I, Vitacolonna M, Orlicky DJ, Roffler SR, Brodt P, Zöller M. 2009. CD44v6 dependence of premetastatic niche preparation by exosomes. *Neoplasia*, Oct;11(10):1093-105

Kadiu I, Narayanasamy P, Dash PK, Zhang W, Gendelman HE. 2012. Biochemical and biologic characterization of exosomes and microvesicles as facilitators of HIV-1 infection in macrophages. *J Immunol.,* 189, (2), 744-54

Kahn R, Mossberg M, Ståhl AL, Johansson K, Lopatko Lindman I, Heijl C, Segelmark M, Mörgelin M, Leeb-Lundberg LM, Karpman D. 2017. Microvesicle transfer of kinin B1-receptors is a novel inflammatory mechanism in vasculitis. *Kidney Int,* Jan;91(1):96-105

Kalyanaraman B, Darley-Usmar V, Davies KJ, Dennery PA, Forman HJ, Grisham MB, Mann GE, Moore K, Roberts LJ 2nd, Ischiropoulos H. 2012. Measuring reactive oxygen and nitrogen species with fluorescent probes: challenges and limitations. *Free Radic Biol Med,* Jan 1;52(1):1-6

Kang JH, Ho JD, Chen YH, Lin HC. 2009. Increased risk of stroke after a herpes zoster attack: a population-based follow-up study. *Stroke,* 40(11):3443-8

Kinchington PR, Cohen JI. 2003. *Varicella-zoster Virus, Virology and Clinical Managment.* Cambridge, Cambridge University Press, 2003, pp 74–104

Kinchington PR, Fite K, Seman A, Turse SE. 2001. Virion Association of IE62, the Varicella-Zoster Virus (VZV) Major Transcriptional Regulatory Protein, Requires Expression of the VZV Open Reading Frame 66 Protein Kinase. *J Virol,* Oct; 75(19): 9106–9113

Kinchington PR, Hougland JK, Arvin AM, Ruyechan WT, Hay J.1992. The varicella-zoster virus immediate-early protein IE62 is a major component of virus particles. *J Virol,* 66(1): 359–366

Kirkham FJ.1999. Stroke in childhood. *Arch Dis Child*, 81,(1), 85-9 2015. The Molecular Basis of Viral Infection. *Progress in Molecular Biology and Translational Science*, 129, 287-297

Knipes DM, Samuel CE, Palese P. 2001. *Virus-host cell interactions. Fields virology*, Lippincott Williams and Wilkins, Philadelphia, PA, p.134–136

Kobayashi T, Vischer UM, Rosnoblet C, Lebrand C, Lindsay M, Parton RG, Kruithof EK, Gruenberg J. 2000. The tetraspanin CD63/lamp3 cycles between endocytic and secretory compartments in human endothelial cells. *Mol Biol Cell,* 11(5):1829-43

Kouwaki T, Okamoto M, Tsukamoto H, Fukushima Y, Oshiumi H. 2017. Extracellular Vesicles Deliver Host and Virus RNA and Regulate Innate Immune Response. *Int J Mol Sci*, Mar 20;18(3)

Kubes P, Suzuki M, Granger DN. 1991. Nitric oxide: an endogenous modulator of leukocyte adhesion. *Proc Natl Acad Sci U S A,* Jun 1; 88(11):4651-5

Kuhlencordt PJ, Gyurko R, Han F, Scherrer-Crosbie M, Aretz TH, Hajjar R, Picard MH, Huang PL. 2001. Accelerated atherosclerosis, aortic aneurysm formation, and ischemic heart disease in apolipoprotein E/endothelial nitric oxide synthase double-knockout mice. *Circulation*, Jul 24; 104(4):448-54

Kumar P, Shen Q, Pivetti CD, Lee ES, Wu MH, Yuan S. 2009. Molecular mechanisms of endothelial hyperpermeability: implications in inflammation. *Expert Rev Mol Med,* 11:e19

Landau WM, Nassief A. 2005. Editorial comment-time to burn the TOAST. *Stroke*, 36, pp. 902-904

Langan SM, Minassian C, Smeeth L, Thomas SL. 2014. Risk of stroke following herpes zoster: a self-controlled case-series study. *Clin Infect Dis*, 58(11):1497-50

Langer RS, Zervas NT, Moskowitz MA. 1981. Perivascular meningeal projections from cat trigeminal ganglia: possible pathway for vascular headaches in man. *Science*, 213, (4504) 228–30

Lanthier S, Armstrong D, Domi T, DeVeber G. 2005. Post-varicella arteriopathy of childhood: natural history of vascular stenosis. *Neurology*, 64, (4) 660-3

Latham SL, Tiberti N, Gokoolparsadh N, Holdaway K, Couraud PO, Grau GE, Combes V. 2015. Immuno-analysis of microparticles: probing at the limits of detection. *Sci Rep*, 10;5:16314

Lawson C, Wolf S. 2009. ICAM-1 signaling in endothelial cells. *Pharmacol Rep,* 61, (1), 22-32

Lee A SY, Burdeinick-Kerr R, Whelan S. PJ. 2013. A ribosome-specialized translation initiation pathway is required for cap-dependent translation of vesicular stomatitis virus mRNAs. *Proceedings of the National Academy of Sciences of the United States of America*, *110*(1), 324–329

Lee JM, Moseley ME, Peterson ED, Turan TN, Valderrama AL, Vinters HV. 2013. An updated definition of stroke for the 21st century: a statement for healthcare professionals from the American Heart Association/American Stroke Association, *Stroke*, 44, (7) 2064-2089

Lee KS, Zhou W, Scott-McKean JJ, Emmerling KL, Cai GY, Krah DL, Costa AC, Freed CR, Levin MJ. 2012. Human sensory neurons derived from induced pluripotent stem cells support varicella-zoster virus infection. PLoS One, 7, (12) e53010

Lee RM. 1995. Morphology of cerebral arteries, *Pharmacol Ther,* 66, 149–173 Liang CC, Park AY, Guan JL. 2007. In vitro scratch assay: a convenient and inexpensive method for analysis of cell migration in vitro. *Nat Protoc,* 2, (2), 329-33.

Li M, Riddle SR, Frid MG, El Kasmi KC, McKinsey TA, Sokol RJ, Strassheim D, Meyrick B, Yeager ME, Flockton AR, McKeon BA, Lemon DD, Horn TR, Anwar A, Barajas C, Stenmark KR. 2011. Emergence of fibroblasts with a proinflammatory epigenetically altered phenotype in severe hypoxic pulmonary hypertension. *J Immunol,* 187(5):2711-22

Liao JK. 2013. Linking endothelial dysfunction with endothelial cell activation. *J Clin Invest,* Feb 1;123(2): 540–541

Liao JK, Shin WS, Lee WY, Clark SL. 1995. Oxidized low-density lipoprotein decreases the expression of endothelial nitric oxide synthase. *J Biol Chem*, 270(1):319–324

Liao F, Ali J, Greene T, Muller WA. 1997. Soluble domain 1 of platelet-endothelial cell adhesion molecule (PECAM) is sufficient to block transendothelial migration in vitro and in vivo. *J. Exp. Med*, 185, 1349–1357

Lindner D, Zietsch C, Tank J, Sossalla S, Fluschnik N, Hinrichs S, Maier L, Poller W, Blankenberg S, Schultheiss HP, Tschöpe C, Westermann D. 2014. Cardiac fibroblasts support cardiac inflammation in heart failure. *Basic Res Cardiol.,* 109, (5), 428

Lo W, Gordon AL, Hajek C, Gomes A, Greenham M, Anderson V, Yeates KO, Mackay MT. 2014. Pediatric stroke outcome measure: predictor of multiple impairments in childhood stroke. *J Child Neurol*., 29, (11) 1524-30

Lo W, Stephens J, Fernandez S. 2009. Pediatric stroke in the United States and the impact of risk factors. *J Child Neurol*, 24, 194–203.

Losurdo G, Giacchino R, Castagnola E, Gattorno M, Costabel S, Rossi A, Amato S, Di Pietro P, Molinari AC. 2006. Cerebrovascular disease and varicella in children. *Brain Dev*, 28: 366–70

Luckett LR, Gallucci RM. 2007. Interleukin-6 (IL-6) modulates migration and matrix metalloproteinase function in dermal fibroblasts from IL-6KO mice *Br J Dermatol,* 156, (6) 1163-71

Lynch JM, Kenyon TK, Grose C, Hay J, Ruyechan WT. 2002. Physical and functional interaction between the varicella zoster virus IE63 and IE62 proteins. *Virology*, 302:71–82

Maaijwee NA, Rutten-jacobs LC, Schaapsmeerders P, Van dijk EJ, De leeuw FE. 2014. Ischaemic stroke in young adults: risk factors and long-term consequences. *Nat Rev Neurol*, 10(6):315-25

Mackay MT, Prabhu SP, Coleman L. 2010. Childhood posterior circulation arterial ischemic stroke. *Stroke* 41,(10), 2201-9

Mackay MT, Wiznitzer M, Benedict SL, Lee KJ, Deveber GA, Ganesan V; International Pediatric Stroke Study Group. 2011. Arterial ischemic stroke risk factors: the International Pediatric Stroke Study. *Ann Neurol.,* 69, (1) 130-40

Mackay MT, Wiznitzer M, Benedict SL, Lee KJ, Deveber GA, Ganesan V; International Pediatric Stroke Study Group. 2011. Arterial ischemic stroke risk factors: the International Pediatric Stroke Study. *Ann Neurol*, 69, 130–40

Madden KP, Karanjia PN, Adams HP Jr, Clarke WR. 1995. Accuracy of initial stroke subtype diagnosis in the TOAST study. Trial of ORG 10172 in Acute Stroke Treatment. *Neurology*, 45(11):1975-9

Ma-Krupa W, Jeon MS, Spoeri S, Tedder TF, Goronzy JJ, Weyand CM. 2004. Activation of arterial wall dendritic cells and breakdown of self-tolerance in giant cell arteritis. *J Exp. Med*, 199, 173–183

Mallick AA, O'Callaghan FJ. 2010. The epidemiology of childhood stroke. *Eur J Paediatr Neurol.*, 14, (3) 197-205

Mallick AA, Ganesan V. 2014. Childhood arterial ischaemic stroke incidence, presenting features, and risk factors: a prospective population-based study. *Lancet Neurol.,* 13, (1) 35-43

Mandell DM, Mossa-Basha M, Qiao Y, Hess CP, Hui F, Matouk C, Johnson MH, Daemen MJ, Vossough A, Edjlali M, Saloner D, Ansari SA, Wasserman BA, Mikulis DJ; Vessel Wall Imaging Study Group of the American Society of Neuroradiology. 2017. Intracranial Vessel Wall MRI: Principles and Expert Consensus Recommendations of the American Society of Neuroradiology. AJNR *Am J Neuroradiol,* Feb;38(2):218-229

Markus A, Grigoryan S, Sloutskin A, Yee MB, Zhu H, Yang IH, Thakor NV, Sarid R, Kinchington PR, Goldstein RS. 2011. Varicella-zoster virus (VZV) infection of neurons derived from human embryonic stem cells: direct demonstration of axonal infection, transport of VZV, and productive neuronal infection. *J Virol,* 85,

(13) 6220-33 Maiellaro K, Taylor WR. 2007. The role of the adventitia in vascular inflammation. *Cardiovasc Res*, 75 640–8

Mathias M, Nagel MA, Khmeleva N, Boyer PJ, Choe A, Durairaj VD, Bennett JL, Mandava N, Gilden D. 2013. VZV multifocal vasculopathy with ischemic optic neuropathy, acute retinal necrosis and temporal artery infection in the absence of zoster rash. *J Neurol Sci*, 325, 180–182

Mause SF, Weber C. 2009. Microparticles: protagonists of a novel communication network for intercellular information exchange. *Circ Res*., 107, 1047-57

McGettrick HM, Smith E, Filer A, Kissane S, Salmon M, Buckley CD, Rainger GE, Nash GB. 2009. Fibroblasts from different sites may promote or inhibit recruitment of flowing lymphocytes by endothelial cells. *Eur J Immunol,* 39 113–25

McHugh L, ArthurJW. 2008. Computational Methods for Protein Identification from Mass Spectrometry Data. *PLoS Comput Biol,* Feb; 4(2): e12

McMurtry MS, Archer SL, Altieri DC, Bonnet S, Haromy A, Harry G, Bonnet S, Puttagunta L, Michelakis ED. 2005. Gene therapy targeting survivin selectively induces pulmonary vascular apoptosis and reverses pulmonary arterial hypertension. *J Clin Invest,* 115(6):1479-91

Meckes DG. 2015. Exosomal communication goes viral. J Virol 89: 5200 –5203

Meckes DG, Gunawardena HP, Dekroon RM, Heaton PR, Edwards RH, Ozgur S, Griffith JD, Damania B, Raab-Traub N. 2013. Modulation of B-cell exosome

proteins by gamma herpesvirus infection. *Proc Natl Acad Sci U S A*, 110:E2925–E2933

Mehta SK, Cohrs RJ, Forghani B, Zerbe G, Gilden DH, Pierson DL. 2004. Stress-induced subclinical reactivation of varicella zoster virus in astronauts. *J Med Virol*, 72 (1) 174–9

Meschia JF, Barrett KM, Chukwudelunzu F, Brown WM, Case LD, Kissela BM, Brown RD, Brott TG, Olson TS, Rich SS, Silliman S, Worrall BB. 2006. Interobserver agreement in the trial of org 10172 in acute stroke treatment classification of stroke based on retrospective medical record review *J. Stroke Cerebrovasc. Dis*, 15, pp. 266-272

Miyazaki Y, Riku Y, Goto Y, Mano K, Yoshida M, Hashizume Y. 2008. VZV vasculopathy associated with myelo-radiculoganglio-meningo-encephalitis: an autopsy case of an immunocompetent 66-year-old male. *J Neurol Sci,* 275:42–5

Mills K, Mills PB, Clayton PT, Johnson AW, Whitehouse DB, Winchester BG. 2001. Identification of alpha(1)-antitrypsin variants in plasma with the use of proteomic technology. *Clin.Chem,* 47(11):2012–2022

Miravet E, Danchaivijitr N, Basu H, Saunders DE, Ganesan V. 2007. Clinical and radiological features of childhood cerebral infarction following varicella zoster virus infection. *Dev Med Child Neurol,* 49, (6) 417–22

Mitzner W, Wagner EM. 2004. Vascular remodeling in the circulations of the lung. *J Appl Physiol* , 97(5):1999-2004

Moffat JF, Greenblatt RJ. 2010. Effects of varicella-zoster virus on cell cycle regulatory pathways. *Curr Top Microbiol Immunol,* 342:67-77

Montalvo EA, Parmley RT, Grose C. 1985. Structural analysis of the varicella-zoster virus gp98-gp62 complex: posttranslational addition of N-linked and O-linked oligosaccharide moieties. *J. Virol,* 53:761-770

Monteventi O, Chabrier S, Fluss J. 2013. Current management of post-varicella stroke in children: a literature review [Article in French]. *Arch Pediatr*, 20, (8) 883-9

Moraitis E, Ganesan V. 2014. Childhood infections and trauma as risk factors for stroke. *Curr Cardiol Rep*, Sep;16(9):527

Moskovitz J, Yim MB, Chock PB. 2002. Free radicals and disease. *Arch Biochem Biophys,* 397:354–359

Muralidharan-Chari V, Clancy JW, Sedgwick A, D'Souza-Schorey C. 2010. Microvesicles: mediators of extracellular communication during cancer progression*. J Cell Sci,* May 15; 123(Pt 10):1603-11

Murray M. Bern. 2017. Extracellular vesicles: how they interact with endothelium, potentially contributing to metastatic cancer cell implants *Clin Transl Med*, 6: 33

Nabata T, Morimoto S, Koh E, Shiraishi T, Ogihara T. 1990. Interleukin-6 stimulates c-myc expression and proliferation of cultured vascular smooth muscle cells. *Biochem Int*, 20(3):445-53

Naess H, Nyland HI, Thomassen L, Aarseth J, Nyland G, Myhr KM. 2002. Incidence and short-term outcome of cerebral infarction in young adults in western Norway. *Stroke*, 33(8):2105–8

Nagel MA, Choe A, Rempel A, Wyborny A, Stenmark K, Gilden D. 2015.

Differential regulation of matrix metalloproteinases in varicella zoster virus-infected human brain vascular adventitial fibroblasts. *J Neurol Sci* , 358, (1-2) 444-6

Nagel MA, Cohrs RJ, Mahalingam R, Wellish MC, Forghani B, Schiller A, Safdieh JE, Kamenkovich E, Ostrow LW, Levy M, Greenberg B, Russman AN, Katzan I, Gardner CJ, Häusler M, Nau R, Saraya T, Wada H, Goto H, de Martino M, Ueno M, Brown WD, Terborg C, Gilden DH. 2008. The varicella zoster virus vasculopathies: clinical, CSF, imaging, and virologic features. Neurology, 70, (11) 853-60

Nagel MA, James SF, Traktinskiy I, Wyborny A, Choe A, Rempel A, Baird NL, Gilden D. 2014. Inhibition of phosphorylated-STAT1 nuclear translocation and antiviral protein expression in human brain vascular adventitial fibroblasts infected with varicella-zoster virus. *J Virol,* 88, (19) 11634-7

Nagel MA, Jones D, Wyborny A. 2017. Varicella zoster virus vasculopathy: The expanding clinical spectrum and pathogenesis. *J Neuroimmunol,* 308:112-117

Nagel MA, Khmeleva N, Boyer PJ, Choe A, Bert R, Gilden D. 2013. Varicella zoster virus in the temporal artery of a patient with giant cell arteritis. *J Neurol Sci,* 335, 228–230

Nagel MA, Mahalingam R, Cohrs RJ, Gilden D. 2010. Virus vasculopathy and stroke: an under-recognized cause and treatment target. *Infect Disord Drug Targets*, 10, (2) 105– 11

Nagel MA, Rempel A, Huntington J, Kim F, Choe A, Gilden D. 2014. Frequency and abundance of alphaherpesvirus DNA in human thoracic sympathetic ganglia. *J Virol*, 88:8189–92

Nagel MA, Russman AN, Feit H, Traktinskiy I, Khmeleva N, Schmid DS, Skarf B, Gilden D. 2013. VZV ischemic optic neuropathy and subclinical temporal artery infection without rash. *Neurology*, 80, 220–222

Nagel MA, Traktinskiy I, Azarkh Y, Kleinschmidt-DeMasters B, Hedley-Whyte T, Russman A, VanEgmond EM, Stenmark K, Frid M, Mahalingam R, Wellish M, Choe A, Cordery-Cotter R, Cohrs RJ, Gilden D. 2011. Varicella zoster virus vasculopathy: analysis of virus-infected arteries. *Neurology,* 77, (4) 364–70

Nagel MA, Traktinskiy I, Stenmark KR, Frid MG, Choe A, Gilden D. 2013. Varicella- zoster virus vasculopathy: immune characteristics of virus-infected arteries. *Neurology,* 80, (1) 62–8

Nahmias AJ, Kibrick S. 1964. Inhibitory effect of heparin on herpes simplex virus. *J Bacteriology*, 87(5):1060-1066

Newsholme P, Haber EP, Hirabara SM, Rebelato EL, Procopio J, Morgan D, Oliveira-Emilio HC, Carpinelli AR, Curi R. 2007. Diabetes associated cell stress and dysfunction: role of mitochondrial and non-mitochondrial ROS production and activity. *J Physiol*, 583:9–24

Noubouossie DF, Whelihan MF, Yu YB, Sparkenbaugh E, Pawlinski R, Monroe DM, Key NS. 2017. In vitro activation of coagulation by human neutrophil DNA

and histone proteins but not neutrophil extracellular traps. *Blood,* 129(8):1021-1029

Owen DJ Crump CM, Graham SC. 2015. Tegument Assembly and Secondary Envelopment of Alphaherpesviruses. *Viruses*, 18;7(9):5084-114

Papaevangelou V, Quinlivan M, Lockwood J, Papaloukas O, Sideri G, Critselis E, Papassotiriou I, Papadatos J, Breuer J. 2013. Subclinical VZV reactivation in immunocompetent children hospitalized n the ICU associated with prolonged fever duration. *Clin Microbiol Infect,* 19, (5) 245–51

Pegtel DM, Cosmopoulos K, Thorley-Lawson DA, van Eijndhoven MA, Hopmans ES, Lindenberg JL, de Gruijl TD, Würdinger T, Middeldorp JM. 2010. Functional delivery of viral miRNAs via exosomes. *Proc Natl Acad Sci U S A,* 6;107(14):6328-33

Peinado H, Aleckovic M, Lavotshkin S, Matei I, Costa-Silva B, Moreno-Bueno G, Hergueta-Redondo M, Williams C, García-Santos G, Ghajar C, Nitadori-Hoshino A, Hoffman C, Badal K, Garcia BA, Callahan MK, Yuan J, Martins VR, Skog J, Kaplan RN, Brady MS, Wolchok JD, Chapman PB, Kang Y, Bromberg J, Lyden D. 2012. Melanoma exosomes educate bone marrow progenitor cells toward a pro-metastatic phenotype through MET. *Nat Med*, 18:883– 891

Petito CK, Cho ES, Lemann W, Navia BA, Price RW. 1986. Neuropathology of acquired immunodeficiency syndrome (AIDS): an autopsy review. *J Neuropathol Exp Neurol*, 45(6):635-46

Pisitkun T, Shen RF, Knepper MA. 2004. Identification and proteomic profiling of exosomes in human urine. *Proc Natl Acad Sci U S A,* 101: 13368

Pober JS, Bevilacqua MP, Mendrick DL, Lapierre LA, Fiers W, Gimbrone MA Jr. 1986. Two distinct monokines, interleukin 1 and tumor necrosis factor, each independently induce biosynthesis and transient expression of the same antigen on the surface of cultured human vascular endothelial cells. *J. Immunol,* 136:1680–1687

Portanova A1, Hakakian N, Mikulis DJ, Virmani R, Abdalla WM, Wasserman BA. 2013. Intracranial vasa vasorum: insights and implications for imaging. *Radiology,* 267, (3) 667-79

Prados-Rosales R, Baena A, Martinez LR, Luque-Garcia J, Kalscheuer R, Veeraraghavan U, Camara C, Nosanchuk JD, Besra GS, Chen B, Jimenez J, Glatman-Freedman A, Jacobs WR Jr, Porcelli SA, Casadevall A. 2011. Mycobacteria release active membrane vesicles that modulate immune responses in a TLR2-dependent manner in mice. *J Clin Invest,* Apr; 121(4):1471-83

Prados-Rosales R, Carreño LJ, Batista-Gonzalez A, Baena A, Venkataswamy MM, Xu J, Yu X, Wallstrom G, Magee DM, LaBaer J, Achkar JM, Jacobs WR Jr, Chan J, Porcelli SA, Casadevall A. 2014. Mycobacterial membrane vesicles administered systemically in mice induce a protective immune response to surface compartments of Mycobacterium tuberculosis. *MBio,* Sep 30; 5(5):e01921-14

Procop GW, Eng C, Clifford A, Villa-Forte A, Calabrese LH, Roselli E, Svensson L, Johnston D, Pettersson G, Soltesz E, Lystad L, Perry JD, Blandford A, Wilson DA, Hoffman GS. 2017. Varicella Zoster Virus and Large Vessel Vasculitis, the Absence of an Association. *Pathog Immun*, 2(2):228-238

Pugazhenthi S, Nair S, Velmurugan K, Liang Q, Mahalingam R, Cohrs RJ, Nagel MA, Gilden D. 2011. Varicella-zoster virus infection of differentiated human neural stem cells. *J Virol* , 85, (13) 6678-86

Pugliese SC, Poth JM, Fini MA, Olschewski A, El Kasmi KC, Stenmark KR. 2015. The role of inflammation in hypoxic pulmonary hypertension: from cellular mechanisms to clinical phenotypes. *Am J Physiol Lung Cell Mol Physiol,* 308(3):L229-52

Putaala J, Metso AJ, Metso TM, Konkola N, Kraemer Y, Haapaniemi E, Kaste M, Tatlisumak T. 2009. Analysis of 1008 consecutive patients aged 15 to 49 with first-ever ischemic stroke: the Helsinki young stroke registry. *Stroke*, 40(4):1195–203

Rahaus M, Desloges N, Wolff MH. 2004. Replication of varicella-zoster virus is influenced by the levels of JNK/SAPK and p38/MAPK activation. *J Gen Virol,* 85:3529–3540

Rahaus M, Desloges N, Wolff MH. 2006. Varicella-zoster virus influences the activities of components and targets of the ERK signalling pathway. *J Gen Virol,* 87:749–758

Rajendran P, Rengarajan T, Thangavel J, Nishigaki Y, Sakthisekaran D, Sethi G, Nishigaki I. 2013. The vascular endothelium and human diseases*. Int J Biol Sci,* Nov 9;9(10):1057-69

Ramakrishnaiah V, Thumann C, Fofana I, Habersetzer F, Pan Q, de Ruiter PE, Willemsen R, Demmers JAA, Stalin Raj V, Jenster G, Kwekkeboom J, Tilanus HW, Haagmans BL, Baumert TF, van der Laan LJW. 2013. Exosome-mediated transmission of hepatitis C virus between human hepatoma Huh7.5 cells. *Proc Natl Acad Sci U S A* 110:13109–13113

Ratajczak J, Miekus K, Kucia M, Zhang J, Reca R, Dvorak P, Ratajczak MZ. 2006. Embryonic stem cell-derived microvesicles reprogram hematopoietic progenitors: evidence for horizontal transfer of mRNA and protein delivery. *Leukemia*, 20: 847–856

Ratajczak J, Wysoczynski M, Hayek F, Janowska-Wieczorek A, Ratajczak MZ. 2006. Membrane-derived microvesicles: important and underappreciated mediators of cell-to- cell communication. *Leukemia,* 20 1487–1495

Rautou PE, Mackman N. 2013. Microvesicles as risk markers for venous thrombosis*.Expert Rev Hematol*, Feb; 6(1):91-101

Reichelt M, Brady J, Arvin AM. 2009. The replication cycle of varicella-zoster virus: analysis of the kinetics of viral protein expression, genome synthesis, and virion assembly at the single-cell level. *J Virol,* 83, (8) 3904-18

Reis AF, Pais P, Monteiro JP. 2014. Chickenpox and stroke in children: case studies and literature review. *Acta Paediatr,* 103(4):e176-80

Reshef E, Greenberg SB, Jankovic J. 1985. Herpes zoster ophthalmicus followed by contralateral hemiparesis: report of two cases and review of literature. *J Neurol Neurosurg Psychiatry*, 48(2):122-7

Rivkin MJ, Bernard TJ, Dowling MM, Amlie-Lefond C. 2016. Guidelines for Urgent Management of Stroke in Children. *Pediatr Neurol,* Mar;56:8-17

Robbins PD, Morelli AE. 2014. Regulation of immune responses by extracellular vesicles. *Nat Rev Immunol* 14:195–208

Roingeard P. 2008. Viral detection by electron microscopy: past, present and future. *Biol Cell,* 100(8):491-501

Rossner R, Kaeberlein M, Leiser SF. 2017. Flavin-containing monooxygenases in aging and disease: Emerging roles for ancient enzymes. *J Biol Chem,* 292(27):11138-11146

Rothwell PM, Coull AJ, Giles MF, Howard SC, Silver LE, Bull LM, Gutnikov SA, Edwards P, Mant D, Sackley CM, Farmer A, Sandercock PA, Dennis MS, Warlow CP, Bamford JM, Anslow P; Oxford Vascular Study. 2004. Change in stroke incidence, mortality, case-fatality, severity, and risk factors in Oxfordshire,UK from 1981 to 2004 (Oxford Vascular Study). *Lancet*, 363:1925–33

Ruyechan WT, Hay J. 2003. *Varicella-zoster Virus, Virology and Clinical Management*. Cambridge, Cambridge University Press, pp 51–73

Sacco RL, Kasner SE, Broderick JP, Caplan LR, Connors JJ, Culebras A, Elkind MS, George MG, Hamdan AD, Higashida RT, Hoh BL, Janis LS, Kase CS,

Kleindorfer DO, Satoh S, Shirane R, Yoshimoto T. 1991. Clinical survey of ischemic cerebrovascular disease in children in a district of Japan. *Stroke*, 22, 586–9

Salazar R, Russman AN, Nagel MA, Cohrs RJ, Mahalingam R, Schmid DS, Kleinschmidt-DeMasters BK, VanEgmond EM, Gilden D. 2011. Varicella zoster virus ischemic optic neuropathy and subclinical temporal artery involvement. *Arch Neurol,* 68, 517–520

Schaefer PW, Hunter GJ, He J, Hamberg LM, Sorensen AG, Schwamm LH, Koroshetz WJ, Gonzalez RG. 2002. Predicting cerebral ischemic infarct volume with diffusion and perfusion MR imaging. *AJNR Am J Neuroradiol.,* 23, (10) 1785-94

Schwechheimer C, Kuehn MJ. Outer-membrane vesicles from Gram-negative bacteria: biogenesis and functions.. Nat Rev Microbiol. 2015 Oct; 13(10):605-19.

Schobess R, Nowak-Göttl U. 2002. Prospective assessment of risk factors for recurrent stroke during childhood–a 5-year follow-up study. Lancet, 360, (9345) 1540–5.

Schorey JS, Bhatnagar S. 2008. Exosome function: from tumor immunology to pathogen biology. *Traffic*, 9, 871–881

Schorey JS, Sweet L. 2008. The mycobacterial glycopeptidolipids: structure, function, and their role in pathogenesis. *Glycobiology* 18, 832–841

Schwechheimer C, Kuehn MJ. 2015. Outer-membrane vesicles from Gram-negative bacteria: biogenesis and functions. *Nat Rev Microbiol,* Oct; 13(10):605-19

Sébire G, Fullerton H, Riou E, DeVeber G. 2004. Toward the definition of cerebral arteriopathies of childhood. *Curr Opin Pediatr,* 16, (6) 617-22

Sébire G, Meyer L. Chabrier S. 1999. Varicella as a risk factor for cerebral infarction in childhood: a case–control study. *Ann Neurol*, 45, (5) 679–80

Simons M, Raposo G. 2009. Exosomes–vesicular carriers for intercellular communication. *Curr Opin Cell Biol*, 21 575–581

Shellhaas RA, Smith SE, O'Tool E, Licht DJ, Ichord RN. 2006. Mimics of childhood stroke: characteristics of a prospective cohort. *Pediatrics*, 118, (2), 704-9

Shi Y, OBrien JE, Fard A, Mannion JD, Wang D, Zalewski A. 1996. Adventitial myofibroblasts contribute to neointimal formation in injured porcine coronary arteries. Circulation, 94 1655–64

Shoyab M, Plowman GD, McDonald VL, Bradley JG, Todaro GJ. 1989. Structure and function of human amphiregulin: a member of the epidermal growth factor family. *Science,* 243(4894 Pt 1):1074-6

Singh P, LeMaire PC, Tan JC, Zeng E, Schorey JS. 2011. Exosomes released from M. tuberculosis infected cells can suppress IFN-g mediated acti- vation of naıve macrophages. *PLoSONE*, 6 e18564

Siow RC, Mallawaarachchi CM, Weissberg PL. 2003. Migration of adventitial myofibroblasts following vascular balloon injury: insights from in vivo gene transfer to rat carotid arteries. *Cardiovasc Res*, 59 212–21

Sloutskin A, Kinchington PR, Goldstein RS. 2013. Productive vs non-productive infection by cell-free varicella zoster virus of human neurons derived from embryonic stem cells is dependent upon infectious viral dose. *Virology*, 443, (2), 285-93

Soneson C, Love MI, Robinson MD. 2015. Differential analyses for RNA-seq: transcript-level estimates improve gene-level inferences. *F1000Res,* 4:1521

Sreenivasan N, Basit S, Wohlfahrt J, Pasternak B, Munch TN, Nielsen LP, Melbye M. 2013. The short- and long-term risk of stroke after herpes zoster - a nationwide population-based cohort study. *PLoS OnE*, 17;8(7):e69156

Smith RS, Smith TJ, Blieden TM, Phipps RP. 1997. Fibroblasts as sentinel cells. Synthesis of chemokines and regulation of inflammation. *Am J Pathol*, 151 317–22

Stack CA, Cole JW. 2017. A Diagnostic Approach to Stroke in Young Adults. *Curr Treat Options Cardiovasc Med*, 25;19(11):84

Stastna M, Van Eyk, JE. 2012. Investigating the Secretome: Lessons About the Cells that Comprise the Heart. *Circ Cardiovasc Genet*, 5(1): o8–o18.

Steiner I, Kennedy PG, Pachner AR. 2007. The neurotropic herpes viruses: herpes simplex and varicella-zoster. *Lancet Neurol,* 6(11):1015–1028

Steinhauser ML, Kunkel SL, Hogaboam CM, Evanoff H, Strieter RM, Lukacs NW. 1998. Macrophage/fibroblast coculture induces macrophage inflammatory protein-1alpha production mediated by intercellular adhesion molecule-1 and oxygen radicals. *J Leukoc Biol,* 64, (5) 636-41

Stenmark KR, Davie N, Frid M, Gerasimovskaya E, Das M. 2006. Role of the adventitia in pulmonary vascular remodeling. *Physiology (Bethesda)*, 21, 134-45

Stenmark KR, Fagan KA, Frid MG. 2006. Hypoxia-induced pulmonary vascular remodeling: cellular and molecular mechanisms. Circ Res, 99, (7) 675-91

Stenmark KR, Yeager ME, El Kasmi KC, Nozik-Grayck E, Gerasimovskaya EV, Li M, Riddle SR, Frid MG. 2013. The adventitia: essential regulator of vascular wall structure and function. *Annu Rev Physiol*, 75():23-47

Stone JR, Bruneval P, Angelini A, Bartoloni G, Basso C, Batoroeva L, Buja LM, Butany J, d'Amati G, Fallon JT, Gittenberger-de Groot AC, Gouveia RH, Halushka MK, Kelly KL, Kholova I, Leone O, Litovsky SH, Maleszewski JJ, Miller DV, Mitchell RN, Preston SD, Pucci A, Radio SJ, Rodriguez ER, Sheppard MN, Suvarna SK, Tan CD, Thiene G, van der Wal AC, Veinot JP. 2015. Consensus statement on surgical pathology of the aorta from the Society for Cardiovascular Pathology and the Association for European Cardiovascular Pathology: I. Inflammatory diseases. *Cardiovasc Pathol*, 24(5):267-78

Storlie J, Carpenter JE, Jackson W, Grose C. 2008. Discordant varicella-zoster virus glycoprotein C expression and localization between cultured cells and human skin vesicles. *Virology*, 382, (2) 171-81

Sweet, L., W. Zhang, H. Torres-Fewell, A. Serianni, W. Boggess, and J. Schorey. 2008. Mycobacterium avium glycopeptidolipids require specific acetylation and methylation patterns for signaling through toll-like receptor 2. J. Biol. Chem. 283: 33221–33231.

Tang XL, Jiang ZY, Dong J, Liu XC, Cai SY, Xiao R, Lu YR. 2006. [Expression of tissue factor induced by IL-6 in HUVEC]. [Article in Chinese]. *Sichuan Da Xue Xue Bao Yi Xue Ban,* 37, (2) 234-7

Tedgui A. 1999. *Biology of the arterial wall*, Springer

Théry C, Ostrowski M, Segura E. 2009. Membrane vesicles as conveyors of immune responses. *Nat Rev Immunol*, 9:581–593

Thiagarajan P, Tait JF. 1990. Binding of annexin V/placental anticoagulant protein I to platelets. Evidence for phosphatidylserine exposure in the procoagulant response of activated platelets. *J. Biol. Chem,* 265, 17420–17423

Thomas SL, Minassian C, Ganesan V, Langan SM, Smeeth L. 2014. Chickenpox and risk of stroke: a self-controlled case series analysis. *Clin Infect Dis*, 58, (1) 61–8

Tieu BC, Lee C, Sun H, Lejeune W, Recinos A 3rd, Ju X, Spratt H, Guo DC, Milewicz D, Tilton RG, Brasier AR. 2009. An adventitial IL-6/ MCP1 amplification loop accelerates macrophage-mediated vascular inflammation leading to aortic dissection in mice. *J Clin Invest*, 119 3637–51

Torrecilhas AC, Schimacher RI, Alves MJM, Colli W. 2012. Vesicles as carriers

of virulence factors in parasitic protozoan diseases. *Microb Infect,* 14, 1465–1474

Trapnell, C., Williams, B.A., Pertea, G., Mortazavi, A., Kwan, G., van Baren, M.J., Salzberg, S.L., Wold, B.J. and Pachter, L. 2010. Transcript assembly and quantification by RNA-Seq reveals unannotated transcripts and isoform switching during cell differentiation. *Nat. Biotechnol*, 28, 511–515

Tuder RM, Archer SL, Dorfmüller P, Erzurum SC, Guignabert C, Michelakis E, Rabinovitch M, Schermuly R, Stenmark KR, Morrell NW. 2013. Relevant issues in the pathology and pathobiology of pulmonary hypertension. *J Am Coll Cardiol,* 62(25 Suppl):D4-12

Valko M, Leibfritz D, Moncol J, Cronin MT, Mazur M, Telser J. 2007. Free radicals and antioxidants in normal physiological functions and human disease. *Int J Biochem Cell Biol*, 39:44–84

vanDongen HM, Masoumi N, Witwer KW, Pegtel DM. 2016. Extracellular Vesicles Exploit Viral Entry Routes for Cargo Delivery. *Microbiol Mol Biol Rev,* 2;80(2):369-86

Wang X, Fang H, Huang Z, Shang W, Hou T, Cheng A, Cheng H. 2013. Imaging ROS signaling in cells and animals. *J Mol Med (Berl).* Aug;91(8):917-27

Wardlaw JM, Dennis MS, Warlow CP, Sandercock PA. 2001. Imaging appearance of the symptomatic perforating artery in patients with lacunar infarction: occlusion or other vascular pathology? *Ann Neurol,* 50, (2) 208-15

Wells PG, McCallum GP, Chen CS, Henderson JT, Lee CJ, Perstin J, Preston

Wiley MJ, Wong AW. 2009. Oxidative stress in developmental origins of disease: teratogenesis, neurodevelopmental deficits, and cancer. *Toxicol Sci,* 108:4–18

Venugopal N. 2017. Head injury, varicella vasculopathy: Differential diagnosis for pediatric retinal arterial occlusion. *Indian J Ophthalmol*, 65(5):424

Verweij MC, Wellish M, Whitmer T, Malouli D, Lapel M, Jonjić S, Früh K. (2015). Varicella Viruses Inhibit Interferon-Stimulated JAK-STAT Signaling through Multiple Mechanisms. Everett RD, ed. *PLoS Pathogens*. 2015;11(5):e1004901

Viedt C, Vogel J, Athanasiou T, Shen W, Orth SR, Kübler W, Kreuzer J. 2002. Monocyte chemoattractant protein-1 induces proliferation and interleukin-6 production in human smooth muscle cells by differential activation of nuclear factor-kappaB and activator protein-1. *Arterioscler Thromb Vasc Biol,* 22, (6), 914-20

Vilela P, Rowley HA. 2017. Brain ischemia: CT and MRI techniques in acute ischemic stroke. *Eur J Radiol,* Nov;96:162-172.

von der Malsburg A, Abutbul-Ionita I, Haller O, Kochs G, Danino D, 2011. Stalk domain of the dynamin-like MxA GTPase protein mediates membrane binding and liposome tubulation via the unstructured L4 loop. *J Biol Chem*, 286: 37858–37865

Wang D, Zhang H, Li M, Frid MG, Flockton AR, McKeon BA, Yeager ME, Fini MA, Morrell NW, Pullamsetti SS, Velegala S, Seeger W, McKinsey TA, Sucharov

CC, Stenmark KR. 2014. MicroRNA-124 controls the proliferative, migratory, and inflammatory phenotype of pulmonary vascular fibroblasts. *Circ Res,* 114(1):67-78

Wilcox JN, Okamoto EI, Nakahara KI, Vinten-Johansen J. 2001. Perivascular responses after angioplasty which may contribute to postangioplasty restenosis: a role for circulating myofibroblast precursors? *Ann N Y Acad Sci*, 947:68-90

Williams LS1, Garg BP, Cohen M, Fleck JD, Biller J. 1997. Subtypes of ischemic stroke in children and young adults. *Neurology*, 49, (6) 1541-5

Willmarth NE, Ethier SP. 2006. Autocrine and juxtacrine effects of amphiregulin on the proliferative, invasive, and migratory properties of normal and neoplastic human mammary epithelial cells. *J Biol Chem*, 281(49):37728-37

Wung BS, Ni CW, Wang DL. 2005. ICAM-1 induction by TNFalpha and IL-6 is mediated by distinct pathways via Rac in endothelial cells. *J Biomed Sci*, 12, (1) 91-101

Yang JJ1, Hill MD, Morrish WF, Hudon ME, Barber PA, Demchuk AM, Sevick RJ, Frayne R. 2002. Comparison of pre- and post contrast 3D time-of flight MR angiography for the evaluation of distal intracranial branch occlusions in acute ischaemic stroke. *AJNR Am J Neuroradiol,* 23, 557– 567

Yawn BP, Wollan PC, Nagel MA, Gilden D. 2016. Risk of Stroke and Myocardial Infarction After Herpes Zoster in Older Adults in a US Community Population. *Mayo Clin Proc*, 91(1):33-44

Yu X, Seitz S, Pointon T, Bowlin JL, Cohrs RJ, Jonjić S, Haas J, Wellish M, Gilden D. 2013. Varicella zoster virus infection of highly pure terminally differentiated human neurons. *J Neurovirol,* 19, (1) 75-81

Zahra S, Anderson JA, Stirling D, Ludlam CA. 2011. Microparticles, malignancy and thrombosis. *Br J Haematol,* Mar;152(6):688-700

Zaiss DMW, Gause WC, Osborne LC, Artis D. 2015. Emerging functions of amphiregulin in orchestrating immunity, inflammation, and tissue repair. *Immunity,* 42(2):216-226

Zerboni L, Sen N, Oliver SL, Arvin AM. 2014. Molecular mechanisms of varicella zoster virus pathogenesis. *Nat Rev Microbiol*, 12, (3), 197-210

Zhao S, Fung-Leung W-P, Bittner A, Ngo K, Liu X. 2014. Comparison of RNA-Seq and Microarray in Transcriptome Profiling of Activated T Cells. Zhang S-D, ed. *PLoS ONE*, 9(1):e78644

Zhou Y, Lee JY, Lee CM, Cho WK, Kang MJ, Koff JL, Yoon PO, Chae J, Park HO, Elias JA, Lee CG. 2012. Amphiregulin, an epidermal growth factor receptor ligand, plays an essential role in the pathogenesis of transforming growth factor-β-induced pulmonary fibrosis. *J Biol Chem,* 287(50):41991-2000

Zhu Z, Gershon MD, Ambron R, Gabel C, Gershon AA. 1995. Infection of cells by varicella zoster virus: inhibition of viral entry by mannose 6-phosphate and heparin. *Proceedings of the National Academy of Sciences of the United States of America*, 92(8):3546-3550

Zimmer JA, Garg BP, Williams LS, Golomb MR. 2007. Age-related variation in presenting signs of childhood arterial ischemic stroke.. *Pediatr Neurol.,* 37, (3), 171-5

Zimmerman GA, Albertine KH, Carveth HJ, Gill EA, Grissom CK, Hoidal JR, Imaizumi T, Maloney CG, McIntyre TM, Michael JR, Orme JF, Prescott SM, Topham MS. 1999. Endothelial activation in ARDS. *Chest*, 116, 18–24